Exploring a high-resolution landscape approach for managing water quality and soil greenhouse gases

Clint Rissmann, Lisa Pearson, Bridget Robson, and Saeed Rahimi

Land and Water Science Report 2022/03
June 2022

Exploring a high-resolution landscape approach for managing water quality and soil greenhouse gases

Prepared by
Rissmann, C., Pearson, L., Robson, B., and Rahimi, S.

Land and Water Science Ltd.
www.landwaterscience.co.nz
231 Dee Street
Invercargill, 9810
New Zealand

Corresponding Author
Clint Rissmann
Email: clint@landwatersci.net

Document Information
Land and Water Science Report No: 2022/03
Report Date: 30.06.2022
Project Number: 21022

Technical Advisors

Applied statistics: Tony Pleasants, Adjunct Professor in Agricultural Analytics, Massey University

Soil nitrous oxide and biogeochemistry: Tim Clough, Lincoln University, Professor, Department of Soil & Physical Sciences

Soil nitrous oxide and biogeochemistry: Troy Baisden, Principal Investigator, Te Pūnaha Matatini Centre of Research Excellence

Geochemistry, Geology, and Hydrochemistry: Professor Matthew Leybourne, Co-Director, Queen's Facility for Isotope Research (QFIR), Department of Geological Sciences and Geological Engineering Queens University, Canada

Document Status: Final

Citation Advice
Rissmann, C., Pearson, L., Robson, B., and Rahimi, S. (2022). Exploring a high-resolution landscape approach for managing water quality and soil greenhouse gases. Land and Water Science Report 2022/03. p133.

Table of Contents

Technical Appendices

Executive Summary

Landscape variability causes major variability in water quality even when land use is the same. Landscape variability also has a big effect on soil GHG production. This report sets out a new, high-resolution physiographic approach[1,2] to mapping the inherent and varied susceptibility of the landscape to land use activities at property scales.

The outputs support the Parliamentary Commissioner for the Environment's quest to find an **integrated landscape approach** to support rural communities and tangata whenua address the interrelated issues of climate change, freshwater quality, soil erosion and biodiversity pressures. It supplies integrated knowledge on the property-scale landscape factors that control water quality and soil nitrous oxide emissions in two trial catchments.

The maps of landscape susceptibility highlight the various contaminants and their forms for the Wairoa Catchment in Northland and Mataura Catchment in Southland. Obviously, land use and land use management needs to vary to be in tune with these varying risks.

Landscape's dominant influence on contaminant production and transport means that much more attention needs to be paid to these spatially driven factors. Doing so presents opportunities.

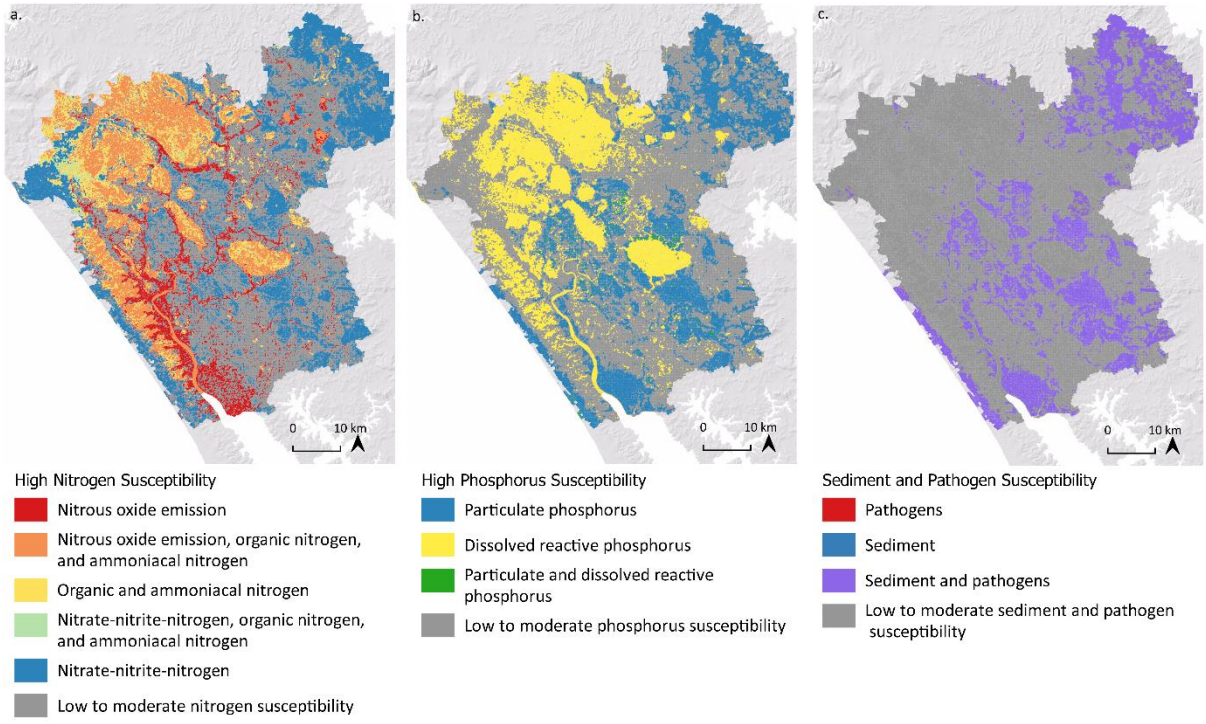

Maps of landscape susceptibility for the Wairoa Catchment, Northland.

[1] Airborne derived radiometric survey (40 x 40 m or 0.16 ha), LiDAR (1 x 1 m), and satellite derived land use intensity, land cover and topography where LiDAR is currently absent.

[2] A physiographic approach involves systematically mapping landscape (climate, topography, hydrology, soils, and geology) to identify key processes that influence the susceptibility of the land to contaminant loss - nitrogen, phosphorous, sediment and pathogens.

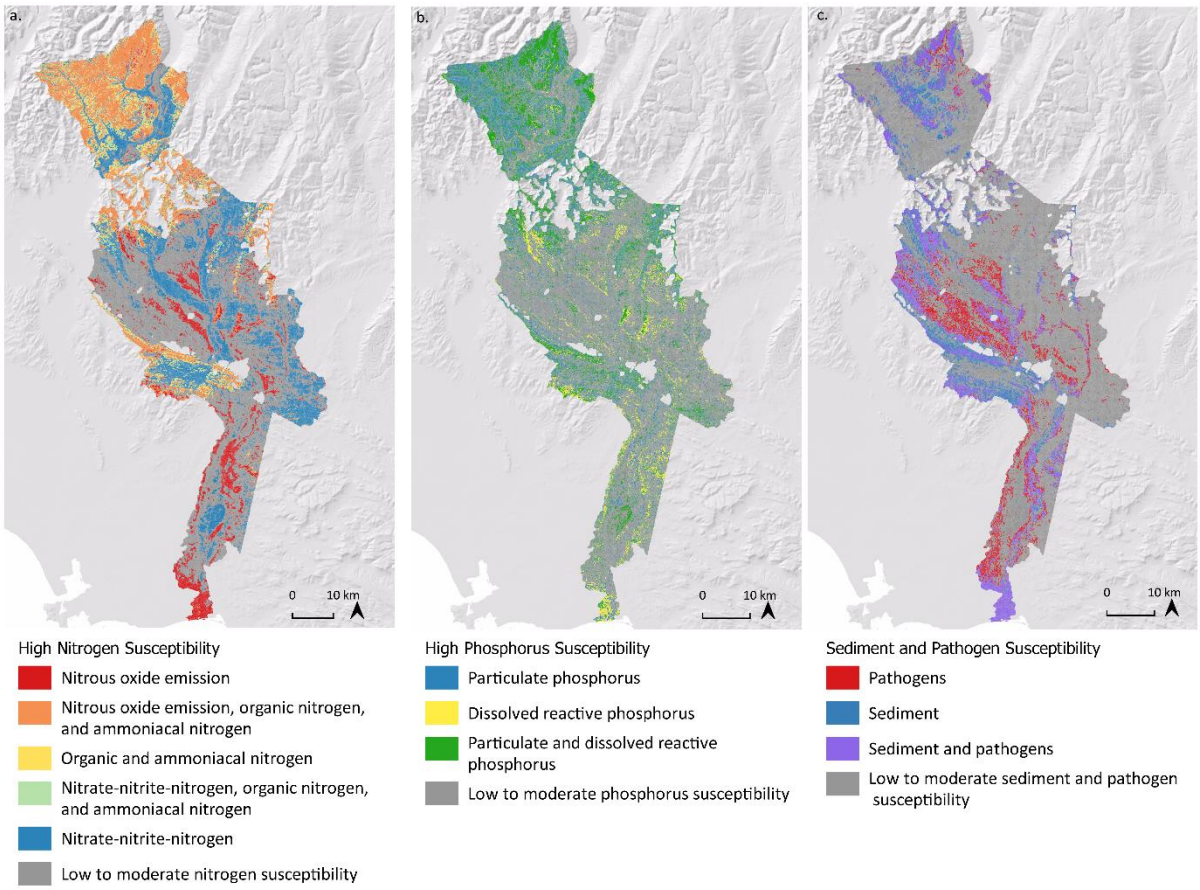

Maps of landscape susceptibility (high) for the Mataura Catchment, Southland.

A heavy focus in some regional plans on single-contaminant or single process (nitrate leaching) has diverted attention from other ways nitrogen is lost, and from other contaminants (phosphorus, sediment, and microbial pathogens). Yet for large areas of NZ's production landscape, these other contaminants present greater risks – where hill country erosion, imperfectly to poorly drained soils, and P losses from reducing aquifers often play a larger role.

Thus, rearranging land use to attenuate nitrate only, while not considering these other risks, often won't improve water quality and may not reduce soil nitrous oxide production. It will also disempower those trying to do the right thing, because the changes they make won't fix the problems they have.

Co-managing biological emissions and forest sinks can be done in an integrated way. A co-management approach means that the landscape can continue to provide a wide range of interrelated environmental, social, and economic services. Effective management of biologically derived greenhouse gases (GHG) will result in the NZ landscape being re-transformed. The consequences to the communities where half our biological gases[3] come from, and where we contemplate storing carbon, will be significant.

Our response to managing GHG can be far more thoughtful than regarding land as just a place to store carbon. An integrated landscape approach lets us also manage other environmental impacts of NZ's land-based sectors.

[3] Methane and nitrous oxide.

1 Introduction

Reading the landscape susceptibility report

This report starts with an overview describing how the landscape approach supports the overall goal of the PCE project - to consider how funds from pricing GHG emission could be put back into rural communities in a way that improves our climate response, reduces soil erosion, and reduces water quality and biodiversity issues. It then explains the approach used to build a picture of the landscape processes that are operating, and the concept that landscape factors control much of contaminant production and transport.

The detail of the methodology is in the five technical appendices. While these appendices are very technical in parts, they also include details that are accessible and interesting to "lay" readers. We would encourage the reader to skim through to find these interesting nuggets.

1.1 Overview

The PCE's 2019 Farms, forests, and fossil fuels report[4] (FFFF) recommends that fossil sources of carbon be dealt with separately from biological sources and sinks.

It concludes that effective management of biologically derived greenhouse gases (GHG) will result in the NZ landscape being re-transformed. The consequences - physical, environmental, cultural, and social - to the communities where half our biological gases[5] come from, and where we contemplate storing carbon, will be significant.

It recommends co-managing biological emissions and forest sinks in an integrated way, as they are often co-produced in NZ landscapes. A co-management approach means that the landscape can continue to provide a wide range of interrelated environmental, social, and economic services. In other words, the Aotearoa New Zealand response to managing GHG needs to be far more thoughtful than regarding land as just a place to store carbon. An integrated landscape approach also lets us look at how to manage other environmental impacts of NZ's land-based sectors.

The PCE's proposition is '*Revenue from pricing biological GHG emissions goes back to places/ people from which they came, to support activities to reduce the risks of climatic and economic disruption'.*

The PCE asks how landscape-based policies could support the three objectives:

- Assisting rural communities to explore locally appropriate ways of tackling GHG emissions, soil erosion and biodiversity loss, while enhancing resilience
- Shifting to climate-resilient landscapes that meet multiple environmental objectives[6]
- Efficiently and equitably reducing biogenic GHGs

Using an integrated landscape-wide approach to manage these environmental impacts could optimise economic and environmental outcomes. The PCE considers that such an approach would require:

1. Integrated knowledge about landscape-scale environmental processes at a macro level, ground-truthed with grassroots knowledge to ensure the micro scale is also accurate

[4] https://www.pce.parliament.nz/publications/farms-forests-and-fossil-fuels-the-next-great-landscape-transformation

[5] Methane and nitrous oxide.

[6] Defined: reducing GHG emissions and soil erosion; improving water quality and biodiversity (or reducing loss)

2. Accurate estimates of farm level emissions, through on-farm measurement
3. Revenue to support activities that reduce the risks of climatic and economic disruption
4. Identifying how landowners and communities are incentivised to act
5. Landowners taking ownership of problems of current land use practices, and deploying new management techniques
6. Land use change to be driven largely by landowners (to rebalance their natural capital).
7. Tools to manage biological sources and sinks
8. Policy tools that go beyond simple economic instruments or regulations
9. Policy responses that better reflect the physical science

This report sets out the mapping component of this PCE exploration of how an **integrated landscape approach** could support rural communities and tangata whenua in addressing the interrelated issues of climate change, freshwater quality, soil erosion and biodiversity pressures.

We note that an integrated landscape approach has physical aspects – it is spatially explicit, place-based, fine-grained, and transparent, and it has social features that relate to how the information set is built and used – it is integrated, bottom up, tailored, and supports collective responsibility. How these aspects have been developed is discussed in detail in the report below.

We also note that this approach uses spatial data in a novel and experimental way to characterise landscape susceptibility to various contaminant-production risks.

2 Land and Water Science Project

The Land and Water Science (LWS) project output detailed below provides positive proof of concept for the value of using a spatial approach to identify landscape susceptibility to contaminant discharges; the Physiographic Approach[7]. It does so by supplying integrated knowledge about landscape-scale controlling factors, at a macro level at two case study catchments[8] in Northland and Southland. The outputs are being ground-truthed with grassroots knowledge at the Southland site to ensure the microscale is also accurate.

The LWS project has created high-resolution maps of the landscape's susceptibility to loss, for factors that control water quality (N and P species, pathogens, and sediment), and soil nitrous oxide. The project:

- Identifies the main controlling landscape factors and associated processes that determine spatial variation in freshwater contaminant concentrations and soil nitrous oxide emissions.
- Produces integrated susceptibility maps for each catchment to help identify the most effective locations for implementing changes to land management practices and land use change.

[7] A physiographic approach involves systematically mapping the biophysical characteristics of a landscape (climate, topography, hydrology, soils, and geology) to identify key processes that influence water quality. The resulting classification of physiographic units and zones can provide useful information about the susceptibility of the land to loss of freshwater contaminants such as nitrogen, phosphorous, sediment and pathogens.

[8] Wendonside (Mataura River catchment Southland), Wairua River (part of Wairoa River catchment Northland)

- Includes updated land use maps for each catchment.

The LWS physiographic outputs for the two case studies includes:

- High-resolution **land use pressure** maps
- High-resolution maps depicting gradients in the susceptibility of **landscape for contaminant loss factors** that control water quality and soil nitrous oxides, and
- An overarching, multi-pollutant classification to support **land use optimisation modelling** by the PCE.

The LWS work stream supports several of the other requirements of the PCE proposed approach. It identifies areas of highest risk and thus areas most appropriate for land use change (#6). It identifies and locates biological sources and sinks in the landscape so that tools to manage these can be applied (relevant to #7). LWS experience with farmer groups provides insights into what motivates farmers to consider change (#4, #5 and #8).

The power to take effective action relies on having knowledge and means. Many farmers are ready and willing to take ownership and act, once they know how contaminants are transported from their property - although they may still need financial support to do so. They are able to put in place effective mitigations because the factors controlling contaminant losses make sense to them. They understand what needs to be done and how to do it (#4, #5 and #6).

The LWS physiographic approach provides insights into the relevant components of the information base required for policy setting (#9). It is clear that many elements of policy need to be strongly spatially informed to be effective. We note that the paucity of relevant environmental monitoring data[9] and the base scale of several input maps (e.g., NZ soil maps) means that risks or susceptibility cannot be confidently expressed in numeric form. Rather, processes and their susceptibility gradients are described with high confidence in relative narrative terms i.e., very low to very high.

The way that the information is provided (educational and map format) strongly supports farmers' agency in their decision-making (#5).

2.1 Application of the approach for the PCE

Policy for managing land, in a way that also supports good water quality, has been relatively unsuccessful in Aotearoa New Zealand to date. The RMA effects-based approach hasn't worked well at managing the cumulative effects of diffuse discharges. The heavy focus in some regional plans on single-contaminant, single process (e.g., leaching only) also diverted attention from the risk of poor outcomes for contaminant loss processes other than nitrate leaching, and for other contaminants (ammoniacal nitrogen, organic nitrogen, phosphorus, sediment, and microbial pathogens).

For large areas of NZ's production landscape, the key contaminant is not nitrate. Across hill country, areas or imperfectly to poorly drained soils, areas with erosion prone geology, and reducing soils and aquifers, other contaminants play a larger role. Thus, rearranging land use to maximise nitrate attenuation without considering risks from sediment, phosphorus, other forms of nitrogen, or pathogens will fail to maintain or improve water quality. It may also have negative effects on soil

[9] Location within a catchment (often bottom end, thus large number of possible sources to try to discern patterns from), data collection frequency (monthly spot samples) and patchy overall coverage in NZ makes it difficult to draw conclusions with confidence. Discussed in many places, including PCE Report Focusing Aotearoa New Zealand's environmental reporting system November 2019.

nitrous oxide production. It will also disempower those trying to do the right thing, because the changes they make won't fix the problems they have.

Resolving multi-contaminant issues requires a holistic understanding of the nature and routes of all contaminant processes, which requires an integrated understanding of the landscape drivers of those.

Responses need to be tailored to those controlling landscape factors[10]. To do this requires a change in focus from trying to control via measuring effects off site, to farmer-centric process control that is well-informed by tools that link directly to property scale (0.25 ha or finer) spatial controlling factors that drive the contaminant risks.

The farmer needs to understand what controlling landscape factors they need to control:

- Where – spatial information, that sets out the site risks
- When? Are there circumstances that make the farm become very vulnerable? Yet more rain on soggy soil? Heavy rain on very dry soil? Differences between air and soil temperature?

2.2 Landscape Susceptibility as part of Environmental Risk

Risk is shown below as the intersection of three factors: land use pressure from the activity, the landscape's inherent susceptibility to contaminant loss, and the vulnerability of downstream receiving environments to contaminant loads (Figure 1).

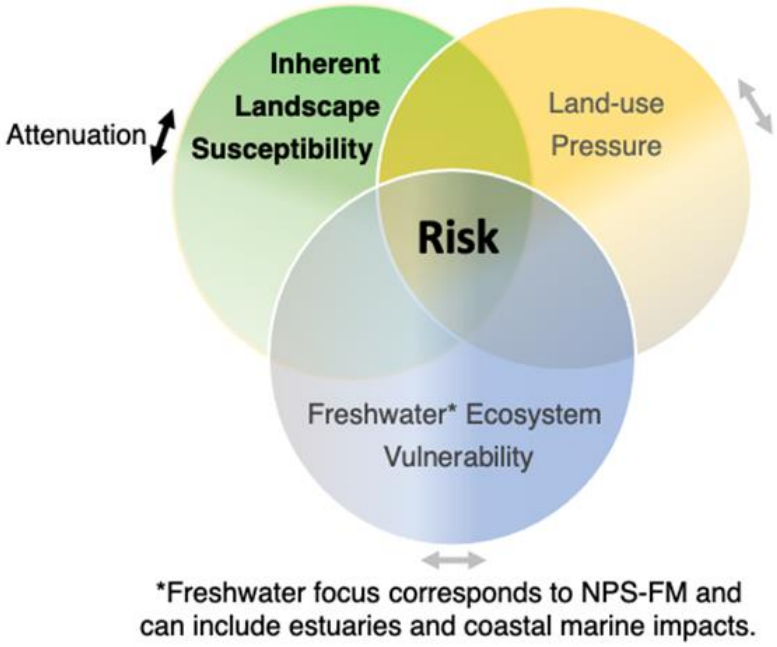

Figure 1. Contaminant risk is the intersection the inherent susceptibility of the landscape for contaminant loss, pressure from land uses, and the vulnerability of the receiving environment. Current levels of emissions and state of a freshwater ecosystem (Ecosystem vulnerability) can also drive the need for reduction. Significantly degraded environments are considered most vulnerable to receiving high contaminant loads, so significant load reductions within the catchment area are likely to be required for water quality improvements to occur.

The LWS work considers the **inherent susceptibility** of the landscape that underlies all production land uses. This spatially driven aspect has seldom been central to regional and national policy on diffuse contaminant management, however the landscape's influence on contaminant production and transport is a dominant one. Internationally, research identifies variation in the landscape as being responsible for the majority of the spatial variability in water quality, relative to land use on its own[11]. The influence of the landscape may be even greater for geologically diverse countries such as Aotearoa New Zealand.

The importance of the landscape is best explained in terms of **controlling landscape factors**. For example, a well-known controlling landscape factor is slope, which explains *some* of the general patterns in erosion and hydrology (Figure 2; Table 1). Heavy rainfall is more likely to run off across the surface in steep hill country relative to flat land, so slope is a controlling landscape factor.

Other controlling factors interact to determine a range of climatic (elevation and aspect), hydrological, microbially mediated redox reactions (e.g., denitrification), chemical and physical weathering processes.

Each controlling landscape factor controls the response of the land-to-land use, determining the particular type and severity of a water quality issue (e.g., nitrate leaching to an aquifer vs. sediment loss from a hill slope). Controlling landscape factors also influence the spatial variability of soil greenhouse gases, with some parts of the landscape consuming GHG and others producing it[12].

As Aotearoa New Zealand is geologically one of the most diverse countries in the world, it is clear that *'one size does not fit all.'* In short, landscapes are far from uniform in their susceptibility to contaminant loss because of land use activities. Diversity in our natural landscape requires that we check how suitable mitigations and land use activities are, given the environmental outcomes from the same type and intensity of land use can vary widely across relatively small scales.

Table 1 sets out a few examples of the controlling factors that influence whether nitrate will leach from a soil, or phosphorus will be mobilised by a storm event.

[11] Becker, J.C., Rodibaugh, K.J., Labay, B.J., Bonner, T.H., Zhang, Y., Nowlin, W.H., (2014). Physiographic gradients determine nutrient concentrations more than land use in a Gulf Slope (USA) river system. Freshw. Sci. 33 (3), 731–744. https://doi.org/10.1086/676635.

Hale, S.S., Paul, J.F. & Heltshe, J.F. (2004). Watershed landscape indicators of estuarine benthic condition. Estuaries, 27(2), pp.283-295.

Johnson, L., Richards, C., Host, G., Arthur, J., (1997). Landscape influences on water chemistry in Midwestern stream ecosystems. Freshw. Biol. 37 (1), 193–208. https://doi.org/10.1046/j.1365-2427.1997.d01-539.x.

King, R.S., Baker, M.E., Whigham, D.F., Weller, D.E., Jordan, T.E., Kazyak, P.F., Hurd, M.K., (2005). Spatial considerations for linking watershed land cover to ecological indicators in streams. Ecol. Appl. 15 (1), 137–153. https://doi.org/10.1890/04-0481.

Shiels, D.R. (2010). Implementing landscape indices to predict stream water quality in an agricultural setting: An assessment of the Lake and River Enhancement (LARE) protocol in the Mississinewa River watershed, East-Central Indiana. Ecological Indicators, 10(6), pp.1102-1110.

[12] Dymond, J. 2010. Soil erosion in New Zealand is a net sink of CO2. *Earth Surface Processes and Landforms*, *35*(15), 1763-1772.

Table 1. Examples of controlling landscape factors and their effect on water quality and soil greenhouse gas emission.

Controlling landscape factor	Example
Topography	Slope, aspect, and terrain ruggedness are important controlling factors. • elevation controls local climatic gradients (e.g., rainfall volume, air temp) • slope position and aspect influence soil moisture, mass wasting (e.g., slips, slides, slumps), and the likely pathway water takes from land to water.
Soil physical properties	Slope, soil drainage class, and permeability interact to determine the pathway water takes to a stream: • vertical percolation of water below the root zone is favoured where soils are permeable and well drained; lateral drainage of water is favoured where soils overlie a slowly permeable layer (e.g., a pan or poorly permeable rock unit); surface runoff is favoured where steep slopes and slowly permeable rock or soil coincide. • vertical percolation of water through the soil plays an important role in the removal of sediment, phosphorus, microbes, and both ammoniacal and organic nitrogen compounds. ○ Permeable and well drained soils are less susceptible to sediment, phosphorus, ammoniacal and organic nitrogen, microbial loss, and soil GHG generation. However, well-drained soils are susceptible to nitrate leaching losses. • Slowly permeable rock and imperfectly to poorly drained soils are more susceptible to surface runoff and the loss of sediment, phosphorus, ammoniacal and organic nitrogen, microbes to waterways. • Areas with slowly permeable and/or imperfectly to poorly drained soils are more susceptible to soil GHG generation.
Organic carbon	The abundance of organic carbon in soil and groundwater systems control phosphorus mobility and nitrate removal. • A groundwater system with high organic carbon is less susceptible to nitrate build than a groundwater system with negligible organic carbon. Organic carbon is the fuel for microbially mediated denitrification. • Soil and groundwater systems with high concentrations of organic carbon are more susceptible to phosphorus loss relative to soils with low organic carbon content.
Rock strength	Rock strength controls mass wasting (e.g., slips, slides, soil creep) and sediment generation. • Weak rocks are more susceptible to failure and associated sediment loss than strong rocks. • Weak rocks fail at lower slopes than strong rocks. • Areas of highly erodible rock tend consume more carbon dioxide than stable landforms. This is due to chemical and biogeochemical weathering processes that consume carbon dioxide.

When farming systems (land use pressure) are overlaid on this variety of landscapes, the contaminant risks vary significantly. Thus, there is no "one size fits all" approach to reducing the effect of farming and contaminant loss. The land's differential susceptibility means the type and severity of water quality and soil GHG effects will vary significantly, even if the farming activity is the same type and intensity (Figure 2).

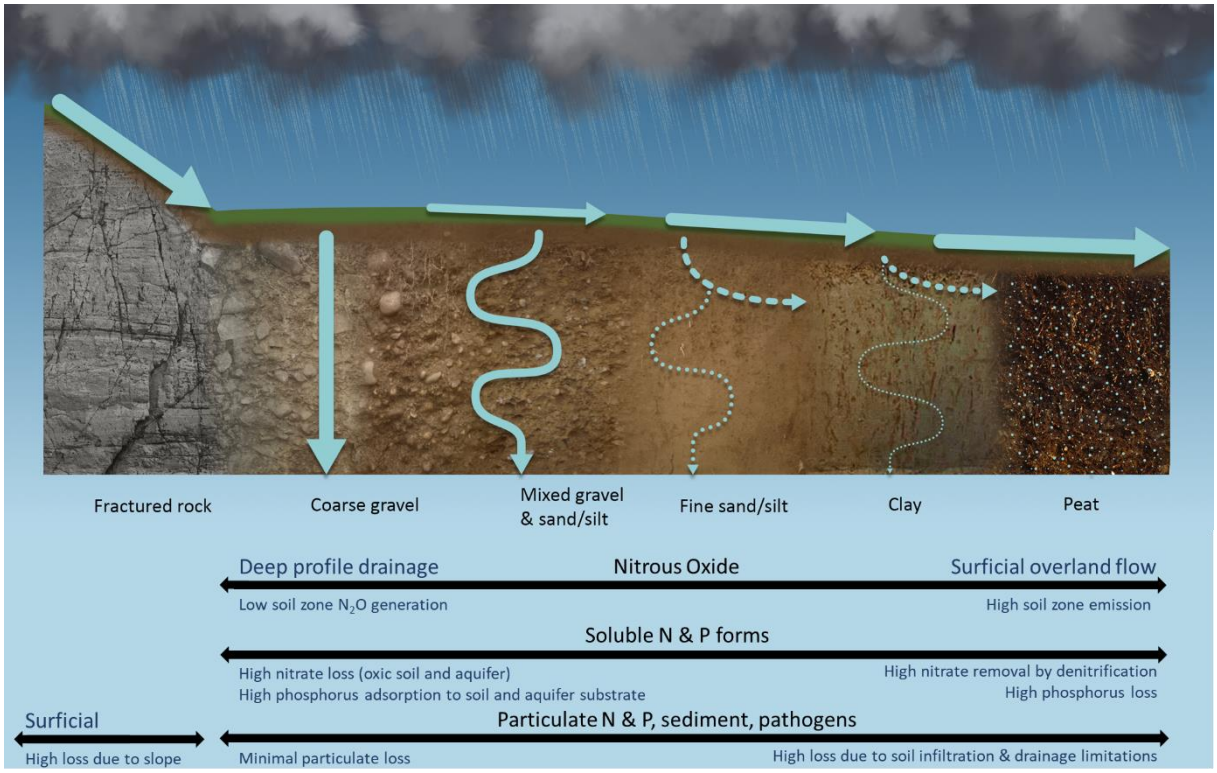

Figure 2. Relationship between controlling landscape factors and susceptibility to nitrous oxide (GHG), nitrogen, phosphorus, sediment, and pathogen loss.

Accounting for landscape susceptibility supports efficient and effective mitigation investment. Identifying the controlling landscape factors that explain significant variation in water quality provides a spatial platform from which to implement suitable management systems and tools. Therefore, understanding the main features and dynamics of our land and water systems *at a farm scale* means we can *predict how they will react* to various production land uses.

When landscape information is used in partnership with local knowledge (land user knowledge) of soil type and variability (heavier vs. lighter soils), hydrological properties (which paddocks run off, which have tiles, which are gravelly), and water quality (farm and catchment monitoring data) it provides a sound platform for developing effective farm management mitigations and for identifying where land use change is needed. Measurement data and partnership with land users supports the identification of the controlling landscape factors that are most relevant to the environmental controls they will use. An emphasis on controlling landscape factors is warranted given that environmental policy is transient, whereas the landscape that underpins production systems is enduring.

3 Project Method

A summary diagram of the method applied to develop maps of landscape susceptibility for the Wairoa and Mataura catchments is provided in Figures 3 and 4. A detailed description of the methodology is provided in Technical Appendix A. Note each region was modelled separately. This was necessary given their *fundamentally* different climatic and geological histories.

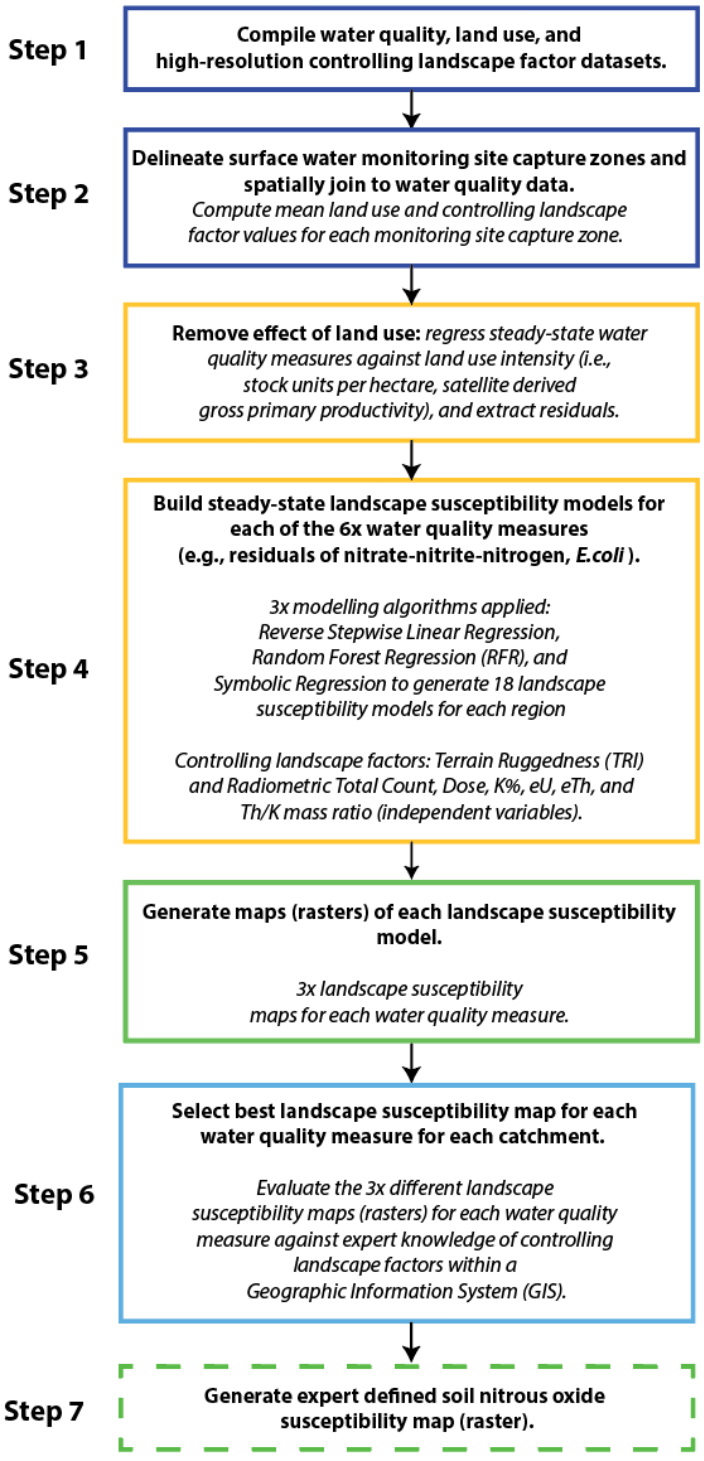

Figure 3. Summary of landscape susceptibility map generation for Wairoa and Mataura catchments.

Steps 1 and 2: Water quality data and maps of controlling landscape factors were combined:

The high-resolution controlling landscape factor datasets used are derived from direct measurement of the environment (see Technical Appendix C for an overview of the controlling factor datasets). Airborne radiometric survey and topographic survey are geophysical techniques that have long been used to provide high-resolution maps of controlling landscape factors[13].

For each region:

- Airborne LiDAR (1 x 1 m) and satellite-derived datasets (13.2 x 13.2 m) were used to build a digital elevation model (DEM).
- Airborne radiometric survey and DEM derived topographic indices were used to represent soil and geological variation at resolutions of 40 x 40 m (0.16 ha):
  - Radiometric survey provides a representation of soil texture, drainage class, organic carbon content, bulk density, and chemical composition.

[13] Beamish, D. (2013a). Gamma ray attenuation in the soils of Northern Ireland, with special reference to peat. Journal of Environmental Radioactivity, 115, 13–27. https://doi.org/10.1016/j.jenvrad.2012.05.031

Beamish, D. (2013b). Peat mapping associations of airborne radiometric survey data. Remote Sensing, 6(1), 521–539. https://doi.org/10.3390/rs6010521

Beamish, D. (2014). Peat mapping associations of airborne radiometric survey data. Remote Sensing, 6(1), 521-539.

Beamish, D. (2016). Soils and their radiometric characteristics, (2011). https://doi.org/10.3318/978-1-908996-88-6.ch19.

Killeen, P. G., C. J. Mwenifumbo, & K. L. Ford. "Tools and techniques: radiometric methods." (2015): 447-524.

Løvborg, L. (1984). The Calibration of Portable and Airborne Gamma-ray Spectrometers - Theory, Problems and Facilities. Riso Report M-2456. p. 207.

Ma, J., Lin, G., Chen, J., & Yang, L. (2010). An improved topographic wetness index considering topographic position. In 2010 18th International Conference on Geoinformatics (pp. 1-4). IEEE.

McKean, J., & Roering, J. (2004). Objective landslide detection and surface morphology mapping using high-resolution airborne laser altimetry. Geomorphology, 57(3-4), 331-351.

Pickup, G., & Marks, A. (2000). Identifying large-scale erosion and deposition processes from airborne gamma radiometrics and digital elevation models in a weathered landscape. Earth Surface Processes and Landforms: The Journal of the British Geomorphological Research Group, 25(5), 535-557.

Raduła, M.W., Szymura, T.H., & Szymura, M. (2018). Topographic wetness index explains soil moisture better than bioindication with Ellenberg's indicator values. Ecological Indicators, 85, 172-179.

Rattenbury, M.S., Cox, S.C., Edbrooke, S.W., & Martin, A.P. (2016) Integrating airborne geophysical data into new geological maps of New Zealand mineral provinces. p.37-44 IN: Christie, A.B. (ed) Mineral deposits of New Zealand: exploration and research. Carlton, Vic.: Australasian Institute of Mining and Metallurgy. Monograph series (Australasian Institute of Mining and Metallurgy) 31.

Rawlins, B. G., Lark, R. M., & Webster, R. (2007). Understanding airborne radiometric survey signals across part of eastern England. Earth Surface Processes and Landforms: The Journal of the British Geomorphological Research Group, 32(10), 1503-1515.

Rawlins, B. G., Marchant, B. P., Smyth, D., Scheib, C., Lark, R. M., & Jordan, C. (2009). Airborne radiometric survey data and a DTM as covariates for regional scale mapping of soil organic carbon across Northern Ireland. European Journal of Soil Science, 60(1), 44-54.

Read, C.F., Duncan, D.H., Ho, C.Y.C., White, M., and Vesk, P.A. (2018). Useful surrogates of soil texture for plant ecologists from airborne gamma-ray detection. Ecology and evolution, 8(4), 1974-1983.

Reinhardt, N., & Herrmann, L. (2019). Gamma-ray spectrometry as versatile tool in soil science: A critical review. Journal of Plant Nutrition and Soil Science, 182(1), 9-27.

    - Radiometric survey also reveals soil hydrological gradients (catenary gradients) associated with slope.
    - Radiometric survey is very good at discriminating the geological provenance of soil and rock.
    - Radiometric survey can be used to identify erosion prone land.
- Sentinel-2 satellite was used to build a representation of land use intensity (Gross Primary Production) at a scale of 10 x 10 m across both regions, generating both winter and summer indices for the last 3 years (see Technical Appendix B).
- The area of radiometric coverage represents 36% of Southland but >90% of the productive land. The area of radiometric survey accounts for 65%, or 3,475 km^2 of the Mataura Catchment. Northland has completed airborne, radiometric cover.
- Five-year median water quality data was compiled for the Northland (n = 69 sites) and Southland (n = 40) State of the Environment (SoE) surface water quality networks. The smaller number of sites for Southland reflect the number of sites that fall within the area of radiometric survey (e.g., radiometric survey was not flown across parts of the Waiau Catchment, the hill country east of the Mataura River, Fiordland, and other areas of conservation land).
- Controlling landscape factors and water quality datasets were spatially joined.

Step 3: Relationships, i.e., a mathematical model, between each water quality measure and land use intensity were generated:

- For each region and each water quality measure a model of the relationship between water quality and land use intensity was generated.
- The portion of spatial variation in water quality that was unexplained by land use intensity, i.e., the 'residual' error in the model, was extracted.
- Our hypothesis is that a significant proportion of the residual error in the land use models is due to controlling landscape factors.

Step 4. The residuals for each water quality measurement and high-resolution datasets of controlling landscape factors were used to derive a mathematical relationship (model).

- The relationship between the residuals of total Kjeldahl nitrogen (TKN represents the organic and ammoniacal nitrogen component of total nitrogen), nitrate-nitrite-nitrogen (NNN), particulate phosphorus (PP is the fraction of phosphorus bound to sediments), dissolved reactive phosphorus (DRP is dissolved in water), *E.coli* (a faecal indicator), total suspended sediment (the sum of sand, silt, clay, and organic matter suspended in water), and turbidity (the scattering of light through water, the more turbid the more scattering) and high-resolution controlling landscape factors were modelled.
- Three different modelling algorithms (i.e., reverse stepwise linear regression, random forest regression, and symbolic regression) were used to generate three separate models of the

relationship between the residuals of each water quality measure and controlling landscape factors. Each algorithm assesses the relative sensitivity (importance) of each controlling landscape factor for each water quality measure, discarding any that do not explain the pattern of variation.

Step 5. The mathematical relationship between water quality residuals and controlling landscape factors was used to build a visual representation ('map') of landscape susceptibility to contaminant loss:

- The models generated in Step 4 were used to build visual-spatial representations ('maps') of the susceptibility of the landscape to total Kjeldahl nitrogen, nitrate-nitrite-nitrogen, particulate phosphorus, dissolved reactive phosphorus, *E.coli*, and sediment[14] for the Wairoa and Mataura catchments. Each model was applied at a pixel-by-pixel level.
- 3x maps (rasters) of landscape susceptibility were generated for each water quality measure. A total of 21 and 18 maps were generated for the Wairoa and Mataura catchments, respectively[15].

Step 6. The maps of landscape susceptibility to organic and ammoniacal nitrogen, particulate phosphorus, dissolved reactive phosphorus, *E.coli*[16], and sediment loss were evaluated against existing models and datasets of water quality controls:

- Expert knowledge of regional topographic, hydrological, soil, and geological controlling factors were used to guide the selection of the best 'map' of the 3x landscape susceptibility maps for each water quality measure.
- Symbolic regression generated the best landscape susceptibility models. It used the Nash-Sutcliffe efficiency criterion as the model search metric. Specifically, symbolic regression appears to be sensitive to multiple different landscape factors that control susceptibility (e.g., dissolved reactive phosphorus susceptibility may be associated with phosphorus rich volcanic rocks, peat wetlands, and coal measures). Reverse stepwise linear regression and random forest regression appear to identify only the main or dominant controlling landscape factor and appeared relatively insensitive to secondary or tertiary controlling factors. Symbolic regression models are also 'white box' models making them more interpretable, which is valuable when seeking to understand 'how' and 'why' variation in landscape susceptibility occurs.

Step 7. A map of landscape susceptibility to soil nitrous oxide emission (N_2O) was generated using the nitrate-nitrite-susceptibility maps and climate data for the Wairoa and Mataura catchments:

- The inverse of the nitrate-nitrite-nitrogen susceptibility map was used to generate a soil zone nitrous oxide susceptibility map.

[14] For the Mataura Catchment, a lack of total suspended sediment (TSS) measures necessitated the use of turbidity as a proxy.

[16] As a proxy for pathogens

- The inverse of nitrate-nitrite-nitrogen susceptibility represents the physical and biogeochemical factors that control soil nitrous oxide generation in the soil.

In addition to soil and geological factors, the Wairoa and Mataura catchments were subdivided into climatic zones according to the controlling factors air temperature and effective precipitation[17]. Warm, moist climate zones are more susceptible to soil nitrous oxide generation than cold, dry climate zones.

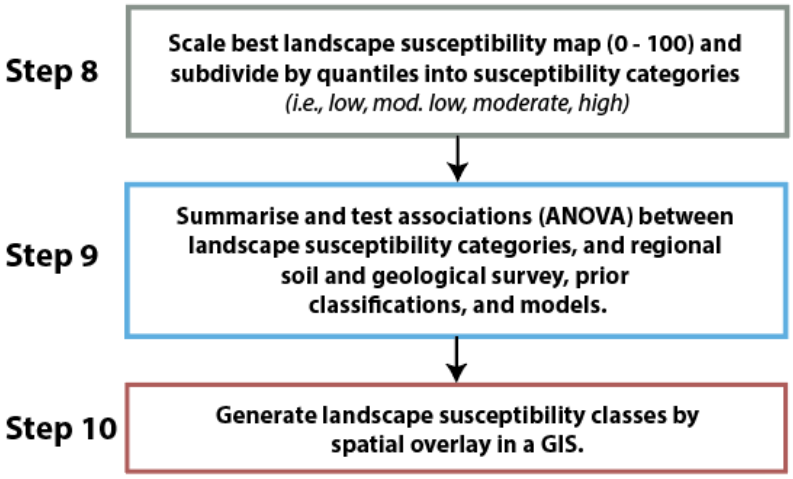

Figure 4. Evaluation and testing of landscape susceptibility maps and generation of an overall landscape susceptibility classification.

Step 8. The best landscape susceptibility maps were scaled from 0 – 100 i.e., from low to high susceptibility, and then subdivided into four categories: low, mod. low, moderate, and high landscape susceptibility.

- The best landscape susceptibility map, from the 3x different algorithms were scaled and a 5 and 95% confidence interval applied.
- The maps were classed by quantiles which subdivided them into four categories: low, mod. low, moderate, and high landscape susceptibility.
- The thresholds in landscape susceptibility were different between the Wairoa and Mataura catchments, reflecting different climatic and geological histories, and associated water quality issues.
- The thresholds were consistent with the dominant water quality issues within each respective catchment.

Step 9. We tested the hypothesis that landscape susceptibility categories are associated with predictable combinations of controlling landscape factors (Technical Appendix E):

- The association between susceptibility classes for each water quality measure and soil nitrous oxide was assessed statistically (Welch's ANOVA and Game-Howell non-parametric post hoc tests) against historic topographic (National 8 m DEM), soil (S-Map/FSL), geological

[17] Effective Precipitation (EP) is the amount of precipitation that is actually added and stored in the soil.

(Q-Map), and water quality classifications (Physiographic Environments of New Zealand, (PENZ)).

- Welch's ANOVA tests were all statistically significant at $\alpha = 0.05$. Post hoc significance tests assess the statistical difference between susceptibility categories and controlling landscape factors.
- Post hoc tests reveal predictable and statistically significant relationships between controlling landscape factors (i.e., Q-Map geological survey, Physiographic Environments of New Zealand and to varying degrees S-Map and FSL) and landscape susceptibility categories.
- Ground truthing activities and local knowledge suggest significant areas of the Mataura Catchment are incorrectly represented by historic soil maps and that soils' effective properties have changed in response to extensive artificial subsurface drainage following the recent dairy boom (c. 2000 – 2018)[18]. More work is required to test the relationship between susceptibility maps and historic soil maps, where there is misalignment. Some of this work is currently being undertaken in partnership with rural catchment groups across Southland.
- Any assessment of controlling landscape factors requires expert knowledge of the *role* of controlling landscape factors and includes consideration of geology, soils, biogeochemistry, hydrogeology, and petrochemistry. Traditional knowledge sets that have been focused on land use only, soils only, hydrology only, agricultural sciences only, do not provide relevant insight.

Step 10. Overall (dominant) landscape susceptibility typologies were generated by overlaying each susceptibility map.

- Following association testing (Step 9), an overall susceptibility class was generated by computing the quantile susceptibility class for each water quality contaminant and soil zone nitrous oxide at a pixel-by-pixel level. This involved stacking each quantile susceptibility raster in the following order to create a unique code (barcode): N_2O-NNN-OAMN-PP-DRP-TURB-*E.coli* [19]. For example, a barcode of 4134321 indicates the following order of susceptibility: N_2O = 4 (High); NNN = 1 (Low); OAMN = 3 (Moderate); PP = 4 (High); DRP = 3 (Moderate); Turbidity = 2 (Moderately low); *E.coli* = 1 (Low). A barcode of 1111111 for a pixel in the integrated classification indicates all susceptibility scores are in the low quantile for the respective catchment.
- The barcode was subsequently converted from a raster layer to a vector polygon to support the multiple fields of the integrated classification. Risk typologies for nitrogen species (including nitrous oxide), phosphorus species, sediment and pathogens were generated by selecting those contaminants with a score of 5 to identify the highest risk contaminants in each polygon (Figures 10 and 11). This layer allows the user to identify and symbolise risk for a single contaminant, or high-risk areas with contaminant species and form. The combined

[18] Artificial drainage of an imperfectly to poorly drained soil enhances drainage and as a result aeration status, and redox potential. Consequently, artificially drained soils are associated with lower denitrification rates than unmodified soils. See: Dowding, P. (1981). The effects of artificial drainage on nitrogen cycle processes. Ecological Bulletins, 615-625.

[19] N_2O = nitrous oxide; OAMN = organic and ammoniacal nitrogen, NNN = nitrate-nitrite nitrogen.

layers were then used to assign landscape susceptibility type. Table 3 provides a breakdown of the area of the 'high' susceptibility categories for the Wairoa and Mataura catchments.

- As an alternative, the end-user could use an equal interval approach to assigning a susceptibility typology and may also choose to vary the number of classes. An overall landscape susceptibility type was generated at a pixel-by-pixel level for nitrogen, phosphorus, sediment and pathogens for the Wairoa and Mataura catchments.
- A susceptibility typology representing the upper quantile, i.e., 'high' was used to assign landscape susceptibility type.

4 Outputs

4.1 Landscape Susceptibility Maps

The landscape susceptibility maps for the Wairoa and the Mataura catchments are provided below (Figure 5 and 6). Each susceptibility layer and the overall susceptibility typologies were provided to the PCE as a GIS package. The soil nitrous oxide susceptibility component is designed to be used in combination with the climate zone classification (Appendix A, Step 7).

Each susceptibility map represents the landscape susceptibility as a range between 0 – 100 or "low to high susceptibility." This scale is subsequently subdivided into four quantiles that distribute pixels into categories that contain an equal number of values. Accordingly, the threshold values identified for each susceptibility layer are area-based (Table 2). Using quantiles to distribute pixels into categories provides a relative sense of susceptibility. However, the susceptibility maps can be subdivided according to equal intervals or other by the end user.

The susceptibility layers do not provide a quantitative assessment of likely loss associated with a land use activity, nor do they account for any possible mitigation of landscape susceptibility. Furthermore, the landscape susceptibility maps generated here do not consider the current state of surface waters, groundwaters, or terminal receiving environment (e.g., estuary). Rather, they seek to provide insight into the probable susceptibility of the landscape to contaminant loss and emission, independent of land use.

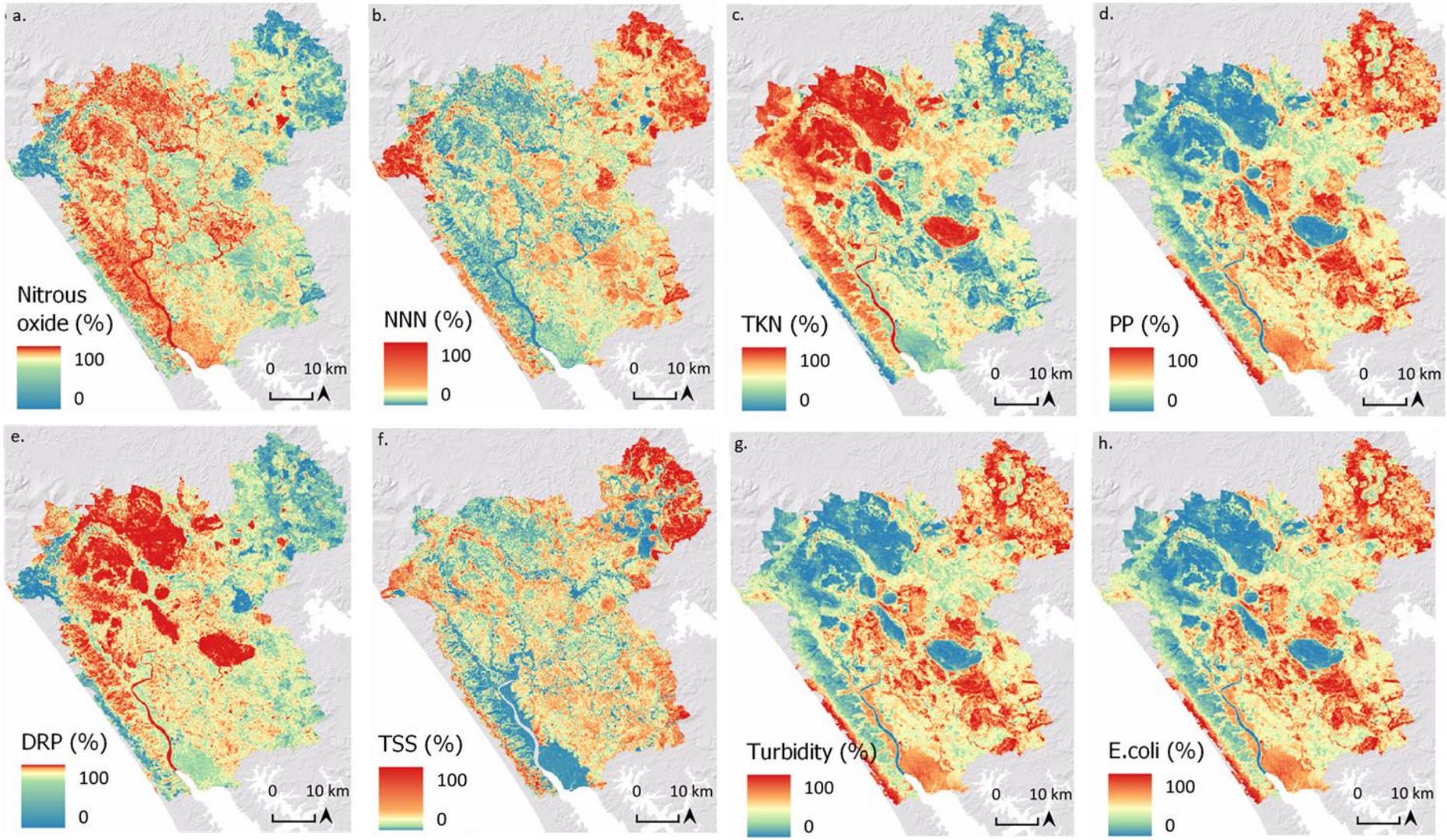

Figure 5. Preferred landscape susceptibility models for the Wairoa Catchment, Northland. NNN = nitrate-nitrite-nitrogen, TKN = total Kjeldahl nitrogen (organic and ammoniacal nitrogen); PP = particulate phosphorus; DRP = dissolved reactive phosphorus; TSS = total suspended sediment; E.coli = indicator for pathogens.

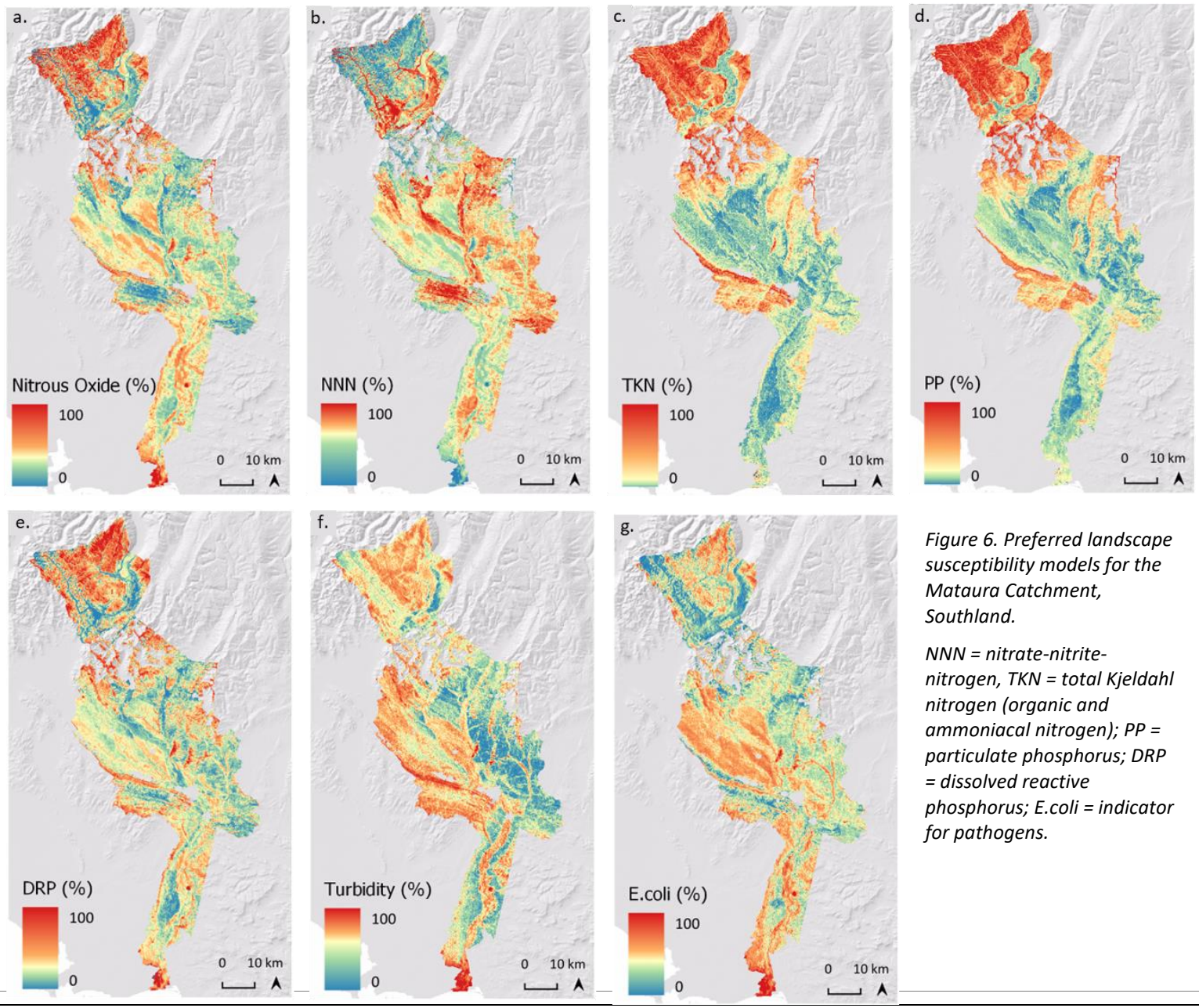

Figure 6. Preferred landscape susceptibility models for the Mataura Catchment, Southland.

NNN = nitrate-nitrite-nitrogen, TKN = total Kjeldahl nitrogen (organic and ammoniacal nitrogen); PP = particulate phosphorus; DRP = dissolved reactive phosphorus; E.coli = indicator for pathogens.

4.2 Landscape Controls over Susceptibility

Examples of landscape susceptibility, as a series of transects, across parts of the Mataura and Wairoa catchments are presented in Figures 7 to 9. The transects demonstrate distinct patterns that relate to existing knowledge of landscape-related controls on water quality and soil nitrous oxide. For example, the transect across the Edendale Terrace and the Mataura River and its floodplains display the susceptibilty of the landscape to nitrate-nitrite-nitrogen loss (Figure 7).

Nitrate-nitrite-nitorgen susceptibility varies with soil drainage class, peaking across the well drained soils of the loess-mantled alluvial gravel aquifer of the Edendale Terrace and the uplifted (Q10) and loess-mantled alluvial terraces that flank the eastern margin of the Mataura Valley. Nitrate-nitrite susceptibility declines sharply at the eastern edge of the Edendale Terrace across an area of peat wetland, before rebounding across the modern-day floodplain of the Mataura River. Susceptibility then decreases towards zero across the large peat wetland in the vicinity of the Mimihau Stream.

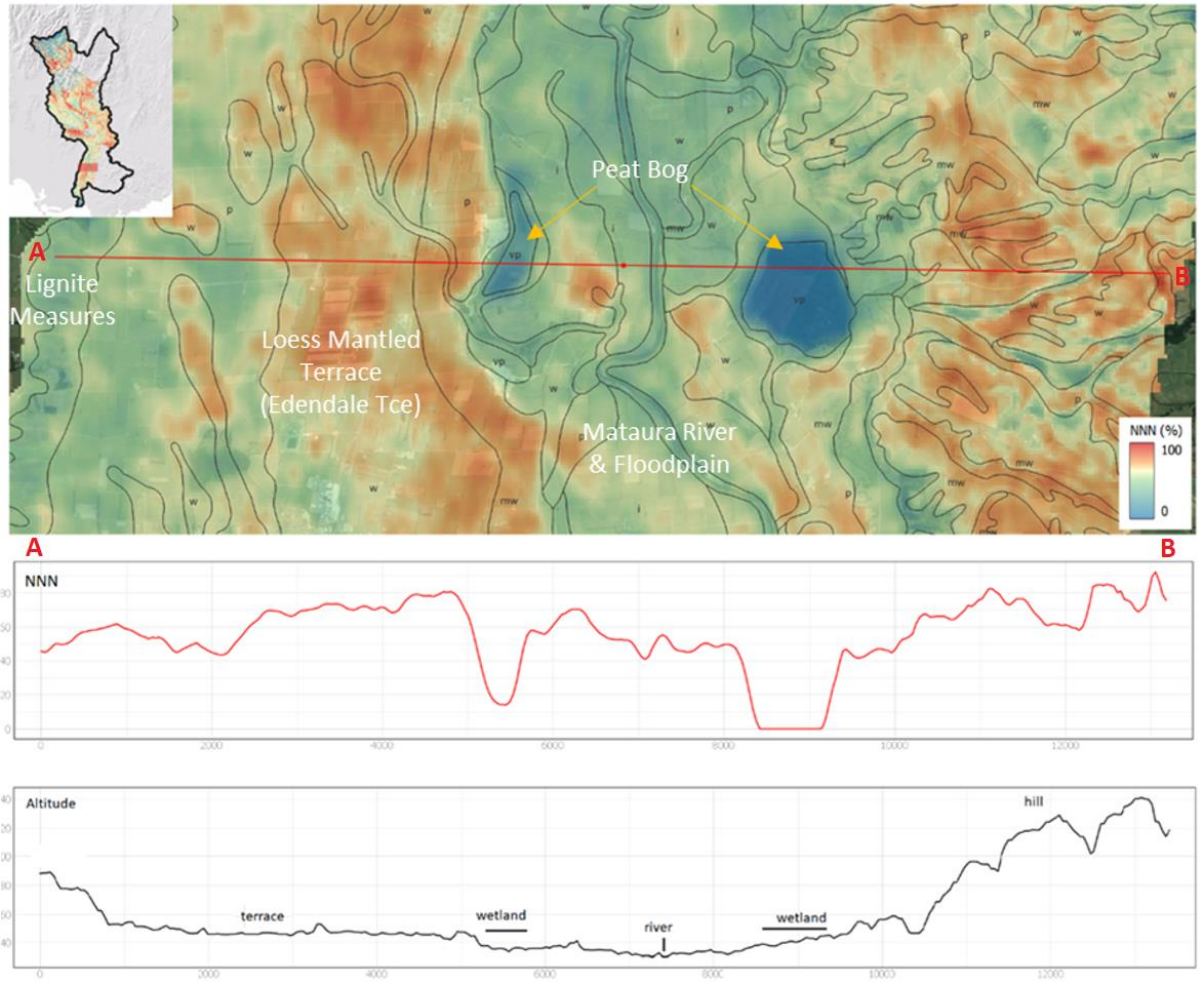

Figure 7. The susceptibility of nitrate-nitrite-nitrogen (NNN) and particulate phosphorus (PP), Edendale area, Mataura Catchment. Black outlines are soil polygons (1:50,000) and drainage class (w = well drained, mw = moderately well drained; i= imperfectly drained; p = poorly drained, and; vp = very poorly drained). Note NNN susceptibility peaks across the well-drained soils of the Edendale Terrace, reaching lowest values across peat bogs, before increasing across the uplifted and loess mantled alluvial terraces of the Mataura Valley. Note PP peaks in association with peat bogs where runoff risk and phosphorus abundance also peak.

A transect across an area of the Wairoa Catchment displays the landscape susceptibility to dissolved reactive phosphorus and sediment (Figure 8). The susceptibility peaks across the Tangihua Range.

Petrochemical analysis of the Tangihua Complex basalts reports P concentrations as high as 6,000 ppm, with typical range of 1,000 – 2,000 ppm (as P_2O_5)[20,21]. Conceptually, weathering of P-rich basalts exposes easily weathered P bearing minerals to dissolution. Dissolved reactive phosphorus susceptibility falls across the well-drained soils of the Whatitiri Maunga[22] which are petrochemically distinct from those associated with the Tangihua Range, with high P-retention and oxidising conditions that favour the retention of P within the soil. Erosion of these soils favours particulate phosphorus loss.

The susceptibility to sediment loss also varies as a function of geology, peaking across the weak (incompetent) sand and mudstones of the Mangakahia Complex. Conceptually, these rocks fail at lower slopes than the strong (competent) rocks of the Tangihua Complex. Sediment susceptibility is also elevated, albeit to a lesser degree than allochthonous sand and mudstones, across the friable clay loam textured soils of the Whatitiri Maunga, which are prone to infiltration excess overland flow and erosion[23]. In these examples, geology is the 1st order control over sediment loss, with soil type and slope playing a secondary role. This finding is consistent with contemporary research into the relative roles of land cover, slope, climate, and geology over chemical load, mass wasting and sediment supply[24].

[20] The USGS notes: Phosphorus is an important element in soil because it is indispensable for biochemical activity in living cells. The average P concentration in the Earth's upper continental crust is approximately 655 milligrams per kilogram (mg/kg). Phosphorus is somewhat enriched in mafic and felsic rocks with an average concentration of about 1,200 mg/kg in mafic rocks, such as basalt, and 750 mg/kg in felsic rocks, such as granite and rhyolite. Phosphorus concentrations in shale average about 800 mg/kg. Limestone (350 mg/kg) and sandstone (30 mg/kg) contain, on average, less P than the other common rock types. Briefly, soil apatite dissolves slowly, and when a soluble phosphate ion (HPO_4^{2-}) is released, it can be immobilized by absorbing to plant roots or by being fixed as iron (Fe) and aluminium (Al) phosphates. Plants can take up HPO_4^{2-}, but they are unable to take up more insoluble forms of P. Phosphate fertilizer is widely applied to many agricultural fields to alleviate soluble P deficiencies. Thus, the distribution of P in soils across the conterminous United States is dependent on the original P concentration of the soil parent material, P transformations and movement during soil formation (weathering and leaching), and certain human activities.

[21]Briggs, R. M. and Searle, E. J. (1975). Tangihua volcanics in the Opouteke—Pakotai area, Northland, New Zealand, New Zealand Journal of Geology and Geophysics, 18:2, 327-341, DOI: 10.1080/00288306.1975.10418203

Nicholson KN, Black PM, Picard C 2000. Geochemistry and tectonic significance of the Tangihua Ophiolite Complex, New Zealand. Tectonophysics 321: 1-15.

[22]More work is required to confirm this response pattern, a query of the GNS Science Pet lab geochemical database would be a useful start.

[23]Northland Regional Soils factsheet notes: These soils are friable and granular (nutty) on top (horizon A) with an accumulation of clay at depth. They have a clay texture, but have only low plasticity, making them 'brittle' and easily destroyed by over-cultivation or compaction when dry. Topsoils can become a fine powdery surface layer known as a 'dust mulch' that seals the surface, repelling water and increasing runoff.

[24]Fratkin, M. M., Segura, C., & Bywater-Reyes, S. (2020). The influence of lithology on channel geometry and bed sediment organization in mountainous hillslope-coupled streams. Earth Surface Processes and Landforms, 45(10), 2365-2379.

Fratkin, M. M. (2018). The Influence of Lithology on the Alluvial Character of Oregon Coast Range Streams.

Mueller, E. R., & Pitlick, J. (2005). Morphologically based model of bed load transport capacity in a headwater stream. Journal of Geophysical Research: Earth Surface, 110(F2).

Porder, S., & Ramachandran, S. (2013). The phosphorus concentration of common rocks—a potential driver of ecosystem P status. Plant and soil, 367(1), 41-55.

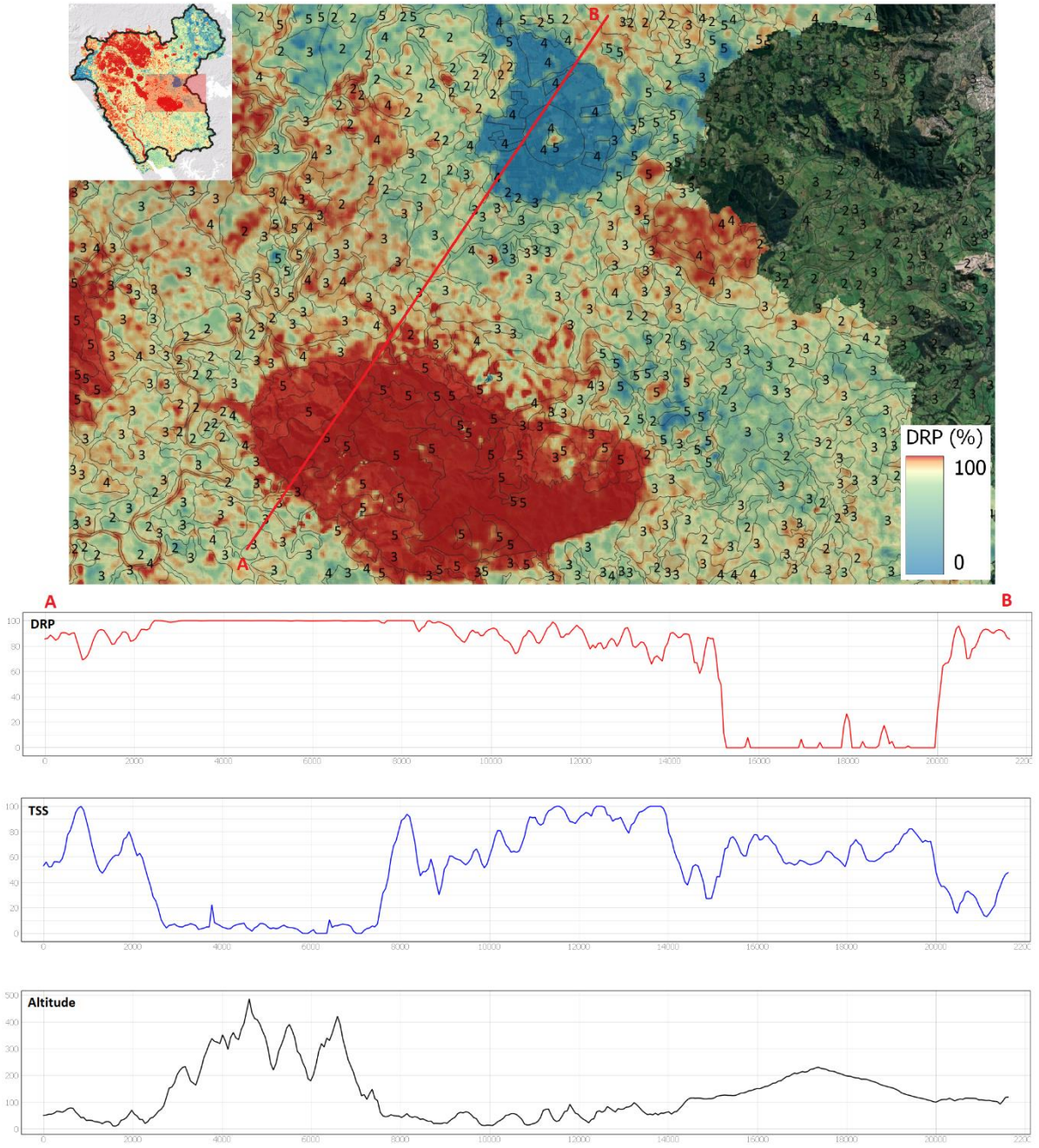

Figure 8. The susceptibility of dissolved reactive phosphorus (DRP), and sediment (TSS), Wairoa Catchment. Black outlines are FSL soil polygons. Note DRP susceptibility peaks across the steep Tangihua Volcanics which contain naturally elevated concentrations of inorganic phosphorus due to their origin as alkali- mid ocean ride basalts. The DRP susceptibility is lowest across the gentle slopes of Whatitiri (Kerikeri Volcanics) volcano which is characterised by well drained volcanic soils with high P-retention. Nitrate-nitrite-nitrogen (not shown) susceptibility also peaks across Whatitiri. Sediment peaks across the weak sedimentary sand and mudstones of the Northland Allochthon, especially the highly incompetent Punakitere sand- and mudstone.

Finally, a transect across the Balfour area of the Waimea Valley, sub catchment of the Mataura River, Southland provides a representation of the landscape susceptibility to soil nitrous oxide emission (Figure 9). Here nitrous oxide susceptibility peaks across the poorly drained, fine textured and slowly permeable soils and reaches lowest values across the well-drained and moderately

permeable Crookston soils in the middle of the transect. Crookston soils are associated with elevated nitrate-nitrite susceptibility and in this location overlie a strongly oxidising aquifer system that hosts some of the highest groundwater nitrate-nitrite-nitrogen concentrations in Southland. An intensive ground truthing programme is underway across this area of the Mataura Catchment to better resolve controlling factors at scales of relevance to land users.

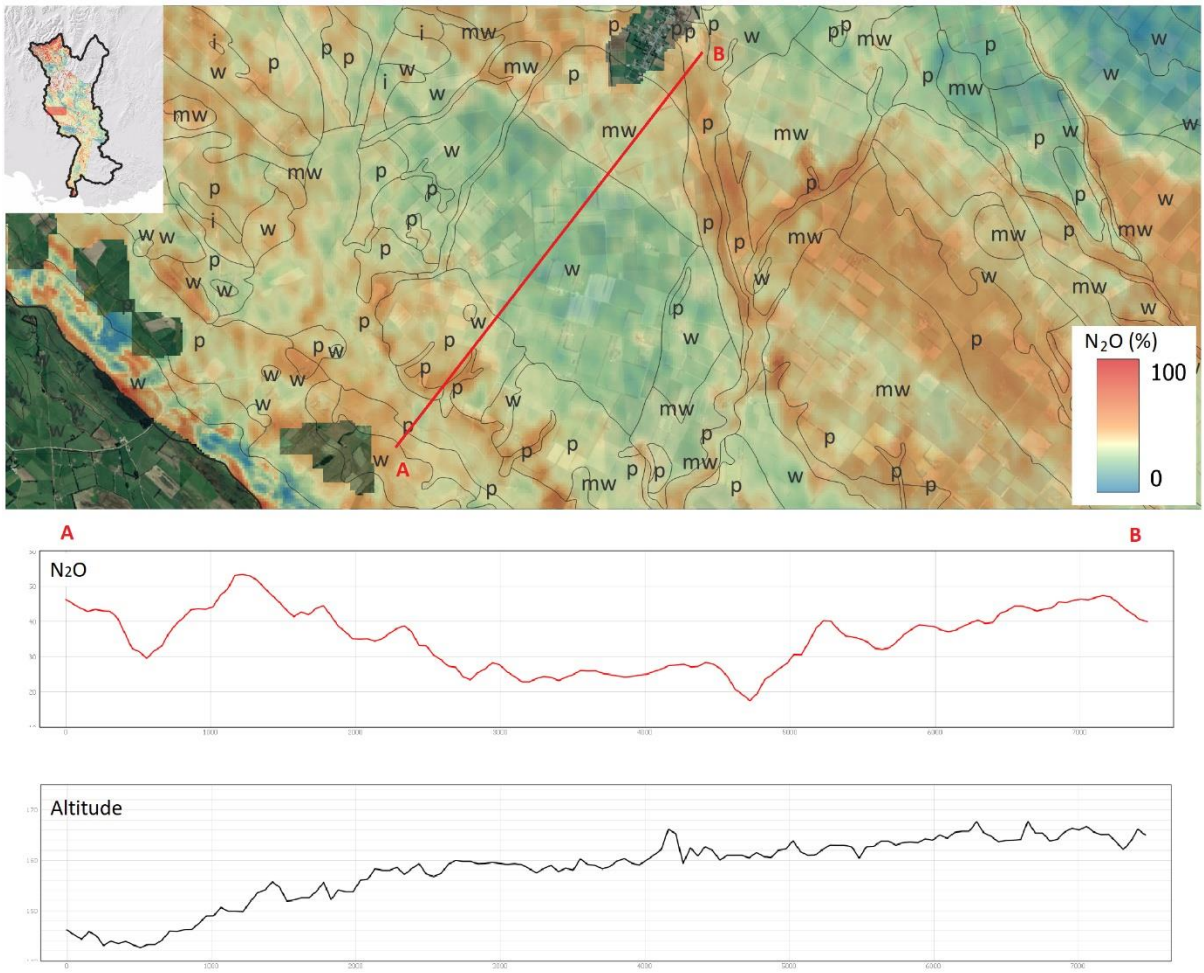

Figure 9. Soil nitrous oxide susceptibility transect across the Balfour alluvial fan area, Waimea Valley, Mataura Catchment. Note soil N_2O susceptibility reaches a minimum as soils transition from poorly drained to well drained across the Balfour groundwater nitrate-nitrite hotspot. Black polygons are soil polygons (1:50,000): w = well drained; mw = moderately well drained; i = imperfectly drained; p = poorly drained. The Balfour and Waimea Plains area falls within the cool dry lowland climate category.

4.3 Combined Susceptibility Typologies

The combined susceptibility typologies support the concept of differential landscape susceptibility (Figures 10 and 11[25]; Tables 2 and 3). They also support the message that resolving multi-contaminant issues requires a holistic understanding of the landscape factors controlling all contaminant processes.

[25] Areas of moderate susceptibility have not been included in the typological maps presented in Figures 10 and 11.

Table 2 provides a summary of the thresholds in landscape susceptibility for the Wairoa and Mataura catchments. Step 8 in Technical Appendix A discusses the association between controlling landscape factors (e.g., geology and soils) and susceptibility typologies for the Wairoa and Mataura catchments, and step 9 describes the results of spatial association testing. Briefly, the patterns of high susceptibility for each catchment corresponds strongly to recognised controlling landscape factors. For example, the higher susceptibility to sediment loss across the Wairoa is consistent with the large area of weak (incompetent) sedimentary sand and mudstones. Table 3 provides a summary of the area of 'high' landscape susceptibility for each catchment.

Table 2. Threshold values for the Wairoa and the Mataura susceptibility models.

	25% threshold	50% threshold	75% threshold	Mean
Wairoa				
N_2O	66.4	80.6	90.1	74.3
NNN	9.9	19.4	33.6	25.7
TKN	34.9	54.2	75.0	54.4
PP	24.8	45.7	65.0	45.5
DRP	74.8	87.3	95.3	80.0
TSS	67.5	81.5	92.7	76.0
Turbidity	24.9	45.9	65.2	45.6
E.coli	24.8	45.7	65.0	45.4
Mataura				
N_2O	25.0	36.3	49.0	38.9
NNN	51.0	63.7	75.0	61.1
TKN	3.2	9.9	38.7	23.8
PP	9.2	18.1	47.5	30.2
DRP	17.4	27.7	42.1	32.2
Turbidity	41.0	60.2	71.2	54.7
E.coli	30.1	42.7	55.2	42.2

Where each thresholds denotes the upper threshold by percent of pixels. N.B. it does not take a lot of E.coli to exceed water quality guidelines.

As Aotearoa New Zealand is geologically one of the most diverse countries in the world, it is clear that *'one size does not fit all.'* In short, landscapes are far from uniform in their susceptibility to contaminant loss. Diversity in our natural landscape requires that we check how suitable mitigations and land use activities are, given the environmental outcomes from the same type and intensity of land use can vary widely across relatively small scales.

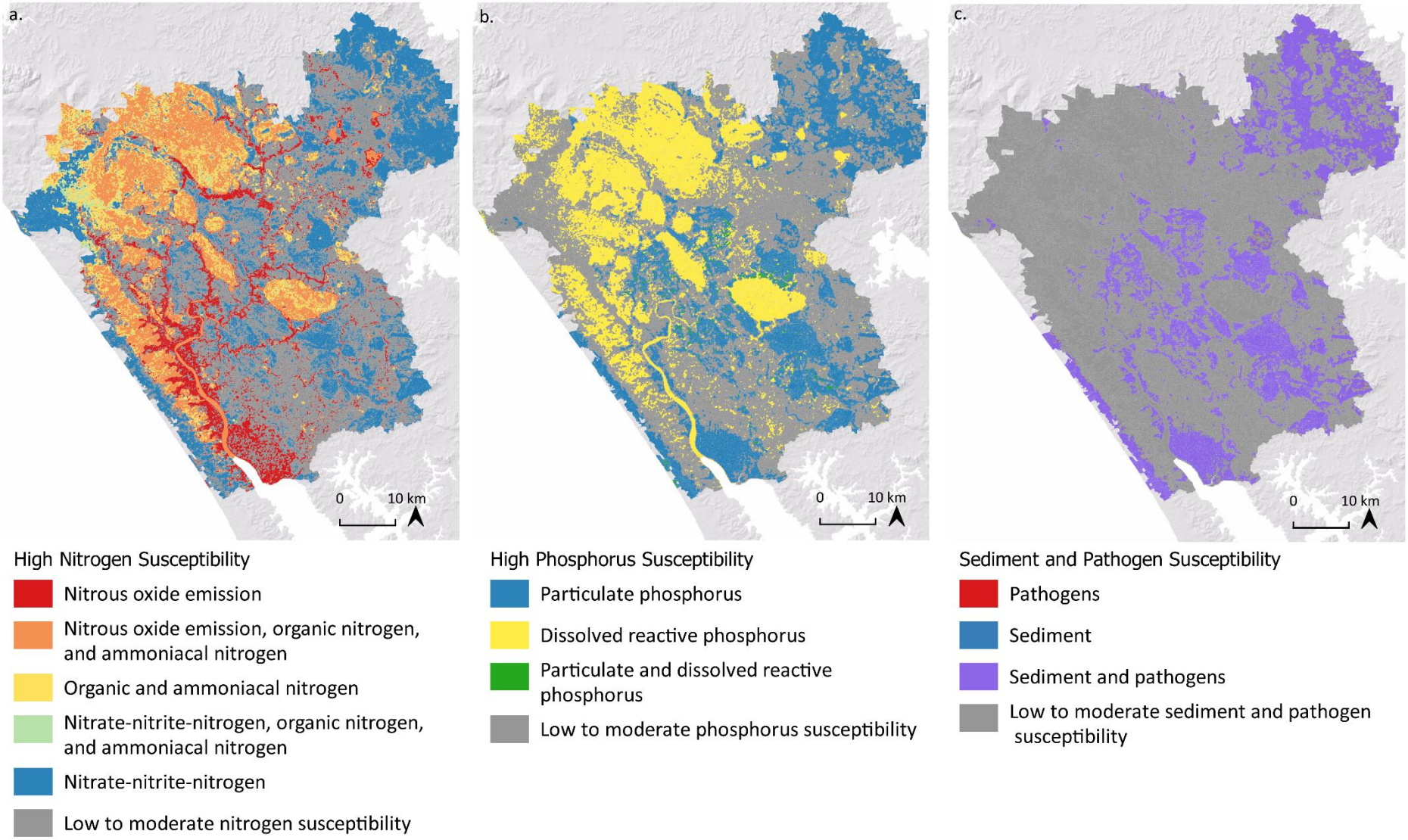

Figure 10. High susceptibility for nitrogen and phosphorus species, sediment, and pathogen loss across the Wairoa Catchment, Northland.

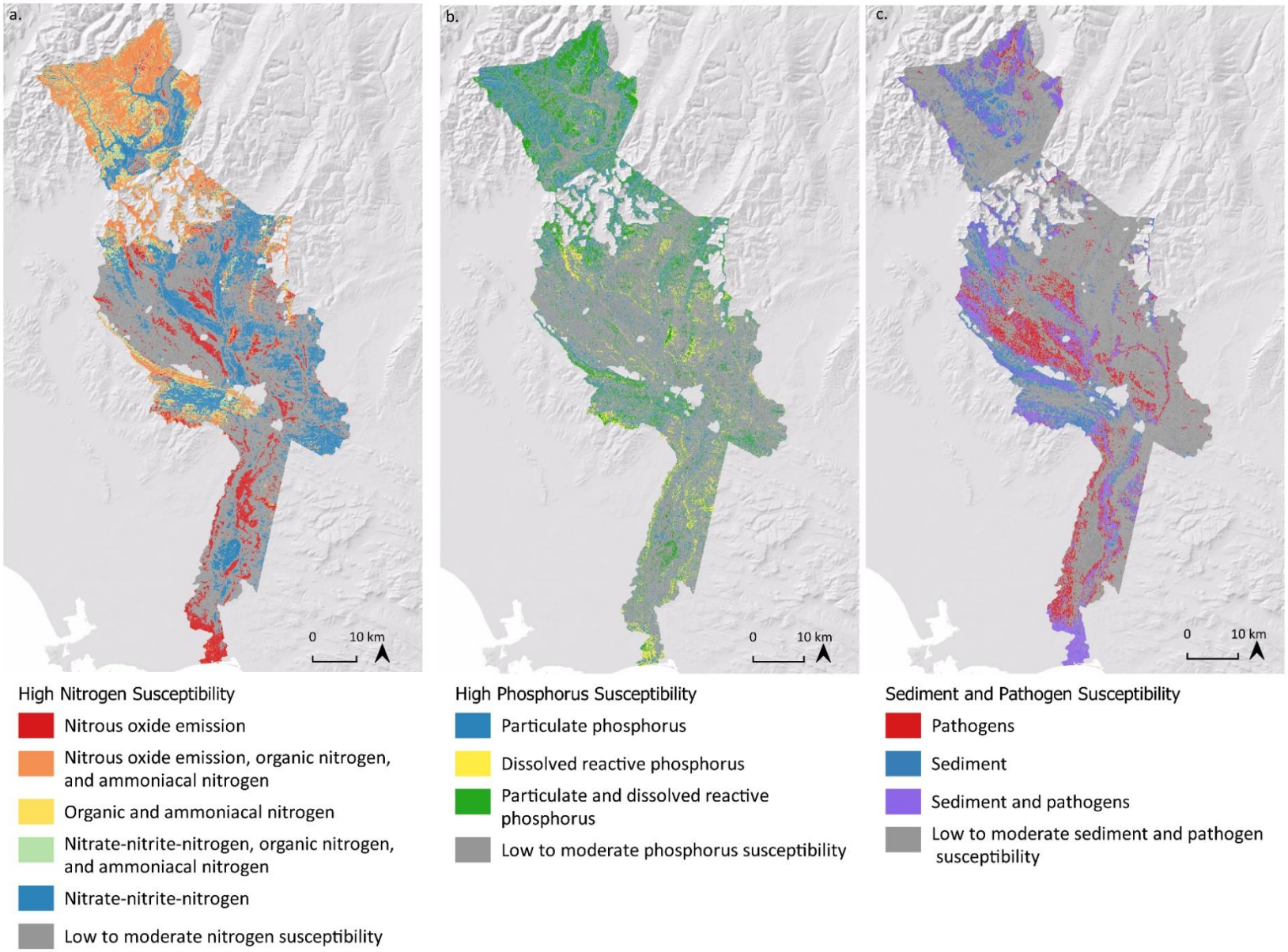

Figure 11. High susceptibility for nitrogen and phosphorus species, sediment, and pathogen loss across the extent of radiometric survey, Mataura Catchment, Southland.

Table 3. Area (ha) of 'high' landscape susceptibility for Wairoa and Mataura catchments.

	Wairoa		Mataura	
	Area (Ha)	Percent (%)	Area (Ha)	Percent (%)
Nitrogen susceptibility				
High N_2O emission	39,474	10.1	31,408	9.1
High N_2O emission and OAMN	58,619	14.9	54,460	15.8
High OAMN	34,892	8.9	22,932	6.7
High NNN and OAMN	4,584	1.2	8,565	2.5
High NNN	93,501	23.8	77,622	22.5
Low to moderate N susceptibility (all forms)	161,283	41.1	149,444	43.4
Phosphorus susceptibility				
Particulate	95,685	24.4	64,067	18.6
Dissolved	95,688	24.4	18,321	5.3
Particulate and dissolved	2,405	0.6	68,922	20.0
Low to moderate P susceptibility (all forms)	198,574	50.6	193,122	56.1
Sediment and Pathogen Susceptibility				
Sediment	460	0.1	35,309	10.3
Pathogens	502	0.1	35,995	10.5
Sediment and pathogens	97,624	24.9	50,778	14.7
Low to moderate sediment and pathogens	293,765	74.9	222,349	64.6

5 Project Commentary and Reflections

International research notes that the landscape may be responsible for a dominant component of the spatial variation in water quality and soil GHG than the direct effect of land use on its own. In a geologically diverse country such as Aotearoa New Zealand, the influence of the landscape may be even more pronounced on the type and severity of water quality and soil GHG emissions. The inherent susceptibility of any landscape means that contaminant risk from land use alters across that landscape even when land use itself remains the same.

In this project, we explored the potential for high-resolution datasets to provide property scale maps of the inherent susceptibility of the landscape, to support a spatially based approach to land use change.

Each map and the overall susceptibility classification generated are independent of land use. It identifies only the landscape derived component that determines water quality contaminant loss and soil nitrous oxide emissions. The controlling landscape factors and dominant processes can be identified at quite fine scale and the resulting susceptibility to the release of various contaminants can be illustrated on maps, as gradations of susceptibility, from very high to very low susceptibility.

It is not yet possible to turn the risk of those effects into numeric datasets, mainly as the approach does not seek to estimate likely yields. However, landscape susceptibility maps may support more realistic estimates of losses when used in combination with a robust, paddock-scale contaminant loss modelling tool. Unfortunately, the current ability of models to reliably simulate quantitative losses at property scales is inherently limited. This is in part due to the coarse scale (1:50,000) of historic soil maps, the inherent complexity of natural processes, and the complexity of land use systems. Furthermore, loss rates from plot trials are insufficient to confidently supply accurate attribution across the majority of New Zealand's landscape, as they tend to be associated with a one-dimensional set of controlling landscape factor settings e.g., well drained soils only, flat land only, a handful of geological settings, and topographic ranges. Thus, extrapolating these studies to

estimate likely loss rates to areas characterised by different sets of controlling landscape factors is unlikely to generate realistic estimates, with the real risk of recommending mitigations or actions that are not relevant. The chances of misalignment are high with real consequences for individual land users who are seeking to operationalise meaningful change at scales finer than existing national scale topographic datasets, soil and geological survey.

Recent innovations in sensor technology and telemetry means that real-time data that helps identify the cause - effect relationship is improving. However, there is still some way to go yet before a narrative expression of the landscape susceptibility could be confidently replaced by a numeric one. The "narrative" approach that uses colour for 'heat maps,' provides useful information for land users to make changes to land management practices that will reduce contaminant discharges.

In terms of the generation of landscape susceptibility maps, some of the most important limitations include:

- The sparsity of regional monitoring networks relative to the scale of variation in controlling factors revealed by LiDAR and radiometric survey.
    - Regional water quality monitoring networks can only provide a gross spatial average of landscape influence.
- Network location (bottom of catchments, with a complex range of activities occurring upstream of the sampling site).
    - More monitoring sites, designed to capture spatial variation in controlling landscape factors are needed.
- Monitoring frequency (1/month spot sample).
    - The present outputs represent a steady-state or long-term average when it is often event-driven export of contaminants that dominate load. Greater sampling frequency is needed, so that periods of peak contaminant export from the land to water are not missed.

Although experimental, the method applied here supports the use of high-resolution data sets such as airborne LiDAR and airborne radiometric survey (at 0.16 ha) to depict the landscape factors that control the susceptibility of the landscape. The value of airborne geophysical datasets as high-resolution surrogates of controlling landscape factors is well-established internationally[9]. This project also demonstrates that it is possible to classify landscape to show comparative susceptibility to a scale that supports effective mitigation actions. However, across Aotearoa New Zealand, the ability to allocate loads and associated yields at catchment scales is highly uncertain[26]. By extension, the ability to estimate losses at property scales is even more uncertain.

Ideally, any attempt to more accurately depict controlling landscape factors so that they can be used to support land user decision making would be combined with property scale ground truthing[27]. A dedicated project employing a grassroots approach to ground truthing of controlling landscape

[26] Snelder, T., Rajanayaka, C., & Fraser, C. (2014). Contaminant load calculator. Envirolink project: "Many studies have found that loads estimated from "infrequent" sampling are highly uncertain. For example, Defew et al. (2013) found phosphorus loads estimated from two weekly sampling could have errors of more than 300% compared to the true loads. In another study Johnes (2007) found loads of total phosphorus estimated from monthly data could have errors in the order of 200 to 500%. Unsurprisingly, these studies found that uncertainties decrease with increased sampling frequency and longer sampling period duration."

[27] Property scale ground-truthing was out of scope.

factors is being supported by an AgMARDT grant across the Mataura Catchment[28]. This project seeks to provide property scale controlling landscape factor knowledge to support land users reduce losses to the environment.

Overall, meaningful guidance needs to be at farm scale, using accurate data.

Land users make operational decisions at paddock scales, but our national soil and geology datasets - that help us deduce spatial variation for water quality and soil GHG issues - are 1:50,000 and 1:250,000. Some models use 1:50,000 scale soil datasets (one data point per 10 - 30 ha) at "block" scales of 1:3,000. This ignores the risks of working to finer scales than historic soil mapping supports. The actual landscape factors that control contaminant losses can be very different from what is mapped, so the site susceptibility assessment and the mitigation measures may well be inappropriate. Such misalignment confers real financial risk to individual property owners, who may be required to invest in expensive mitigations that are not suited to the inherent susceptibility of the landscape.

Overall our current inability to scale down to provide farm scale data means that farm mitigation guidance and policy are much less effective than they could be. There are perils of using averages in an environment where averages can mask large ranges. This becomes a significant issue when investment grade decisions, on mitigations at an individual farm level need to be made.

From our work partnering with catchment groups in Southland, we can see the benefits of the spatially based analysis to support farmers' quest for knowledge on how to improve their systems. We strongly support using this as an empowerment tool to co-design solutions with farmers. We've seen how effective it can be for behaviour change if we follow these steps:

- **Identify** the controlling landscape factors in partnership with land users across a property or catchment.
- **Validate** the controlling landscape factors using high-resolution datasets and ground-truthing (soil augering, soil pits; soil, surface, and groundwater sampling) in partnership with land users' local knowledge of their land.
- **Communicate** the relationship between controlling landscape factors and water quality and soil GHG susceptibility in partnership with land users.
- **Collectively respond** to the controlling factors through spatially targeted mitigations and farm system optimisation.

The above approach can also support land use change, although such a step may require significant financial support.

5.1 Where to next?

This project's scope was to explore the production of high-resolution, landscape susceptibility maps for two catchments that can be used to help identify the most effective locations for implementing changes to land management practices and land use change.

As noted above, areas of disagreement between historic soil maps and radiometric survey-derived soil properties require further ground truthing to confirm aspects of the susceptibility outputs. Relevant ground truthing would include soil auger/pits and testing soil water, surface, and ground

[28] https://www.thrivingsouthland.co.nz/beyond-regulation-mataura-catchment-project/

water, in partnership with rural communities. Water quality datasets are also often only able to provide long term trend data[29] and are often located at the bottom of large catchments, where it's difficult to unravel the importance of controlling landscape factors. Supplementary water quality monitoring providing localised data would greatly assist in confirming the circumstances that produce contaminant pulses, so that appropriate mitigations can be designed.

We used three well-known statistical analyses to confirm the data validity, however there are other statistical tools or methodological approaches that could draw out further inferences from the data sets we have.

This work concentrates on the spatial aspects of contaminant risks, noting that these vary hugely across the landscape. Not central to this study, but we note that temporal variations in water quality effects are also large. This is obviously a related topic, but one that requires specific attention, and would use specialised analysis and mathematical modelling that can assess dynamic feedback loops.

As businesspeople, land users want confidence that any investment they make will result in meaningful change. Without property, and ideally paddock-scale resolution over the controlling landscape factors, investment in mitigation or land use change could be misaligned with controlling landscape factors. For example, a model or suite of mitigation actions (e.g., FEP) that identifies an area of imperfectly to poorly drained soils - incorrectly mapped as well drained - will provide erroneous estimates of losses and/or be used to recommend mitigations or land use changes that are unlikely to improve environmental outcomes. Misalignments such as these are not currently accounted for in most model uncertainty estimates, planning scenarios, or assessments of the economic cost to reduce contaminant loss. Large property scale uncertainty in historic maps of controlling landscape factors and the sparsity of water quality monitoring networks confer major limitations for any quantitative or policy framework seeking to fairly allocate contaminant losses at property scales.

Ground truthing of the susceptibility maps generated for the Mataura Catchment is being supported by an AgMARDT grant to Thriving Southland. The outputs of the AgMARDT project are non-regulatory, seeking only to empower land users to reduce losses from the land.

Extending a landscape approach to support land users meet their environmental targets would require greater investment. Such investment is required to support a model of property scale validation of controlling landscape factors in partnership with rural communities, as well as for the acquisition of high-resolution airborne geophysical datasets. Although satellite datasets are useful, they are limited to absorbance and reflectance of vegetation or bare ground and do not provide an understanding of the subsurface environment. Geophysical methods employing passive or direct measures of controlling landscape factors are far more effective tools.

[29] PCE environmental reporting system 2019 report overview page 4 "But when we try to find out what's happening on our land or what's happening to our water, there are huge gaps. How can we make economically efficient or socially fair environmental rules if we can't measure authoritatively what's happening to the physical resource base on which our wellbeing ultimately depends?"

Technical Appendices

Table of Contents

List of Figures

Appendix A

Appendix B

Appendix C

Appendix D

Appendix E

List of Tables

Appendix A

Appendix B

Appendix C

Technical Appendix A: Methodology

An overview of the experimental methodology developed for this work is provided below with a summary of each step provided in Figures A.1 and A.2. The methodology was applied separately to the datasets for each region.

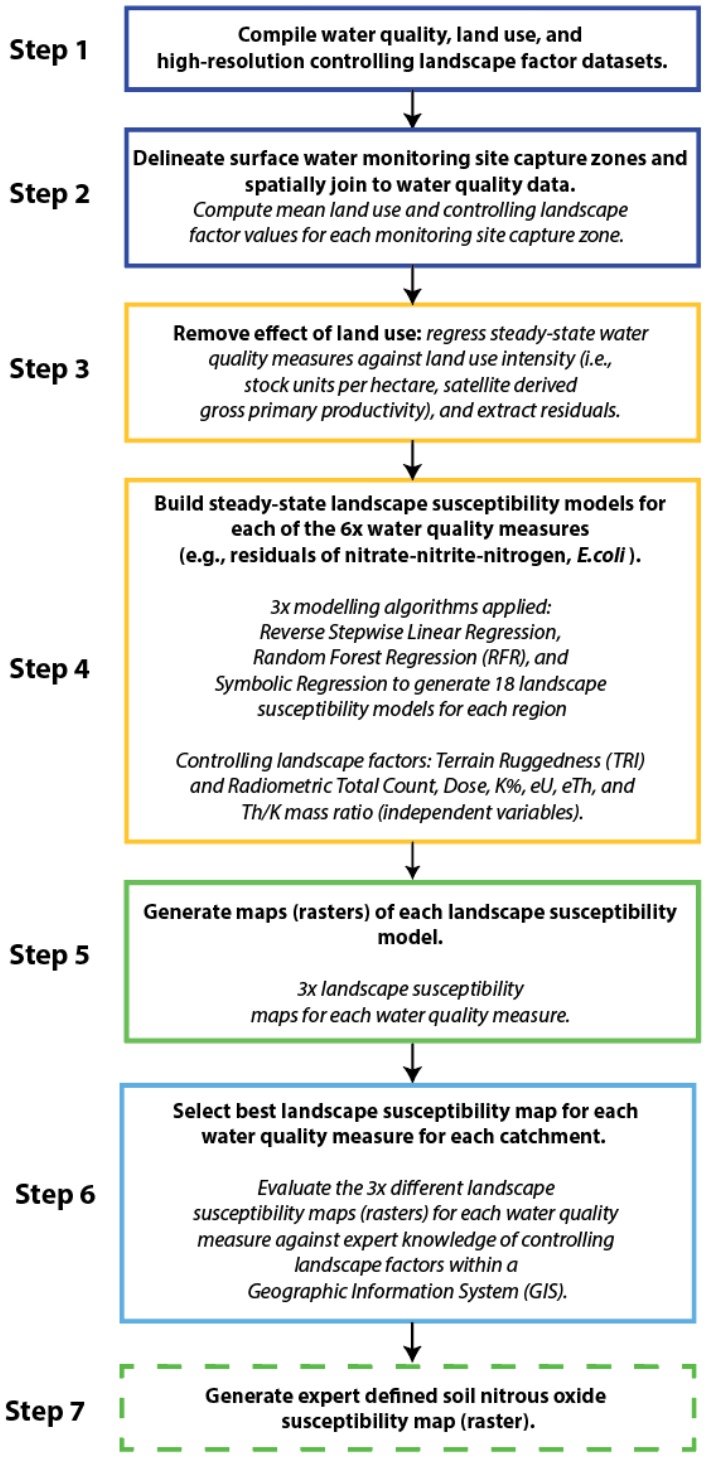

Figure A.1. Summary of landscape susceptibility map generation for Wairoa and Mataura catchments.

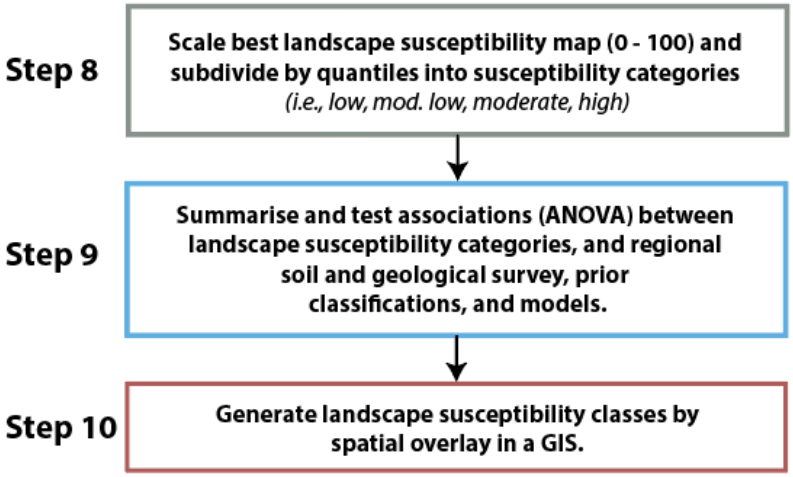

Figure A.2. Evaluation and testing of landscape susceptibility maps and generation of an overall landscape susceptibility classification.

Step 1. Compile water quality, land use, and controlling landscape factor datasets

Water quality datasets

Water quality data sets were compiled from each regional council's state of environment surface water monitoring network. The Northland time series comprised 4,170 measures for 69 long-term monitoring sites for the 2015 - 2019 calendar years. The Southland time series comprised 4,076 measures for 59 long-term monitoring sites for 2017 – 2022 (March) calendar years. The Southland dataset was subsequently reduced to 40 sites that contain at least 70% of their capture zone within the area of radiometric survey.

Outliers associated with raw, time-series water quality data were evaluated using the 'quantile range outlier' method in JMP Statistical Software (JMP, v 16.2)[30]. This method uses the quantile distribution of the values to locate extreme values. Extreme values are found using a multiplier of the interquantile range, the distance between two specified quantiles. A small number of sites with recognised issues associated with saltwater intrusion, stagnation due to low flows, and field sampling error (turbidity) were identified, and the affected water quality measures removed. Median values were then computed for each water quality measure for each site and the data standardised[31]. Median values were considered to provide the best representation of the long-term steady-state sources supplying a stream.

Land use intensity

Land use layers include stocking rates for low and high producing grassland and a satellite-derived measure of Gross Primary Productivity (GPP). The satellite derived GPP layers for Northland and

[30] https://www.jmp.com/support/help/en/16.2/#page/jmp/launch-the-explore-outliers.utility.shtml?os=win&source=application#ww355398

[31] https://towardsdatascience.com/how-and-why-to-standardize-your-data-996926c2c832

Southland have a resolution of 10 x 10 m and include coverage of production forestry and natural state areas. Sensitivity analysis indicates the GPP index is a strong proxy for distributed land use intensity (Technical Appendix B). Land use intensity rasters were standardised using the grid standardisation tool in QGIS[32].

Controlling landscape factors

The controlling landscape factors selected for this project are listed in Table A.1 with summary figures of each provided in Figures A.3 and A.4. A brief literature review of the use of terrain and airborne radiometric survey for the detection and mapping of organic carbon, soil (texture, bulk density, drainage class), geology (rock and sediment geochemistry and weathering), and geomorphic (soil catenary, mass wasting, geomorphic surface age) are provided in Technical Appendix C. Controlling landscape factor rasters were standardised using the grid standardisation tool in QGIS (Montanagne et al., 2009). The benefit of using recent airborne radiometric survey is that it captures the effective properties of the soil landscape, which has been heavily modified by management including wholesale modification of the hydrological properties of soil by compaction and artificial drainage[32].

Table A.1. Controlling landscape factors.

Controlling landscape factors	Units	Resolution
Terrain Ruggedness Index (TRI)		1 x 1 m LiDAR Northland; LWS composite DEM Southland
Radiometric Total Count (Northland)	cps	Airborne Gamma-ray Spectroscopy
Radiometric DOSE (air) (Southland)	nGy/h	Airborne Gamma-ray Spectroscopy
Radiometric percent Potassium (K)	%	Airborne Gamma-ray Spectroscopy
Radiometric Uranium (U)	Ppm	Airborne Gamma-ray Spectroscopy
Radiometric Thorium (Th)	Ppm	Airborne Gamma-ray Spectroscopy
Radiometric Th/K mass ratio		Airborne Gamma-ray Spectroscopy

cps = counts of gamma radiation per second; nGy/h = nano Grays per hour; ppm = parts per million.

[32]https://docs.qgis.org/2.6/en/docs/user_manual/processing_algs/saga/grid_calculus/gridstandardisation.html

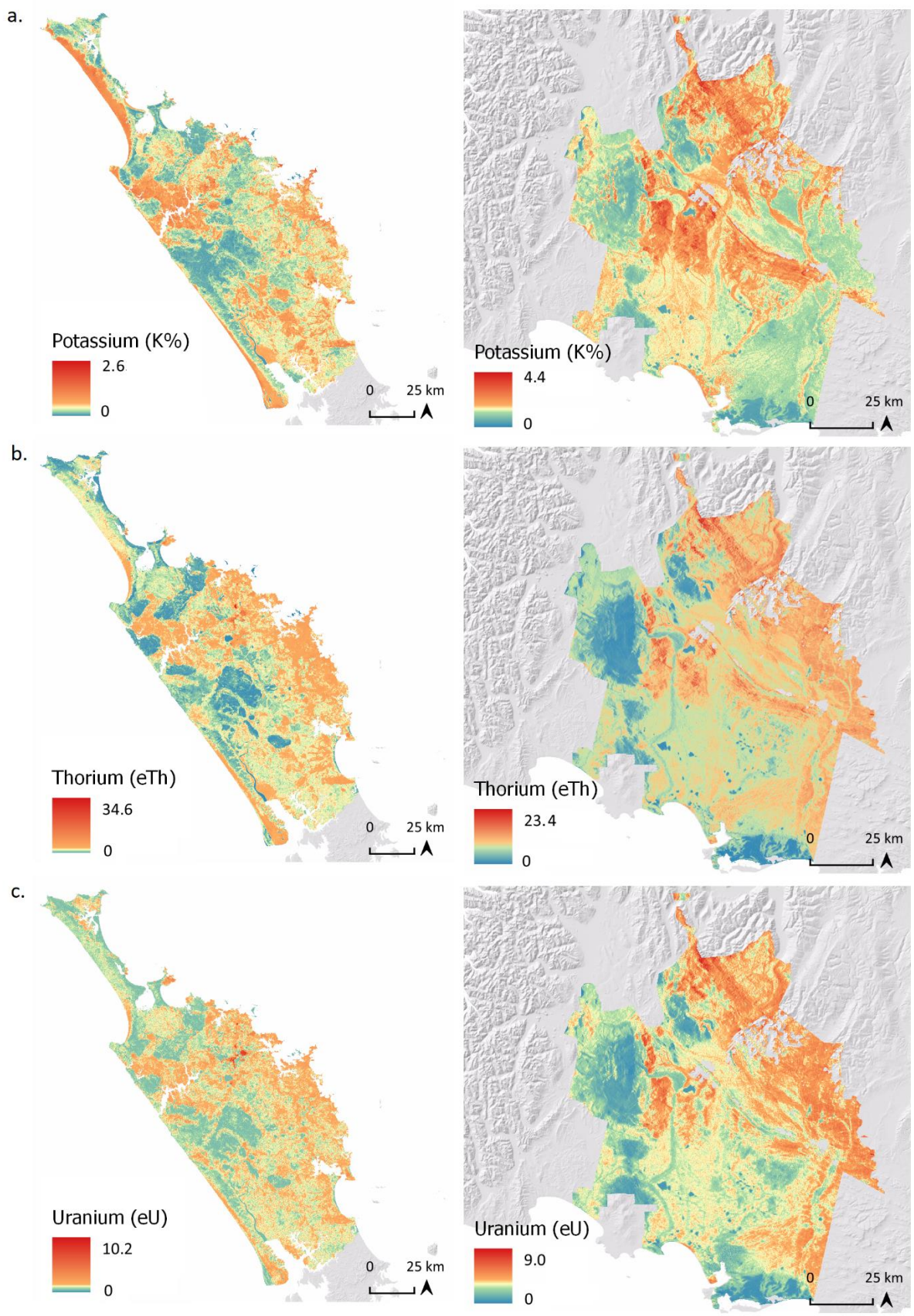

Figure A.3. Northland (left) and Southland (right) for a) potassium (K%), b) thorium (eTh), and c) uranium (eU). Area mapped represents the extent of the radiometric survey for each region.

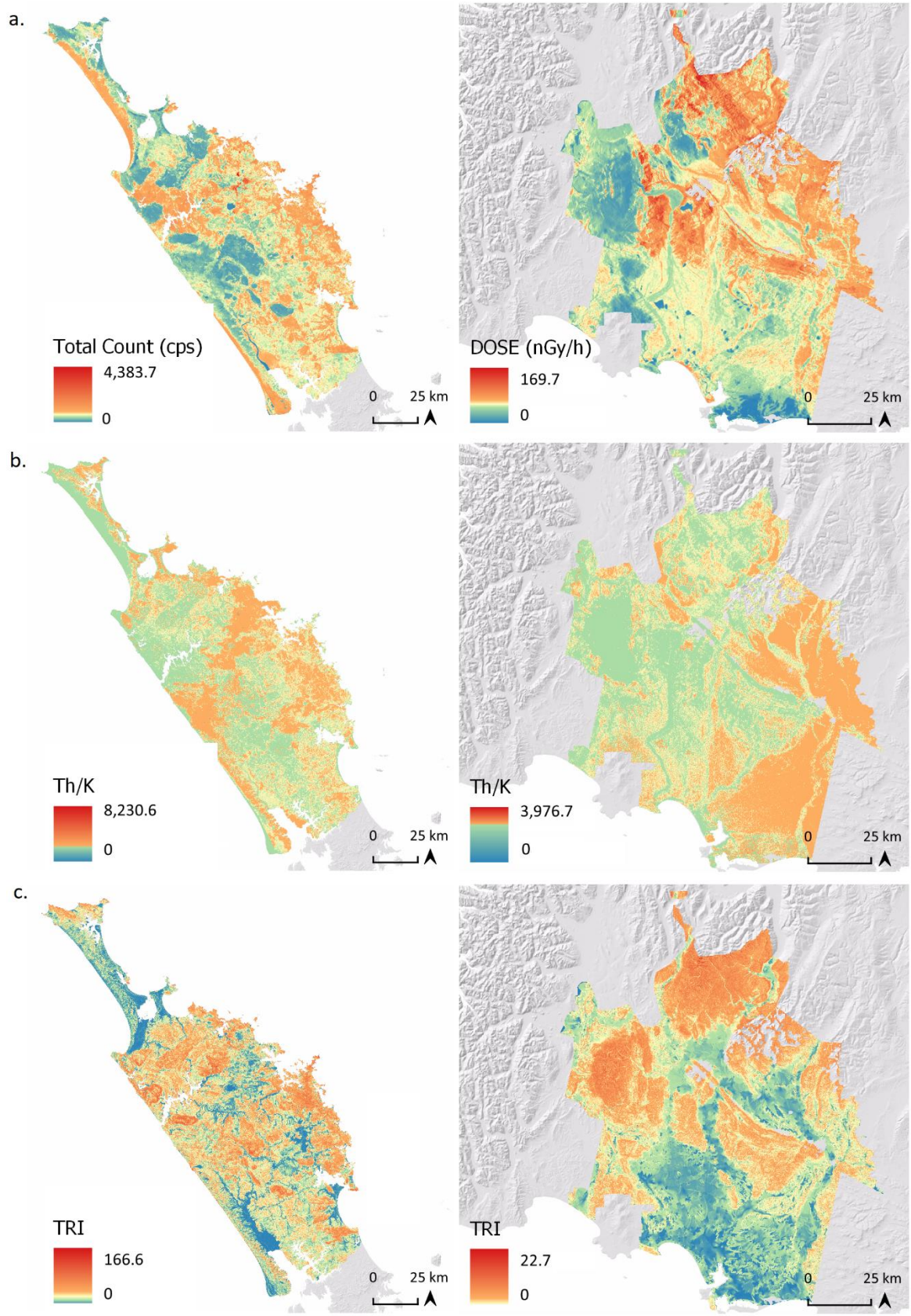

Figure A.4. Northland (left) and Southland (right) for a) total count (count per second) or DOSE (nGy per hour) b) thorium to potassium mass ratio (Th/K), and c) terrain ruggedness index (TRI). Area mapped represents the extent of the radiometric survey for each region.

Step 2. Capture zones and data join

For each water quality monitoring site with high-resolution data coverage, a capture zone was generated (Figure A.5 and A.6). This represents the surface water drainage basin (the area of land contributing drainage water to a monitoring point in the stream). Mean values of land use intensity and controlling landscape factors were then calculated for each capture zone using the Zonal Statistics tool in QGIS (QGIS, v 3.16, 2022)[33]. The mean scores for land use intensity and controlling landscape factors were then spatially joined to median values for each monitoring site.

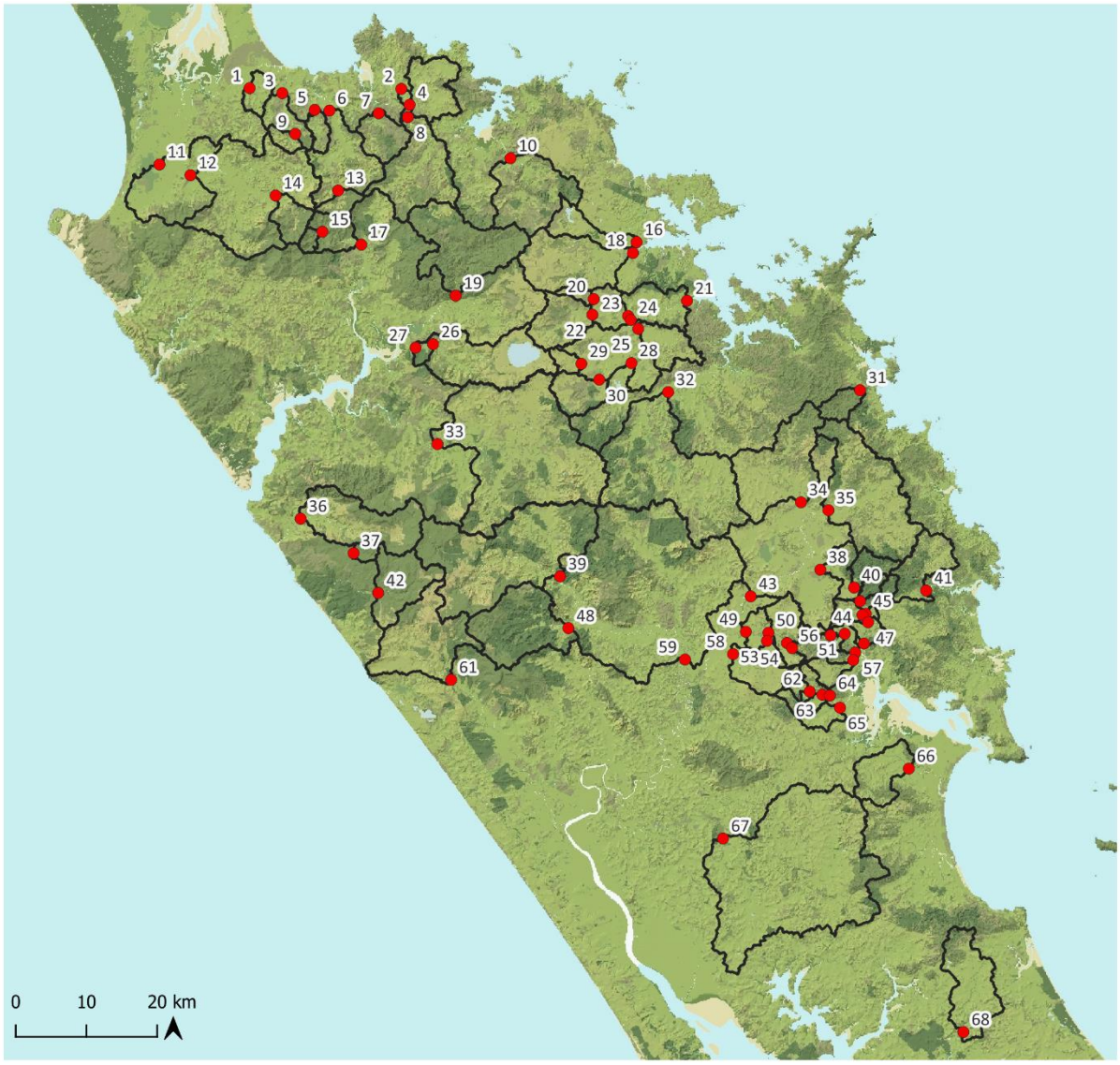

Figure A.5. Northland's water quality monitoring sites and associated capture zones. See Table A.2 for site names.

[33] https://docs.qgis.org/2.18/en/docs/user_manual/plugins/plugins_zonal_statistics.html

Table A.2. Northland water quality monitoring sites.

ID	Site name	ID	Site name
1	Aurere at Pekerau Road	38	Mangahahuru at Apotu Road Bridge
2	Oruaiti at Windust Road	39	Mangakahia at Twin Bridges
3	Parapara at Taumata Road	40	Mangahahuru at Main Road
4	Stony at Sawyer Road	41	Ngunguru at Coalhill Lane
5	Paranui at Paranui Road	42	Waipoua at SH12
6	Oruru at Oruru Road	43	Wairua at Purua
7	Kenana at Kenana Road	44	Mangakino at Mangakino Lane
8	Oruaiti at Sawyer Road	45	Mangakino U/S Waitaua Confluence
9	Parapara at Parapara Toatoa Road	40	Mangahahuru at Main Road
10	Kaeo at Dip Road	41	Ngunguru at Coalhill Lane
11	Awanui at Waihue Channel	42	Waipoua at SH12
12	Awanui at FNDC take	43	Wairua at Purua
13	Peria at Honeymoon Valley Road	44	Mangakino at Mangakino Lane
14	Victoria at Victoria Valley Road	45	Mangakino U/S Waitaua Confluence
15	Tapapa at SH1	46	Waitaua at Vinegar Hill Road
16	Waipapa at Landing	47	Hatea at Whangarei Falls
17	Mangamuka at Iwitaua Road	48	Opouteke at Suspension Bridge
18	Kerikeri at Stone Store	49	Mangere at Knight Road
19	Waipapa at Forest Ranger	50	Mangere at Kokopu Road
20	Waipapa at Waimate North Road	51	Waiarohia at Whau Valley
21	Waitangi at Wakelins	52	Pukenui at Kanehiana Drive
22	Waitangi at Waimate North Road	53	Mangapiu at Kokopu Road
23	Waitangi at SH10	54	Mangere at Kara Road
24	Waiaruhe at Puketona	55	Hatea at Mair Park
25	Mania at SH10	56	Mangere at Wood Road
26	Utakura at Okaka Road	57	Waiarohia at Second Avenue
27	Utakura at Horeke Road	58	Waipao at Draffin Road
28	Watercress at SH1	59	Mangakahia at Titoki
29	Pekepeka at Ohaeawai	60	Raumanga at Bernard Street
30	Waiaruhe D/S Mangamutu Confluence	61	Kaihu at Gorge
31	Punaruku at Russell Road	62	Otaika at Cemetery Road
32	Waiharakeke at Stringers Road	63	Otakaranga at Otaika Valley Road
33	Punakitere at Taheke	64	Otaika at Otaika Valley Raod
34	Waiotu at SH1	65	Puwera at SH1
35	Whakapara at Cableway	66	Ruakaka at Flyger Road
36	Waimamaku at SH12	67	Manganui at Mitaitai Road
37	Wairau at SH12	68	Hakaru at Topuni

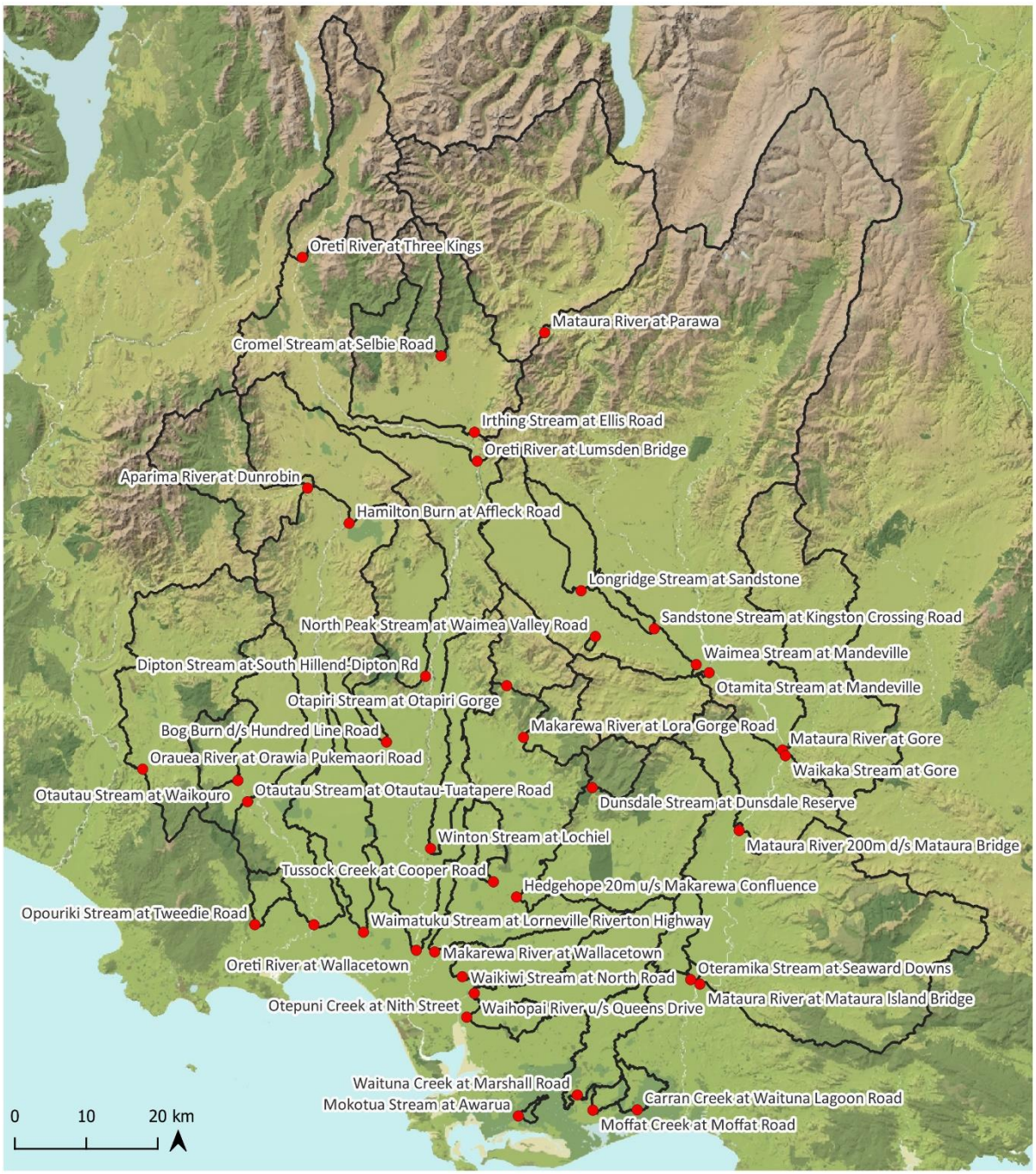

Figure A.6. Southland's water quality monitoring sites and associated capture zones. Sites have been restricted to those with complete or near complete radiometric coverage.

Step 3. Removing the effect of land use

Models were fitted between each water quality measure and proxies of land use intensity provided by PENZ land use intensity layers (Rissmann et al., 2019) and Sentinel-2 satellite derived Gross Primary Production (Figure A.7). Random forest regression was chosen as the preferred modelling approach for extracting the unexplained variation, i.e., residual error, in the water quality data, given its ability to identify the relative importance of the independent variables, especially compared to

simple least squares regression, which we trialled. We hypothesise that some of the unexplained error in each land use model is likely due to controlling landscape factors.

Figure A.7 and A.8 show the proxies of land use intensity for the Wairoa and the Mataura, respectively. The performance of each random forest regression model for each water quality measure and each region is summarised in Table A.3.

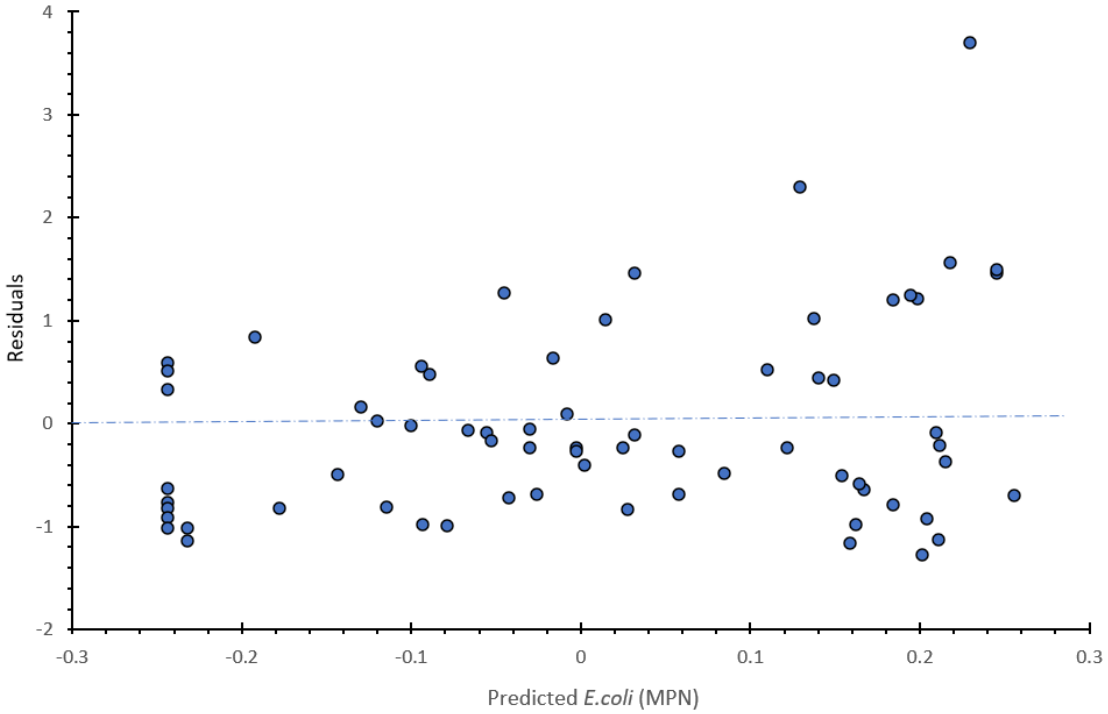

Figure A.7. Residuals extracted from the random forest regression model of land use intensity and median E.coli for the Northland region. Note the deviation from '0' on the Y-axis denotes the unexplained component of the prediction for each water quality site.

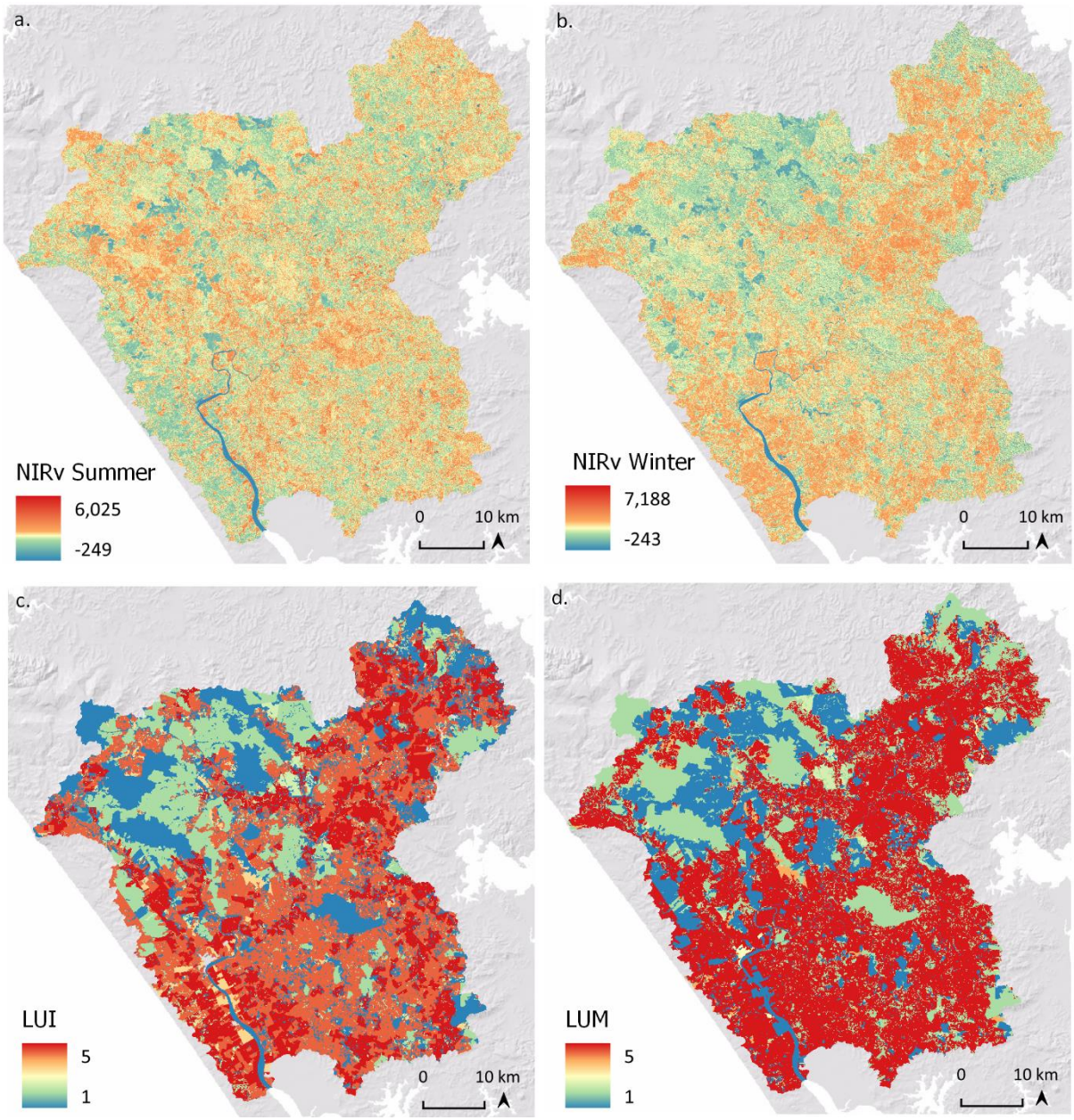

Figure A.8. Proxy for land use intensity from Sentinel-2 satellite derived Gross Primary Production a) summer near infrared vegetation index, b) winter near infrared vegetation index (see Appendix B) and Physiographic layers c) land use intensity and d) microbial intensity from Rissmann et al. (2019).

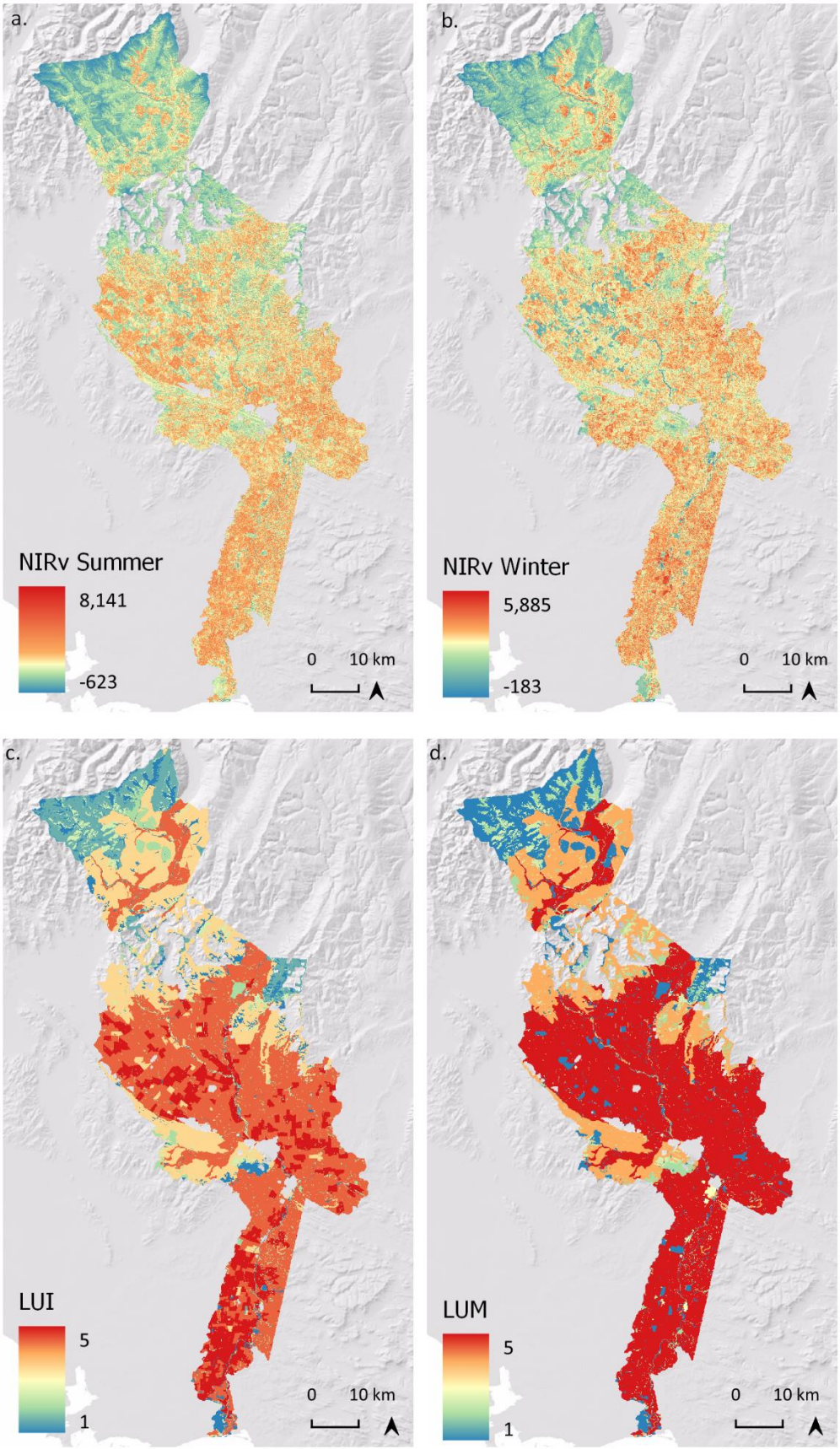

Figure A.9. Proxy for land use intensity from Sentinel-2 satellite derived Gross Primary Production a) summer near infrared vegetation index, b) winter near infrared vegetation index (see Appendix B) and physiographic layers c) land use intensity and d) microbial intensity from Rissmann et al. (2019).

Table A.3. Performance of random forest regression for land use and steady state water quality models

	R^2	RMSE	MAE
Northland			
NNN_LU	0.62	0.41	0.35
TKN_LU	0.69	0.35	0.26
PP_LU	0.63	0.59	0.46
DRP_LU	0.61	0.61	0.49
TSS_LU	0.73	0.59	0.49
Turbidity_LU	0.60	0.75	0.60
*E.coli*_LU	0.56	0.81	0.61
Southland			
NNN_LU	0.86	0.55	0.34
TKN_LU	0.81	0.13	0.10
PP_LU	0.79	0.46	0.35
DRP_LU	0.79	0.64	0.39
Turbidity_LU	0.87	0.49	0.31
*E.coli*_LU	0.76	0.55	0.37

Cross validated R^2; RMSE = Root Mean Squared Error; MAE = Mean Absolute Error. NNN = nitrate-nitrite nitrogen; TKN = total Kjeldahl nitrogen; PP = particulate phosphorus; DRP = dissolved reactive phosphorus; TSS = total suspended sediment; LU = denotes the use of land use layers as the independent variables.

Step 4. Landscape susceptibility models

Reverse stepwise linear regression, random forest regression, and symbolic regression were used to fit models between the residuals of each water quality measure and controlling landscape factors (Table A.4; Table A.5).

Reverse stepwise regression (Burnham and Anderson, 2004) and random forest regression (Brieman, 2001) are familiar modelling approaches, so they are not described here. Symbolic regression, a genetic programming algorithm, is less well known (Smits and Kotanchek, 2005). For this experimental work, symbolic regression was applied to identify the most accurate and least complex mathematical representation of the relationship between the controlling landscape factors and the residuals of each water quality indicator using the TuringBot Python library source code (TuringBot, 2022; see also Ashok et al., 2020).

As an evolutionary algorithm, symbolic regression evolves towards a single best model, sifting through billions of different combinations of controlling landscape factors and mathematical operators, discarding those that do not improve the accuracy or reduce the complexity of the model. Unlike traditional regression methods, which optimise the parameters of pre-defined models, symbolic regression learns both the model structure and its parameters simultaneously. The latter is highly advantageous as the model is interpretable, providing an output of each controlling landscape factor's sensitivity and its magnitude of response to each water quality measure. The transparency provided by symbolic regression has been used to test controlling landscape factor hypotheses (Rissmann et al. 2019).

As part of the symbolic regression approach, the Nash-Sutcliffe efficiency criterion was used as the model search metric to guide the evolutionary search for the best model (Nash and Sutcliffe, 1970). The efficiency (E) proposed by Nash and Sutcliffe (1970) is defined as one minus the sum of the absolute squared differences between the predicted and observed values normalised by the

variance of the observed values. It is commonly used in hydrological modelling approaches to provide an objective assessment of the 'closeness' of the simulated behaviour to the observed measurements (Krause et al., 2005). As well as specifying the Nash-Sutcliffe efficiency criteria as the evolutionary search metric, a Pareto chart was used to guide model selection, using the trade-off between error and model complexity.

Table A.4. Random forest variable importance for the Northland and Southland datasets.

	TRI	TC/DOSE	K%	eTh	eU	Th/K
Northland						
NNN	0.046	0.193	0.083	0.333	0.013	0.058
TKN	0.227	0.186	0.071	0.023	0.125	0.019
PP	0.098	0.033	0.103	0.025	0.101	0
DRP	0.095	0.038	0.024	0.001	0.002	0.001
Turbidity	0.062	0.052	0.017	0.029	0.205	0.001
TSS	0.001	0.05	0.042	0.043	0.054	0.006
E.coli	0.003	0.121	0.146	0.068	0.017	0.015
Southland						
NNN	0.027	0.112	0.053	0.094	0.204	0.018
TKN	0	0	0.002	0.002	0.002	0.060
PP	0.04	0	0.034	0.184	0.001	0.055
DRP	0	0	0	0.018	0.013	0.023
Turbidity	0.042	0.004	0.076	0.090	0.008	0.124
E.coli	0.020	0.014	0.125	0.069	0.038	0.097

NNN = nitrate-nitrite nitrogen; TKN = total Kjeldahl nitrogen; PP = particulate phosphorus; DRP = dissolved reactive phosphorus; TSS = total suspended sediment.

Table A.5. Table of landscape susceptibility models and their performance metrics by region.

Measure	Method	R^2	RMSE	Landscape Susceptibility Models for Symbolic Regression and Reverse Stepwise Linear Regression.
Northland				
NNN	SR	0.83	0.21	0.174411*(-1.1908-(0.0100389/Th_K_Ratio)+Th-(((TRI_LiDAR+((-0.0292084)/(TC-0.0129464+0.934022*Th_K_Ratio)))/(-0.0304227+TRI_LiDAR-Th-TC))*Th_K_Ratio))+(0.0410165/(-0.808886-Th))-(0.0393437/(Th_K_Ratio-0.686486*U+((-0.000931305)/U)+Th_K_Ratio))
	RF	0.87	0.23	
	RSLR	0.32	0.46	-0.041005427 + -0.155105837 * TRI LiDAR + 0.4223139723 * Th + - 0.225477873 * U + -0.213370798 * Th K Ratio
TKN	SR	0.85	0.21	-0.273371+((0.930555-((0.0045209/(1.0566-Th))/(0.0431945+K)))*TC)-(0.0266384/(-2.30925+K))-Th+((-0.532215+TRI_LiDAR)/(-2.61705-(((1.90845+Th_K_Ratio)*K+1.6853+TC)*Th)-Th_K_Ratio))
	RF	0.72	0.27	
	RSLR	0.43	0.43	-0.099309109 +-0.220166403 * TRI LiDAR + 1.319890301 * TC + -1.378148232 * Th + 0.1491827238 * Th K Ratio
PP	SR	0.71	0.45	(K-Th)*(0.0620697*((Th+((-0.212435)/(0.111865+U))-3.25426)*(((-0.160856)/((1.06321-Th)*(-0.402638+Th)))+(-2.76669+2.7122*TRI_LiDAR))-((1.01271+TRI_LiDAR)/K)+U))
	RF	0.68	0.39	
	RSLR	0.32	0.73	-0.096122417 + 1.439422546 * TC +-1.513141441 * Th
DRP	SR	0.81	0.43	(-0.34861)*((U/(Th_K_Ratio+0.95409-(0.0349557/Th_K_Ratio)))-(K-(0.858784+(((0.00345718/(0.0397125+K))/(1.12983*K-Th))+0.213*Th_K_Ratio-((-0.0357383)/(TC-(1.98654-K)))))))
	RF	0.62	0.37	
	RSLR	0.25	0.68	-0.060977807 + -0.549562222 * TC + 0.4880515001 * K
TSS	SR	0.81	0.37	(0.155759+((-0.0148782)/Th))*(((0.0532237/(TRI_LiDAR-0.725638))+(Th*((TRI_LiDAR/(0.0405432+K))+((0.0531918/(0.0980227+TC))+((0.0171707/(Th-Th_K_Ratio-0.0965399))/(0.048882+Th_K_Ratio))-TRI_LiDAR))+(1.41113-(TRI_LiDAR/((1.21956+Th)*TC)))))*K-1.2288)
	RF	0.65	0.51	
	RSLR	0.25	0.84	0.0827494116 + 4.5140242619 * TC +-1.271872156 *K +-2.994224863 * Th +-0.801870025 * U
Turbidity	SR	0.73	0.46	TC-(Th-0.0894125-(0.147936*(TRI_LiDAR+((-0.459059)*(Th_K_Ratio+(-3.35495-((-0.678453)/(0.855639+Th+((TRI_LiDAR-U+((TRI_LiDAR-Th-8.06534)*Th_K_Ratio))*(Th_K_Ratio+0.00284263)))))))*(Th_K_Ratio-((0.0997927/(0.0239508+Th_K_Ratio))+(-0.354028+TRI_LiDAR)))))
	RF	0.62	0.71	
	RSLR	0.34	0.81	-0.028523262 + -0.407306401 * TRI LiDAR + 1.7672610677 * TC + -1.839390037 * Th
E.coli	SR	0.68	0.41	K*(0.0362078/((Th+0.0506505)*(U+TRI_LiDAR)-0.00674078))-(0.14017*TC*K+(0.125826-(TC+(((-0.00695158)/(-0.0224951*U+Th_K_Ratio+0.0677356))-Th))))
	RF	0.88	0.27	
	RSLR	0.20	0.77	-0.067646446 + -0.293989722 * TRI LiDAR + 1.2609503765 * TC +-0.725384011 * Th + -0.488604539 * U

SR = symbolic regression; RF = random forest; RSLR = reverse stepwise linear regression. NNN = nitrate-nitrite nitrogen; TKN = total Kjeldahl nitrogen; PP = particulate phosphorus; DRP = dissolved reactive phosphorus; TSS = total suspended sediment.

Measure	Method	R^2	RMSE	Landscape Susceptibility Model for SR and RSLR.
Southland				
NNN	SR	0.95	0.19	0.398689*(0.850439*U-TRI+(DOSE-Th)+((0.0301069/(-0.0227661+K))-0.447107)+((-0.389214)*(((DOSE+((-0.406103)/(-0.0597559+U)))*TRI+1.52009+U)*(0.207207+((-0.0132965)/(TRI-0.997259))+Th))/(0.133958+DOSE+TRI-(0.0139462/K))))
	RF	0.96	0.35	
	RSLR	0.54	0.64	-0.063248747 + -0.720698685 * TRI + 8.8181561672 * DOSE + -3.554390004 * K + -2.663067885 * Th + -2.877434505 * U
TKN	SR	0.89	0.19	(2.76365-(U-Th)-(Th_K/(0.0601245+(DOSE/0.794082)+K)))*(-0.109939+TRI)/((-1.03419+Th_K+K)*K+(0.016296/((0.767755+K)*((DOSE+0.849663)*(-0.438024*DOSE+DOSE*K))))-6.75519)
	RF	0.91	0.19	
	RSLR	0.55	0.57	0.1720672499 + -0.432760358 * TRI + -0.278994489 * DOSE
PP	SR	0.88	0.20	(((-0.00506426)/Th_K)+(0.576036*((0.296398/(0.820816*TRI+Th+DOSE))+0.321883+TRI)))/(-2.2733+(((-0.0613457)/(-0.0293555*U+DOSE))-DOSE))
	RF	0.77	0.27	
	RSLR	0.42	0.68	0.1845487497+ -0.32535182 * TRI + -2.674557364 * DOSE + 1.4088536664 * Th + 1.0242883376 * U + -0.652268113 * Th_K_Ratio
DRP	SR	0.86	0.19	((0.310314+TRI)/((((-1.19936)/(-0.014489-TRI))+TRI)*Th_K-K-2.19665))+((0.112313*(0.810593+Th_K)/(U+(TRI+((Th_K-0.706794)*Th))))-((-0.0118615)*((TRI/U)-(-5.72897*DOSE*Th_K))))
	RF	0.43	0.32	
	RSLR	0.26	0.84	0.22459625 + -0.567599494 * TRI + -0.257538196 * Th_K_Ratio
Turbidity	SR	0.79	0.22	-0.189132+Th-(DOSE+(0.0169272/(K+(-0.218938*Th))))+((0.571341/((Th-((0.973226/TRI)-(0.000316418/DOSE)))*Th_K+2.09474+K))+((-0.0336359)/(0.789917+K))-(0.190935*(TRI-K)))
	RF	0.84	0.26	
	RSLR	0.44	0.71	0.2617979996 + -0.3230177 * TRI + -3.387434941 * DOSE +2.1553494117 * Th + 1.0187974815 * U + -0.788557436 * Th_K _ratio
E.coli	SR	0.81	0.20	((-0.0290281)/(K-(0.014551+Th_K)))+((0.102361/((0.701526-Th_K)*(U-(K-((-0.00731469)*((0.983572/(-0.0901662+Th))+(2.8916/(K+U-Th_K))+((0.233198+K)/(-0.0316769+Th_K))))+TRI))))-((-0.18305)*(DOSE-(1.2318+TRI))))
	RF	0.75	0.41	
	RSLR	0.10	0.87	0.089861 + -0.282532416 * TRI

SR = symbolic regression; RF = random forest; RSLR = reverse stepwise linear regression. NNN = nitrate-nitrite nitrogen; TKN = total Kjeldahl nitrogen; PP = particulate phosphorus; DRP = dissolved reactive phosphorus; TSS = total suspended sediment.

Step 5. Applying the landscape susceptibility models to produce maps

Three landscape susceptibility rasters ('maps') were created for each water quality measure using the models tabulated in Table A.4. Each landscape susceptibility model was applied at a pixel-by-pixel level within QGIS (QGIS, v 3.16, 2022) or via R (R Core Team, 2017) for the Wairoa and Mataura catchments. The resultant susceptibility maps for individual water quality measures have a resolution of 0.16 ha (40 x 40 m) for both the Wairoa and Mataura catchments.

Figures A.10 to A.22 show the outputs of the 3 different models (Reverse Stepwise Linear Regression, Random Forest Regression, and Symbolic Regression) for each water quality measure and catchment.

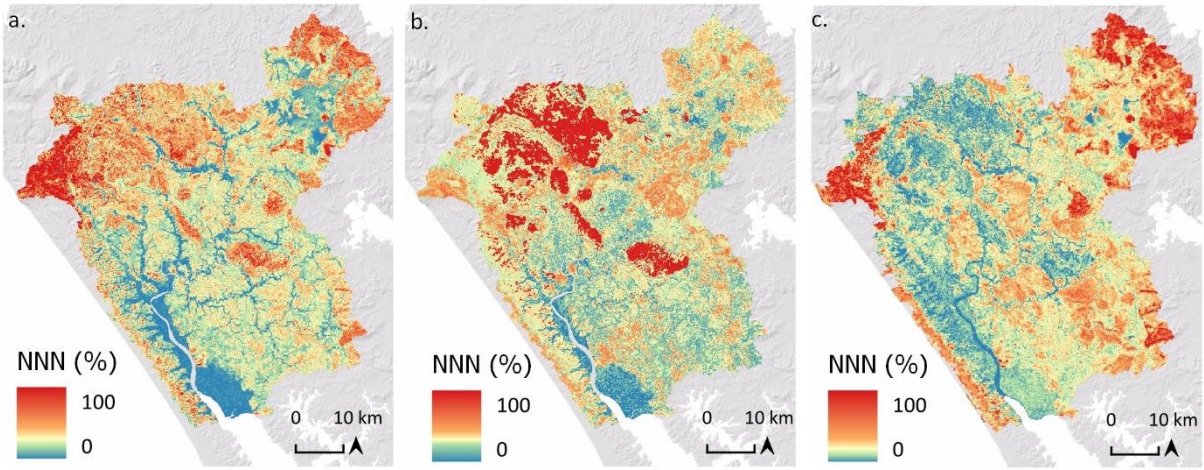

Figure A.10. Nitrate-nitrite-nitrogen models by a) reverse stepwise linear regression, b) random forest regression, and c) symbolic regression for the Wairoa catchment.

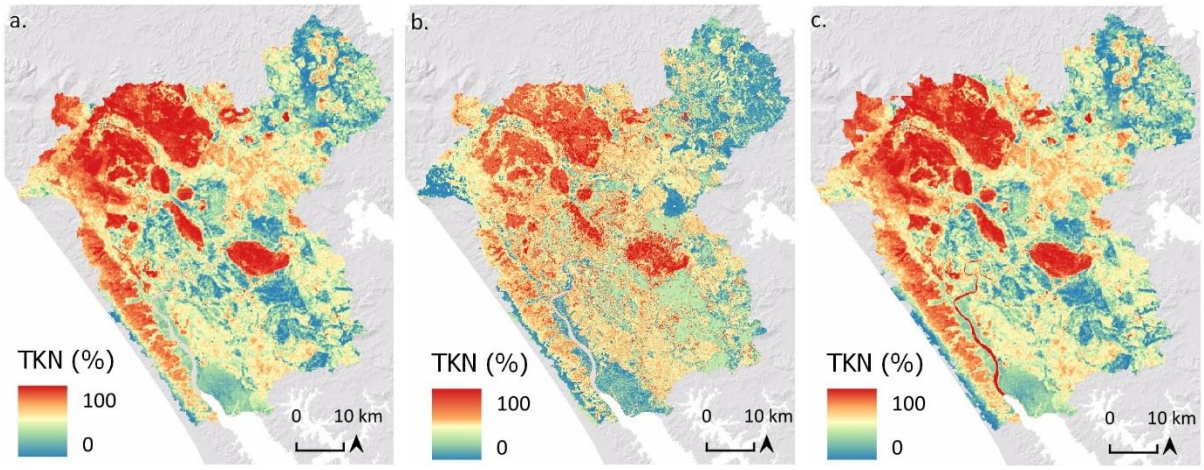

Figure A.11. Organic and ammoniacal nitrogen models (measured by TKN) by a) reverse stepwise linear regression, b) random forest regression, and c) symbolic regression for the Wairoa catchment.

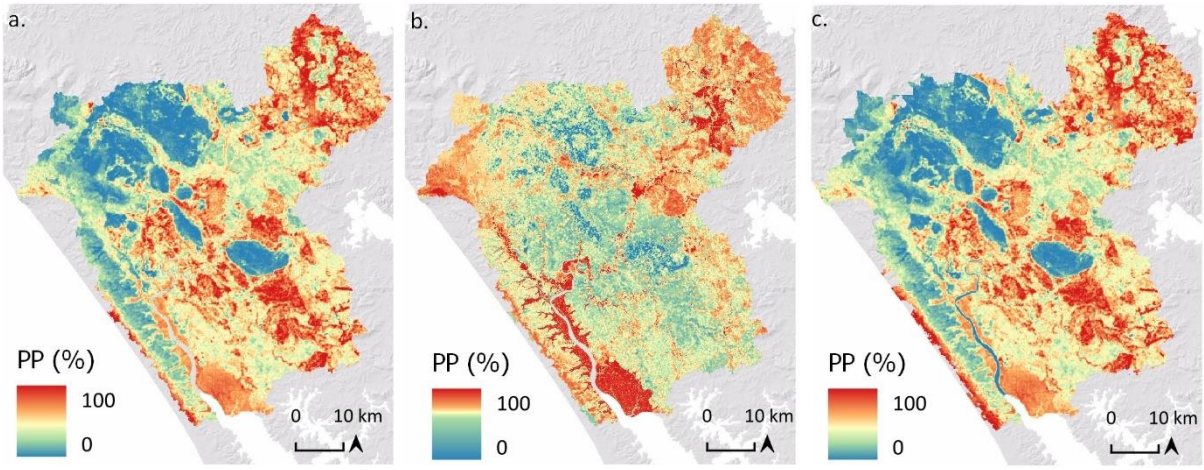

Figure A.12. Particulate phosphorus models by a) reverse stepwise linear regression, b) random forest regression, and c) symbolic regression for the Wairoa catchment.

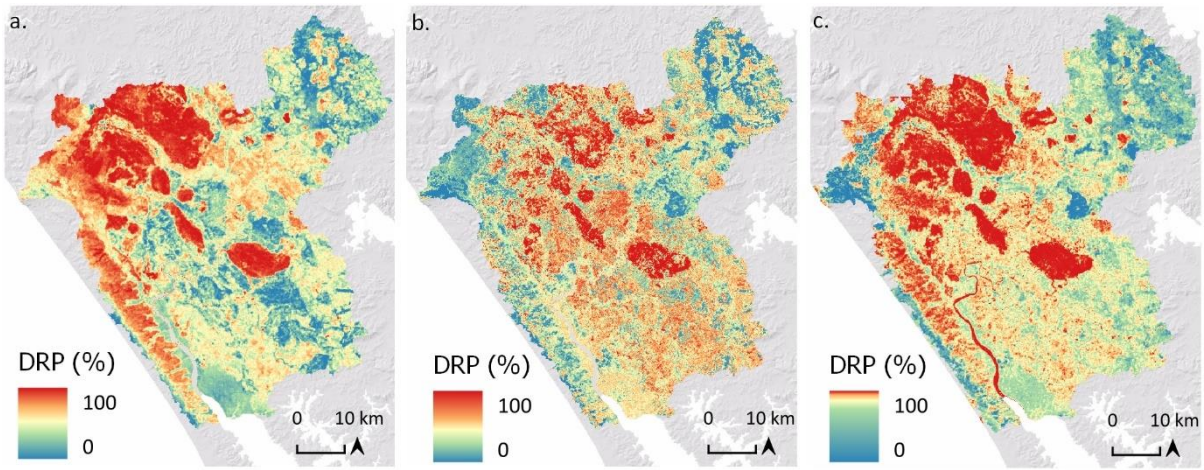

Figure A.13. Dissolved reactive phosphorus models by a) reverse stepwise linear regression, b) random forest regression, and c) symbolic regression for the Wairoa catchment.

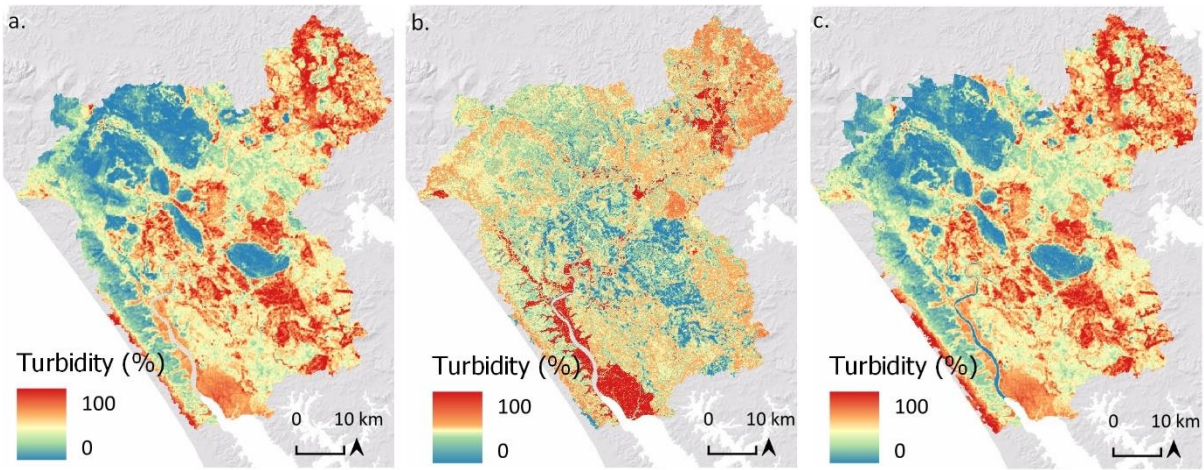

Figure A.14. Turbidity models by a) reverse stepwise linear regression, b) random forest regression, and c) symbolic regression for the Wairoa catchment.

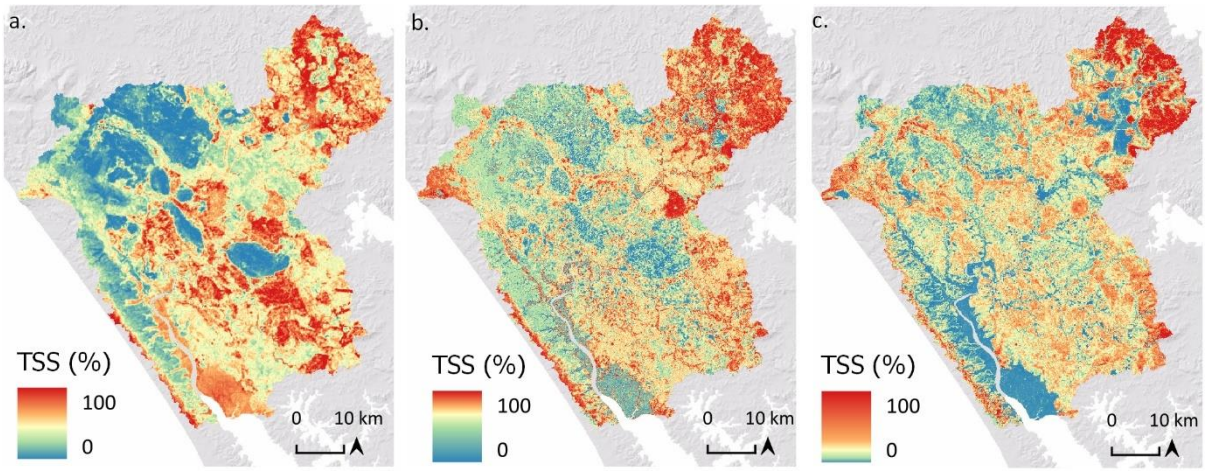

Figure A.15. Total suspended sediment models by a) reverse stepwise linear regression, b) random forest regression, and c) symbolic regression for the Wairoa catchment.

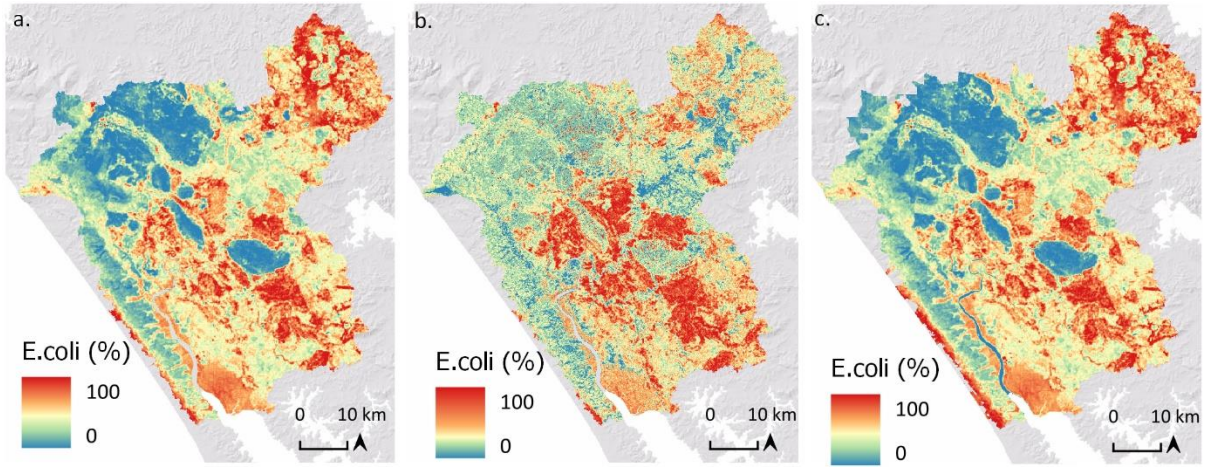

Figure A.16. E. coli models by a) reverse stepwise linear regression, b) random forest regression, and c) symbolic regression for the Wairoa catchment.

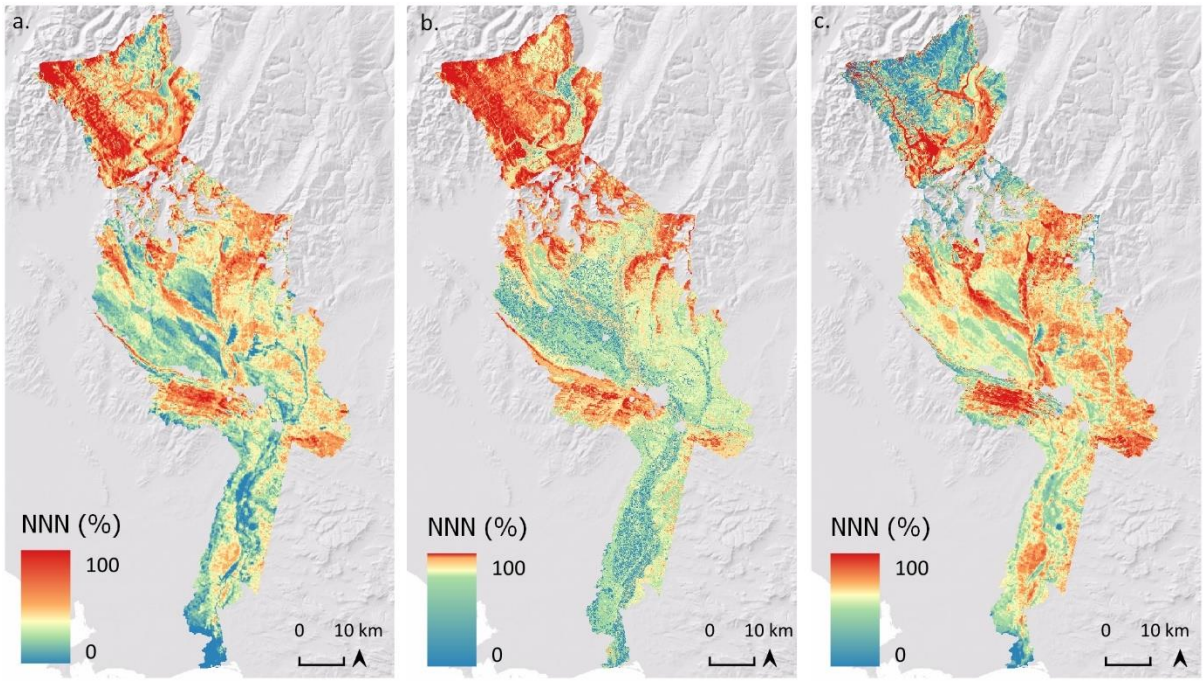

Figure A.17. Nitrate-nitrite-nitrogen models by a) reverse stepwise linear regression, b) random forest regression, and c) symbolic regression for the Mataura catchment.

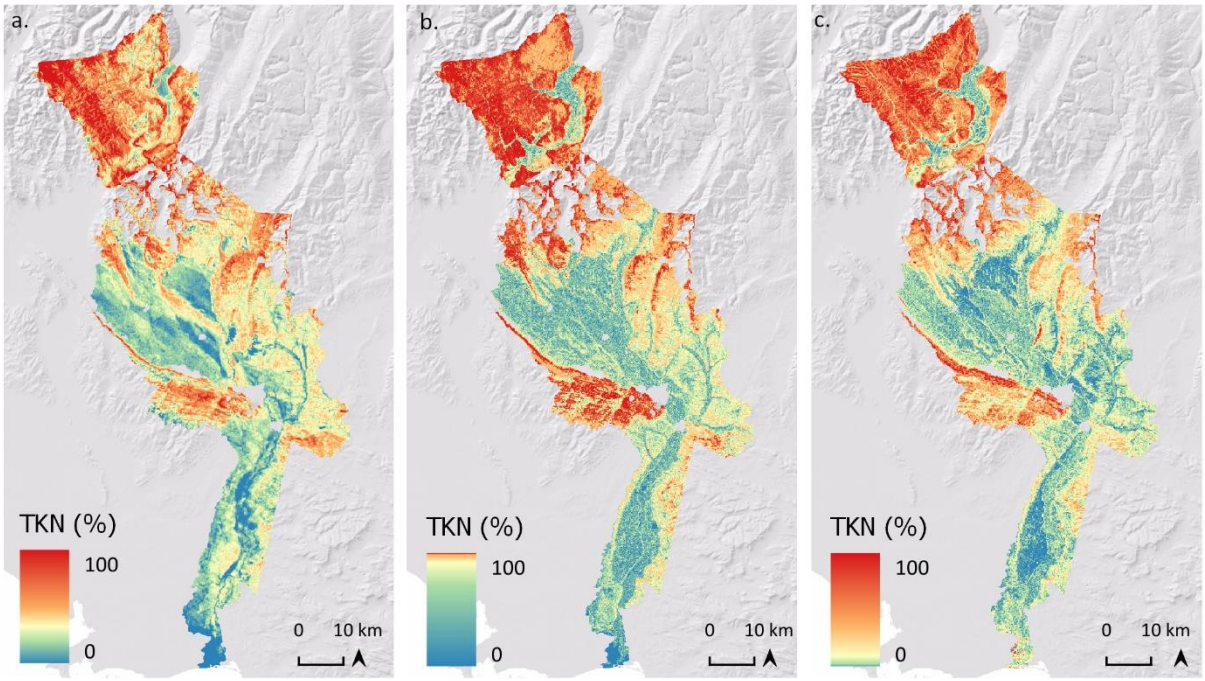

Figure A.18. Organic and ammoniacal nitrogen models (measured by TKN) by a) reverse stepwise linear regression, b) random forest regression, and c) symbolic regression for the Mataura catchment.

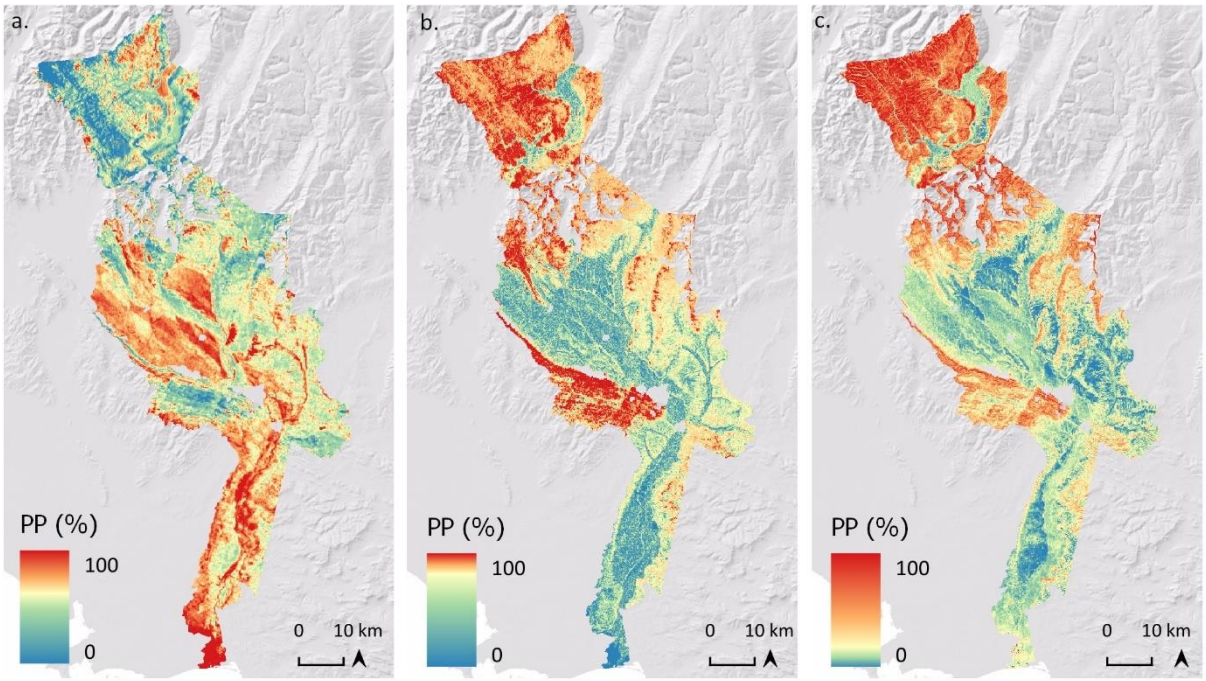

Figure A.19. Particulate phosphorus models by a) reverse stepwise linear regression, b) random forest regression, and c) symbolic regression for the Mataura catchment.

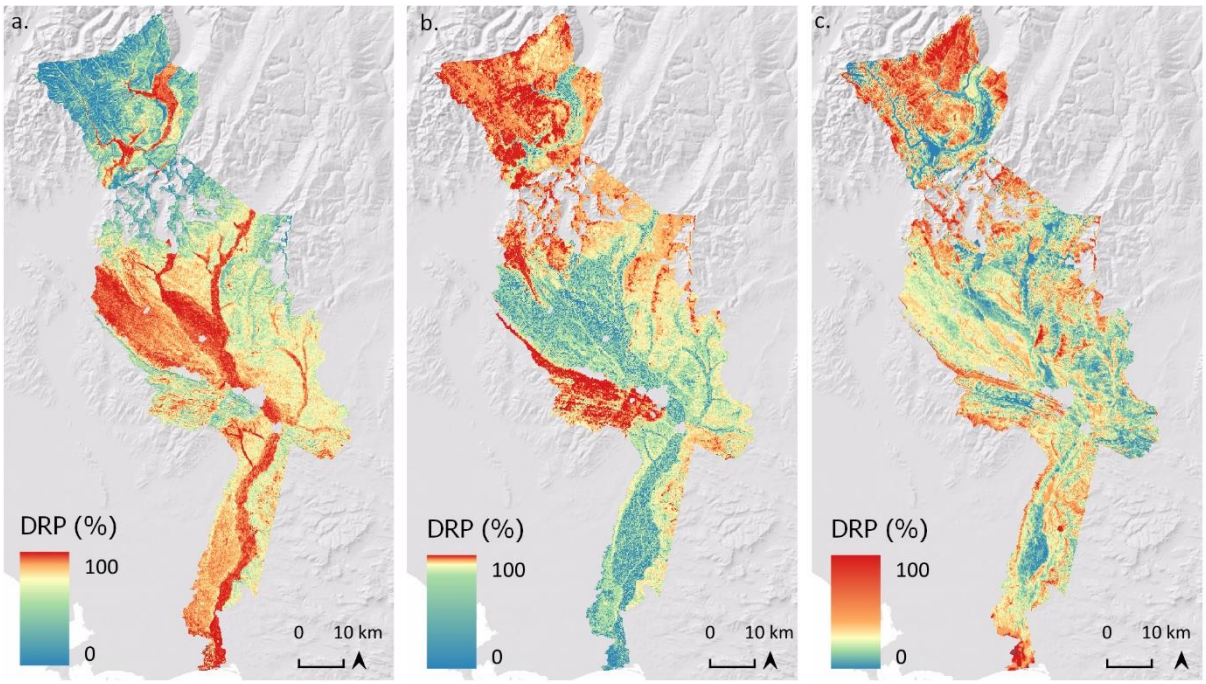

Figure A.20. Dissolved reactive phosphorus models by a) reverse stepwise linear regression, b) random forest regression, and c) symbolic regression for the Mataura catchment.

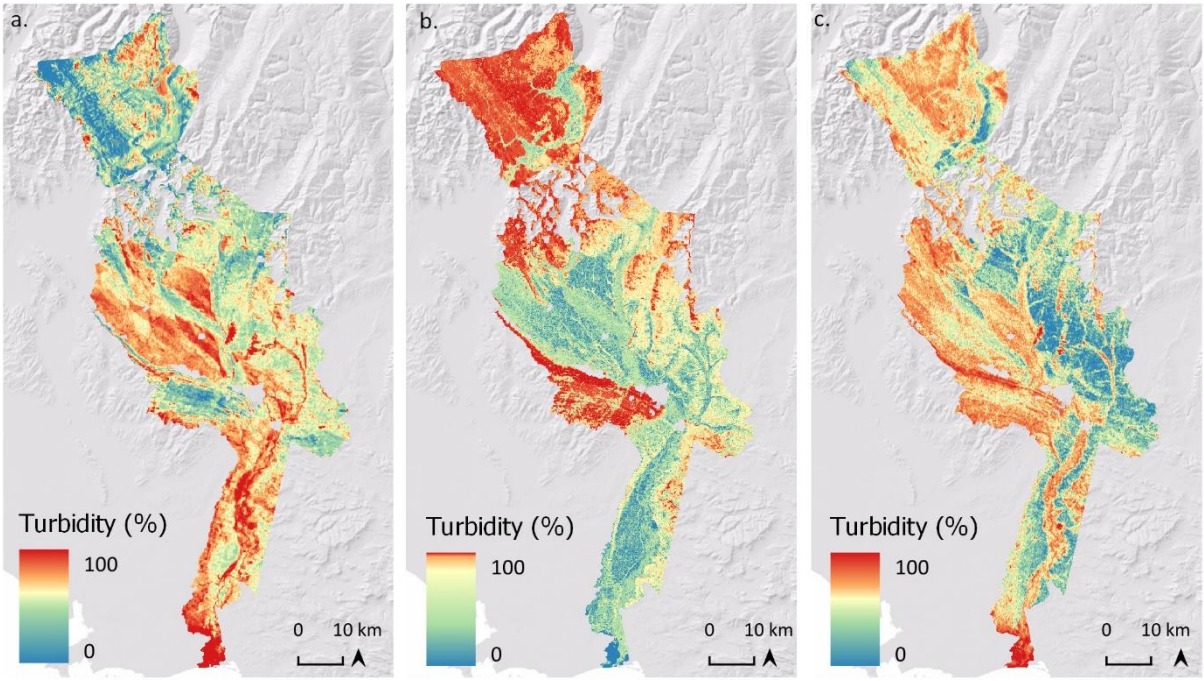

Figure A.21. Turbidity models by a) reverse stepwise linear regression, b) random forest regression, and c) symbolic regression for the Mataura catchment.

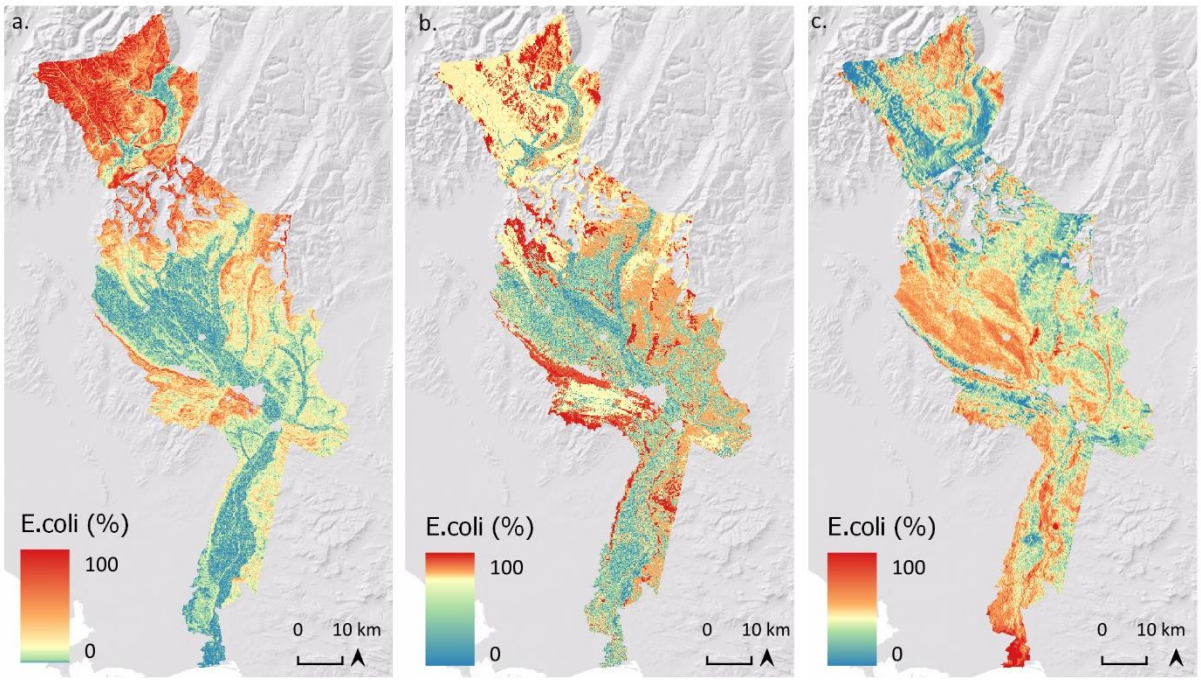

Figure A.22. E. coli models by a) reverse stepwise linear regression, b) random forest regression, and c) symbolic regression for the Wairoa catchment.

Step 6. Selection of susceptibility models

The rasters generated by reverse stepwise linear regression, random forest regression, and symbolic regression were imported into QGIS. The authors then evaluated each landscape susceptibility raster

against local knowledge of spatial variation in the controlling landscape factors. The expert assessment included cross-referencing each raster to regional soil and geological surveys and hydrochemical signatures of dominant processes in soil water, surface waters, and ground waters.

In addition to comparing each susceptibility raster against controlling landscape factors, each was compared to the other. Expert judgment was then used to select the model that in the author's opinion best represents spatial variation in landscape susceptibility.

Symbolic regression, which uses the Nash-Sutcliffe efficiency criterion (Nash and Sutcliffe, 1970) as the model search metric, generated the best landscape susceptibility models. Specifically, symbolic regression appears to be sensitive to multiple different landscape factors that control susceptibility (e.g., dissolved reactive phosphorus susceptibility may be associated with phosphorus rich volcanic rocks, peat wetlands, and coal measures). Reverse stepwise linear regression and random forest regression appear to identify only the main or dominant controlling landscape factor and appeared relatively insensitive to secondary or tertiary controlling factors (e.g., identifying only wetlands or only phosphorus rich rocks as the dominant controlling factor). Symbolic regression models are also 'white box' models making them more interpretable, which was valuable when evaluating 'how' and 'why' variation in landscape susceptibility occurs.

Step 7. Soil nitrous oxide (N_2O) landscape susceptibility model

The role and relative contribution of controlling landscape factors on soil nitrous oxide emission is currently poorly quantified, with most studies focusing solely on the relative contribution from land use, or where landscape factors are considered do not provide a quantitative assessment of the role of landscape. However, a recent meta-data synthesis based on 6,016 field observations from 219 articles including four New Zealand studies by Li et al. (2022), provides a quantitative assessment of the importance of landscape factors. The work of Li et al. (2022) notes that soil moisture (19.0%) and mean annual temperature (18.0%) accounted for 37% of the variation in soil nitrous oxide emissions on a global scale, with a further 9.4% of variation associated with differences in ecosystem type, e.g., forest vs wetland, cropland vs grassland. Li et al. (2022) attributed the remaining 53.6% of the variation to soil N content (i.e., nitrate, ammonium, and soil organic N).

Of the soil N content, nitrate-nitrite concentration within the soil was identified as the single most sensitive predictor of emissions (Li et al. 2022), which is consistent with a strong land use control. However, soil redox conditions also influence the relative abundance of nitrate-nitrite nitrogen versus less labile ammoniacal and organic nitrogen (Bartlett, 1993; Sutherland et al. 1993). Therefore, as Li et al (2022) did not assess the role of soil redox we expect some of the variation in N_2O emissions explained by soil nitrate-nitrite-nitrogen to reflect spatial and temporal variation in soil redox conditions in addition to land use. Using the study of Li et al. (2022), controlling landscape factors may account for at least 50% of the variation in soil nitrous oxide. Please note that Li et al. (2022) did not identify soil pH as a highly influential controlling factor.

As discussed in the literature review accompanying this report, redox processes determined by soil saturation govern denitrification, coupled nitrification-denitrification, and nitrifier denitrification pathways that generate soil zone nitrous oxide (Technical Appendix D). These reaction pathways are directly related to soil zone redox potential and associated nitrate-nitrite-nitrogen susceptibility[34]. As nitrate-nitrite production is favoured in soils that seldom saturate, the inverse of the landscape

[34] The work of Giltrap et al. (2010) provides an important overview of the reaction processes specific to soil nitrous oxide production and the application of a multi-process modelling framework to assessing soil nitrous oxide emissions across New Zealand.

susceptibility model for nitrate-nitrite-nitrogen was utilised as the basis for depicting landscape susceptibility to nitrous oxide emission (Figure A.23). The main advantage of using the nitrate-nitrite-nitrogen landscape susceptibility layer reflects the use of in-stream concentrations to reveal the effective landscape gradients controlling denitrification, nitrification-denitrification and nitrifier denitrification pathways that generate soil zone nitrous oxide.

As noted by Li et al. (2022), climatic factors also control soil zone nitrous oxide generation. Therefore, each catchment was subdivided into climatic classes using the River Environment Classification (Snelder et al., 2010). Across the Wairoa and Mataura catchments, climate classes are strongly correlated with local topography and associated lowland, hill, and steep land landscape settings. Warm, wet climate zones are more susceptible to nitrous oxide loss than cold, dry climate zones (Figure A.22). Climate zones were ranked from coldest and driest to warmest and wettest.

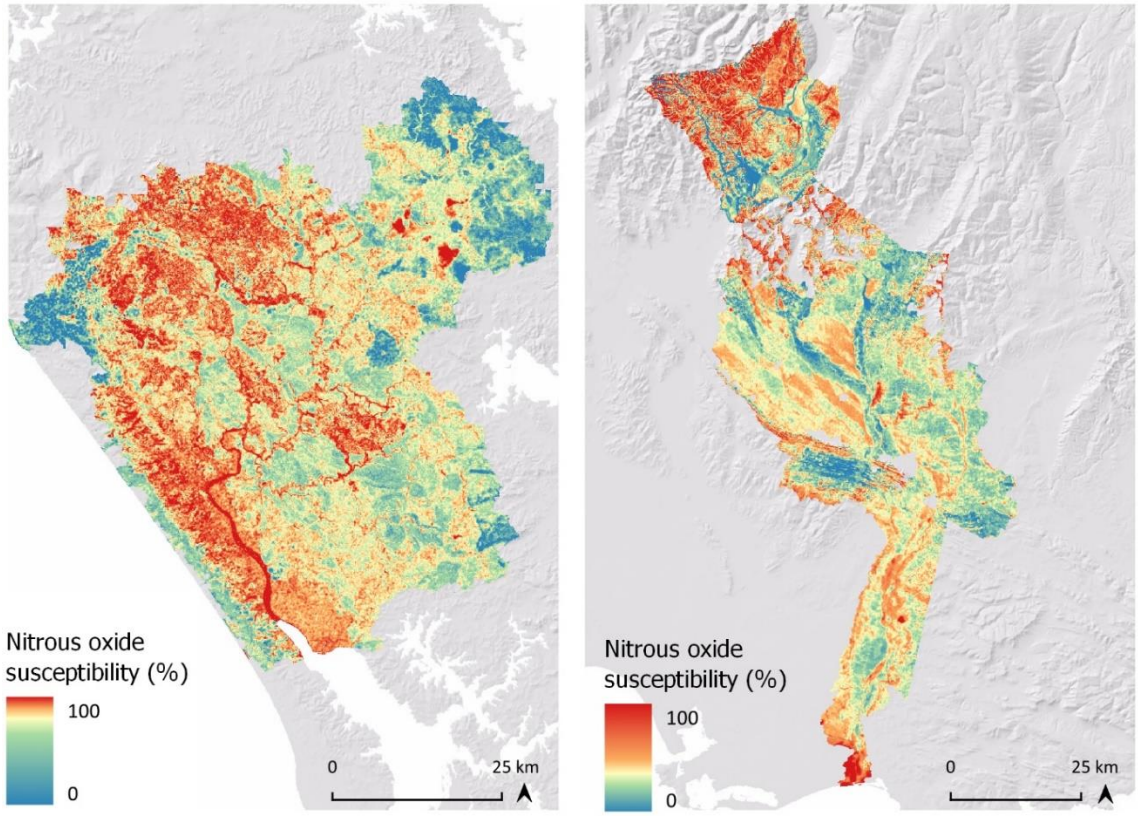

Figure A.23. The landscape susceptibility classification for soil zone nitrous oxide for the Wairoa and Mataura.

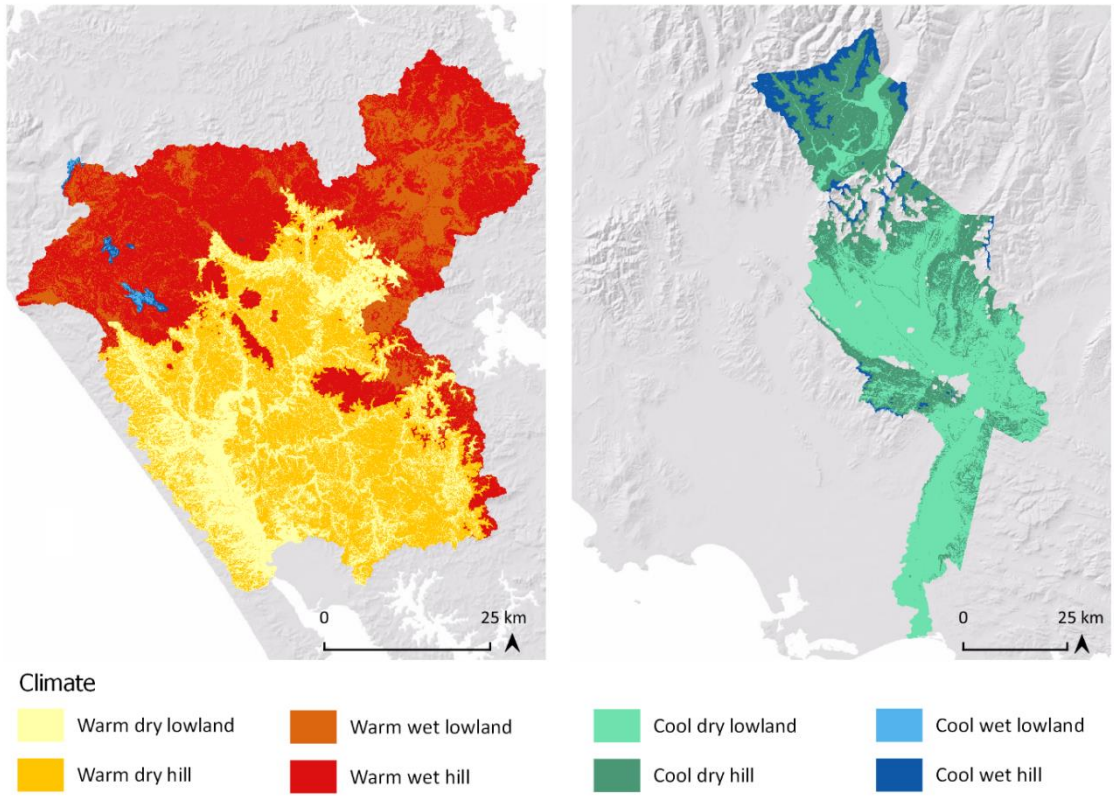

Figure A.24. The climate classification for the Wairoa and Mataura where warm is ≥ 12°C mean annual temperature and cool >12°C, dry is ≤500 mm effective rainfall and wet is >500 mm. A slope threshold of 8°discrimnates lowland from hill classes.

This work does not seek to estimate nitrous oxide emissions. Rather it seeks to identify the inherent susceptibility of the landscape to soil zone nitrous oxide generation, independent of land use. The work of Giltrap et al. (2010, 2013) provides a process based methodology that was used to estimate soil nitrous oxide emissions across New Zealand, with historic soil survey (1:50,000) forming the biophysical basis for emissions estimation. The work of Giltrap et al. identified the high uncertainties in soil nitrous oxide emission factors were primarily due to the high uncertainty of the soil parameters within the selected soil categories and that uncertainty in soil parameters contributed much more to the uncertainty in N_2O emissions than the inter-annual weather variability. The need for more resolved soil maps as a means to reduce uncertainty in N_2O emissions estimates supports the need for paddock and often sub-paddock scale variability in the landscape factors that control variability in soil GHG emissions and water quality.

Step 8. Scaling and categorisation of susceptibility models

The preferred (Step 6) susceptibility rasters were scaled from 0 - 100 (lowest to highest susceptibly). Quantiles were then used to subdivide each landscape susceptibility map into 4 ordinal categories:

- Q1 = low susceptibility
- Q2 = moderately low susceptibility
- Q3 = moderate susceptibility
- Q4 = high susceptibility

where each quartile incorporates 25% of the pixels. The susceptibility thresholds for each quantile differ for each region and for each water quality measure (Table A.6).

Table A.6. Quartile thresholds for the Wairoa and the Mataura susceptibility models.

	1st Quantile	2nd Quantile	3rd Quantile	Mean
Wairoa				
N_2O	66.4	80.6	90.1	74.3
NNN	9.9	19.4	33.6	25.7
TKN	34.9	54.2	75.0	54.4
PP	24.8	45.7	65.0	45.5
DRP	74.8	87.3	95.3	80.0
TSS	67.5	81.5	92.7	76.0
Turbidity	24.9	45.9	65.2	45.6
E.coli	24.8	45.7	65.0	45.4
Mataura				
N_2O	25.0	36.3	49.0	38.9
NNN	51.0	63.7	75.0	61.1
TKN	3.2	9.9	38.7	23.8
PP	9.2	18.1	47.5	30.2
DRP	17.4	27.7	42.1	32.2
Turbidity	41.0	60.2	71.2	54.7
E.coli	30.1	42.7	55.2	42.2

The differences in susceptibility thresholds between each catchment are consistent with the dominant water quality issues for each catchment. For example, nitrate-nitrite-nitrogen is not a significant water quality issue across either Northland or the Wairoa Catchment, due to the large area of reducing soils and lithologies. Rather, the large area of reducing soils and lithologies favours soil zone nitrous oxide, ammoniacal and organic nitrogen loss and dissolved reactive phosphorus loss. With regard to the high dissolved reactive phosphorus susceptibility, the large area of P-rich basalts of the Tangihua Complex also play an important role. Susceptibility to sediment loss is also elevated across the Wairoa Catchment. These patterns are consistent with regional water quality network data (Rissmann et al., 2018; Pearson and Rissmann, 2020; Rissmann and Pearson, 2020)[35]. Due to warm moist climate and large area of fine texture and imperfectly to poorly drained soils, soil zone nitrous oxide susceptibility is elevated across a significant area of the Wairoa Catchment.

Across the Mataura Catchment nitrate-nitrite-nitrogen susceptibility is significant (at least within the area with radiometric coverage). This reflects larger areas of well drained and artificially drained soils that favour nitrate-nitrite generation and export. A greater area of well drained soils with moderate to high permeability equates to a lower inherent landscape susceptibility to soil zone nitrous oxide emission (Figure 8). The cool dry lowland climate is another controlling factor that limits the landscapes' susceptibility to soil zone nitrous oxide emissions across the Mataura Catchment.

Landscape susceptibility to *E.coli* loss[36] is challenging, due to the complexity of environmental controls and low natural abundances in natural state areas. The models of *E.coli* susceptibility were the worst performing and the most challenging to explain. However, it only takes a small amount of *E.coli* to exceed national guidelines.

Different controlling landscape factors will result in different water quality and soil nitrous oxide related issues. For example, dissolved reactive phosphorus, nitrous oxide, and sediment are the main susceptibilities for the Wairoa Catchment, whereas nitrate-nitrite-nitrogen dominates the Mataura.

The main differences in landscape susceptibility between the two catchments is thought to reflect different geological and climatic histories and as a result a different pattern of controlling landscape factors. Specifically, the Mataura Catchment is geomorphically youthful, with numerous cycles of glacial activity over the Quaternary geological epoch, generating large volumes of sediment from Alpine areas and depositing these across the lowland areas of the Mataura Catchment. Mudstones are largely absent from the Mataura as are basalts. Felsic sedimentary and metamorphic (schist) lithologies dominate, with small areas of ultramafic rock (e.g., Livingstone Volcanics) and large areas of loess-mantled alluvial floodplains. The relatively youthful and permeable alluvial gravel deposits of the Mataura Catchment are overlain by loess. Loess thickness varies with alluvial surface age and proximity to the Mataura River and its floodplain. Large areas of peat wetland occur within the recent (Quaternary) floodplain of the Mataura River and at its southernmost extent. This generalised setting favours nitrate-nitrite-nitrogen susceptibility, relative to the Wairoa Catchment.

The Northland landscape is old and highly weathered, with no history of glaciation nor significant volcanic ash deposits. Approximately half of the catchment is characterised by weak and highly erodible sedimentary rocks, including large areas of erosion prone sand- and mudstones. Mudstones favour the development of poorly permeable clay-rich soils that are prone to runoff. The low permeability of local geologies and the fine texture and dominance of imperfect to poorly drained soils favours reducing conditions within soil and groundwater systems. Reducing conditions in turn favour denitrification, soil nitrous oxide production, and enhanced mobility of dissolved reactive phosphorus.

Ancient greywacke basement, Waipapa Group, also outcrops in the east and northeast of the Wairoa Catchment. These rocks are deeply weathered and prone to erosion. Weak sedimentary units, deep weathering, and fine textured and slowly permeable soils also favour mass wasting (e.g., slips, slumps, earth flows, soil creep) and fluvial erosion of the soil mantle. The weak sedimentary rocks of the Wairoa Catchment contrast with a large area of strong basaltic rocks that were rafted in (Tangihua Complex) or erupted through (Waipoua Basalt) and flooded over the top of the sedimentary sequence. These strong rocks are characterised by lower susceptibility to mass wasting processes and their attendant sediment generation, except where they overlie weak sedimentary units. Petrochemical data suggests that the basaltic rocks of the Tangihua Complex and Waipoua Basalts contain naturally elevated concentrations of inorganic P and inferred susceptibility to dissolved reactive phosphorus loss. Elevated landscape susceptibility to dissolved reactive phosphorus, is therefore thought to reflect a combination of reducing lithologies and soils and rock units with naturally elevated inorganic P concentrations.

[36] *E. coli* being a proxy for microbial pathogens.

Step 9. Statistical testing of the association between landscape susceptibility categories and historical datasets of controlling landscape factors

Given the experimental nature of this work, it was important to test if the property scale landscape susceptibility maps make sense in terms of historical representations of geological (Q-Map) and soil (S-Map/FSL) surveys. Despite differences in the resolution and inferred distribution of controlling landscape factors between the high-resolution datasets and historic soil and geological survey, a component of agreement – at least at a high level was anticipated.

To test the association between landscape susceptibility categories and historical topographic and geological survey sub-catchment areas were selected for the Wairoa and Mataura catchments (Figure A.25), namely:

Wairoa:

- Tangihua area
- Whakapara area

Mataura:

- Mid-Mataura
- Upper Mataura

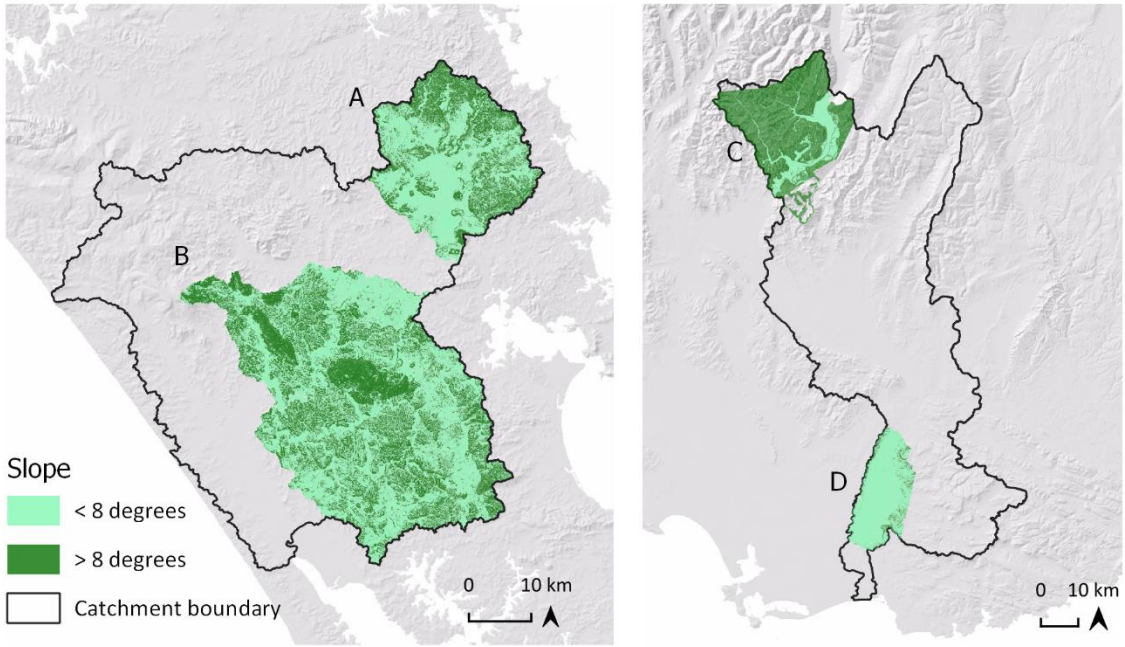

Figure A.25. Association testing areas. Left Wairoa Catchment, Northland. A = Whakapara Area, B = Tangihua Area. Right Mataura Catchment, Southland. C = upper-Mataura area, D = mid-Mataura area.

These areas were selected as they represent physiographic 'endmembers,' for each respective catchment i.e., each area is characterised by different combinations of controlling landscape factors. Subdividing these by physiographic setting provides landscape context to the results of statistical testing. The susceptibility rasters for each area were clipped and vectorised. Vectorising a raster file involves joining all adjacent pixels of the same category to produce an irregular shape or polygon. For every polygon (Table A.7), overall mean scores of elevation and slope, numeric soil (FSL and S-Map) and geological (Q-Map) factors were computed. Mean scores for per cent overland flow of

effective runoff (OLF %), soil profile drainage (vertical percolation), artificial drainage, soil reduction potential, and geological reduction potential were also calculated using the Physiographic Environments of New Zealand (PENZ) layers (Pearson and Rissmann, 2021). The PENZ layers are based on 1:50,000 LRI and S-Map and, to a lesser degree, the 1:250,000 Q-Map series; as such, they have the exact resolution as the layers they are derived from. The Real Centroid plugin in QGIS was used to assign geological or soil descriptors (string) to each polygon, for example Main Rock, Rock Class, Rock Group, Stratigraphic Age, Soil Type (NZSC), Soil Series and other to each polygon.

Table A.7. Number of susceptibility polygons by sub catchment area for the Wairoa and Mataura catchments.

	Count DRP susceptibility	Count Turbidity susceptibility	Area (ha)
Tangihua	5,980	5,501	136,940
Whakapara	5,426	2,160	53,098
Wairoa Total	11,406	7,661	190,038
	Count NNN susceptibility	Count PP susceptibility	Area (ha)
Upper-Mataura	35,835	31,043	77,782
Mid-Mataura	1,510	4,354	36,483
Mataura Total	37,345	35,397	114,265

The tabulated data were ranked and z-scored using the inverse-normal transformation function in excel prior to application of Welch's Analysis of Variance (ANOVA)[37]. One-way analysis of variance determines whether differences between the means of at least three groups are statistically significant. Welch's ANOVA was preferred as it can be used when data violates the assumption of homogeneity of variance, which is common issue of environmental datasets. The Games-Howell non-parametric test was then applied to all Welch's ANOVA runs that produced statistically significant results, using the raw untransformed data[38]. An alpha level of 0.05 was specified for both tests, with a secondary alpha of 0.15 also applied to the Games-Howell post-hoc significance tests.

For both Welch's ANOVA and Games-Howell post-hoc test, geological unit and susceptibility class were utilised as the grouping factors to test if numeric scores of historical soil (FSL and S-Map), geological (Q-Map), and the Physiographic Classification of New Zealand (PENZ) dataset varied in a predictable manner. Specifically, we sought to test whether there was evidence for:

1. A systematic and expected pattern of association between geological unit and susceptibility classes and controlling landscape factors that are consistent with previous physiographic classifications and physiographic knowledge of the Northland and Southland regions, and;
2. Predictable and statistically significant differences in the controlling landscape factors, provided by historic soil and geological survey, between susceptibility classes.

A summary of the controlling landscape factors tested and the results of Welch's ANOVA are summarised in Table A.7. **The results of Games-Howell post-hoc tests for each subcatchment of the**

[37] Welch's ANOVA was preferred as it can be used when data violates the assumption of homogeneity of variance (Toothaker, 1993; Kirk, 2012).

[38] The Games-Howell post-hoc test is a non-parametric approach to compare combinations of groups or treatments. It is similar to Tukey's test in its formulation. However, the Games-Howell test does not assume equal variances and sample sizes. The test was designed based on Welch's degrees of freedom correction and uses Tukey's studentised range distribution. The Games-Howell test is performed on the ranked variables and does not rely on equal variances and sample sizes, it is often recommended over other approaches such as Tukey's test.

Wairoa and Mataura catchments are presented in Technical Appendix E and provide strong evidence in support of points 1 and 2 above. Further, association testing is being undertaken as part of the AgMARDT funded project for the Mataura Catchment.

Table A.8. Association testing for areas within the Wairoa and Mataura catchments.

Susceptibility Layer (0.16 ha)	Subcatchment	Historical soil, geological, and PENZ controlling landscape factors (1:50,000 to 1:250,000 scale)	Welch's ANOVA results
Nitrate-nitrite-nitrogen	mid-Mataura, upper-Mataura	Soil drainage class, soil reduction potential (SRP), slope, and rock class.	All test were statistically significant at 0.05.
Particulate phosphorus	mid-Mataura, upper-Mataura	Slope, soil reduction potential (SRP), percent overland flow (OLF) of effective precipitation, depth to a slowly permeable horizon.	All test were statistically significant at 0.05.
Sediment	Tangihua, Whakapara	Geological unit, slope, elevation, soil reduction potential, geological reduction potential, soil P-retention class, depth to slowly permeable soil horizon.	All test were statistically significant at 0.05.
Dissolved reactive phosphorus	Tangihua, Whakapara	Geological unit, slope, elevation, soil reduction potential, geological reduction potential, soil P-retention class, depth to slowly permeable soil horizon.	All test were statistically significant at 0.05.

Step 10. Overall susceptibility class (typology)

Following association testing, an overall susceptibility class was generated by computing the quantile susceptibility class for each water quality contaminant and soil zone nitrous oxide at a pixel-by-pixel level. This involved stacking each quantile susceptibility raster in the following order to create a unique code (barcode): N_2O-NNN-OAMN-PP-DRP-TURB-*E.coli*. For example, a barcode of 4134321 indicates the following order of susceptibility: N_2O = 4 (High); NNN = 1 (Low); OAMN = 3 (Moderate); PP = 4 (High); DRP = 3 (Moderate); Turbidity = 2 (Moderately low); *E.coli* = 1 (Low). A barcode of 1111111 for a pixel in the integrated classification indicates all susceptibility scores are in the low quantile for the respective catchment.

The barcode was subsequently converted from raster layer to a vector polygon to support the multiple fields of the integrated classification. Risk typologies for nitrogen species, phosphorus species, sediment and pathogens were generated by selecting those contaminants with a score of 5 to identify the highest risk contaminants in each polygon (Figure 10 and 11). This layer allows the user to identify and symbolise risk for a single contaminant, or high-risk areas with contaminant species and form. Importantly, there were very few classes where a single contaminant dominates, or where there is uniformly low or uniformly high landscape susceptibility for all contaminants.

This is just one way of presenting a combined susceptibility classification and outputs can be presented in alternative ways to best suit the needs of the PCE and other users. We would recommend the use of the continuous scaled susceptibility layers to best inform catchment prioritisation and land use change modelling (see Technical Appendix E).

References

Ashok, D., Scott, J., Wetzel, S., Panju, M., & Ganesh, V. (2020). Logic guided genetic algorithms. arXiv preprint arXiv:2010.11328.

Bartlett, R. J., & James, B. R. (1993). Redox chemistry of soils. Adv. Agron, 50(151208), 7.

Breiman, L. (2001). Random forests. Machine learning, 45(1), 5-32.

Burnham, K. P., & Anderson, D. R. (2004). Multimodel Inference: Understanding AIC and BIC in Model Selection. Sociological Methods and Research 33:261–304.

Crops for Southland. 2002. Topoclimate Southland Soil Map. Venture Southland.

Giltrap, D. L., Li, C., & Saggar, S. (2010). DNDC: A process-based model of greenhouse gas fluxes from agricultural soils. Agriculture, Ecosystems & Environment, 136(3-4), 292-300.

Giltrap, D. L., Ausseil, A. G. E., Thakur, K. P., & Sutherland, M. A. (2013). Investigating a method for estimating direct nitrous oxide emissions from grazed pasture soils in New Zealand using NZ-DNDC. Science of the Total Environment, 465, 7-16.

JMP®, Version 16.2. SAS Institute Inc., Cary, NC, 1989–2021.

Kirk, R.E. (2012). Experimental design: Procedures for the behavioural sciences. Sage Publications.

Krause, P., Boyle, D. P., & Bäse, F. (2005). Comparison of different efficiency criteria for hydrological model assessment. Advances in geosciences, 5, 89-97.

Li, Z., Zeng, Z., Song, Z., Tian, D., Huang, X., Nie, S., & Niu, S. (2022). Variance and main drivers of field nitrous oxide emissions: A global synthesis. Journal of Cleaner Production, 131686.

Nash, J. E., & Sutcliffe, J. V. (1970). River flow forecasting through conceptual models part I—A discussion of principles. Journal of hydrology, 10(3), 282-290.

Pearson, L., & Rissmann, C. (2020). Application of Physiographic-based modelling to estimate contaminant load to the Hokianga Harbour.

Pearson, L. and Rissmann, C. (2021). Physiographic Environments of New Zealand: Inherent susceptibility of the landscape for contaminant loss. Land and Water Science Report 2021/25. p60.

QGIS.org, 2022. QGIS Geographic Information System. QGIS Association. http://www.qgis.org

R Core Team (2017). R: A language and environment for statistical computing. R Foundation for Statistical Computing, Vienna, Austria. URL https://www.R-project.org/.

Rissmann, C.W.F., Pearson, L.K., Beyer, M., Couldrey, M.A., Lindsay, J.L., Martin, A.P., Baisden, W.T., Clough, T.J., Horton, T.W. & Webster-Brown, J.G. (2019). A hydrochemically guided landscape classification system for modelling spatial variation in multiple water quality indices: Process-attribute mapping. Science of the Total Environment, 672, pp.815-833.

Smits, G. F., & Kotanchek, M. (2005). Pareto-front exploitation in symbolic regression. In Genetic programming theory and practice II (pp. 283-299). Springer, Boston, MA.

Snelder, T., Biggs, B., and Weatherhead, M. (2010). New Zealand River Environment Classification User Guide. Ministry for the Environment, ME 1026.

Sutherland, R. A., Van Kessel, C., Farrell, R. E., & Pennock, D. J. (1993). Landscape-scale variations in plant and soil nitrogen-15 natural abundance. Soil Science Society of America Journal, 57(1), 169-178.

Toothaker, L.E. (1993). Multiple comparison procedures (No. 89). Sage.

TuringBot Software. (2022). Avenida Paulista 807 23º Andar, Conj. 2315 Bela Vista 01311915 São Paulo, SP Brazil https://turingbotsoftware.com

Westerhoff, R., White, P., & Miguez-Macho, G. (2018). Application of an improved global-scale groundwater model for water table estimation across New Zealand. Hydrology and Earth System Sciences, 22(12), 6449-6472

Technical Appendix B. Land use and landscape susceptibility outputs

This technical appendix provides a summary of the land use maps that will be used by the PCE to support land use change modelling. A section on the derivation of satellite derived Gross Primary Production (GPP), which was utilised as one of three land use intensity models for removing the effect of land use, is also provided (Step 3 in Technical Appendix A).

Literature Review on Contaminant Yields from Agriculture and Forestry

Land use pressure and the inherent susceptibility of a landscape are the two major controls over environmental contamination. Here different land uses, stock unit densities, and estimated yields of nitrogen, phosphorus, sediment, and *E. coli* are presented for each land use type. The estimated loss rates for these contaminants vary between land uses. Tables B.1 to B.4 represents the estimated yields of nitrogen, phosphorus, sediment, and *E. coli* for six major land use classes, reported for New Zealand (Ledgard, 2013).

Table B.1. Nitrogen yields from different land use types in New Zealand. Data gathered from a systematic review of New Zealand literature on contaminant losses.

Land use	loss (kg/ha/yr)		Location	Reference
	Mean	Range		
Cropland – annual	45	10-140	Canterbury, NZ wide	Ledgard, 2013; Monaghan et al., 2010; Srinivasan et al., 2021; Thriving Southland and Land Pro.
Dairy	40	22-100	NZ wide	Srinivasan et al., 2021; Thriving Southland and Land Pro
Deer	9.5	7-12	NZ wide	Srinivasan et al., 2021
Indigenous vegetation	2	1-7.1	NZ wide	Srinivasan et al., 2021
Drystock (Beef and Sheep)	11.5	4-40	NZ wide	Srinivasan et al., 2021
Plantation Forestry	2	0.5-5	NZ wide	Ledgard, 2013

Table B.2. Phosphorus yields from different land use types in New Zealand. Data gathered from a systematic review of New Zealand literature on contaminant losses.

Land use	loss (kg/ha/yr)		Location	Reference
	Mean	Range		
Cropland – annual	1	0.1-2.9	NZ wide	Srinivasan et al., 2021
Dairy	1.3	0.6-1.9	NZ wide	Srinivasan et al., 2021; McDowell et al., 2020
Deer	1.3	0.2-2.8	NZ wide	Srinivasan et al., 2021
Indigenous vegetation	0.3	0.1-0.6	NZ wide	Srinivasan et al., 2021
Drystock (Beef and Sheep)	0.9	0.3-1.6	NZ wide	Srinivasan et al., 2021; McDowell et al., 2020
Plantation Forestry	0.3	0.1-1.3	Southland, NZ wide	Ledgard, 2013; Monaghan et al., 2007; Srinivasan et al., 2021

Table B.3. Sediment yields from different land use types in New Zealand. Data gathered from a review of New Zealand literature on contaminant losses.

Land use	loss (kg/ha/yr)		Location	Reference
	Mean	Range		
Cropland – annual				
Dairy	247	60-330	NZ wide	Ledgard, 2013; McDowell and Wilcock, 2008
Deer	1567	1000-2034	NZ wide	Ledgard, 2013; McDowell and Wilcock, 2008
Indigenous vegetation	163	27-320	NZ wide	Monaghan et al., 2010
Drystock (Beef and Sheep)	877	598-1156	NZ wide	McDowell and Wilcock, 2008
Plantation Forestry	767	34-500	NZ wide	Ledgard, 2013; Monaghan et al., 2010

Table B.4. E. coli yields from different land use types in New Zealand. Data gathered from a systematic review of New Zealand literature on contaminant losses. With CFU/h/yr unit.

Land use	loss (CFU/ha/yr)		Location	Reference
	Mean	Range		
Cropland – annual				
Dairy	8.54×10^{10}		NZ wide	McDowell and Wilcock, 2008
Deer	1.8×10^{11}		NZ wide	McDowell and Wilcock, 2008
Indigenous vegetation				
Drystock (Beef and Sheep)	8.6×10^{9}		NZ wide	McDowell and Wilcock, 2008
Plantation Forestry				

Land Use Map and Pastoral Grazing Pressure

Two major sets of data are used as a proxy for land use in New Zealand: Land Use Carbon Analysis System (LUCAS; Ministry for the Environment, 2020) and Land Cover Database (LCDBv5; Manaaki Whenua Landcare Research, 2019). To classify land use in this study, these data sets are combined with the following to generate a property scale land use pressure layer with estimates of stock units and effective hectares:

1. NZ Property Titles (Land Information New Zealand, 2021)
2. NZ Livestock numbers grid APS (Livestock_grid, Ministry for the Environment and Statistics New Zealand, 2017)
3. Physiographic Environments of New Zealand (Pearson and Rissmann, 2021)

In the Mataura catchment, Environment Southlands Land Use map was also used to inform land use classes (Pearson and Couldrey, 2016). This data source has more information over stock type and is retained with the Mataura catchment dataset. Figure B.1 describes the steps conducted to generate the Land Use Pressure layer, with the resultant land use maps presented in Figure B.2 for the Wairoa catchment, Northland, and Figure B.3 for the Mataura catchment, Southland. It is worth noting that we base our analysis on a general assumption that High-producing Grasslands (HpG) has 1.5 times more capacity to feed stock than Low-producing Grasslands (LpG). In other words, we assume that 1 km^2 of HpG host 1.5 times more stock-units than 1 km^2 of LpG.

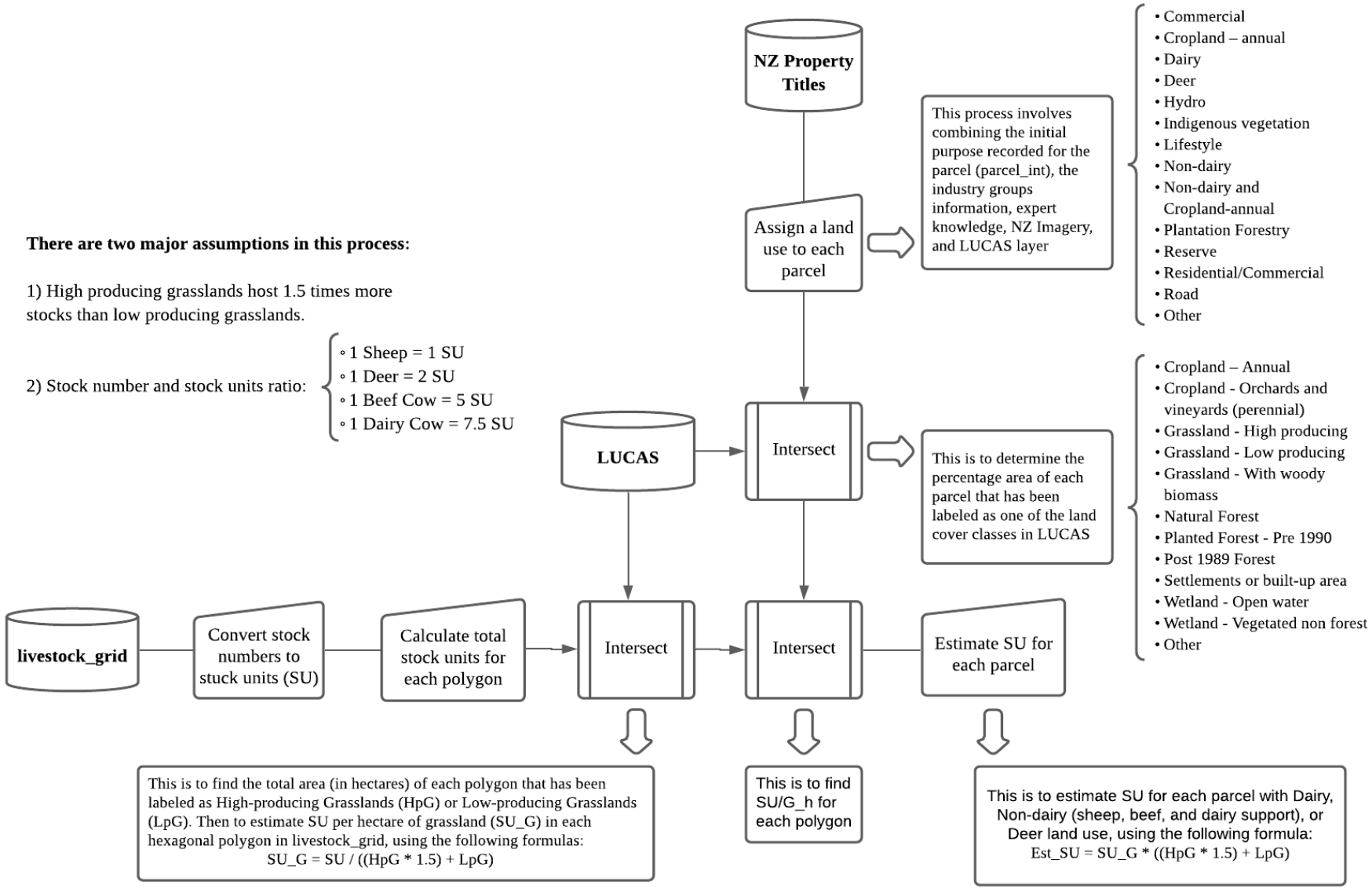

Figure B.1. A flowchart diagram describing the steps to generate the Land Use Pressure layer.

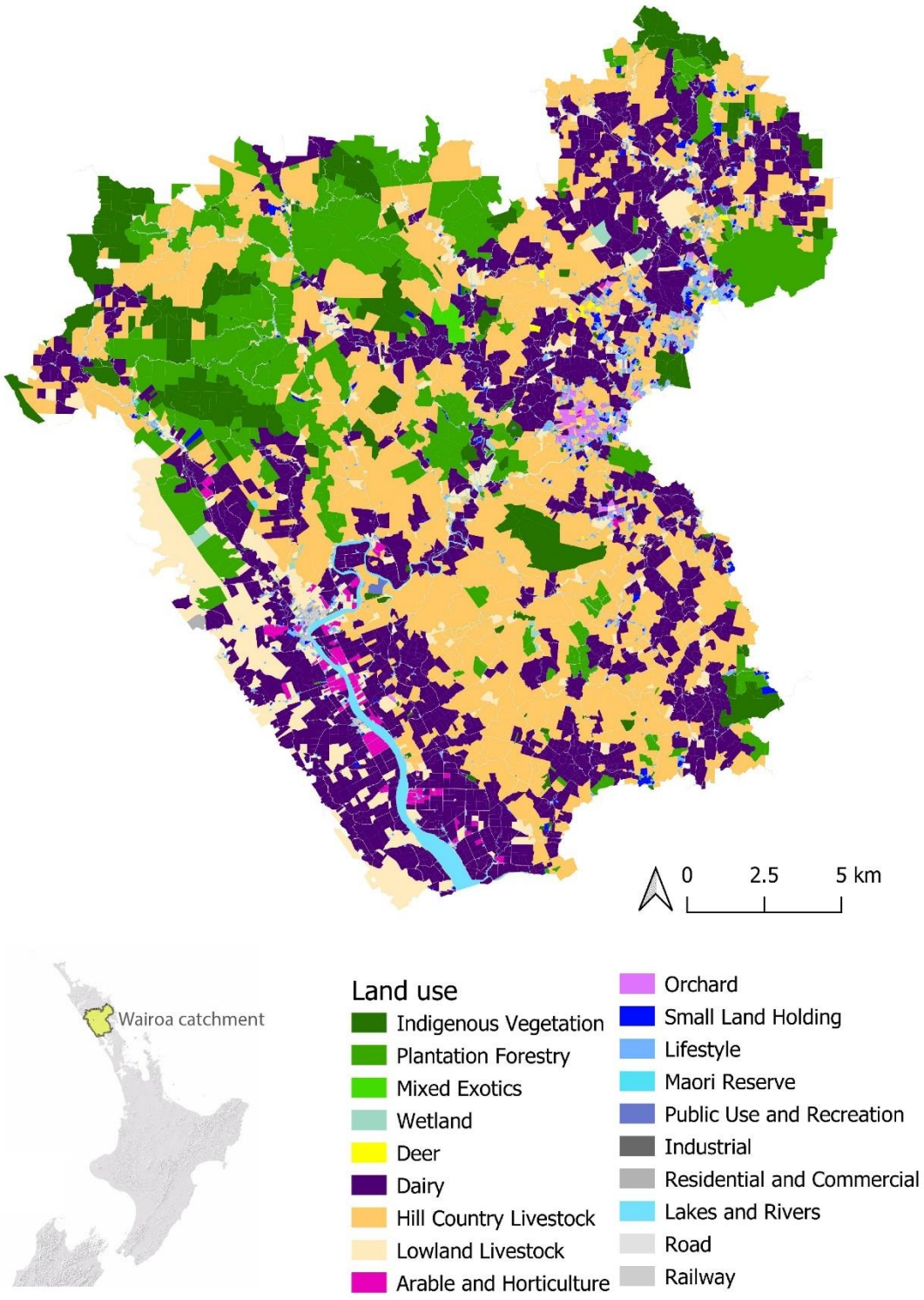

Figure B.2. Land use in the Wairoa catchment, Northland.

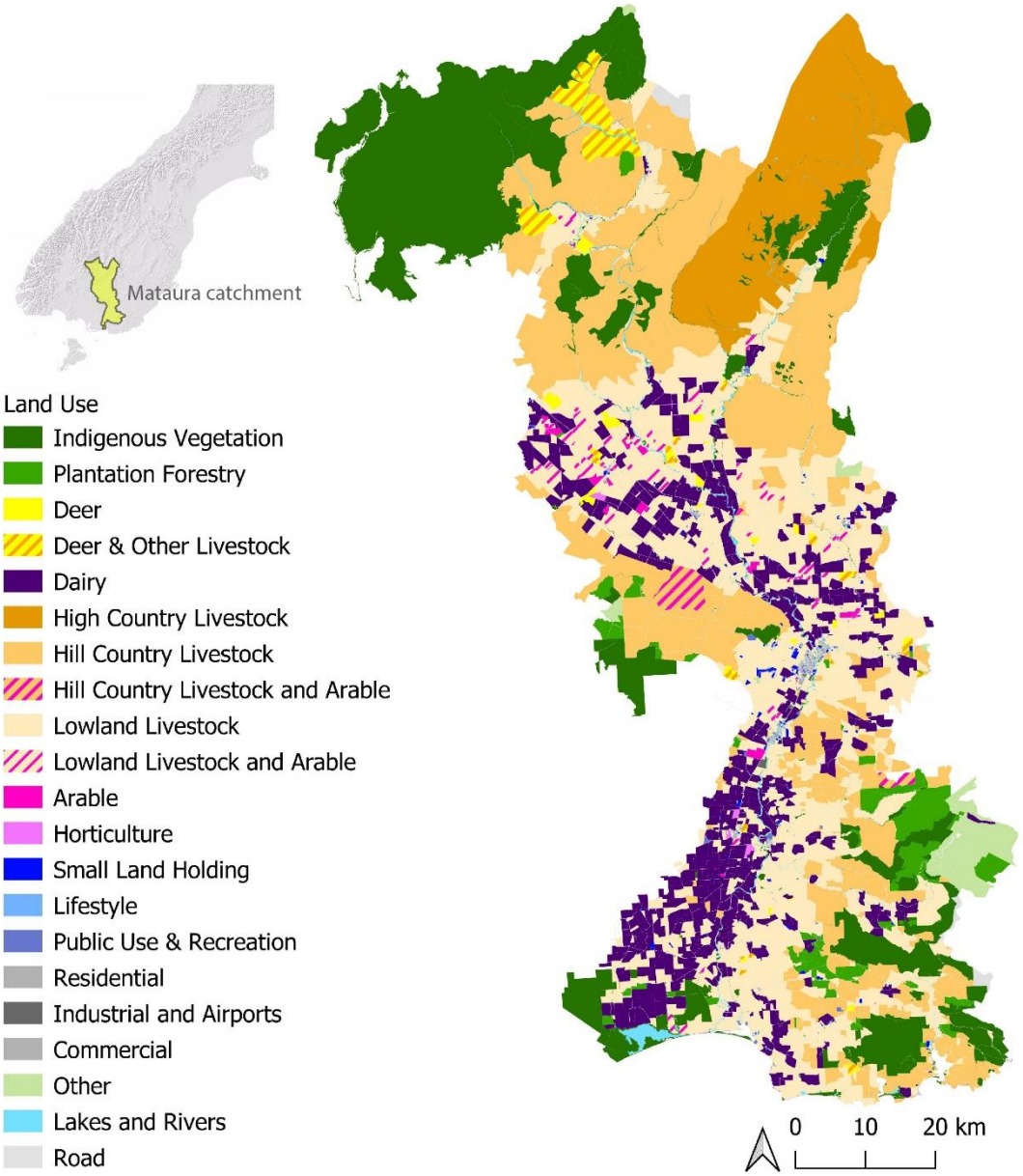

Figure B.3. Land use in the Mataura catchment, Southland.

The total number of land parcels by enterprise type and their respective area is summarised in Figure B.4 for both catchments.

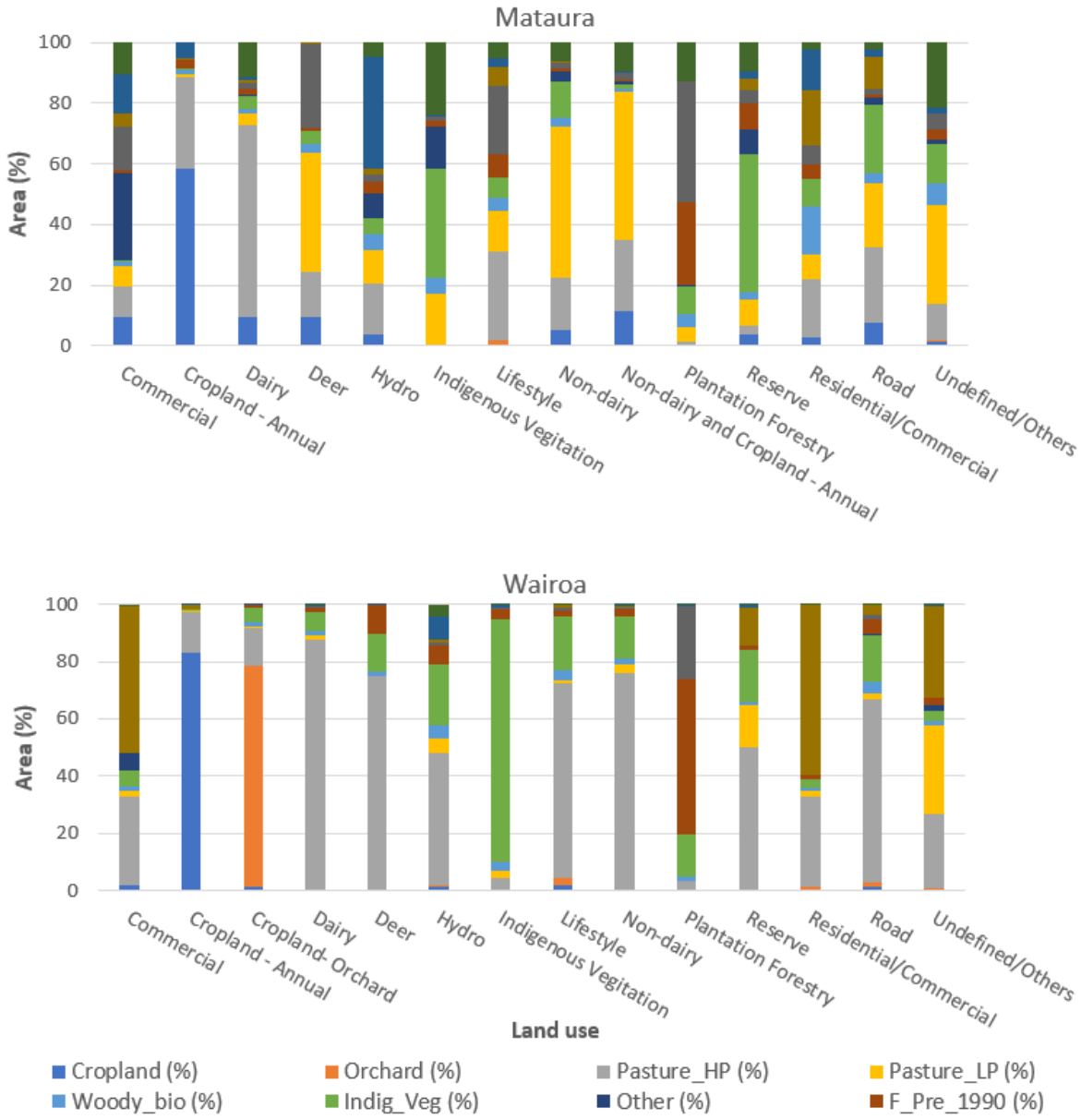

Figure B.4. The total area of parcels in each land use class, labelled with different land cover classes in LUCAS for each study area.

A detailed land use survey completed by farmers across Wendonside Catchment, Northern Southland in 2021, was used to validate stocking rate estimates (Figure B.5). The estimated versus reported stocking rates were within 5%. Within the Wairoa Catchment, primary industry bodies were used to validate the spatial accuracy of the land use layer.

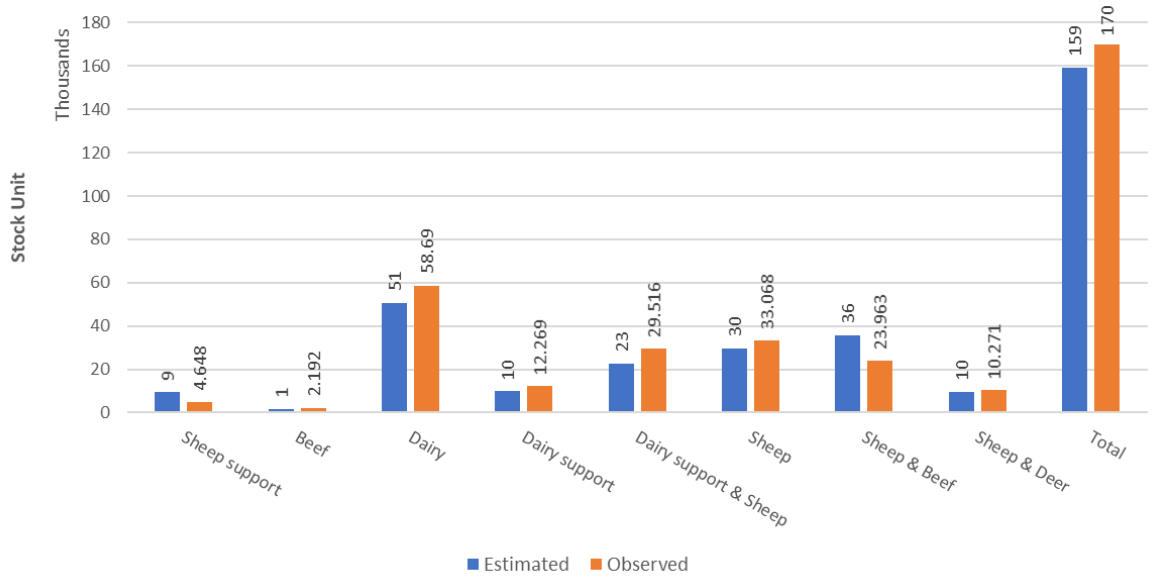

Figure B.526. A comparison between the estimated and reported (observed) stock units for northern Southland (northern Southland catchment groups).

Gross Primary Production

Spectral information of Copernicus Sentinel-2 satellite data (processed by the European Space Agency) can be used for estimating nitrogen uptake by vegetation providing a measure of gross primary production (Sharifi, 2020). Assessment of various spectral indices against plant nitrogen content indicate that a simple red-edge ratio is the best performing index. For example, in a 3-year project measuring maize nitrogen uptake across three different locations and growing conditions, Sharifi (2020) identified a R^2 = 0.91 and RMSE = 11.34 kg/N/ha. This and other studies of a wide range of production systems, climate settings, and landscapes support the potential of the spectral analysis of simple red-edge ratio as a strong proxy for plant N content (see Berger et al., 2020).

There are various satellite derived vegetation indices (see Chenzong, et al., 2017; Xing et al., 2021). Among these indices, the normalised difference vegetation index (NDVI), is the most common measure of vegetation cover (see Huang et al., 2021). However, NDVI is also known to saturate fast when the vegetation is dense, which is often the case in New Zealand. In this study, we use the near-infrared reflectance of vegetation (NIRv) to address saturation limitations of NDVI and generate a high-resolution proxy of land use intensity (see Camps-Valls et al., 2021). NIRv is the product of total scene NIR reflectance (NIRT) and NDVI, which is calculated as follows (Badgley et al., 2017):

$$NIRv = ((NIR - Red) / (NIR + Red))* NIR \quad \text{(Eq. B1)}$$

To derive the NIRv for the spring – summer (October – March = S_NIRv) and autumn through winter (May – August, W_NIRv) for both catchments, the Google Earth Engine was implemented to:

- Create a Sentinel-2 Surface Reflectance (S2SR) collection for summer and winter across each study area. Note that each Sentinel-2 image is a composite of several images (i.e., the winter composite is comprised of approximately 18 images, where each image is a stack of 12 raster layers corresponding to 12 bands in Sentinel-2).
- Each composite is built from 80% cloud-free data, with any pixels obscured by cloud and clouds' shadows removed from the resulting composite.

- The median cloud-free pixels from all images are combined to generate a cloud-free composite image for each season.
- The NIRv formula (Eq. B1) is applied to Summer and Winter composites, see Table B.5 for a list of bands in Sentinal-2 imagery.
- The S_NIRv and W_NIRv layers were downloaded.

Table B.5. Band spatial resolution, central wavelength and bandwidth of the Sentinel-2 image.

Band	Spatial Resolution	Central Wavelength (µm)	Description
B1	60 m	0.44	Ultra-blue (Coastal and Aerosol)
B2	10 m	0.49	Blue
B3	10 m	0.56	Green
B4	10 m	0.66	Red
B5	20 m	0.70	Visible and Near Infrared (VNIR)
B6	20 m	0.74	Visible and Near Infrared (VNIR)
B7	20 m	0.78	Visible and Near Infrared (VNIR)
B8	10 m	0.84	Visible and Near Infrared (VNIR)
B8a	20 m	0.86	Visible and Near Infrared (VNIR)
B9	60 m	0.94	Short Wave Infrared (SWIR)
B10	60 m	1.37	Short Wave Infrared (SWIR)
B11	20 m	1.61	Short Wave Infrared (SWIR)
B12	20 m	2.19	Short Wave Infrared (SWIR)

After obtaining the S_NIRv and W_NIRv, mean winter and summer NIRv scores were calculated for each polygon for each regional PLM. Mean scores were also calculated for each of the 145 capture zones across Southland and Northland. To assess the statistical significance of the NIRv as a proxy of land use intensity, a constant was added to any negative values and all scores were log10 transformed and reverse, stepwise, regression applied.

Median NNN and *E. coli* for the 145 long-term monitoring sites were regressed against 10 different variables, one at a time, to find the best single predictor that can represent the land use intensity (2018-2020). *E. coli* and NNN were chosen as they are considered strong indicators of land use intensity.

Following is a list of the model fit parameters and a concise description from Dormann (2020):

- Residuals: The residuals are the difference between the observed *E. coli* and NNN values and the predicted *E. coli* and NNN by the model. The distribution of the residuals must be symmetrical around the mean value (0). Far residual values from zero, means that the model predicts certain points (either the upper or the lower limits, depending on the sign of the median) less accurately than other points in the observations (in simple words, the model is biased).
- Coefficient - estimate: The coefficients are two unknown constants that represent the intercept and slope terms in the linear model. A higher slope shows a stronger effect of a predictor on the response variable (i.e., median *E. coli* and NNN).

- Coefficient - t value: This is a measure of how many standard-deviations the coefficient estimate is from zero. A large t value from zero would suggest that the null hypothesis (i.e., that there is no relationship between NIRv and NNN/*E.coli*) can be rejected.
- Coefficient – p-value: This coefficient is calculated based on t value, indicating the probability of observing any value equal or larger than t. A small p-value shows that it is unlikely to observe a relationship between a predictor and *E. coli* or NNN due to chance. In the other words, p-value indicates how significant a variable is in predicting *E. coli* or NNN. Generally, a predictor with the p-value of 5% or less is considered significant.
- Residual standard error: This is a measure of the quality of a linear regression fit. every linear model in theory is assumed to contain an error term (ε) indicating that the response variable can almost never be perfectly predicted, in real world practices. The Residual Standard Error is the average amount that the observed *E. coli* or NNN deviates from the true regression line in the model.
- Multiple R-squared: This measure indicates that what percentage (between 0 and 1) of the variation within *E. coli* or NNN is explained by a predictor. In a simplistic interpretation, multiple R-squared shows how well our model is fitting the data. Although, a higher R-squared is more desirable, this measure alone should not be used to evaluate the model performance. This is because, adding more predictors to a model almost always increases the R-squared, even if they aren't related to *E. coli* or NNN in any way.
- F-statistic: This is a good indicator of whether there is a relationship between a predictor and *E. coli* or NNN. The further the F-statistic is from 1 the better it is. Like p-value, F-statistic is used to decide whether we can reject the null hypothesis (a.k.a. there is no relationship between a predictor and *E. coli* or NNN) or not.

Table B.6 demonstrates the above-described measures for simple regression models between *E. coli* or NNN and each predictor. Note that, according to these measures, NIRv performed better than the other 9 predictors for modelling *E. coli* or NNN. Table B.7 also shows that NIRv is the best predictor among these 10 variables for modelling *E. coli*. Figure B.6 shows the Residuals are normally distributed around the mean when regressing NNN and *E. coli* on NIRv. Figure B.7 provides an example of the NIRv in the Mataura catchment.

Table B.6. Simple regression model between NNN and each predictor at a time. The colour code indicates the preference, from high (dark blue) to low (light blue).

Covariates	Estimate	t value	Pr(>|t|)	RSE	R^2	F-statistic
Area	-5.538E-02	-6.630E-01	5.080E-01	1.002E+00	3.067E-03	4.400E-01
Elevation	-3.672E-01	-4.721E+00	5.550E-06	9.334E-01	1.348E-01	2.228E+01
Slope	-6.817E-01	-1.114E+01	2.000E-16	7.342E-01	4.647E-01	1.241E+02
TRI	-6.356E-01	-9.844E+00	2.000E-16	7.748E-01	7.748E-01	9.690E+01
DOSE	-4.744E-01	-6.444E+00	1.660E-09	8.834E-01	2.250E-01	4.153E+01
K	4.568E-01	6.140E+00	7.690E-09	8.927E-01	2.087E-01	3.771E+01
U	5.635E-01	8.157E+00	1.590E-13	8.290E-01	3.176E-01	6.654E+01
Th	5.184E-01	7.249E+00	2.410E-11	8.581E-01	2.687E-01	5.255E+01
Th/K	-6.556E-02	-7.860E-01	4.330E-01	1.001E+00	4.298E-03	6.173E-01
NIRv	7.377E-01	1.307E+01	2.000E-16	6.775E-01	5.442E-01	1.708E+02

Table B.7. Simple regression model between E. coli and each predictor at a time. The colour code indicates the preference, from high (dark blue) to low (light blue).

Covariates	Estimate	t value	Pr(>|t|)	RSE	R^2	F-statistic
Area	-5.119E-02	-1.168E+00	2.448E-01	4.000E-01	9.718E-03	1.364E+00
Elevation	-2.462E-01	-3.096E+00	2.375E-03	3.888E-01	6.450E-02	9.584E+00
Slope	-7.518E-02	-1.648E+00	1.015E-01	3.981E-01	1.917E-02	2.717E+00
TRI	-5.420E-02	-1.402E+00	1.632E-01	3.991E-01	1.394E-02	1.965E+00
DOSE	2.237E-01	2.388E+00	1.830E-02	3.939E-01	3.940E-02	5.701E+00
K	1.517E-01	1.716E+00	8.839E-02	3.977E-01	2.075E-02	2.945E+00
U	1.807E-01	2.223E+00	2.786E-02	3.950E-01	3.432E-02	4.940E+00
Th	2.438E-01	2.523E+00	1.278E-02	3.930E-01	4.378E-02	6.363E+00
Th/K	3.179E-01	1.364E+00	1.749E-01	3.993E-01	1.320E-02	1.860E+00
NIRv	1.783E+00	7.126E+00	5.110E-11	3.440E-01	2.676E-01	5.078E+01

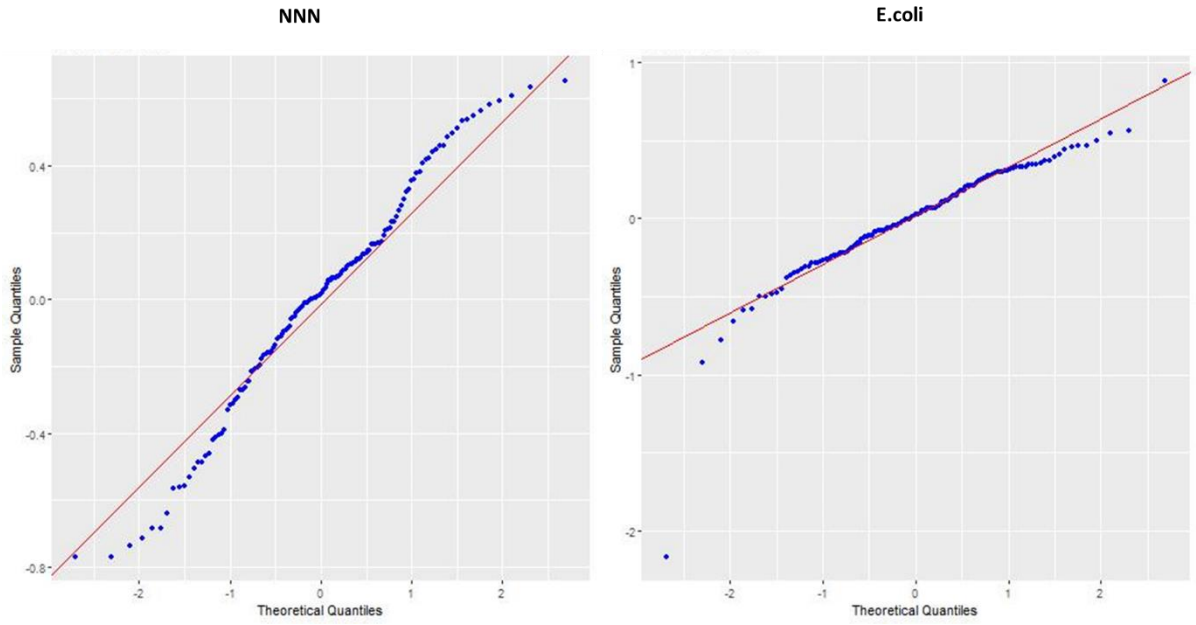

Figure B.6. Residual Normality Test for regressing NNN and E. coli on NIRv. The residuals in both models are normally distributed, which implies that the models predict all points in the observations with the same accuracy.

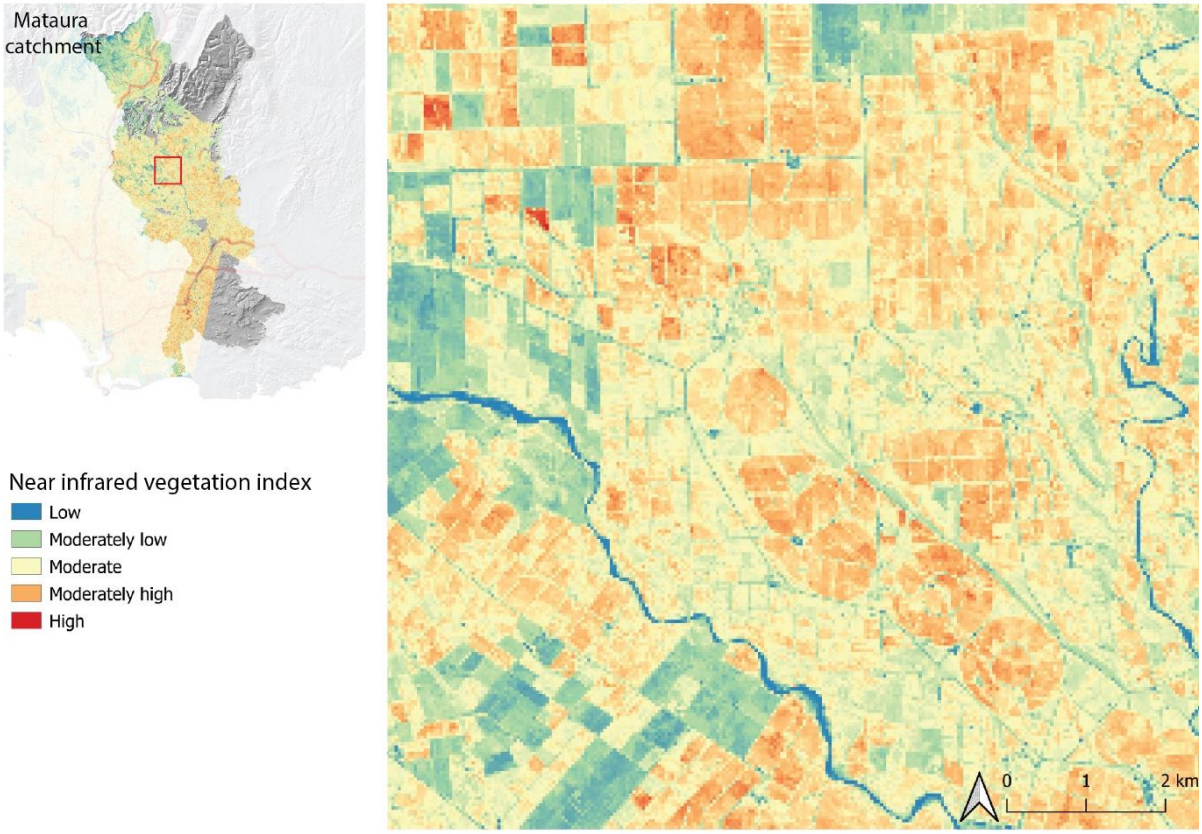

Figure B.7. Near infrared vegetation index (winter) for the Mataura Catchment. Where low is 0, moderately low is 1500, moderate is 3000, moderately high is 4500, and high is 6000 Gross Primary Production (GPP). The highest rates of GPP are associated with irrigated land (circular areas of centre pivots).

Land Use Intensity and Effective Farm Area

A strength of the above methods is the ability to estimate effective area, the area used for production, on a farm and relative stock unit intensity through both the StatsNZ reported stock data and a relative gross primary production measure according to the near infrared vegetation index. Figure B.8 shows the relative intensity of a property based on the average winter near infrared vegetation index. Effective farm area can be displayed by overlaying the land cover classification over the land use map.

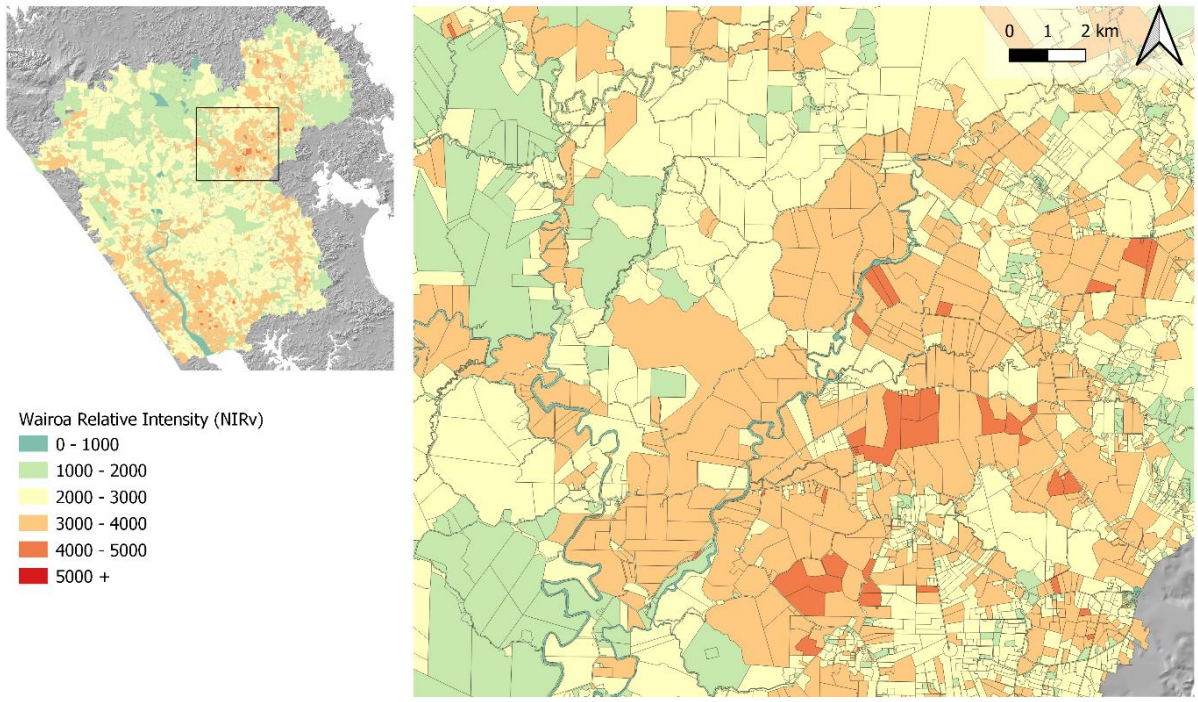

Figure B.8. Relative intensity as depicted by the winter average near infrared vegetation index for the Wairoa catchment.

References

Badgley, G., Field, C. B., Berry, J. A. (2017). Canopy near-infrared reflectance and terrestrial photosynthesis, Science Advances, 3(3).

Berger, K., Verrelst, J., Féret, J. B., Wang, Z., Wocher, M., Strathmann, M., ... & Hank, T. (2020). Crop nitrogen monitoring: Recent progress and principal developments in the context of imaging spectroscopy missions. Remote Sensing of Environment, 242, 111758.

Chenzong, L., Jinru, X., Baofeng, S. (2017). Significant Remote Sensing Vegetation Indices: A Review of Developments and Applications, Journal of Sensors, 1687-725X.

Dormann, C. F. (2020). Calibration of probability predictions from machine-learning and statistical models. Global Ecology and Biogeography, 29(4), 760-765.

Huang, S., Tang, L., Hupy, J.P. et al. (2021). A commentary review on the use of normalized difference vegetation index (NDVI) in the era of popular remote sensing. J. For. Res. 32, 1–6.

Land Information New Zealand. (2021). NZ Property Titles. https://data.linz.govt.nz/layer/50804-nz-property-titles/

Ledgard, G. (2013). Nitrogen, Phosphorus and Sediment losses from rural land uses in Southland. Environment Southland, Technical Report, (2013-7), 85.

McDowell, R. W., & Wilcock, R. J. (2008). Water quality and the effects of different pastoral animals. New Zealand Veterinary Journal, 56(6), 289-296.

McDowell, R. W., Monaghan, R. M., Smith, C., Manderson, A., Basher, L., Burger, D. F., ... & Depree, C. (2020). Quantifying contaminant losses to water from pastoral land uses in New Zealand III. What could be achieved by 2035?. New Zealand Journal of Agricultural Research, 1-21.

Ministry for the Environment and Statistics NZ. (2019). Livestock numbers grid APS 2017. https://data.mfe.govt.nz/layer/99906-livestock-numbers-grid-aps-2017/

Ministry for the Environment. (2020). LUCAS NZ Land Use Map 1990 2008 2012 2016 v008. https://data.mfe.govt.nz/layer/52375-lucas-nz-land-use-map-1990-2008-2012-2016-v008/

Monaghan, R. M., Wilcock, R. J., Smith, L. C., Tikkisetty, B., Thorrold, B. S., & Costall, D. (2007). Linkages between land management activities and water quality in an intensively farmed catchment in southern New Zealand. Agriculture, ecosystems & environment, 118(1-4), 211-222.

Monaghan, R. M., Semadeni-Davies, A., Muirhead, R. W., Elliott, S., & Shankar, U. (2010). Land use and land management risks to water quality in Southland. Report prepared for Environment Southland.

Manaaki Whenua Landcare Research. (2019). LCDB v5.0 - Land Cover Database version 5.0, Mainland New Zealand. https://lris.scinfo.org.nz/layer/104400-lcdb-v50-land-cover-database-version-50-mainland-new-zealand/

Pearson, L., & Couldrey, M. (2016). Methodology for GIS-based land use maps for Southland. Technical Report-Environment Southland Publication 2016-10, 167p.

Pearson, L. and Rissmann, C. (2021). Physiographic Environments of New Zealand: Inherent susceptibility of the landscape for contaminant loss. Land and Water Science Report 2021/25. p60.

Sharifi, A. (2020). Using sentinel-2 data to predict nitrogen uptake in maize crop. IEEE Journal of Selected Topics in Applied Earth Observations and Remote Sensing, 13, 2656-2662.

Srinivasan, M. S., Muirhead, R. W., Singh, S. K., Monaghan, R. M., Stenger, R., Close, M. E., ... & Hodson, R. (2021). Development of a national-scale framework to characterise transfers of N, P and Escherichia coli from land to water. New Zealand Journal of Agricultural Research, 64(3), 286-313.

Xing, N., Huang, W., Ye, H., Ren, Y., & Xie, Q. (2021). Joint Retrieval of Winter Wheat Leaf Area Index and Canopy Chlorophyll Density Using Hyperspectral Vegetation Indices. Remote Sensing, 13(16), 3175.

Technical Appendix C. High-resolution controlling landscape factor datasets

Airborne gamma ray spectroscopic survey

Airborne gamma ray spectroscopy (AGRS) provides a measure of the strength of gamma radiation emitted from naturally occurring radioisotopes within the uppermost surface of the Earth (Løvborg, 1984; IAEA, 2003). As described by Beamish (2014), the airborne survey method employs a gamma ray detector (crystal scintillator) tuned to detect ^{40}K and estimate uranium (^{238}U) and thorium (^{232}Th) through the radon daughter ^{214}B in its decay chain and thorium (^{232}Th) via ^{208}Tl in its decay chain (Table C.1). Potassium (^{40}K) is measured directly at 1.461 MeV (megaelectronvolt). Secular equilibrium in the decay chains of ^{238}U and ^{232}Th is assumed and the ground concentration results are reported as equivalent uranium (eU, ppm) and equivalent thorium (eTh, ppm). Potassium is reported as %K.

Table C.1. Spectral energy ranges of the airborne radiometric data (after Beamish, 2014).

Window	Nuclide	Energy Range (MeV)
Potassium (%K)	^{40}K (1.46 MeV)	1.37–1.57
Thorium (eTh)	^{208}Tl (2.61 MeV)	2.41–2.81
Uranium (eU)	^{214}Bi (1.76 MeV)	1.66–1.86

Most of the gamma radiation emitted to the atmosphere is derived from shallow depths with approximately 90% coming from the top 300–500 mm for dry material with a bulk density of 1.5 g cm^{-3} (Grasty, 1975; Wilford et al., 1997). However, emanation depths may exceed several metres across areas of low bulk density soils, e.g., peat (Rawlins et al., 2007, 2009; Beamish, 2013a;b; 2014; 2016; Gatis et al., 2019). Radiometric data are typically displayed using a red, green, blue (RGB) ternary, where red is the potassium gamma count, green is the thorium count and blue is the uranium count. The raw ternary data image is provided in Figure C.1 for the Northland Region and Figure C.2 for the Southland Region. Areas with high attenuation, such as wetlands and mafic/ultramafic geologies, appear as dark areas in a ternary diagram.

For the Southland and Northland regions, a scintillator was mounted on an aircraft and flown at a sensor height of 50 m, along hundreds of flight lines with a lateral spacing of 200 m and tie lines every 2,000 m (Thomson Aviation, 2016). During surveying, gamma-ray emission is recorded every second, resulting in ground measures that are between 40 and 70 m apart. The sensor footprint is elliptical and the area contributing to 90% of the signal intensity covers 109,000 m^2 (11 ha) resulting in some overlap along the flight path (IAEA, 2003; Beamish, 2014). Within the sensor ellipse, the greatest signal contribution comes from directly beneath the aircraft and decays exponentially with lateral distance from the flight line.

The imagery derived from the survey has a nominal resolution of 40 m (0.16 ha) across lowland areas and 50 m (0.25 ha) across high-relief areas, making it finer than existing soil and geological polygons. However, at a lateral spacing of 200 m, small-scale variation falling between the lateral extent of the sensor ellipsoids may be missed. Lateral flight line spacings of 50–100 m are recommended for detection of small-scale (< 20 m x 20 m) features such as minor wetlands, springs, seeps and small ponds or lakes.

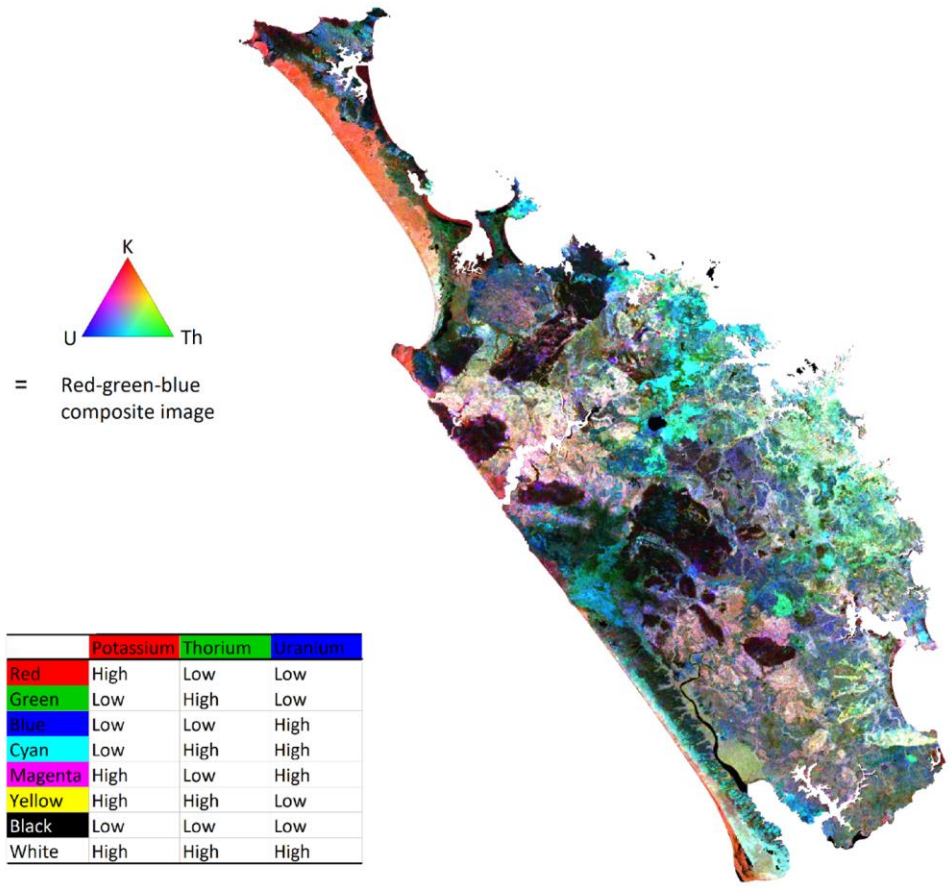

	Potassium	Thorium	Uranium
Red	High	Low	Low
Green	Low	High	Low
Blue	Low	Low	High
Cyan	Low	High	High
Magenta	High	Low	High
Yellow	High	High	Low
Black	Low	Low	Low
White	High	High	High

Figure C.1. Airborne Gamma-Ray Spectroscopy (AGRS) ternary for the Northland Region (NZP&M, 2011). Table of colours produced by variable mixing of K, eTh and eU.

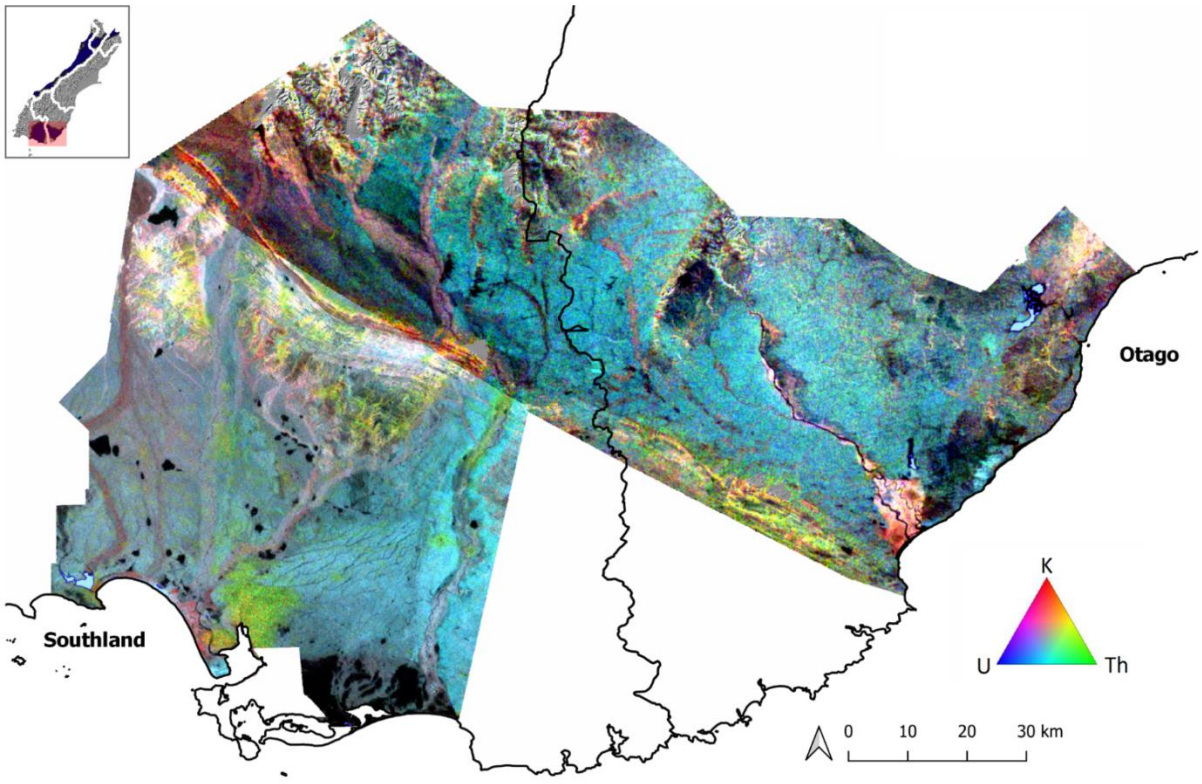

Figure C.2. Airborne gamma ray spectroscopy ternary image for the Southland Otago survey area (from Rissmann et al., 2020). Inset shows the extent of radiometric coverage for the South Island of New Zealand.

The mapping of soil hydrological properties using radiometrics relies on an assessment of the attenuation of gamma radiation by the air-liquid-solid phases that constitute rock and soil (Løvborg, 1984; Rawlins et al., 2007, 2009; Beamish, 2013a;b; 2014; 2016; Gatis et al., 2019). This differs from geological, soil and landscape stability mapping, which is focused on interpreting the spatial variation in potassium (K), equivalent thorium (eTh) and equivalent uranium (eU) and relevant mass ratios (i.e., eU/eTh, K/eTh) with regard to geological and geomorphic gradients (Pickup and Marks, 2000).

Gamma ray attenuation primarily occurs via incoherent scattering of gamma rays by electrons associated with earth materials and water. The degree of attenuation is determined by the density of electrons and is a product of both the dry bulk density and the volumetric water content of the earth material[39]. Importantly, relative to rock and soil, liquid water has a greater electron density and, as such, is a stronger attenuator of gamma rays[40] (Løvborg, 1984). Therefore, the maximum gamma ray signal (S) emitted from a particular depth in centimetres (d) is given by:

$$S(d) = (1 - \exp(-0.046*\rho*d))*100, \qquad \text{(Eq. C.1)}$$

where ρ is the dry bulk density of the material in g.cm^{-3} (Taylor et al., 2002). The factor 0.046 is an assumed mass attenuation coefficient for the material and the energy considered. This expression indicates that about 90% of the radiometric signal comes from the top 30 cm of the soil when the average dry bulk density is 1.6 g cm^{-3} (Beamish, 2014; Figure C.3). For a lower dry bulk density and for the very low densities of some organic soils (c. 0.1 g cm^{-3}), the emission profile will be deeper c. ≥ 100–500 cm. These theoretical emission depths represent maximum values and are modified by volumetric water content. Laboratory and field-based studies note a quasi-linear relationship between volumetric water content and gamma ray attenuation, with a 10% increase in attenuation for every 10% increase in volumetric water content (Grasty and Minty, 1995; Cook et al., 1996; IAEA, 2003).

Figures C.3a and C.3b from Beamish (2013a) are examples of the relationship between soil dry bulk density and volumetric water content. Specifically, reference mineral soils of lower bulk density (1.1 g cm^{-3}) have a shallower attenuation curve than mineral soils with a higher bulk density (1.6 g cm^{-3}). Figure C.3 displays attenuation curves for five soils and two different rock types in terms of their degree of water saturation.

As expected, there is a strong correlation between porosity, density and volumetric water content and resultant gamma ray attenuation. At full saturation, attenuation approaches 100% for the peat soil. Most critical here is that water content is the dominant factor governing attenuation in low-density soils such as peat. Gamma ray attenuation approaches 100% for standing water with a depth of ≥ 0.9 m. Lakes greater than 1 m deep are often used to assess the 100% attenuation baseline in radiometric surveys.

Another relevant feature of low-density organic soils is the lesser concentration of radiogenic minerals. This equates to lower emanation power relative to mineral soils. Due to the strong attenuation capacity of water and the naturally low radionuclide concentration of organic matter, areas of organic and especially wet organic soils are commonly associated with the lowest gamma ray emanation signature. In short, the attenuation of gamma ray emission by low-density earth materials such as peat is highly detectable (Beamish, 2013a;b; 2014; 2016; Gatis et al., 2019).

[39] Because air is part of the airborne measurement it is ignored with the electron density governed by the dry bulk density and volumetric water content of the earth material. There is little variation in electron density for earth materials with different geochemical composition with the exception of ore-grade deposits of heavy atoms with an atomic number > 30 (Løvborg, 1984).

[40] Water's greater electron density is due to the absence of a neutron within the nucleus of the hydrogen atom.

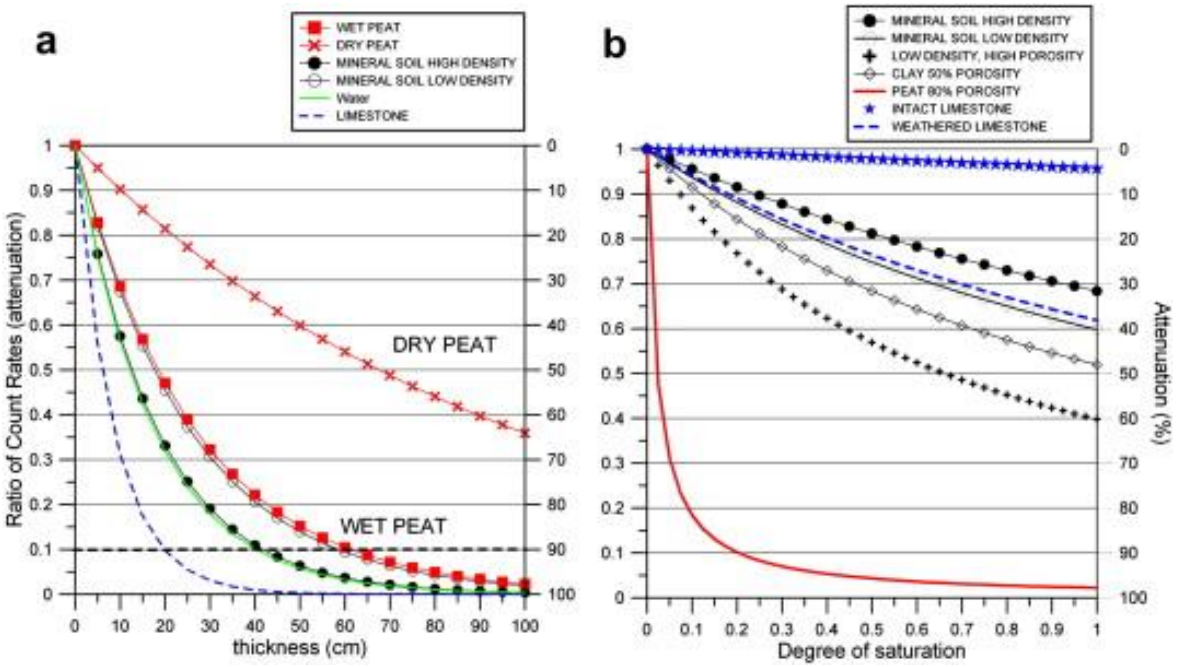

Figure C.3. Theoretical attenuation behaviour of soil/bedrock types from Beamish (2013a). a) Variation with thickness assuming a uniform half-space. A 90% attenuation level is shown by the horizontal dashed line. b) Variation with degree of saturation (soil moisture or moisture content).

Total gamma count is measured as absorbed dose rate (DOSE) in air using ground contributions from radiometric survey (IAEA, 2003):

$$\text{DOSE (nGy·h}^{-1}\text{)} = 13.078*\%K + 5.675*eU + 2.494*eTh, \qquad \text{(Eq. C.2)}$$

where 1 Gy (Gray) is equivalent to one joule of energy absorbed per kilogram of matter deposited in a medium by ionising radiation. Equation C.2 excludes contributions from artificial (man-made) sources by limiting the energy range from 1.37 to 2.81 MeV (IAEA, 2003). Importantly, as DOSE covers a wider spectral range it offers a higher signal-to-noise ratio than the individual radio components and, therefore, it is more sensitive at detecting gamma ray attenuation relative to individual spectra (Beamish, 2014; Gatis et al., 2019).

Topographic Indices

Geomorphometry (geomorphic topographic indices), has been used to identify and better understand the underlying susceptibility of the landscape to mass wasting and erosion (Riley et al., 1999; Guzzetti et al., 2012; Różycka et al., 2015). An underlying assumption of these approaches, and that of the classification applied here, is that mass movements, or large-scale erosional processes, such as tunnel gullying, markedly change slope surface characteristics, and these can be detected by quantitative, objective DEM (digital elevation model) analysis. This type of approach is considered particularly attractive for large areas, where the systematic visual interpretation of a DEM is challenging. A common premise in such studies is that sliding and then deposition of the failed mass, often disintegrated *en route*, will result in a considerable increase in local topographic complexity relative to adjacent, unaffected slopes (e.g., McKean and Roering, 2004; Booth et al., 2009).

One of the key geomorphometric algorithms used for identifying and better understanding the controls over mass wasting is Terrain Ruggedness (McKean and Roering, 2004; Booth et al., 2009; Guzzetti et al., 2012; Różycka et al., 2015). The Terrain Ruggedness (or Roughness) Index (TRI) reveals the change of slope and aspect over distances in a relief; or in GIS terms, the elevation

difference between adjacent cells of a Digital Elevation Model (DEM). Studies applying TRI note that areas with higher scores more commonly exhibit signs of mass wasting (Guzzetti et al., 2012; Różycka et al., 2015). Furthermore, areas of recent mass wasting show higher overall TRI relative to areas of older mass wasting reflecting erosion and subsequent weathering and recovery of the regolith. Accordingly, TRI has been used as a proxy for inferring the age of mass wasting events by comparing TRI scores and other indices of weathering within a similar geostructural setting (LaHusen et al., 2016).

Rode and Seibert (1999) found that although topography was a useful predictor of wetland occurrence across hill country areas, it was less diagnostic across lower relief areas. They attributed the poorer performance to estimate wetland occurrence across lowland areas to the relatively poor resolution (50 x 50 m) of the Digital Elevation Model (DEM) used for their assessment. Later, Sørensen and Seibert (2007) evaluated the effects of DEM resolution over the performance of topographic indices, i.e., the Topographic Wetness Index (TWI), for identifying wetness gradients and noted enhanced resolution across low-relief areas associated with higher resolution DEM (i.e., LiDAR). More recently, Radula et al. (2018) noted that topographic indictors of wetness were a more sensitive determinant of soil moisture distribution than bioindicators (e.g., Ellenberg's indicator values from a satellite-based assessment of vascular plant form, cover, and structure).

Despite the obvious value of topographic indices of wetness, a fundamental limitation of DEM based approaches is the assumption of a uniformly impervious surface. Such an assumption ignores the inherent geological and edaphic controls over infiltration rate and water table depth, restricting the resolution of wetness indices based purely upon topographically driven water routing algorithms (Ma et al., 2010).

The assumption of uniform permeability contrasts with a radiometric-based assessment of wetness gradients that is sensitive to soil textural and drainage class controls over water content. For example, Read et al. (2018) identified radiometric data as a useful surrogate for soil texture in terms of providing constraint over the sand and clay content of soils that were poorly defined at the resolution of traditional soil classifications across a 40,000 km^2 area of South Australia. Dent et al. (2013) also noted the usefulness of radiometrics for identifying and mapping soil textural class across an 82,000 km^2 area of forested land across the south-central portion of the province of British Columbia.

Rissmann et al. (2019) noted that radiometrics objectively discriminated the spatial distribution of soil textural fractions (e.g., sand vs clay) across Northland, New Zealand (13,940 km^2). Specifically, soils across areas of sandstone (e.g., Ruatangata Sandstone) showed lower gamma ray attenuation and distinct spectral signatures relative to soils formed in adjacent allochthonous mudstones (e.g., Whangai Formation). These observations are consistent with the NZ Soil Bureau's evaluation of soil–landscape relationships across Northland, i.e., that soil texture, permeability, and depth to slowly permeable layer exhibit a spatial correlation to the texture of the primary parent material (NZ Soil Bureau, 1954). Specifically, soils formed in mudstones tend to exhibit both higher clay content and poorer internal drainage than soils formed in sandstones that have low clay content. Therefore, the integration of digital terrain and radiometric imagery is considered a more robust approach to the discrimination of landscape attributes.

References

Beamish, D. (2013a). Gamma-ray attenuation in the soils of Northern Ireland, with special reference to peat. Journal of Environmental Radioactivity, 115, 13–27. https://doi.org/10.1016/j.jenvrad.2012.05.031

Beamish, D. (2013b). Peat mapping associations of airborne radiometric survey data. Remote Sensing, 6(1), 521–539. https://doi.org/10.3390/rs6010521

Beamish, D. (2014). Peat Mapping Associations of Airborne Radiometric Survey Data, 521–539. https://doi.org/10.3390/rs6010521

Beamish, D. (2016). Soils and their radiometric characteristics. In M.E. Young (ed.). Unearthed: impacts of the Tellus surveys of the north of Ireland. Dublin. Royal Irish Academy. DOI:10.3318/ 978-1-908996-88-6.ch19

Booth, A. M., Roering, J. J. and Perron, J. T. (2009). Automated landslide mapping using spectral analysis and high-resolution topographic data: Puget Sound lowlands, Washington, and Portland Hills, Oregon. Geomorphology. https://doi.org/10.1016/j.geomorph.2009.02.027

Cook, S.E., Corner, R.J., Groves, P.R. and Grealish, G.J. (1996). Use of airborne gamma ray images as a rapid -radiometric data for soil mapping. Australian Journal of Soil Research 34, 183–194.

Dent, D. L., MacMillan, R. A., Mayr, T. L., Chapman, W. K., & Berch, S. M. (2013). Use of airborne gamma radiometrics to infer soil properties for a forested area in British Columbia, Canada. Journal of Ecosystems and Management, 14(1).

Gatis N., Luscombe D.J., Carless D., Parry L.E., Fyfe R.M., Harrod T.R., Brazier R.E., Anderson K. (2019). Mapping upland peat depth using airborne radiometric and lidar survey data. Geoderma, 335, 78–87. https://doi.org/10.1016/j.geoderma.2018.07.041

Grasty, R.L., and Minty, B.R.S. (1995). A guide to the technical specifications for airborne gamma-ray surveys. AGSO Australian Geological Survey Organisation, Record 1996/60.

Grasty, R.L. (1975). Atmospheric absorption of 2.62 MeV gamma ray photons emitted from the ground. Geophysics 40: 1058–1065.

Guzzetti, F., Mondini, A. C., Cardinali, M., Fiorucci, F., Santangelo, M., and Chang, K. T. (2012). Landslide inventory maps: New tools for an old problem. Earth-Science Reviews. Elsevier B.V. http://doi.org/10.1016/j.earscirev.2012.02.001

International Atomic Energy Agency. (2003) Guidelines for Radioelement Mapping Using Gamma Ray Spectrometry; IAEA: Vienna, Austia, 2003

LaHusen, S. R., Duvall, A. R., Booth, A. M. and Montgomery, D. R. (2016). Surface roughness dating of long-runout landslides near Oso, Washington (USA), reveals persistent postglacial hillslope instability. Geology 44: 111–114.

Løvborg, L. (1984). The Calibration of Portable and Airborne Gamma-ray Spectrometers - Theory, Problems and Facilities. Risø Report M-2456. p. 207.

Ma, J., Lin, G., Chen, J., & Yang, L. (2010). An improved topographic wetness index considering topographic position. In 2010 18th International Conference on Geoinformatics (pp. 1-4). IEEE.

McKean, J. and Roering, J. (2004). Objective landslide detection and surface morphology mapping using high-resolution airborne laser altimetry. Geomorphology. https://doi.org/10.1016/S0169-555X(03)00164-8

NZP&M (2011). Detailed Airbourne Magnetic, Radiometric and Digital Terrain Survey for the Northland Project. Ministry of Economic Development New Zealand Unpublished Mineral Report MR4800

Pickup, G. and Marks, A. (2000). Identifying large-scale erosion and deposition processes from airborne gamma radiometrics and digital elevation models in a weathered landscape. Earth Surface Processes and Landforms, 25: 535-557

Raduła, M.W., Szymura, T.H., and Szymura, M. (2018). Topographic wetness index explains soil moisture better than bioindication with Ellenberg's indicator values. Ecological Indicators, 85, 172-179.

Rawlins, B.G., Lark, R.M., Webster, R. (2007). Understanding airborne radiometric survey signals across part of eastern England. Earth Surf. Process. Landf. 32, 1503–1515. https://doi.org/10.1002/esp.1468.

Rawlins, B.G., Marchant, B.P., Smyth, D., Scheib, C., Lark, R.M., Jordan, C. (2009). Airborne radiometric survey data and a DTM as covariates for regional-scale mapping of soil organic carbon across Northern Ireland. Eur. J. Soil Sci. 60, 44–54. https://doi.org/10.1111/j.1365-2389.2008.01092.x.

Read, C.F., Duncan, D.H., Ho, C.Y.C., White, M., and Vesk, P.A. (2018). Useful surrogates of soil texture for plant ecologists from airborne gamma-ray detection. Ecology and evolution, 8(4), 1974-1983.

Riley, S. J., DeGloria, S. D. and Elliot, R. (1999): A terrain ruggedness index that quantifies topographic heterogeneity. Intermountain Journal of Sciences 5: 23 – 27.

Rissmann, C., Pearson, L., Lindsay, J., and Couldrey, M. (2019). Mapping of Northland's Wetness Gradients utilising Radiometric and Satellite imagery – GIS Metadata. Land and Water Science Report 2019/38

Rissmann, C., Pearson, L., Shi, Y., and Lawrence, C. (2020). Radiometric and Terrain Derived Erosion Susceptibility Classification for the Southland Region. Land and Water Science Report 2020/28. p82.

Rodhe, A., and Seibert, J. (1999). Wetland occurrence in relation to topography: A test of topographic indices as moisture indicators. Agricultural and Forest Meteorology, 98–99, 325–340. http://doi.org/10.1016/S0168-1923(99)00104-5

Różycka, M., Migoń, P., & Michniewicz, A. (2015). Topographic Wetness Index and Terrain Ruggedness Index in geomorphic characterisation of landslide terrains, on examples from the Sudetes, SW Poland. Zeitschrift Für Geomorphologie. http://doi.org/10.1127/zfg

Sørensen, R., and Seibert, J. (2007). Effects of DEM resolution on the calculation of topographical indices: TWI and its components. Journal of Hydrology, 347(1-2), 79-89.

Taylor, M. J., Smettem, K., Pracilio, G., & Verboom, W. (2002). Relationships between soil properties and high-resolution radiometrics, central-eastern Wheatbelt, Western Australia. Exploration geophysics, 33(2), 95-102.

Wilford, J.R., Bierwirth, P.N., and Craig, M.A. (1997). Application of airborne gamma-ray spectrometry in soil/regolith mapping and applied geomorphology. AGSO Journal of Australian Geology & Geophysics, 17(2): 201-216

Technical Appendix D. Soil Nitrous Oxide Susceptibility Literature Review

Landscape controls over soil zone nitrous oxide (N_2O) emissions

Of the GHGs associated with agriculture, nitrous oxide (N_2O) is of particular concern due to its global warming potential (>298 times more powerful than carbon dioxide (CO_2) for a 100-year timeline; IPCC, 2014) and has ozone-depleting capabilities (Ravishankara et al., 2009; Signor et al., 2013; Samad et al., 2016). In most countries, nitrous oxide emissions typically contribute less than 10% of the carbon dioxide equivalent (CO_2eq) GHG emissions. However, in New Zealand nitrous oxide contributes ≥17% of the nation's total GHG emissions on a carbon dioxide equivalent basis, due to the dominance of the agricultural sector (de Klein and Ledgard, 2005). Accordingly, the reduction of even a small proportion of the mass of nitrous oxide emitted from the soil zone could result in a disproportionate benefit relative to reductions in carbon dioxide or methane.

In soils, microbially mediated pathways for the formation of nitrous oxide and dinitrogen (N_2) include nitrification, nitrifier-denitrification, and denitrification (Firestone et al., 1980; Clough et al., 2006; Balaine et al., 2016; Wrage-Monning et al., 2018; Stein, 2019; Li et al., 2021; Figure D.1). Nitrification converts ammonium (NH_4^+) to nitrite (NO_2^-) and subsequently to nitrate (NO_3^-) under aerobic (oxygenated) conditions. As soil oxygen levels decline to <5%, nitrifier-denitrification begins converting nitrate and nitrite nitrogen to nitrous oxide (partial or incomplete denitrification). If the soil becomes anoxic (no oxygen present), complete denitrification occurs to N_2 gas (Clough et al., 2006; Balaine et al., 2016; Li et al., 2021). Complete denitrification and the production of N_2 is the endpoint of 'true' denitrification, whereas N_2O is produced as a result of suboxia or removal of the intermediate product. Nitrifier denitrification produces nitrous oxide via the reduction of nitrite to nitric oxide (NO), which is further reduced to N_2O (Stein, 2019). The transformations are carried out by autotrophic nitrifiers. Nitrifier denitrification differs from coupled nitrification-denitrification (where denitrifies reduce nitrite or nitrate that was produced by nitrifiers).

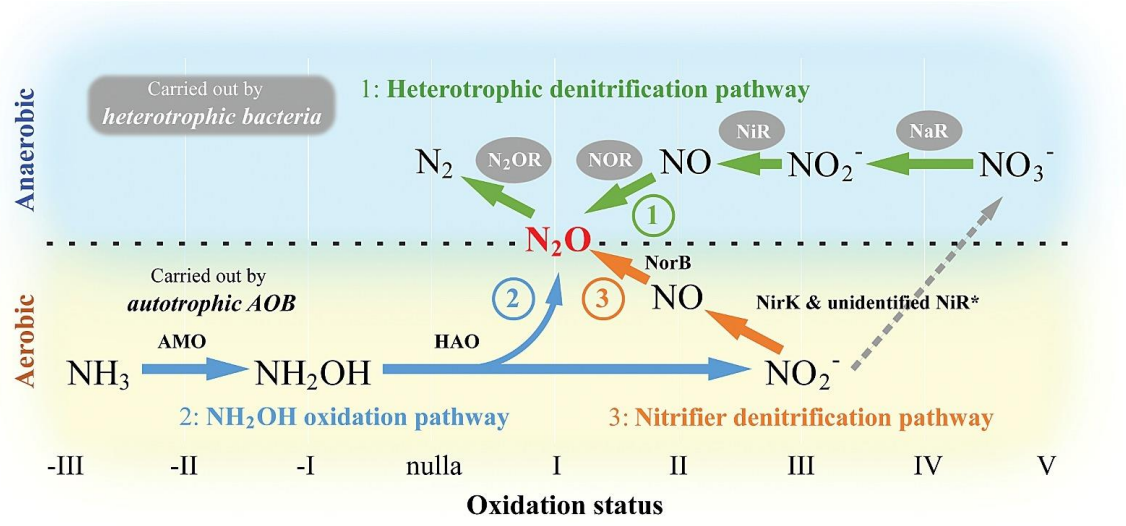

Figure D.1. Soil zone N_2O production pathways (after Duan et al., 2017): the heterotrophic denitrification pathway employed by heterotrophic denitrifiers, the NH_2OH oxidation pathway and the nitrifier denitrification pathway employed by ammonia-oxidising bacteria (AOB). AMO: ammonium monooxygenase; HAO: hydroxylamine oxidoreductase; NirK: copper-containing nitrite reductase; NorB: membrane-bound nitric oxide reductase; NaR: nitrate reductase; NiR: nitrite reductase; NOR: nitric oxide reductase; N2OR: nitrous oxide reductase.

Denitrification, both nitrifier and true denitrification, are widely recognised as the main pathway generating nitrous oxide in agricultural soils (Smith et al., 2004; Giles et al., 2012; Morley et al., 2014;

Balaine et al., 2016; Samad et al., 2016; Li et al., 2021). Therefore, understanding the factors controlling the sequential reduction of nitrate to nitrous oxide instead of inert N_2 is critical when seeking to assign an inherent susceptibility to N_2O loss to the landscape.

The main controlling factor over N_2O generation is the tendency of a soil to become saturated with water. The soil physical factors that control saturation include texture (clay, silt, sand, gravels) and internal drainage (Stepniewski et al., 1994 and references therein). Soil texture and structure influences the volume of void space and the conductivity of water to drain. Soils with coarse textures have large void spaces and are highly conductive while fine textured silt and clay soils have a low conductivity and water drains more slowly through the soil as a result. Internal drainage refers to the ability of soil water to percolate to depth (drain under gravity). Soils with poor internal drainage do not tend to drain to depth with water perching (held) in the soil resulting in saturation.

Where soils are well drained and highly permeable, saturation is less likely and susceptibility of the soil to N_2O production is low. Soil saturation may occur intermittently in well drained soils that are fine textured due to infiltration exceeding soil permeability, meaning the soil pore space fills up faster than it can drain. Where soils are both fine textured and imperfectly to poorly drained the susceptibility of the soils to become saturated is enhanced as internal drainage is restricted increasing the likelihood N_2O is produced.

N_2O production occurs under soil saturation because the supply of O_2 from the atmosphere is restricted to the microbial community. Microbial communities continue to rapidly consume any remaining oxygen in the soil (both free and dissolved in water). Nitrifier-denitrification commences under these suboxic conditions and N_2O production starts. When the soil dries out, soil pores are resupplied with oxygen and the soil microbial community returns to the nitrification pathway and N_2O production ceases. However, if a soil remains saturated for an extended period, all the oxygen is consumed, and the soil becomes anoxic. Under anoxic conditions, the amount of N_2O produced will depend on the relative abundance of NO_3^-. If the soil has a low abundance of NO_3^- the production of N_2O will be limited. Animal urine patches are often the main hotspots of N_2O production, especially for cattle, where the larger volume of urine excreted can result in localised soil saturation, whilst also containing abundant organic nitrogen which is rapidly converted by soil microbes to ammonium and then nitrate. Commonly, wetting and drying of saturation prone soils results in pulses of N_2O production.

The upper most horizon of the soil, the 'A' horizon in most agricultural soils, is the most dynamic in terms of soil water and associated oxygen supply. Here, the 'A' horizon is the interface between the atmosphere and subsoil horizons and can transition rapidly from unsaturated to saturated in response to precipitation or irrigation events. A high degree of transience in 'A' horizon water content is recognised as an important driver of N_2O emissions (pers. com. Prof. Tim Clough, June 2021).

Soil drainage and permeability and hence the susceptibility of a soil to produce nitrous oxide is dependent on slope, soil texture, and internal drainage (Stepniewski et al., 1994; Schaetzl et al., 2009). Areas of shallow water table, especially where the water table moves up and down a lot may also be areas of elevated susceptibility to N_2O production (e.g., riparian soils).

The

References

Balaine, N., Clough, T. J., Beare, M. H., Thomas, S. M., & Meenken, E. D. (2016). Soil gas diffusivity controls N_2O and N_2 emissions and their ratio. Soil Science Society of America.

Clough, T. J., Kelliher, F. M., Wang, Y. P., & Sherlock, R. R. (2006). Diffusion of ^{15}N-labelled N_2O into soil columns: a promising method to examine the fate of N_2O in subsoils. Soil Biology and Biochemistry, 38(6), 1462-1468.

Duan, H., Ye, L., Erler, D., Ni, B. J., & Yuan, Z. (2017). Quantifying nitrous oxide production pathways in wastewater treatment systems using isotope technology–a critical review. Water Research, 122, 96-113.

Firestone, M. K., Firestone, R. B., & Tiedje, J. M. (1980). Nitrous oxide from soil denitrification: factors controlling its biological production. Science, 208(4445), 749-751.

Giles, M., Morley, N., Baggs, E. M., & Daniell, T. J. (2012). Soil nitrate reducing processes–drivers, mechanisms for spatial variation, and significance for nitrous oxide production. Frontiers in Microbiology, 3, 407.

Giltrap, D. L., Li, C., & Saggar, S. (2010). DNDC: A process-based model of greenhouse gas fluxes from agricultural soils. Agriculture, Ecosystems & Environment, 136(3-4), 292-300. https://doi.org/10.1016/j.agee.2009.06.014

IPCC, 2014: *Climate Change 2014: Synthesis Report*. *Contribution of Working Groups I, II and III to the Fifth Assessment Report of the Intergovernmental Panel on Climate Change* [Core Writing Team, R.K. Pachauri and L.A. Meyer (eds.)]. IPCC, Geneva, Switzerland, 151 pp.

de Klein, C. A. M. De, & Ledgard, S. F. (2005). Nitrous oxide emissions from New Zealand agriculture – key sources and mitigation strategies. 77–85.

Li, Y., Clough, T.C., Moinet, G., David. W. (2021). Emissions of nitrous oxide, dinitrogen and carbon dioxide from three soils amended with carbon substrates under varying soil matric potential. European Journal of Soil Science. 10.1111/ejss.13124.

Morley, N. J., Richardson, D. J., & Baggs, E. M. (2014). Substrate Induced Denitrification over or under Estimates Shifts in Soil N_2/N_2O Ratios, 9(9), 1 6.https://doi.org/10.1371/journal.pone.0108144

Ravishankara, A. R., Daniel, J. S., & Portmann, R. W. (2009). Nitrous oxide (N_2O): the dominant ozone-depleting substance emitted in the 21st century. Science, 326(5949), 123-125.

Samad, M., Biswas, A., Bakken, L.R., Clough, T.J., de Klein, C.A.M., Richards, K.G., Lanigan, G.J., & Morales, S. (2016). Phylogenetic and functional potential links pH and N_2O emissions in pasture soils. Nature Publishing Group, 1–10. https://doi.org/10.1038/srep35990

Schaetzl, R. J., Krist, F. J., Stanley, K., & Hupy, C. M. (2009). The natural soil drainage index: an ordinal estimate of long-term soil wetness. Physical Geography, 30(5), 383-409.

Signor, D., & Cerri, C. E. P. (2013). Nitrous oxide emissions in agricultural soils: a review. Pesquisa Agropecuária Tropical, 43(3), 322-338.

Smith, W., Grant, B., Desjardins, R., Lemke, R. & Li, C., (2004). Estimates of the interannual variations of N_2O emissions from agricultural soils in Canada. Nutrient Cycling in Agroecosystems. 68. 37-45. 10.1023/B:FRES.0000012230.40684.c2.

Stein, L. Y. (2019). Insights into the physiology of ammonia-oxidizing microorganisms. Current Opinion in Chemical Biology, 49, 9-15.

Stepniewski, W., Gliński, J., & Ball, B. C. (1994). Effects of compaction on soil aeration properties. In Developments in agricultural engineering (Vol. 11, pp. 167-189). Elsevier.

Wrage-Mönnig, N., Horn, M. A., Well, R., Müller, C., Velthof, G., & Oenema, O. (2018). The role of nitrifier denitrification in the production of nitrous oxide revisited. Soil Biology and Biochemistry, 123, A3-A16.

Technical Appendix E. Games-Howell post-hoc tests results for subcatchments of the Wairoa and Mataura

Mataura Catchment

The Mataura Catchment is geomorphically youthful when contrast with the Wairoa Catchment. It has been shaped by recent Quaternary glacial activity, with a large area of alluvial floodplains and areas of glacial till in the upper mountainous portion of the catchment. Loess, a silt sized particle, mantles a large area of the catchment, with the thickest deposits directly adjacent to the modern-day floodplain of the Mataura River and its tributaries. As geomorphic surface age increases, the thickness of loess also increases.

Nitrate-nitrite-nitrogen susceptibility

Nitrate and nitrite are produced from the mineralisation of organic nitrogen. It is but one of the forms of nitrogen that contribute to nitrogen load. Organic and ammoniacal nitrogen are other, often overlooked forms of nitrogen, which contribute to contaminant loads. Nitrate and nitrite are highly mobile species due to their negative charge and their large, hydrated radius. Their negative charge and large size when hydrated mean they are not held by areas of positive charge in soil or groundwater systems.

Nitrate and nitrite can be removed via denitrification, a microbially mediated reduction – oxidation reaction. Soil zone denitrification is favoured where soils are prone to saturation whereas denitrification in groundwater systems is associated with an abundance of organic carbon or reduced iron (pyrite and glauconite). Soil zone denitrification may produce nitrous oxide, a potent GHG, whereas denitrification in a saturated groundwater system commonly generates benign N_2 gas.

The landscape factors controlling the susceptibility of the landscape to nitrate-nitrite-nitrogen leaching loss include soil water residence time, soil drainage, and organic carbon content. Importantly, nitrate-nitrite-nitrogen leaching occurs even where there are no aquifers, with leached nitrate moving laterally through the subsoil as horizon permeable flow or along a contact with a slowly permeable layer (bedrock).

Particulate phosphorus susceptibility

Particulate phosphorus is particle bound, moving with sediment as it is carried to stream by surface runoff or via artificial subsurface drainage. Particulate phosphorus can be made up of organic or inorganic forms. Both organic and inorganic forms of P have a high affinity for negatively charged surfaces. Soils with high P-retention that are eroded may carry large quantities of bound P, as particulate, to waterways.

In general, the susceptibility of a geological unit and associated soil to mass wasting and sediment loss is a strong control over the likelihood that particulate phosphorus will be an issue (Ward et al., 1990; Kronvang, 1992; Berhe et al., 2018). By comparison, dissolved reactive phosphorus, the fraction of P 'dissolved' in water is controlled by parent material composition and redox status[41].

[41] Dissolved reactive phosphorus may not always be dissolved. Rather, they represent the P molecules that can pass through a ≤0.45 um filter. Some of the smallest P molecules exist as colloids that may be neutrally charged and highly mobile.

Mid-Mataura, Mataura Catchment, Southland

The mid-Mataura area includes the loess mantled Edendale terrace and alluvial aquifer system, the modern-day floodplain of the Mataura River and areas of East Southland Group sediments (Lignite), peat wetlands (organic soils), uplifted alluvial terraces, and sandstones of the Murihiku Terrane. Much of the area is of low relief (Figure E.1).

Alluvial gravels of Quaternary age are 83% of the area of the mid-Mataura (30,396 ha). The Ferndale Group, Taringatura Group, and Gore Lignite Measures bedrock are a further c. 14% by area. Their components: Ferndale Group (8%) is described as a "Sandstone and interbedded mudstone with minor shellbeds; and conglomerate and coal" by geological survey (Q-Map). The Gore Lignite Measures (2%) are described as "Sandstone with lignite and carbonaceous mudstone; mudstone; claystone and minor conglomerate." by geological survey (Q-Map) and the Taringatura Group (4%) is described as "Sandstone with minor tuff; mudstone; tuff; shellbeds and granitic conglomerate." The remaining geological units make up <3% by area.

According to Q-Map, peat makes up 1% by area of the Quaternary alluvial deposits. However, recent work (Rissmann et al. 2020) suggest this an underestimate. Of the Quaternary gravels, 94% by area or 28,572 ha are designated as Q6, Q5, and Q4 in age. These deposits are described by geological survey (Q-Map) as "Schist-greywacke-quartz sandy gravel: sandy gravel in outwash and alluvial terraces." Approximately 1% by area are Q1 or recent alluvium. The oldest Quaternary alluvial Q10 – Q8 deposits make up the uplifted terraces that flank the eastern boundary of the Mataura River and its floodplain.

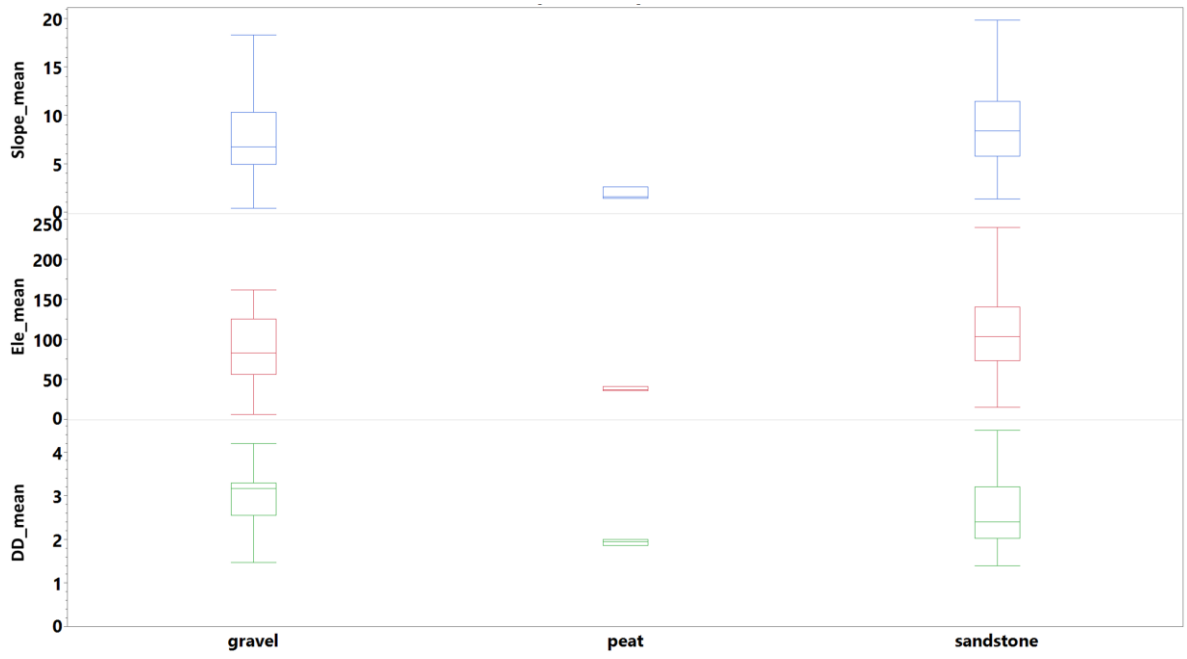

Main Rock (Q-Map)	Elevation (m RSL)	Slope (□□	Profile Drainage (DD)
Gravel	82.8	6.7	3.2
Peat	36.5	1.6	1.9
Sandstone	103.4	8.4	2.4

Figure E.1. Slope, elevation relative to sea level, and soil profile drainage (S-Map, 1:50,000) by Main Rock (Q-Map, 1:250,000).

The sandstones of the Ferndale Group, Taringatura Group, and Gore Lignite Measures occupy the highest elevation areas of the mid-Mataura and have the steepest slope. The large area of alluvial gravels has the second highest elevation and slope, and peat deposits occupy the lowest elevation areas and are also characterised by the lowest slope of all units. According to soil survey (S-Map, 1:50,000), soil drainage class is lowest for peat, and highest for gravel. Sandstones have an intermediate drainage class, best characterised as imperfectly to poorly drained (Figure E.2). Permeabilities are moderate, with lower permeabilities across loess mantled gravels.

Isolating the large area of alluvial deposits and grouping by stratigraphic age identifies the oldest alluvial deposits as occupying the highest elevation areas and steepest slopes. The large area of Q6 – Q4 gravels, which includes the loess mantled Edendale Terrace, are associated with lower elevation and slope. According to soil survey, soil profile drainage is similar between the alluvial gravel deposits and lowest for Q1 aged peat. Overall, the alluvial gravels have moderate permeability with lower permeabilities associated with the loess mantled Edendale Terrace. Peat has the lowest permeability according to soil survey.

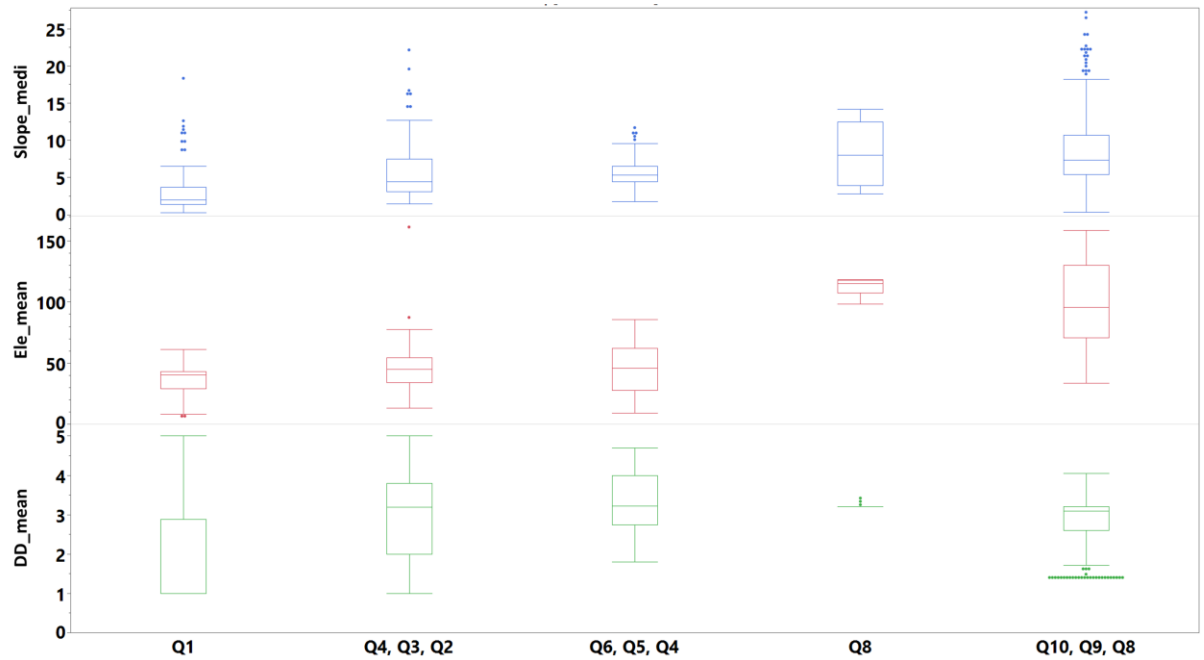

Stratigraphic Age (Q-Map)	Slope (°)	Elevation (m RSL)	Profile Drainage (DD)	Range Slope	Range Elevation	Range Profile Drainage
Q1	2.0	40.4	1.0	18.1	55.7	4.0
Q4, Q3, Q2	4.6	44.9	3.2	20.7	148.3	4.0
Q6, Q5, Q4	5.4	45.6	3.2	9.9	76.7	2.9
Q8	8.0	114.9	3.2	10.3	20.0	0.2
Q10, Q9, Q8	7.3	95.9	3.1	27.6	125.0	2.7

Figure E.2. Median slope, elevation relative to sea level, and soil drainage (DD) class (S-Map, 1:50,000) by stratigraphic age of alluvial gravel deposits (Q-Map, 1:250,000) for the mid-Mataura area.

Nitrate-nitrite-nitrogen susceptibility

The association between nitrate-nitrite-nitrogen susceptibility class and soil drainage class from historic soil survey (S-Map, 1:50,000), supports the controlling landscape factor hypothesis that the susceptibility of the landscape to nitrate leaching increases as soil drainage class increases (Figure E.3).

The systematic increase in soil drainage class with nitrate-nitrite-nitrogen susceptibility class is consistent with controlling factor theory for nitrate leaching, with higher rates of leaching losses as internal soil drainage shifts from very poor (peat/organic soils) to well drained (mineral soils) soils. The 95% confidence interval for susceptibility class 1 is large. This is consistent with historic soil survey having missed significant areas of organic soils within the mid-Mataura catchment (Rissmann et al., 2020a). Where organic soils have not been identified the soil drainage class is overestimated.

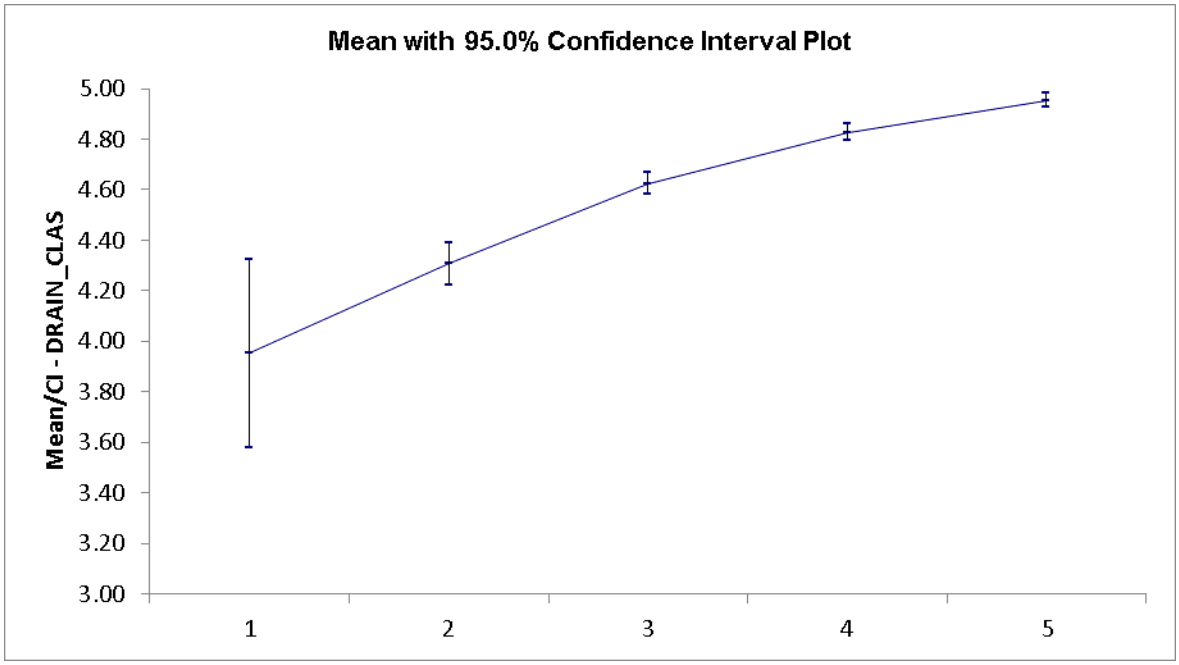

Games-Howell Probabilities (α = 0.05; 0.15)	1	2	3	4	5
1		0.3438	0.0067	0.0003	0.0000
2			0.0000	0.0000	0.0000
3				0.0000	0.0000
4					0.0000
5					

Figure E.3. Games-Howell post hoc test of soil drainage class (FSL, 1:50,000) vs. nitrate-nitrite-nitrogen susceptibility class (1 = 0 – 20; 2 = 21 – 40; 3 = 41 – 60; 4 = 61 – 80; 5 = 81 – 100) for the mid-Mataura subcatchment. Susceptibility class 1 is not statistically different from class 2.

The association between nitrate-nitrite-nitrogen susceptibility class and soil reduction potential, a proxy for soil zone denitrification from the Physiographic Environment Classification of New Zealand (PENZ; 1:50,000; Pearson & Rissmann, 2021), supports the controlling landscape factor hypothesis that the susceptibility of the landscape to nitrate leaching increases as soil reduction potential decreases (Figure E.4)[42]. Specifically, as soil reduction potential decreases the capacity of the soil to attenuate nitrate also decreases, reflecting a decrease in soil zone denitrification. Soils with high soil reduction potential can attenuate a significant proportion of nitrate that is generated. The 95% confidence interval for susceptibility class 1 is large. This is consistent with historic soil survey having missed significant areas of organic soils within the mid-Mataura catchment (Rissmann et al., 2020a). Where organic soils have not been identified soil reduction potential is underestimated.

[42] A similar pattern is observed for Geological Reduction Potential from PENZ.

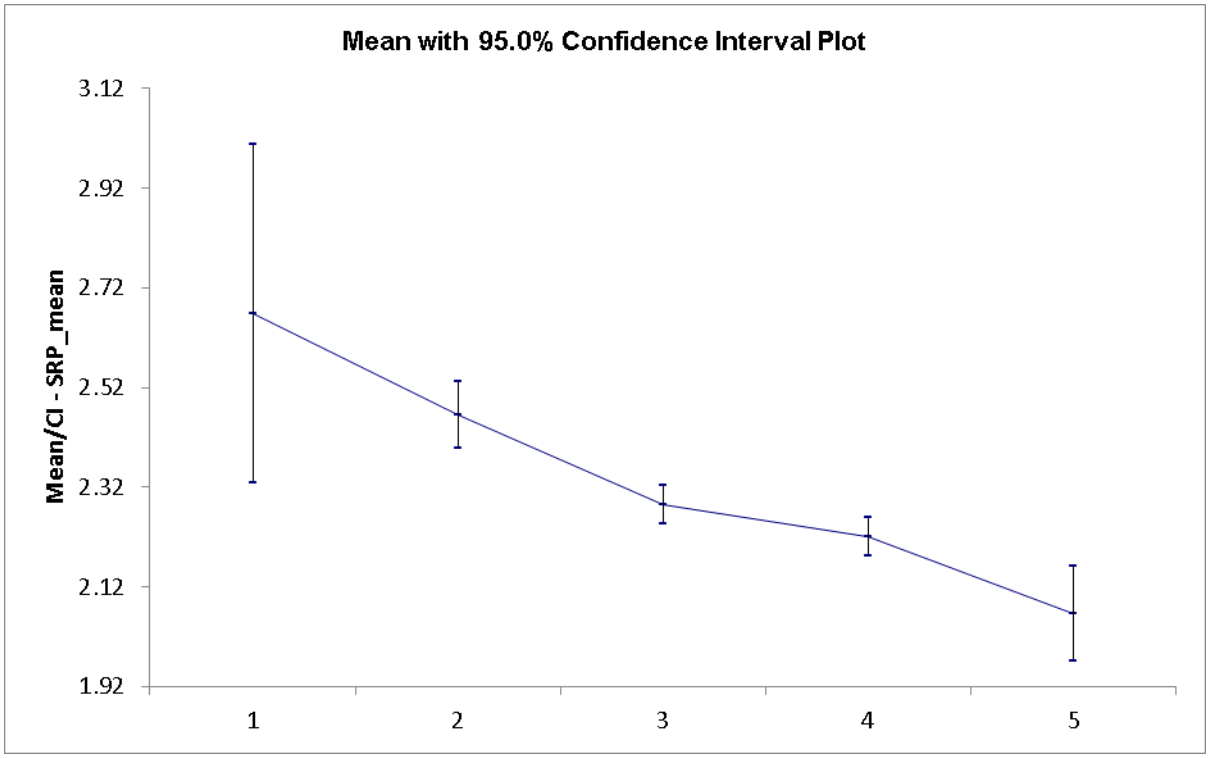

Games-Howell Probabilities (α = 0.05; 0.15)	1	2	3	4	5
1		0.7626	0.1772	0.0797	0.0103
2			0.0000	0.0000	0.0000
3				0.1315	0.0002
4					0.0264
5					

Figure E.4. Games-Howell post hoc test of soil reduction potential (SRP) class (PENZ, 1:50,000) vs. nitrate-nitrite-nitrogen susceptibility class (1 = 0 – 20; 2 = 21 – 40; 3 = 41 – 60; 4 = 61 – 80; 5 = 81 – 100) for the mid-Mataura subcatchment. Susceptibility class 1 is not statistically at α = 0.05 or 0.15 from class 2. Susceptibility class 3 is not statistically different from class 1.

Overall, the pattern of nitrate-nitrite-nitrogen susceptibility is consistent with established controlling landscape factor theory and prior physiographic modelling of the mid-Mataura area (Rissmann et al., 2016, 2019, 2021).

Particulate phosphorus susceptibility

Particulate phosphorus susceptibility is primarily a factor of geology. Geology controls the abundance of inorganic phosphorus, slope and soil physical and chemical characteristics that determine water infiltration, drainage, and the likelihood of a soil saturating. Typically, where geology is relatively uniform and the slope is low e.g., <4 - 8°, soil physical hydrological properties are the dominant control over particulate phosphorus susceptibility with slope the dominant control across high relief areas (Rissmann et al. 2020b).

Application of the Games-Howell post hoc test to Main Rock class (Q-Map) reveals that Quaternary alluvium has a significantly lower susceptibility to particulate phosphorus loss than the sandstones and mudstones of the Ferndale Group, Gore Lignite Measures, and Taringatura Group (Figure E.5). The strongly contrasting susceptibilities between rock classes are consistent with the controlling factor hypothesis that geological control over slope, soil thickness and the tendency of a soil to

become saturated with water controls the particulate phosphorus loss. Specifically, thin soils overlying slowly permeable rock is more likely to saturate and runoff than a highly permeable and well-drained soil that occupies a low-relief area.

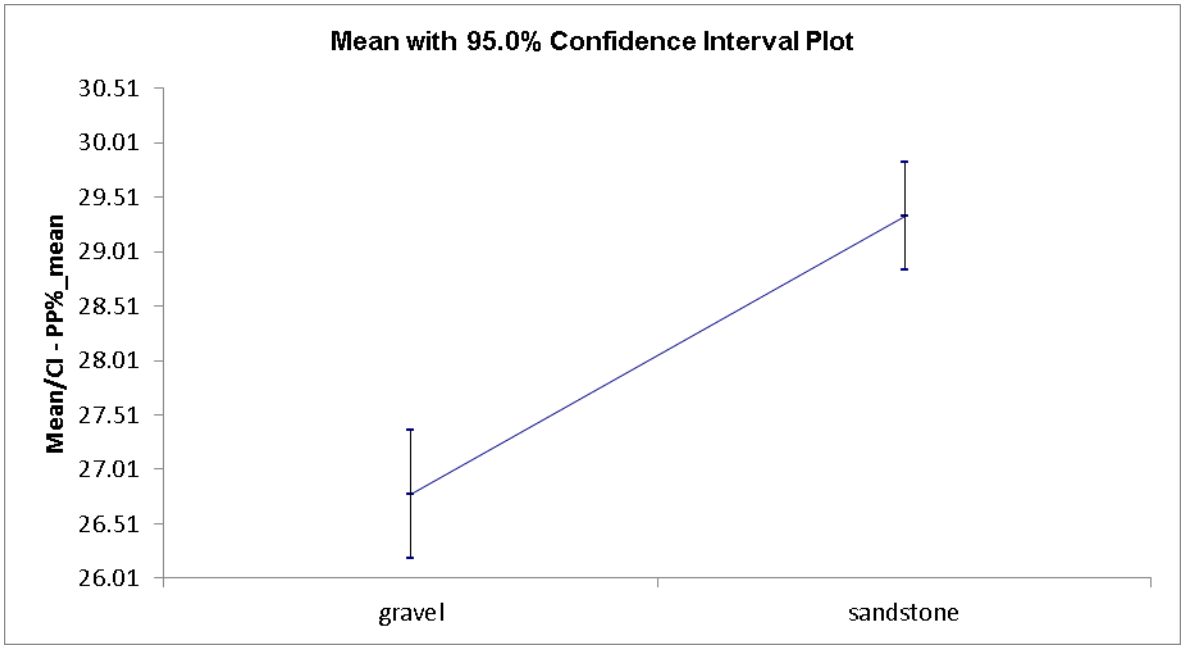

Games-Howell Probabilities (α = 0.05, 0.15)	Alluvium	Sandstone
Alluvium (gravel, sand, silt, clay)		0.0000
Sandstone		

Figure E.5. Games-Howell post hoc test of Q-Map derived 'Main Rock' vs. particulate phosphorus susceptibility class percentage for the mid-Mataura subcatchment. Welch's ANOVA was statistically significant at α= 0.05. The alluvial gravel class includes peat deposits. The sandstone class includes the Gore Lignite Measures, Ferndale, and Taringatura groups.

Application of the Games-Howell post hoc test supports the controlling landscape factor hypothesis that as slope increases the susceptibility of the landscape to particulate phosphorus loss also increases (Figure E.6). Susceptibility classes 1 and 2 are associated with low relief <8° areas, with the main differences between these two classes a factor of soil permeability and drainage.

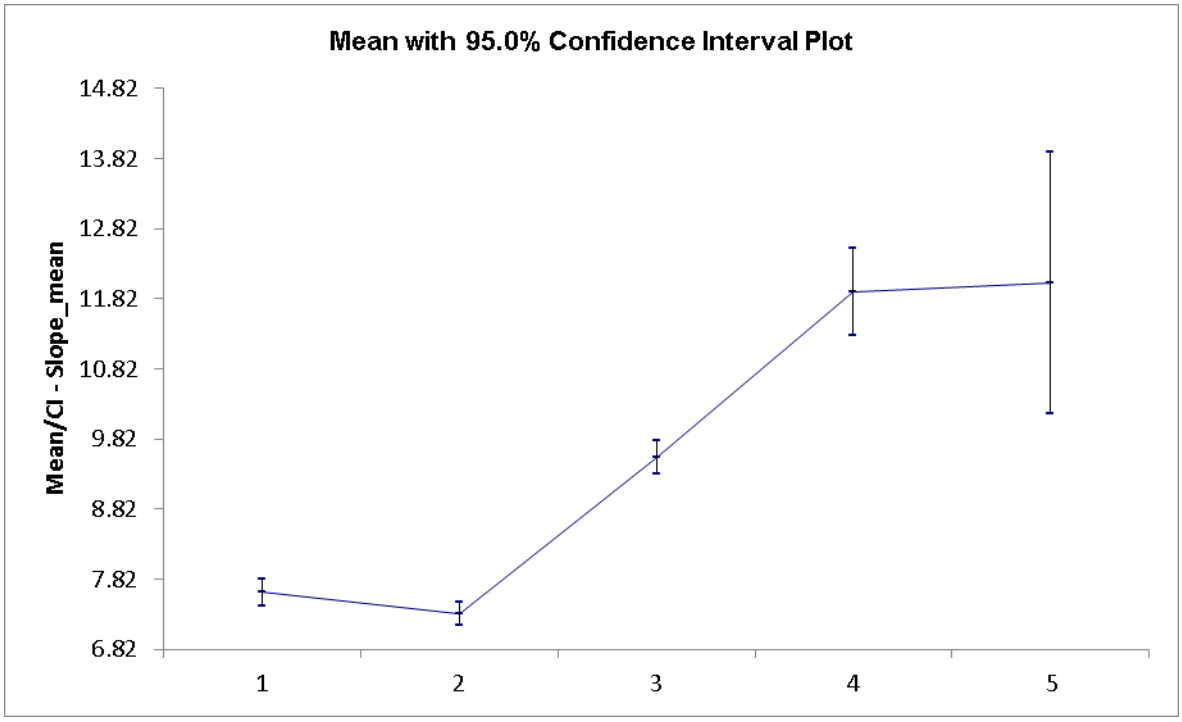

Games-Howell Probabilities (α = 0.05, 0.15)	1	2	3	4	5
1		0.1129	0.0000	0.0000	0.0001
2			0.0000	0.0000	0.0000
3				0.0000	0.0732
4					0.9999
5					

Figure E.6. Games-Howell post hoc test of slope (8 m DEM) vs. particulate phosphorus susceptibility class (1 = 0 – 20; 2 = 21 – 40; 3 = 41 – 60; 4 = 61 – 80; 5 = 81 – 100) for the mid-Mataura subcatchment. Susceptibility class 5 is not significantly different from class 4.

The depth to a slowly permeable horizon (DSLO) is considered an important landscape factor controlling the susceptibility of the landscape to particulate phosphorus loss. When soils are thin or a pan occurs close to the topsoil, soils are more likely to become saturated. Saturated soils produce greater quantities of overland flow. The Games-Howell post hoc test indicates an association between the depth to a slowly permeable layer and particulate phosphorus susceptibility (Figure E.7). Specifically, particulate phosphorus susceptibility increases as the depth to a slowly permeable layer decreases. Hill soils are often thin, especially where the slope is steep. Such soils can saturate more rapidly than deep, well drained soils. In areas of rock outcrop, the absence of soil favours runoff. The depth to a slowly permeable layer is deepest for classes 1 and 2. Classes 5 is associated with the steepest parts of the mid-Mataura, at some nominal threshold, slope overwhelms the influence of soil depth.

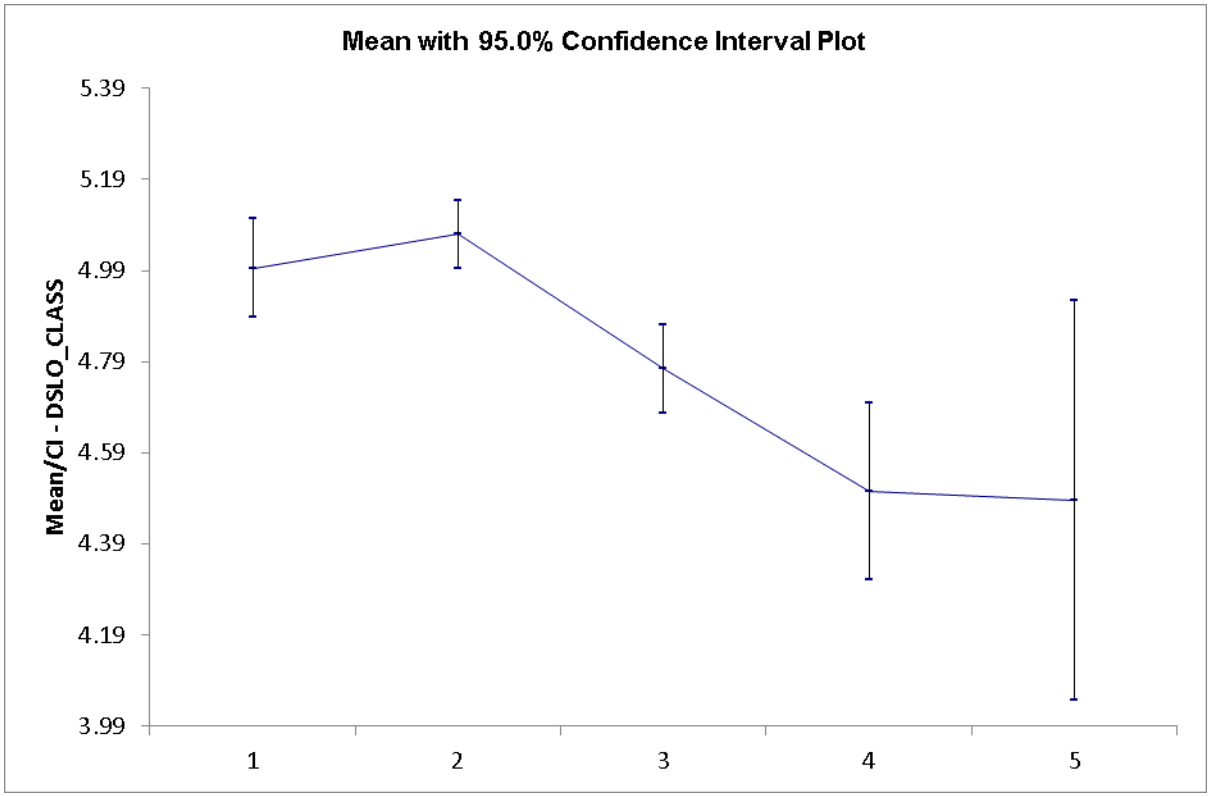

Games-Howell Probabilities (α = 0.05, 0.15)	1	2	3	4	5
1		0.8086	0.0246	0.0001	0.1726
2			0.0000	0.0000	0.0788
3				0.1046	0.6988
4					1.0000
5					

Figure E.7. Games-Howell post hoc test of depth to a slowly permeable horizon (1:50,000) vs. particulate phosphorus susceptibility class (1 = 0 – 20; 2 = 21 – 40; 3 = 41 – 60; 4 = 61 – 80; 5 = 81 – 100) for the mid-Mataura subcatchment. Depth to a slowly permeable horizon decreases across the particulate phosphorus susceptibility classes. This reflects the control of slope over the thickness of soil.

The percent of overland flow (surface runoff) from PENZ (1:50,000) incorporates slope, soil hydrological properties, and mean annual precipitation to provide an estimate of the per cent of mean annual precipitation than runs off across the landscape. As such, for a relatively homogenous geological setting such as the mid-Mataura, overland flow (OLF) combines the two most important factors that control the susceptibility of the landscape to particulate phosphorus loss. The Games-Howell post hoc test reveals a strong and systematic increase in OLF with particulate phosphorus susceptibility (Figure E.8). Classes 1 and 2 are associated with low-relief areas of the mid-Mataura, the loess mantled Edendale Terrace and the modern-day floodplain of the Mataura River. The main difference between classes 1 and 2 is soil drainage and associated soil reduction potential, with the soils associated with class 2 characterised by a larger proportion of imperfectly to poorly drained and slowly permeable soils.

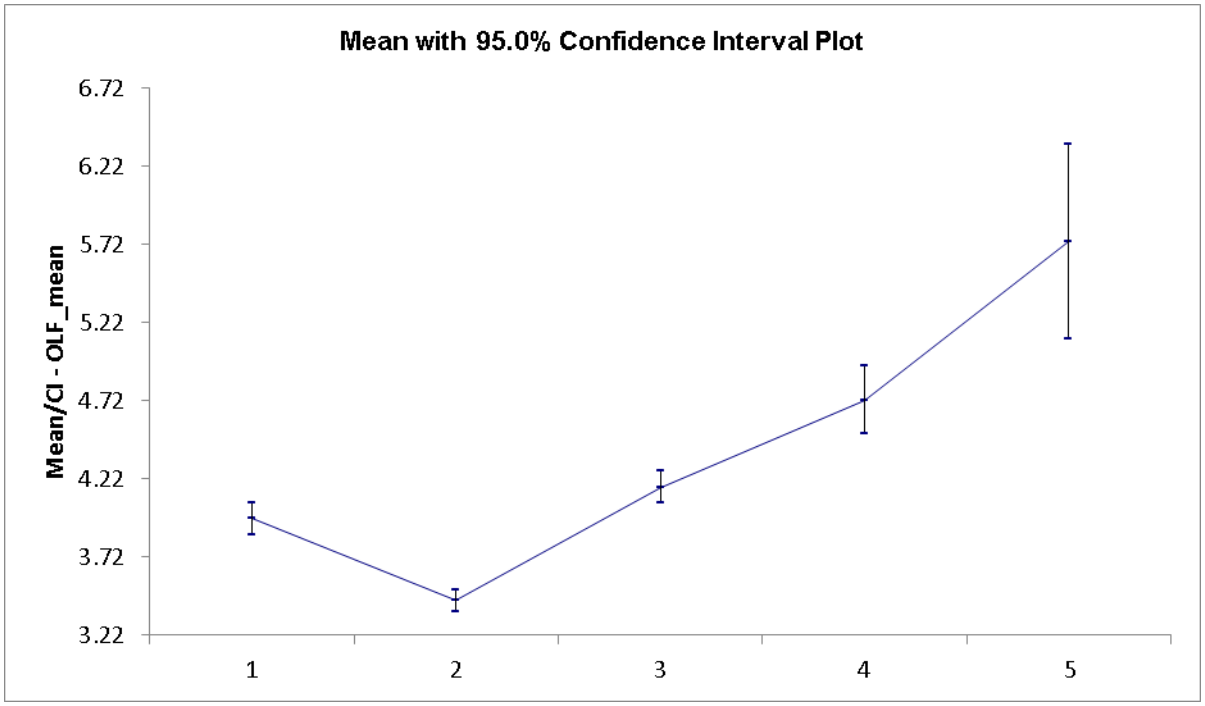

Games-Howell Probabilities (α = 0.05, 0.15)	1	2	3	4	5
1		0.0000	0.0584	0.0000	0.0000
2			0.0000	0.0000	0.0000
3				0.0000	0.0001
4					0.0242
5					

Figure E.8. Games-Howell post hoc test of percent overland flow of effective precipitation (PENZ; 1:50,000) vs. particulate phosphorus susceptibility class (1 = 0 – 20; 2 = 21 – 40; 3 = 41 – 60; 4 = 61 – 80; 5 = 81 – 100) for the mid-Mataura subcatchment.

In summary, the associations between data-driven susceptibility classes and historic soil and geological survey are consistent with established controlling landscape factor theory, and previous physiographic classification and testing of the mid-Mataura area (Rissmann et al., 2016, 2019). Specifically, where there is limited contrast in the inorganic phosphorus content of rock and sediment, slope and soil physical hydrological factors govern the susceptibility of the landscape to particulate phosphorus loss.

Upper-Mataura (Eyre Mountains)

The upper-Mataura is a steep, mountainous hill and high-country catchment characterised by weakly metamorphosed sandstones (psammite) and schist (pelitic schist, semi-schist) of the Caples Terrane (Figure E.9). Caples Terrane bedrock makes up 78% by area or 60,668 ha. Quaternary alluvium makes up the second largest geological unit by area at 19% or 14,658 ha. Glacial till makes up 2% of the area or 1,705 ha and is described by geological survey (Q-Map, 1:250,000) as “Undifferentiated till consisting of variably weathered, generally bouldery angular gravel with minor sand in cirque moraines.” The remaining geological units make up <2% by area and were excluded from analysis.

Geological survey defines the lithological units of the Caples Terrane as:

- schist: “Well foliated psammitic and pelitic schist with incipient segregation, minor greenschist and metachert, with quartz veins common.”

- Semischist: “Well foliated psammitic and pelitic semischist, phyllite, minor greenschist, metachert and metaconglomerate”.
- Sandstone: “Sandstone and mudstone with minor volcanic bands and broken formation texture.”

The petrochemistry of the Caples Terrane bedrock and the alluvial sediments it has generated are assumed to be broadly similar in terms of electron donors and inorganic P concentrations. Assumption of similar electron donor and P abundance is consistent with a common geological provenance for Caples Terrane bedrock facies (see Mortimer and Roser, 1992; Pound et al., 2014).

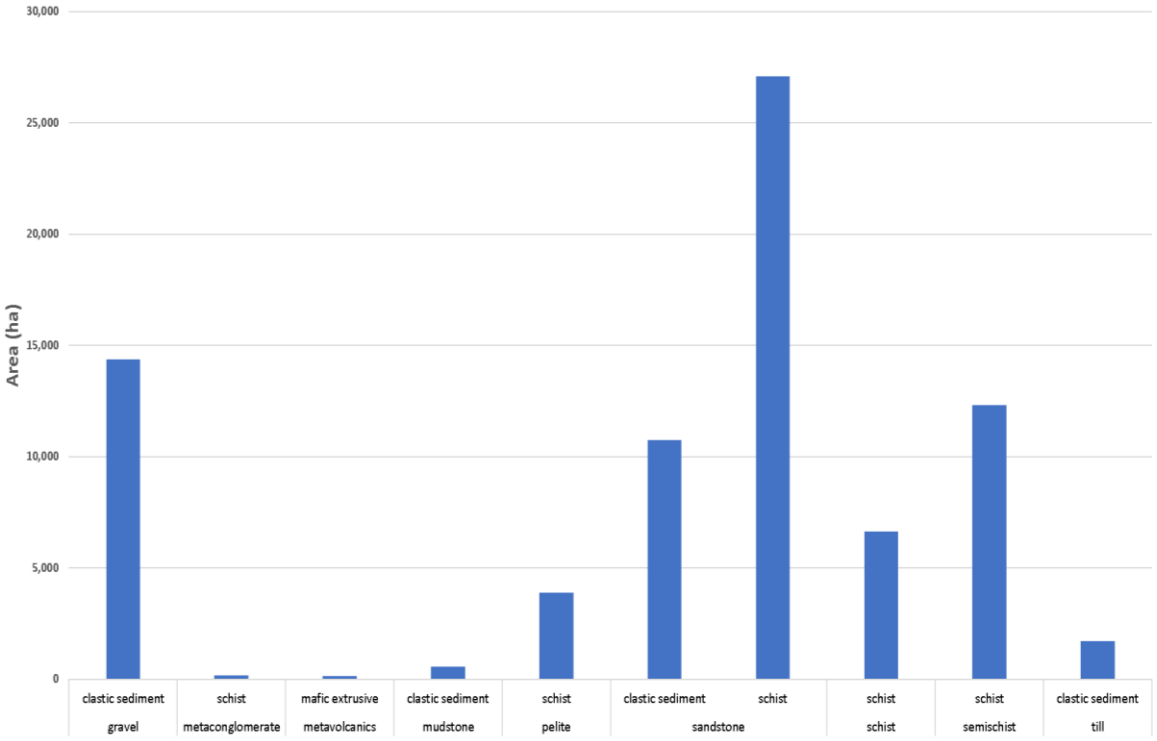

Figure E.9. Area (hectares) by Main Rock and Rock Class (Q-Map, 1:250,000) for the upper Mataura area.

According to geological survey, the small area of glacial till has the highest median elevation, followed by schist, sandstone, and semischist units of the Caples Terrane (Figure E.10). Quaternary alluvium has the lowest median elevation and slope. Semischist, sandstone and schist have similar median slope values that range between 20 – 22°. Most of the area of high elevation bedrock is sparsely vegetated. Valley fill, mainly as Quaternary alluvium is farmed except where the valley fill is associated with high elevation alpine valleys.

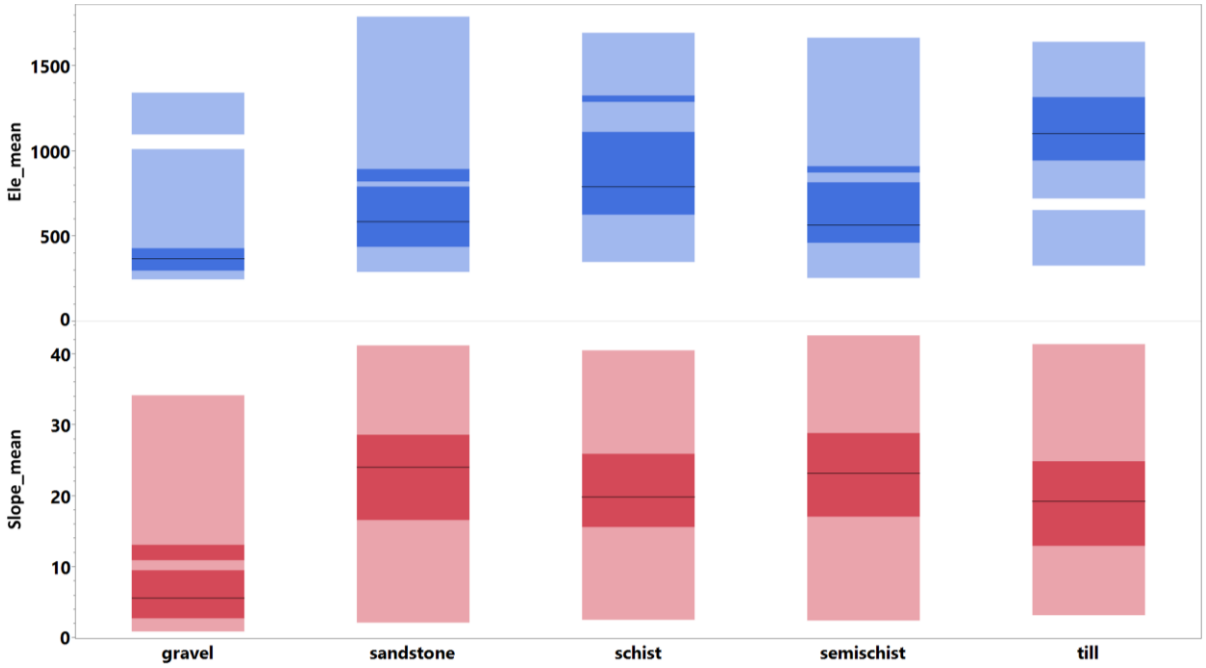

ROCK_GROUP	Slope (°)	Elevation (m RSL)	Slope Range	Elevation Range
gravel	11	391	40	1382
sandstone	21	754	55	1581
schist	20	944	44	1422
semischist	22	738	61	1737
till	19	1118	42	1314

Figure E 10. Slope and elevation by Rock Group (Q-Map, 1:250,000) for the upper Mataura area. Tabulated values for median and range. Lighter shaded region represents the 99% probability region; the darker shaded region represents the 50% probability region. Nonparametric density estimated by applying a Gaussian kernel to the data after the points have been interpolated to a grid.

According to soil survey (FSL, 1:50,000), depth to a slowly permeable layer (DSLO) is deepest for sandstone, followed by semischist, and shallowest for schist (Figure E.11). Till and gravel both have a similar DSLO. Soil drainage class is highest for till and sandstone and lowest for gravel, followed by schist. Soil permeability is variable within each rock group, with sandstone, and semischist characterised by moderate permeability and Quaternary alluvium with a greater proportion of moderate over rapid permeability (Figure E.12). Schist and glacial till exhibit a mix of moderate, moderate over rapid, and moderate over slow permeability.

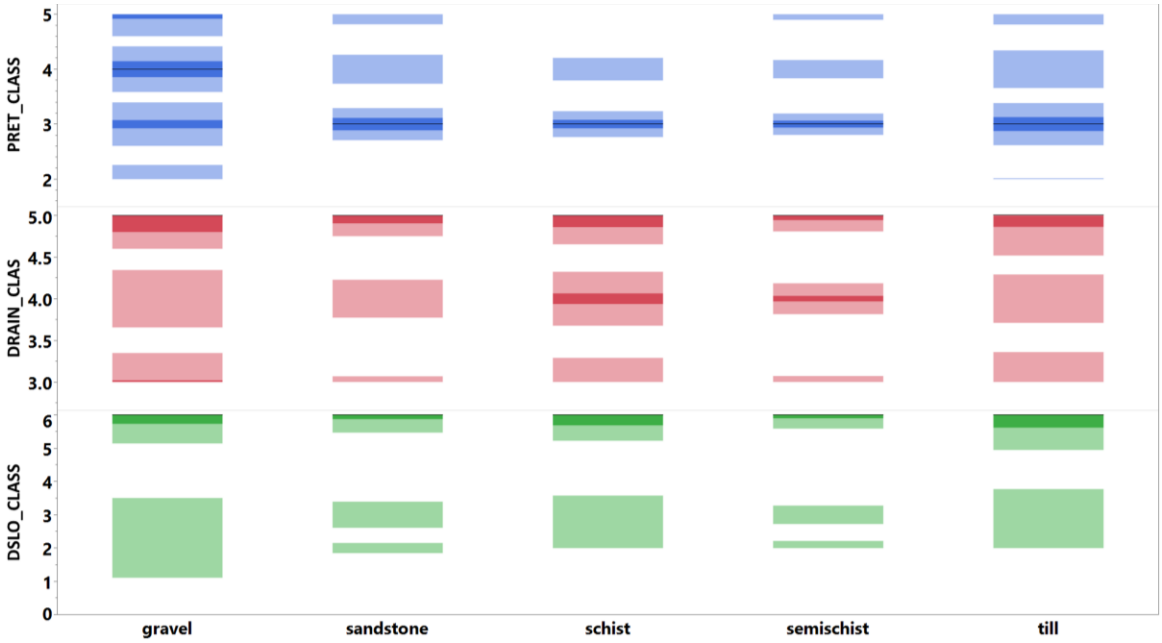

ROCK_GROUP	PRET_CLASS	DSLO_CLASS	DRAIN_CLASS	Min. PRET	Min. DSLO	Min. DRAIN	Max. PRET	Max. DSLO	Max. DRAIN
till	3.3	5.0	4.7	2	2	3	5	6	5
sandstone	3.4	5.7	4.7	2	1	3	5	6	5
semischist	3.3	5.6	4.5	2	2	3	5	6	5
schist	3.3	4.9	4.4	2	2	3	5	6	5
gravel	3.9	5.1	4.3	2	1	3	5	6	5

Figure E.11. Phosphorus retention class, depth to slow permeable layer (DSLO), and soil drainage class from soil survey (FSL, 1:50,000) by geological unit (Q-Map, 1:250,000). Lighter shaded region represents the 99% probability region; the darker shaded region represents the 50% probability region. Nonparametric density estimated by applying a Gaussian kernel to the data after the points have been interpolated to a grid. Tabulated mean, minimum, and maximum.

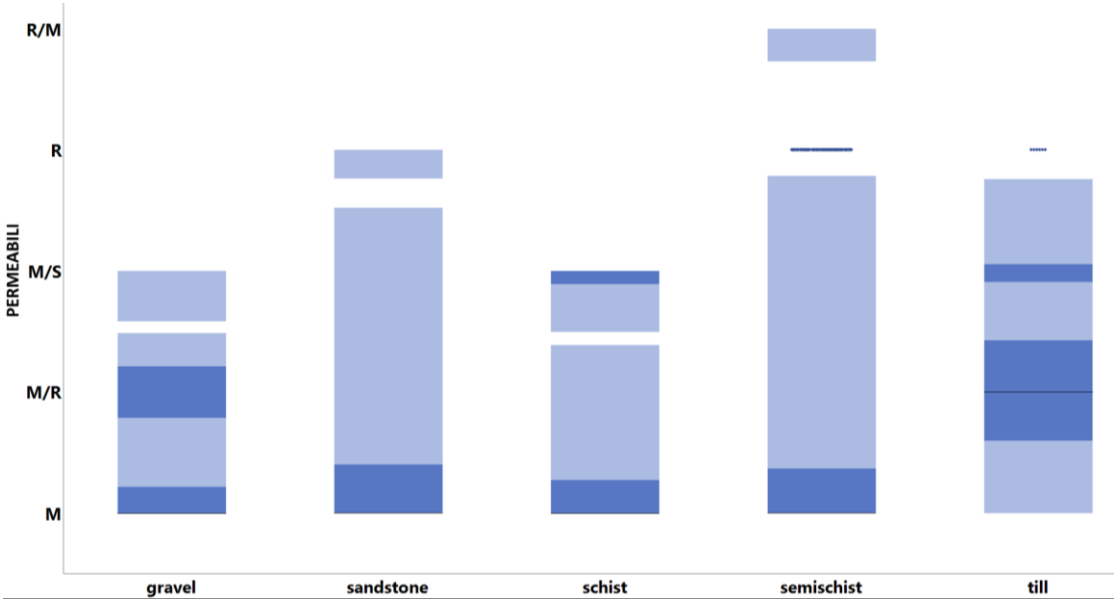

Figure E.12. Soil permeability from soil survey (FSL 1:50,000), by Rock Group (Q-Map, 1:250,000). Lighter shaded region represents the 99% probability region; the darker shaded region represents the 50% probability region. Nonparametric density estimated by applying a Gaussian kernel to the data after the points have been interpolated to a grid.

Nitrate-nitrite-nitrogen susceptibility

The Games-Howell post hoc test indicates that nitrate-nitrite-nitrogen susceptibility is lowest for schist, followed by the semischist of the Caples Terrane (Figure E.13). Sandstone, which has the deepest DSLO, and highest drainage class scores also has the highest susceptibility to nitrate-nitrite-nitrogen leaching of the bedrock units. Glacial till has the second highest susceptibility, which according to soil survey is probably due to rapid permeability and the deepest DSLO score. Overall, Quaternary alluvial valley fill is associated with the highest nitrate-nitrite-nitrogen susceptibility of all the geological units that characterise the upper Mataura.

The strongly contrasting susceptibilities are a factor of geological control over slope, soil water residence time, and - across areas of steep alpine and hill country - the thin soil cover. Thin soils overlying slowly permeable rock is more likely to saturate than thick, well drained soils. Soils that saturate will actively denitrify; soils that do not saturate do not denitrify. Further, the residence time of water in steep alpine and hill country environments is much shorter than that occurring in lowland settings. Soil where waters have a greater residence time favour the generation of nitrate-nitrite.

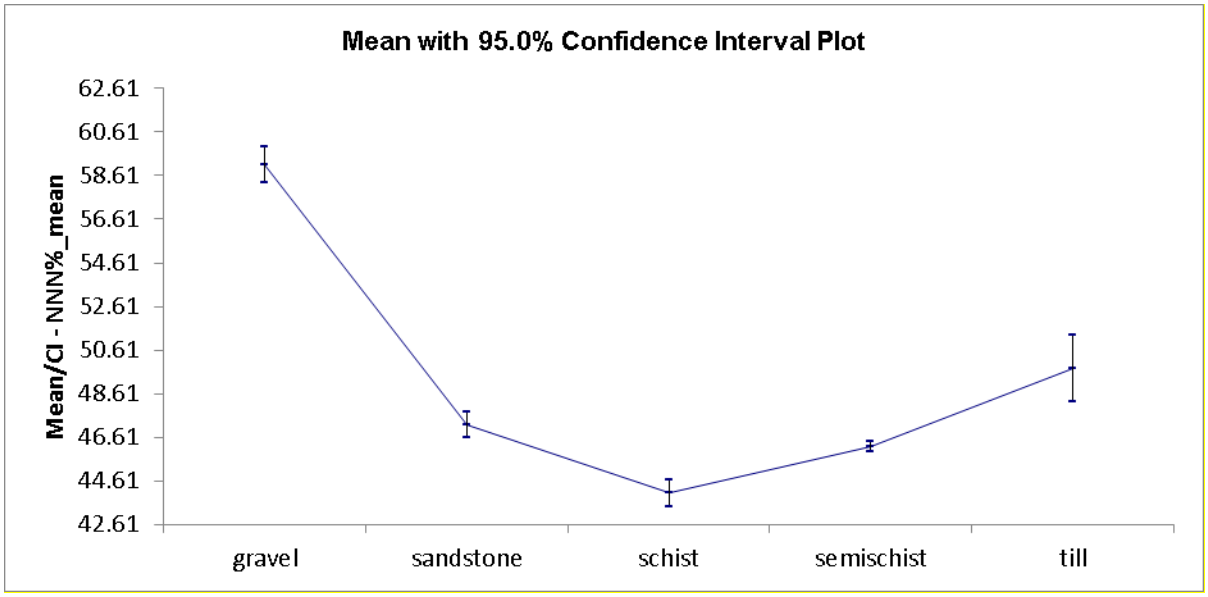

Games-Howell Probabilities α = 0.05, 0.15	gravel	sandstone	schist	semischist	till
gravel		0.0000	0.0000	0.0000	0.0000
sandstone			0.0000	0.0134	0.0159
schist				0.0000	0.0000
semischist					0.0000
till					

Figure E.13. Games-Howell post hoc test of 'Rock_Class' (Q-Map, 1:250,000) vs. nitrate-nitrite-nitrogen susceptibility class (1 = 0 – 20; 2 = 21 – 40; 3 = 41 – 60; 4 = 61 – 80; 5 = 81 – 100) for the upper-Mataura subcatchment. Welch's ANOVA was statistically significant at α= 0.05.

Application of the Games-Howell post hoc test indicates that the susceptibility to nitrate leaching increases as slope decreases (Figure E.14). The increase in nitrate-nitrite-nitrogen susceptibility with decreasing slope is consistent with controlling factor theory. Specifically, as slope decreases, soil thickness increases, along with the increasing residence time of water within the soil zone, favouring nitrate-nitrite-nitrogen production and leaching.

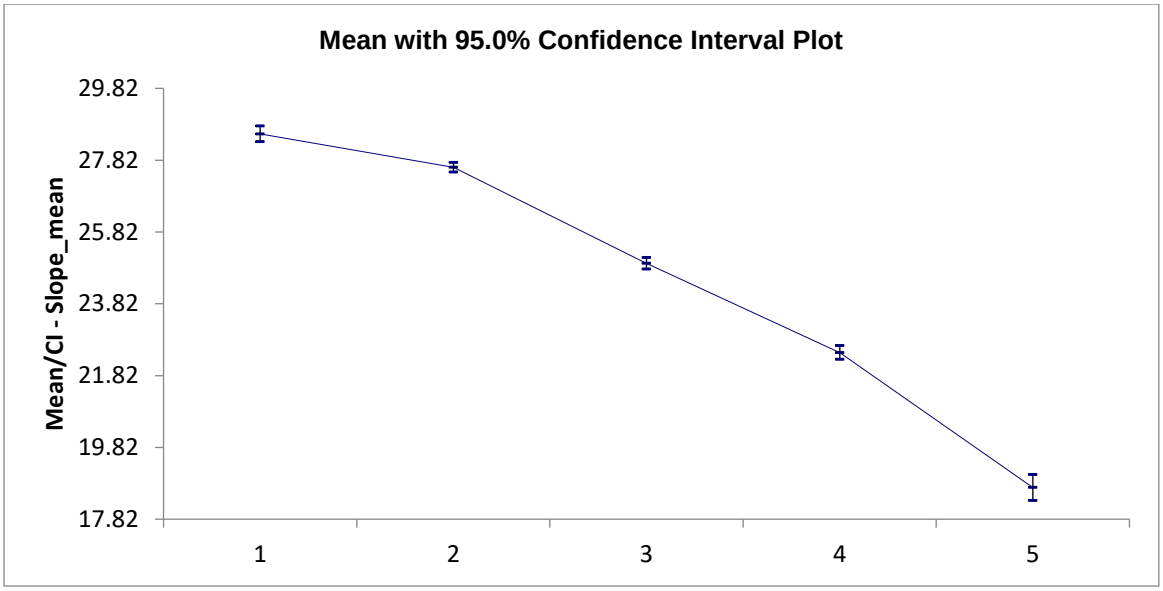

Games-Howell Probabilities α = 0.05, 0.15	1	2	3	4	5
1		0.0000	0.0000	0.0000	0.0000
2			0.0000	0.0000	0.0000
3				0.0000	0.0000
4					0.0000
5					

Figure E.14. Games-Howell post hoc test of slope vs. nitrate-nitrite-nitrogen susceptibility class (1 = 0 – 20; 2 = 21 – 40; 3 = 41 – 60; 4 = 61 – 80; 5 = 81 – 100) for the upper-Mataura area.

In summary, the associations between nitrate-nitrite-nitrogen susceptibility and established controlling landscape factors represented by historic soil and geological survey are consistent with controlling landscape factor theory. Geology is the first order control over the susceptibility of the upper Mataura area to nitrate-nitrite-nitrogen leaching susceptibility. Geology controls slope, slope controls soil drainage, and the relative residence time of water in contact with the soil zone.

Association testing reveals that the low relief areas of Quaternary valley fill have the highest susceptibility to nitrate-nitrite-nitrogen leaching, and areas of steep land above the treeline the lowest. This susceptibility pattern is consistent with established controlling landscape factor theory for nitrate-nitrite-nitrogen susceptibility and with historic physiographic classifications of the Southland region (Rissmann et al., 2016, 2019).

Particulate phosphorus susceptibility

Applying the Games-Howell post hoc test to Rock Group (Q-Map) shows that Quaternary valley fill has a significantly lower susceptibility to particulate phosphorus loss than Caples Terrane bedrock and glacial till (Figure E.15). The strongly contrasting susceptibilities between the Quaternary valley fill and bedrock is consistent with geological control over slope and runoff. Soil permeability, depth to a slowly permeable layer, and drainage class are secondary to slope, but also contribute to spatial variation in the susceptibility of the upper Mataura to particulate phosphorus loss.

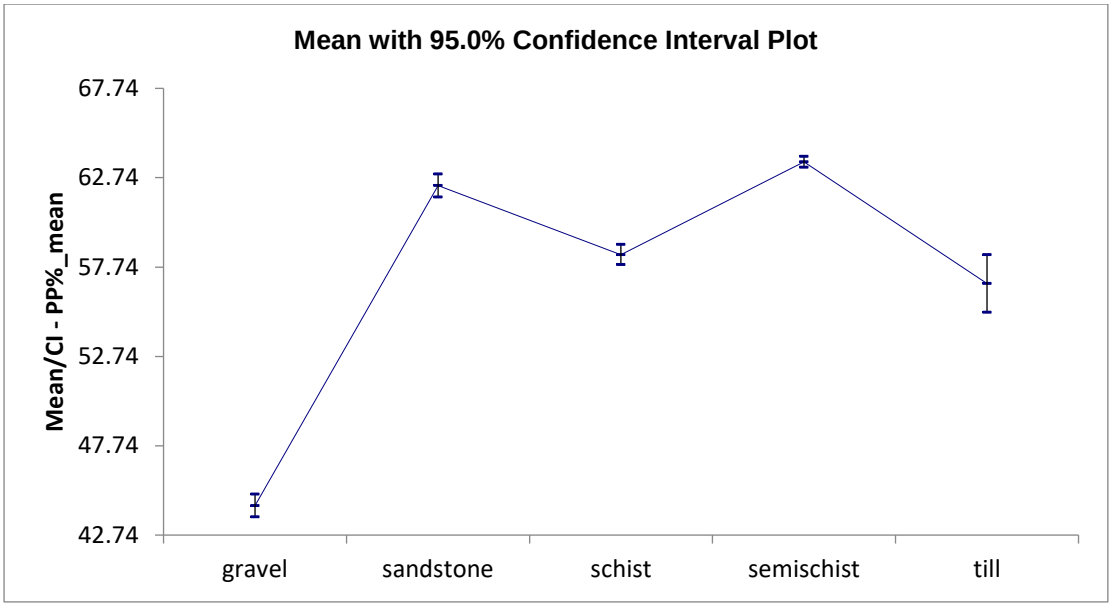

Games-Howell Probabilities	α = 0.05, 0.15	gravel	sandstone	schist	semischist	till
gravel			0.0000	0.0000	0.0000	0.0000
sandstone				0.0000	0.0026	0.0000
schist					0.0000	0.3351
semischist						0.0000
till						

Figure E.15. Games-Howell post hoc test of Q-Map derived 'Rock_Group' vs. particulate phosphorus susceptibility class (1 = 0 – 20; 2 = 21 – 40; 3 = 41 – 60; 4 = 61 – 80; 5 = 81 – 100) for the upper-Mataura subcatchment. Welch's ANOVA was statistically significant at α= 0.05. The susceptibility of glacial till is not significantly different from schist.

The percent of overland flow (surface runoff) from PENZ incorporates slope, soil hydrological properties, and mean annual precipitation to provide an estimate of the percent of mean annual precipitation than runs off across the landscape (Figure E.16). Overland flow (OLF, 1:50,000) therefore combines the two most important factors controlling the susceptibility of the landscape to particulate phosphorus loss. Applying the Games-Howell post hoc test to particulate phosphorus susceptibility class reveals a strong positive association between susceptibility and OLF (Figure E.17).

Application of Welch's ANOVA and Games-Howell post hoc tests reveal a systematic increase in particulate phosphorus susceptibility by percent overland flow. Susceptibility classes 1 and 2 are dominated by Quaternary alluvial valley fill and classes 3 – 4 by the bedrock facies of the Caples Terrane.

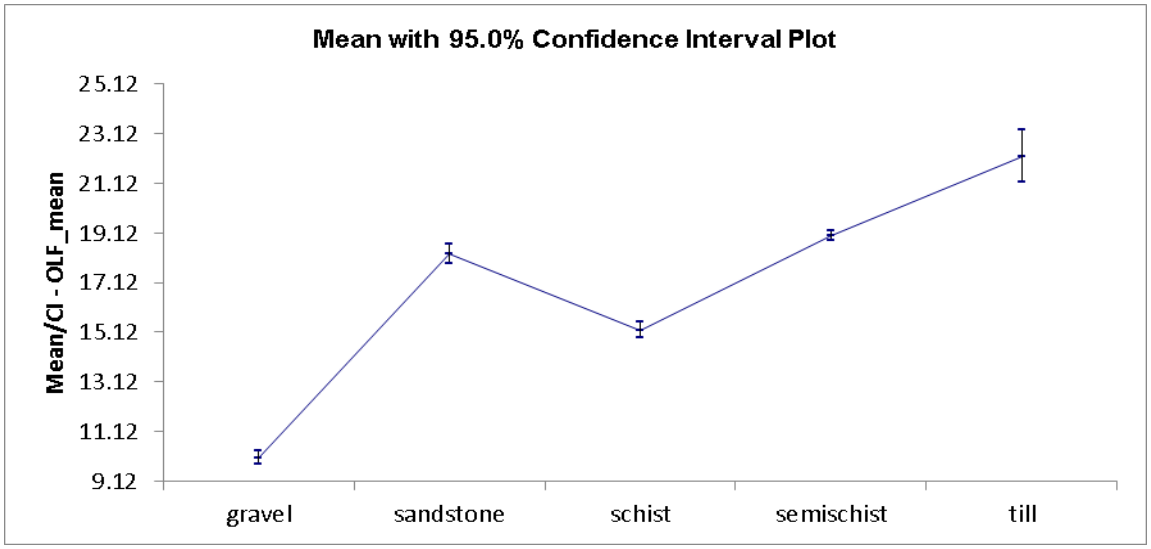

Games-Howell Probabilities	α = 0.05, 0.15	gravel	sandstone	schist	semischist	till
gravel			0.0000	0.0000	0.0000	0.0000
sandstone				0.0000	0.0120	0.0000
schist					0.0000	0.0000
semischist						0.0000
till						

Figure E.16. Games-Howell post hoc test of per cent overland flow (OLF) (PENZ, 1:50,000) vs. particulate phosphorus susceptibility class (1 = 0 – 20; 2 = 21 – 40; 3 = 41 – 60; 4 = 61 – 80; 5 = 81 – 100) for the upper-Mataura subcatchment.

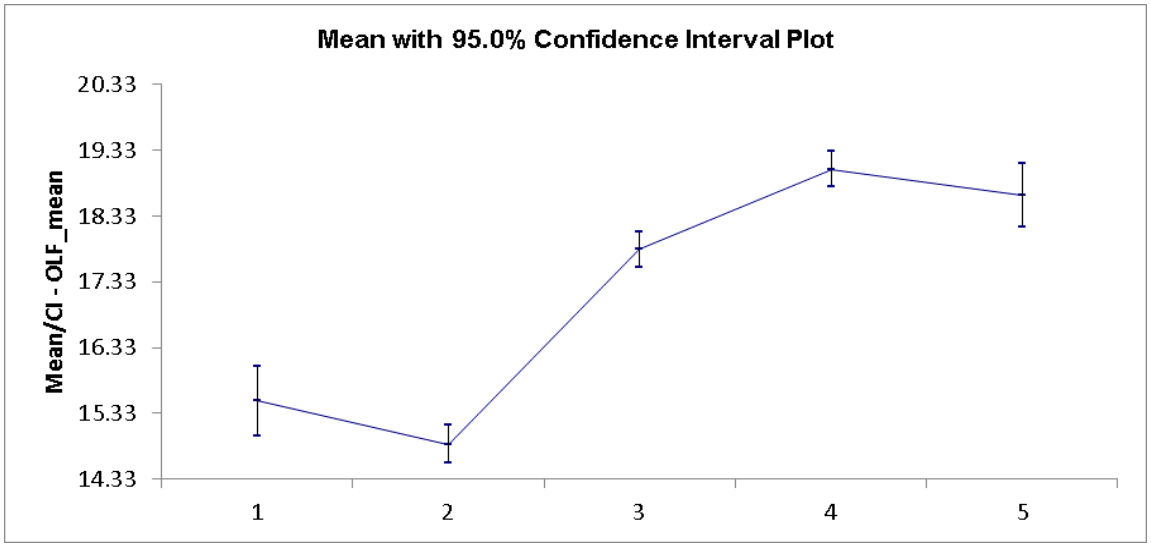

Games-Howell Probabilities	α = 0.05, 0.15	1	2	3	4	5
1			0.2158	0.0000	0.0000	0.0000
2				0.0000	0.0000	0.0000
3					0.0000	0.0293
4						0.6442
5						

Figure E.17. Games-Howell post hoc test of particulate phosphorus susceptibility by Rock Group (Q-Map, 1:250,000). Phosphorus susceptibility class (1 = 0 – 20; 2 = 21 – 40; 3 = 41 – 60; 4 = 61 – 80; 5 = 81 – 100) for the upper-Mataura area. Classes 1 and 2, and 4 and 5 are not significantly different.

In summary, the association between particulate phosphorus susceptibility and controlling landscape factors represented by historic soil and geological survey are consistent with established controlling landscape factor theory for areas of relatively homogenous geology and with historic physiographic classifications of the Southland region (Rissmann et al., 2016, 2019).

Wairoa Catchment

Northland has a large area of allochthonous rocks that originated from outside the region, having been rafted-in and juxtaposed by tectonic processes[43].

The Northland Allochthon is characterised by the strong basalts of the Tangihua Complex, which originated as mid-ocean ridge basalts, and a complex array of weak sedimentary sand and mudstones of the Mangakahia Complex. Autochthonous rocks (those rocks and sediments that formed *in situ*) include: the youthful (Pleistocene) Kerikeri Volcanic Group basalts that intruded through the deep greywacke basement (Waipapa Group, within which we have included the Mesozoic sandstones of the Waitemata Group) that underlies the region; and the overlying allochthonous sedimentary units, mantling the landscape with low relief lava flows (e.g., Kerikeri area) or generating basaltic volcanoes characterised by gentle slopes and scoria cones (e.g., Whatitiri Maunga). Holocene River Deposits occupy low lying valleys, amongst the large area of hill and steep lands.

Northland is geologically more complex than Southland, with a greater variety of geological materials that are physically and chemically very different. Northland and the Wairoa Catchment have not experienced recent glaciation nor widespread volcanism. Geomorphically Northland hosts the oldest landscape in New Zealand. The strongly contrasting geologies and general antiquity of the landscape means the controlling factors that govern landscape susceptibility in other regions of New Zealand should not be extrapolated to Northland and the Wairoa Catchment, without careful consideration of their relevance.

Sediment susceptibility

Sediment is a mix of organic and inorganic materials of varying particle size. Sediment is derived from the regolith, the weathered portion of the earth's crust, or because of mass failure of unweathered or weakly weathered rock or sediment. Soil forms a component of the regolith and represents the uppermost portion of the land surface. Sediment is lost through mass wasting processes in which rock and soil fail and move down slope under the influence of gravity, and via erosion, the transport of earth materials by wind and water.

As a heterogenous mix of earth materials, sediment is associated with microbial, biomolecular (fluvic and humic acids), major, minor, and trace ion constituents. Nutrients such as ammoniacal and organic nitrogen, particle bound inorganic and organic phosphorus, and microbes are often attached to sediment and transported with sediment to waterways. Sediment quality – in terms of its chemical and biological associations - is seldom considered by New Zealand's environmental research community, rather the mass of sediment, mainly as sand, silt, and clay is the primary focus. However, the mass wasting or erosion of a small amount of sediment from an area with elevated P, N, and microbial content can have a disproportionate effect on the internal eutrophication of waterways, relative to a small volume of sediment from an area with low P, N, and microbial content (Boynton et al., 1995; Ekholm and Lehtoranta, 2012; Joshi et al., 2015; Kleinmanet al., 2019; Moncelon et al, 2021). A failure to consider the nutrient and microbial load of sediment, vis a viz,

[43] Allochthonous geological materials have originated in locations remote to where they now reside.

sediment quality will fail to identify the drivers of internal eutrophication of streams, lakes, estuaries, and harbours[44].

Of the drivers of sediment generation and loss to waterways it is well established that, *geology is the first order control over the susceptibility of any landscape to mass wasting and erosion* (Morel et al., 2003; Mueller and Pitlick, 2013; Fratkin et al., 2020). In the case of mass wasting, weak rocks fail at lesser slopes than strong rocks, with the corollary that generally stronger rocks are associated with steeper slopes. Geology therefore determines the topography of the landscape, which also influences local climatic gradients and, as a result, the type and density of vegetation cover. Geology in combination with topography, climate, and vegetation also determines the physical and biogeochemical character of soils, including their susceptibility to mass wasting and erosion.

Dissolved reactive phosphorus susceptibility

Dissolved reactive phosphorus as measured in freshwater comprises the $\leq$0.45 μm fraction and may be comprised of organic and inorganic P molecules. Some of the small organic and inorganic phosphorus molecules may occur as nanometer sized colloids, which are highly mobile under a specific range of conditions. The main controls over dissolved reactive phosphorus includes chemical weathering, i.e., both hydrolysis of primary minerals to form clays and chemical dissolution (e.g., limestone) and redox reactions.

Oxides and oxyhydroxides are the main minerals that sequester and hold on to phosphorus in the environment. They are also responsible for the brown and red colours of weathered soil and rock and are indicative of an oxidising environment, one characterised by abundant oxygen. When oxides and oxyhydroxides are subject to low oxygen environments they dissolved, releasing any stored P into solution. As such, redox indirectly controls the mobility of dissolved reactive phosphorus via the reductive dissolution of the oxides and oxyhydroxides of iron, manganese, and aluminium. Accordingly, under low oxygen conditions, dissolved reactive forms of phosphorus may be highly mobile and easily transported through porous media to stream or groundwater. For these reasons, peat deposits, organic soils, and poorly drained soils are more susceptible to dissolved reactive phosphorus loss. Groundwater systems that are strongly anoxic can also produce significant amounts of dissolved reactive phosphorus. However, for most groundwater systems, dissolved reactive phosphorus is geogenic or 'naturally' derived. Exceptions occur in areas of peat soils and aquifers where intensive land use on reducing soils that overlie reducing groundwater systems may result in elevated dissolved reactive phosphorus leaching and accumulation in groundwater. Accordingly, it is well established internationally that *geology is the first order control over the susceptibility of the landscape to dissolved reactive phosphorus loss* (Porder et al., 2013).

Tangihua, Wairoa Catchment, Northland

The weak allochthonous and mudstones of the Mangakahia Complex make up 58% of the Tangihua area (Figure E.18). The Holocene River deposits of the Tauranga Group are 10%, the Tangihua Complex (8%), and Kerikeri Volcanic Group (6%). The marine sandstones of the Mesozoic aged Waitemata Group make up 5% by area. The remaining geological units total <3% in area and were excluded from analysis.

The Mangakahia Complex is comprised of a range of weak, allochthonous sand, silt, and mudstones (e.g., Punakitere Sandstone, Ruarangi Siltstones, Whangai Mudstones). Geological survey (Q-Map, 1:250,000) describes the Tangihua Complex as "Mainly basalt pillow lava, with subvolcanic intrusives of basalt, dolerite and gabbro." The Tangihua Complex is allochthonous, originating as mid ocean

[44] https://www.usgs.gov/special-topics/water-science-school/science/phosphorus-and-water

ridge basalts (MORB). Tauranga group sediments are described as “Unconsolidated to poorly consolidated mud, sand, gravel and peat deposits of alluvial, colluvial and lacustrine origins,” and the youthful Kerikeri (Pleistocene) Volcanic Group as basalt lava flows and volcanic plugs. The Mesozoic aged Waitemata Group is described as “Laminated to thin-bedded, calcareous siltstone with rare, interbedded shelly sandstone.”

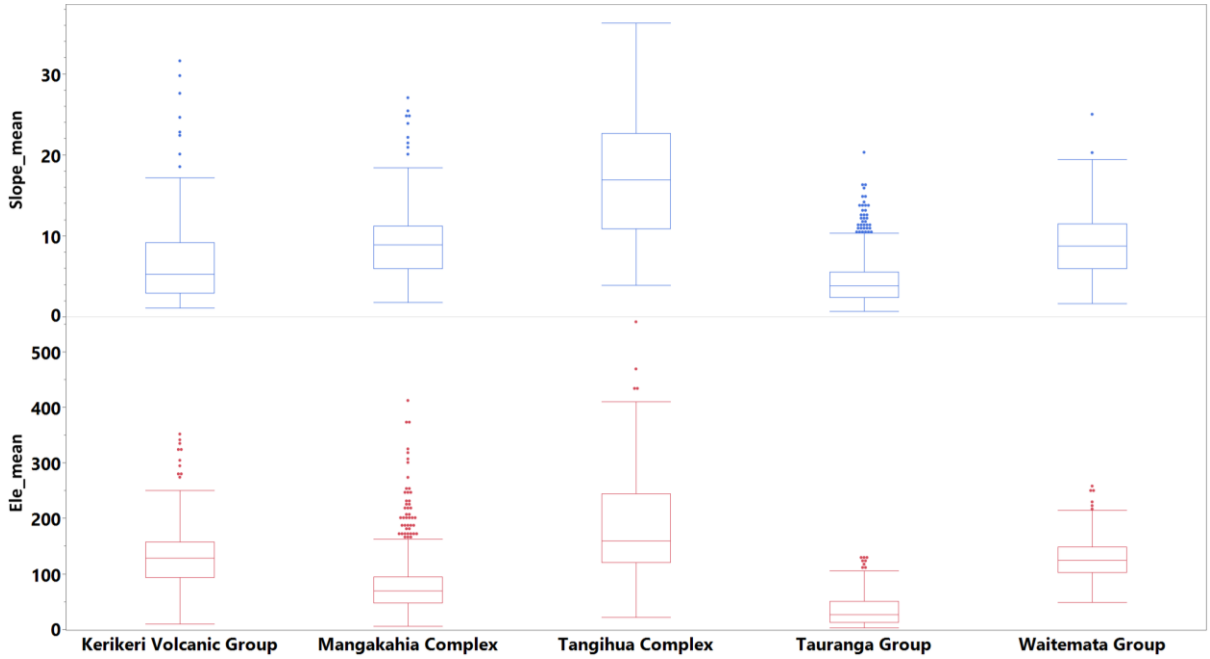

Geological Unit	N Rows	Elevation (m RSL)	Slope (°)	Min. Elevation	Min. Slope	Max. Elevation	Max. Slope
Kerikeri Volcanic Group	240	128.8	5.4	9.6	1.1	351.6	31.6
Mangakahia Complex	2744	69.5	8.9	5.5	1.8	412.1	27.0
Tangihua Complex	385	159.4	16.9	21.9	3.9	553.8	36.3
Tauranga Group	545	28.3	3.9	3.2	0.7	129.7	20.3
Waitemata Group	548	124.5	8.8	48.5	1.7	258.0	25.0

Figure E.18. Box and Whisker plots of elevation in metres relative to sea level (m RSL) and slope (°) vs. main geological unit (Q-Map) across the Tangihua area. Median, minimum, and maximum values in table.

Hill country is the dominant landform across the Tangihua area, with the highest elevation and steepest land associated with the competent rock of the Tangihua Complex. The youthful Whatitiri Maunga is a symmetrical basalt volcanic cone of the Kerikeri Volcanic Group with gentle slopes and deep, well drained soils that overlie a fractured basalt aquifer system. The sedimentary rocks of the Mangakahia Complex include large areas of sandstone and mudstone, much of it very weak (incompetent) and prone to mass wasting and erosion. The soils formed in the sand and mudstones are clay-rich, imperfectly to poorly drained, and moderately to slowly permeable. Due to the large area (70%) of slopes ≥12° the soils of the Tangihua Complex are thin. Bedrock occurs close to and in places at the surface – there is thus limited unconsolidated regolith available for export. Streams draining the Tangihua Complex rocks have high clarity relative to streams draining the weak sedimentary sand and mudstones of the Northland Allochthon and the Waipapa Group greywackes (Northland Regional Council surface water quality monitoring data).

The strong basalts of the Tangihua Complex make up by far the highest elevation and relief geological unit of the Tangihua area. The weak sedimentary units of the Mangakahia Group and the strong but deeply weathered marine sandstones of the Waitemata Group have significantly lower mean slope values and elevation. The Whatitiri Maunga is the dominant landform feature of the Kerikeri Volcanic Group within the Tangihua area and is characterised by the second highest elevation yet has the second lowest mean slope. Basalt volcanoes are typically characterised by low relief due to the low viscosity of basaltic lava. The unconsolidated Holocene River deposits of the Tauranga Group occupy the lowest elevation parts of the Whakapara area and are characterised by the lowest relief.

According to soil survey (FSL, 1:50,000), soil drainage class is lowest for the Mangakahia Complex, Waitemata Group, and Tauranga Group geological units and highest for the Kerikeri Volcanic Complex and Tangihua Complex (Figure E.19A systematic and expected pattern of association between susceptibility classes and controlling landscape factors that are consistent with previous physiographic classifications and physiographic knowledge of the Northland and Southland regions, and). Depth to a slowly permeable layer (e.g., bedrock or low permeability soil horizon) is shallowest for the imperfect to poorly drained soils of the Mangakahia Complex and Waitemata Group, and deepest for the well-drained basalt soils of the Tangihua Complex (but only where the slope is <12°) and Kerikeri Volcanic Group. Tauranga Group Holocene River deposits have smaller number of soils with a slowly permeable layer than the hill country soils formed in the Mangakahia Complex and Waitemata Group sedimentary rocks. The clay-rich soils formed in the weak sedimentary sand and mudstones of the Mangakahia Complex are characterised by the lowest permeability followed by the soils formed in Waitemata Group, and Tauranga Group geological units. The soils of the Kerikeri Volcanics and Tangihua Complex have moderate permeability.

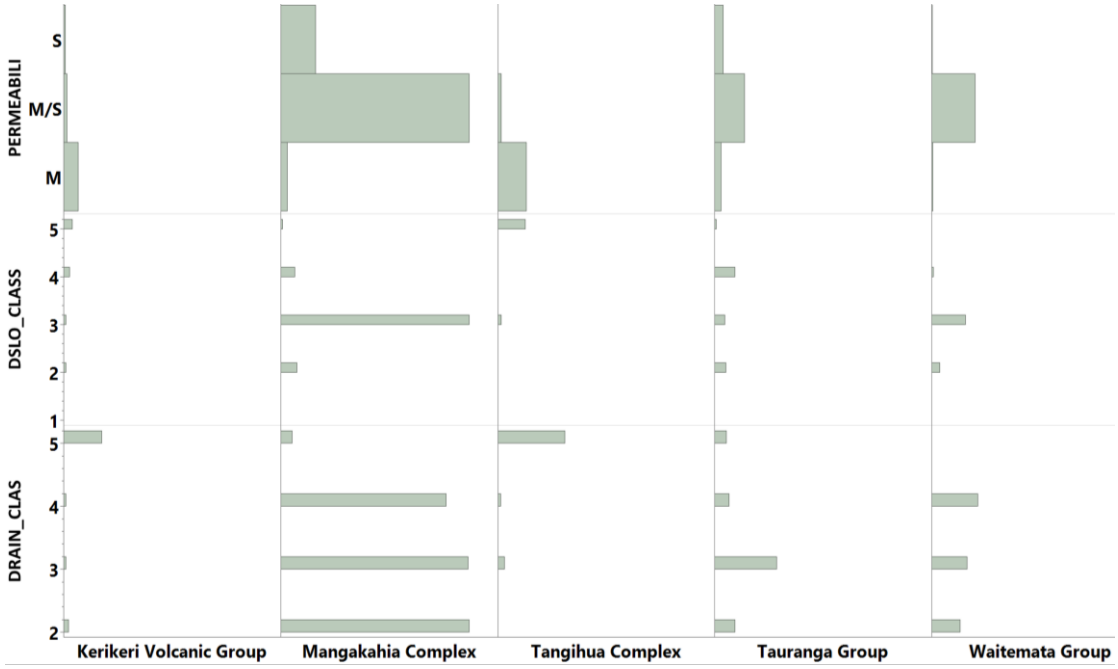

Geological Unit	N Rows	DRAIN_CLASS	DSLO_CLASS
Kerikeri Volcanic Group	240	5	4
Mangakahia Complex	2,744	3	3
Tangihua Complex	385	5	5
Tauranga Group	545	3	4
Waitemata Group	548	3	3

Figure E.19. Median permeability (M = moderate; M/S moderate over slow; S = Slow), depth to slowly permeable layer (DSLO), and soil drainage class (FSL) by main geological unit (Q-Map) for the Whakapara area.

Rissmann et al. (2018) identified that mass wasting and erosion were strongly linked to rock type and the geostructural relationships (i.e., tectonic, and stratigraphic) between the allochthonous and autochthonous rocks of the Northland Region. They noted that the weak sedimentary mud and sandstones of the Northland Allochthon were associated with the greatest number of mass wasting and erosional features followed by the deeply weathered greywacke basement rock of the Waipapa Group that outcrops across eastern Northland.

Geostructural relationships controlling mass wasting and erosion susceptibility included the association between young flood basalts that intruded through and overtop of weak allochthonous sedimentary units. Undercutting and dispersion of the weak mudstone units drives instability, the form of mass movement and erosion. Areas of contact between the highly competent basalts of the Tangihua Complex and weak sedimentary mud and sandstones are another geostructural setting associated with elevated mass wasting and erosion susceptibility. The deeply weathered regolith of the Mesozoic Waitemata Group sandstones and Waipapa Group Eastern Basement rocks were also identified as having an elevated susceptibility to mass wasting and erosion.

An independent assessment of the geologically-based mass wasting, and erosion susceptibility classification of Rissmann et al. (2018) found a high degree of correspondence between the mass wasting and erosion classes and the number, size, and type of mass wasting and erosional features across Northland (McDonald et al., 2020). In the following, it is critical to note that *rock strength*, not slope, is the main driver of mass wasting and resultant sediment generation across Northland. Specifically, weak rocks fail at lower slope angles than strong rock and weak rocks and seldom attain the same elevation or slope angles than strong rock.

Sediment susceptibility

Application of Welch's ANOVA and the Games-Howell post hoc test to the most important geological units of the Tangihua area are consistent with the controlling landscape factors rock strength, weathering, and geostructural origin as the main drivers of the susceptibility of the Tangihua area to sediment loss (Figure E.20 and E.21). Specifically, the weak (structurally incompetent) sedimentary rocks of the Mangakahia Complex have by far the highest susceptibility to mass wasting and erosion. The deeply weathered sandstones of the Waitemata Group and the Holocene River deposits of the Tauranga Group have significantly lower susceptibilities to sediment loss but are still elevated relative to the competent rocks of the Tangihua Complex and Kerikeri Volcanic Complex (Whatitiri Maunga). The pattern of susceptibility is consistent with controlling factor hypothesis that relate the susceptibility of sediment loss to the geostructural evolution of the geological unit and its strength (Rissmann et al., 2018).

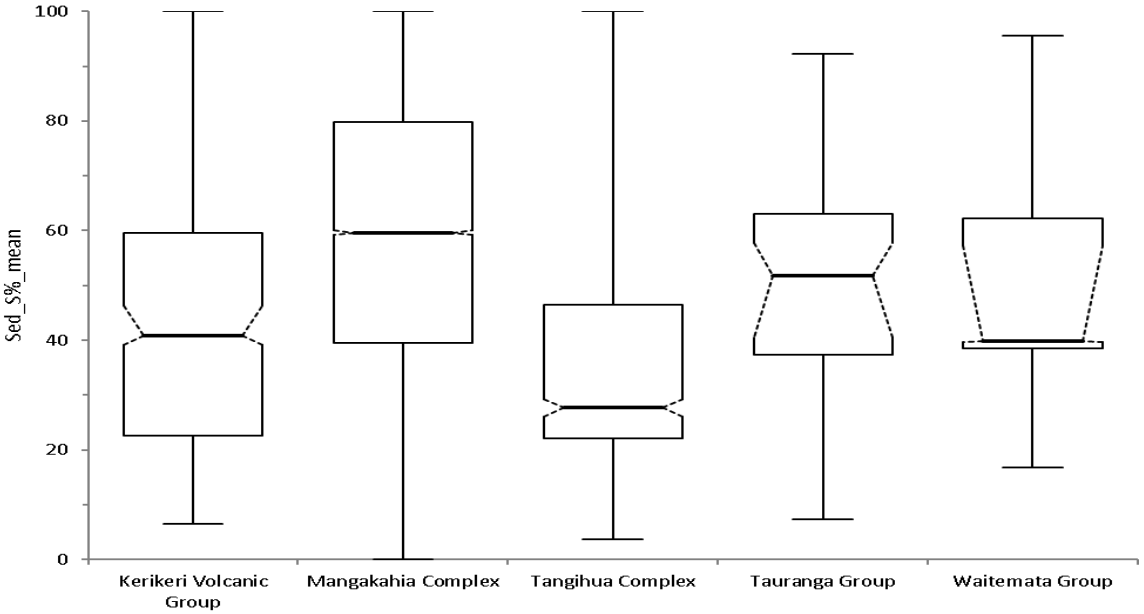

Geological Unit	Minimum	1st Quartile	Median	95% CI		3rd Quartile	Maximum
Mangakahia Complex	0.0	39.5	59.6	59.3	60.1	79.7	100.0
Tauranga Group	7.3	37.3	51.8	40.6	57.8	63.0	92.3
Kerikeri Volcanic Group	6.5	22.6	40.8	39.2	46.3	59.6	100.0
Waitemata Group	16.7	38.6	39.9	39.7	57.3	62.2	95.5
Tangihua Complex	3.7	22.1	27.8	26.1	29.2	46.4	100.0

Figure E.20. Box and whisker plot of landscape susceptibility to sediment loss (%) by main rock unit for the Tangihua area, Wairoa Catchment, Northland.

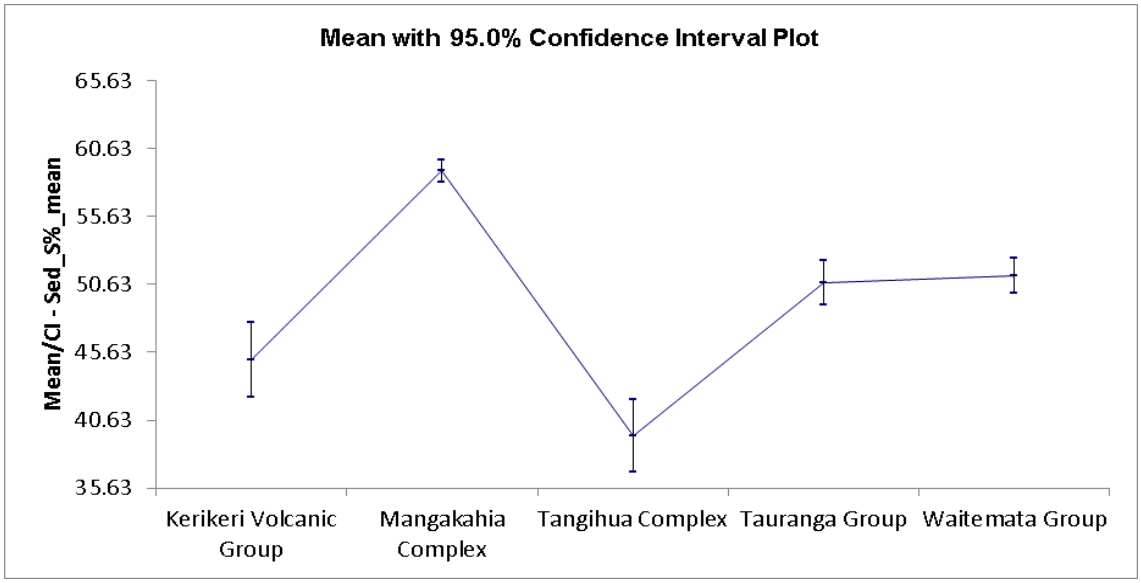

Games-Howell Probabilities ($\alpha = 0.05, 0.15$)	Kerikeri Volcanic Group	Mangakahia Complex	Tangihua Complex	Tauranga Group	Waitemata Group
Kerikeri Volcanic Group		0.0000	0.0356	0.0040	0.0005
Mangakahia Complex			0.0000	0.0000	0.0000
Tangihua Complex				0.0000	0.0000
Tauranga Group					0.9876
Waitemata Group					

Figure E.21. Games-Howell post hoc test of the dominant lithologies (Q-Map, 1:250,000) vs. sediment susceptibility for the Tangihua area. Welch's ANOVA was statistically significant at α= 0.05.

Application of the same tests to main geological units of the Tangihua area by slope supports the controlling factor hypothesis that *geostructural setting and rock strength, not slope, controls the susceptibility of the Tangihua area to sediment loss* (Figure E.22). Specifically, the strong basaltic rock of the Tangihua Complex has by far the steepest slopes. The Mangakahia Complex and Mesozoic sandstones of the Waitemata Group have half the median slope of the Tangihua Complex and yet much higher susceptibilities due to structural incompetence and deeply weathered regolith, respectively. The Kerikeri Volcanic Complex (Whatitiri Maunga) and Tauranga Group have the lowest median slope values. Due to the steepness of the Tangihua Complex (>70% by area is ≥12°, with 36% ≥20° by area) the regolith is weathering limited, relative to Waitemata Group sandstones and allochthonous sand and mudstones of the Mangakahia Group. In other words, the Tangihua Complex has a lesser volume of unconsolidated material available for loss across the Tangihua area. By comparison, the Mangakahia Complex, Waitemata Group, and Tauranga Group geological units have an abundance of unconsolidated or weakly consolidated material available for export.

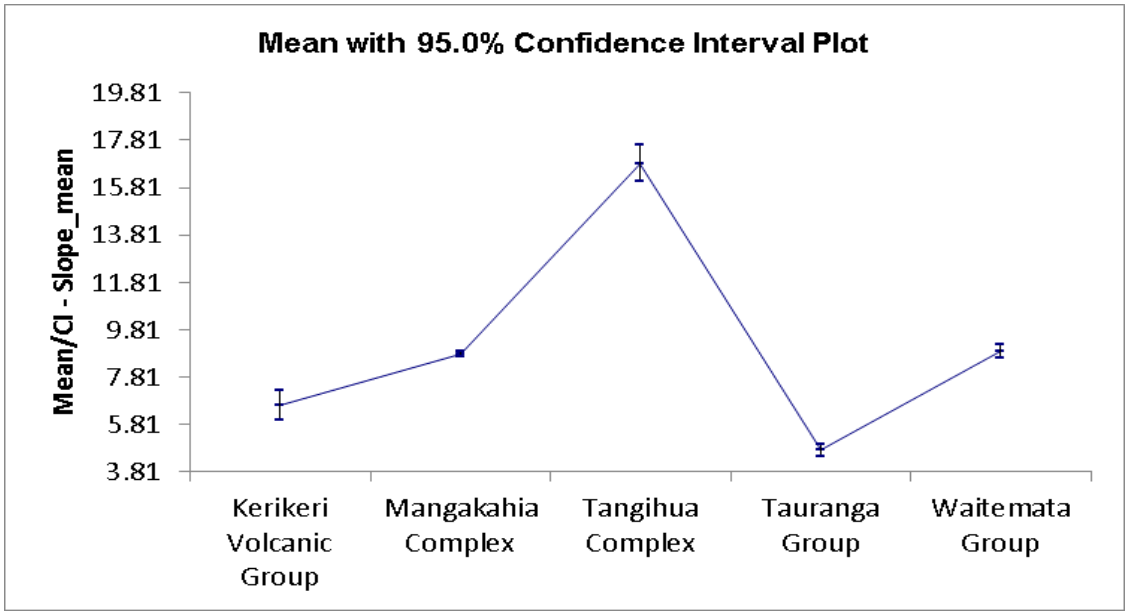

Games-Howell Probabilities (α = 0.05, 0.15)	Kerikeri Volcanic Group	Mangakahia Complex	Tangihua Complex	Tauranga Group	Waitemata Group
Kerikeri Volcanic Group		0.0000	0.0000	0.0000	0.0000
Mangakahia Complex			0.0000	0.0000	0.9192
Tangihua Complex				0.0000	0.0000
Tauranga Group					0.0000
Waitemata Group					

Figure E.22. Games-Howell post hoc test of the dominant lithologies (Q-Map, 1:250,000) vs slope for the Tangihua area. Welch's ANOVA was statistically significant at α= 0.05. The Waitemata Group is not significantly different from the Mangakahia Complex.

Geology also controls the texture and permeability of soils, which in turn influences susceptibility to sediment loss. For example, the soils formed in the youthful basalts of the Kerikeri Volcanic Group are well structured, well drained, and moderately permeable. By comparison, soils formed in the Mangakahia Complex and Waitemata Complex soils are poorly structured, fine textured and imperfectly to poorly drained, with lower permeability. *Soil physical properties in combination with slope control the susceptibility of the landscape to overland flow and fluvial erosion*. Welch's ANOVA and Games-Howell post hoc tests reveal a significant relationship between the main geological units

and overland flow (Figure E.23). Application of the same tests to overland flow by sediment susceptibility supports the dominant role of geology, not slope, over sediment loss (Figure E.24).

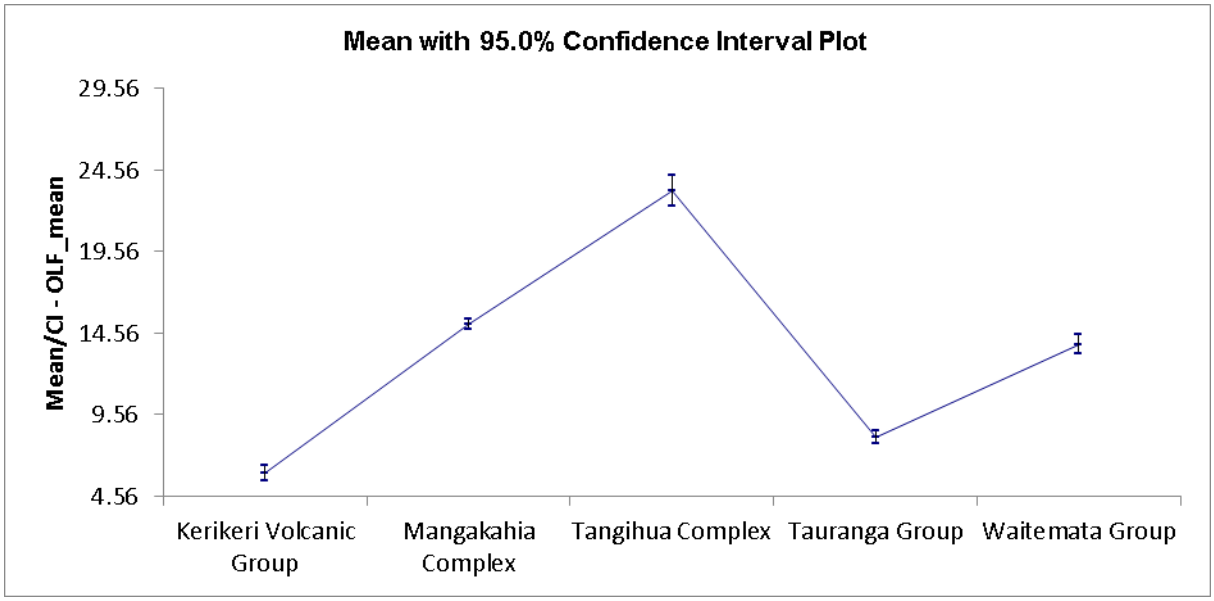

Games-Howell Probabilities (α = 0.05, 0.15)	Kerikeri Volcanic Group	Mangakahia Complex	Tangihua Complex	Tauranga Group	Waitemata Group
Kerikeri Volcanic Group		0.0000	0.0000	0.0000	0.0000
Mangakahia Complex			0.0000	0.0000	0.0033
Tangihua Complex				0.0000	0.0000
Tauranga Group					0.0000
Waitemata Group					

Figure E.23. Percent overland flow (OLF) of effective precipitation (PENZ, 1:50,000) by main geological unit for the Tangihua area. Welch's ANOVA was significant at $\alpha = 0.05$.

Application of Welch's ANOVA and Games-Howell post hoc test to overland flow by susceptibility class is presented in Figure E.24. As slope is a key control over OLF, the outputs of Games-Howell post hoc test support the importance of geological unit strength and consolidation status, not fluvial surface erosion, as the main driver of sediment loss across the Tangihua area. However, we note that fluvial erosion of a toe slope may initiate mass movement.

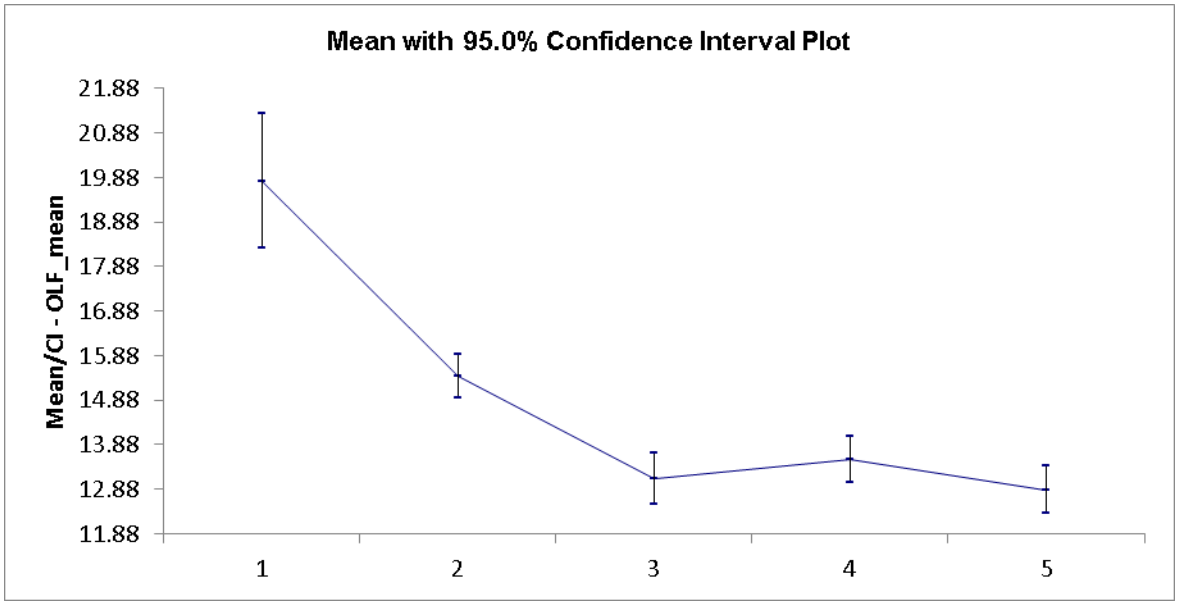

Games-Howell Probabilities (α = 0.05, 0.15)	1	2	3	4	5
1		0.0000	0.0000	0.0000	0.0000
2			0.0000	0.0000	0.0000
3				0.8238	1.0000
4					0.7708
5					

Figure E.24. Percent overland flow of effective precipitation (OLF) by sediment susceptibility class for the Tangihua area. Classes 3, 4 and 5 are not significantly different from each other at an $\alpha = 0.05$.

In summary, the association between sediment susceptibility and controlling landscape factors represented by historic soil and geological survey are consistent with established controlling landscape factor theory for areas of heterogenous geology and with historic physiographic classifications of the Northland region (Rissmann et al., 2018; Rissmann and Pearson, 2020; McDonald et al., 2020; Pearson and Rissmann, 2020). Notably, *geology, not slope is the first order control over the susceptibility of the landscape to sediment loss* across the Tangihua area, an observation that is well supported by sediment generation research (Morel et al., 2003; Mueller and Pitlick, 2013; Fratkin et al., 2020) and the sediment susceptibility map generated for this study.

Dissolved reactive phosphorus susceptibility

Application of Welch's ANOVA and the Games-Howell post hoc test to the main geological units of the Tangihua area reveal a strong and statistically significant pattern of dissolved reactive phosphorus susceptibility that is explained by the combination of physical and chemical weathering and microbially mediated redox processes (Figure E.25). Specifically, the high-relief Tangihua Complex rocks are associated with the highest dissolved reactive phosphorus susceptibility. These rocks originated as mid-ocean ridge basalts and have an alkali character and as such contain naturally elevated concentrations as inorganic phosphorus, mainly as orthophosphate. The concentration of inorganic phosphorus averages between 1,000 – 2,000 ppm as P_2O_5, with concentrations as high as 6,000 ppm as P_2O_5 reported in the geochemical literature for the Tangihua Complex (Briggs and Searle, 1975; Nicholson et al., 2000; Porder et al., 2013). The Tangihua Complex is steep across the Tangihua area and does not have a deep regolith. It thus has high rates of chemical and physical weathering. Weathering releases inorganic phosphorus into solution. Streams

originating from natural state areas in the Tangihua Complex, have dissolved reactive phosphorus concentrations that exceed ecological thresholds (Pearson and Rissmann, 2020; Northland Regional Council surface water quality data).

The Whatitiri Maunga (Kerikeri Volcanic Group) is associated with the lowest dissolved reactive phosphorus susceptibility across the Tangihua area. Although, the Whatitiri Maunga hosts well drained soils that are moderately permeable and have high phosphorus retention due to oxidising conditions and an abundance of the oxides and oxyhydroxides of iron and aluminium. Accordingly, the susceptibility to dissolved reactive phosphorus is low relative to the Tangihua Complex.

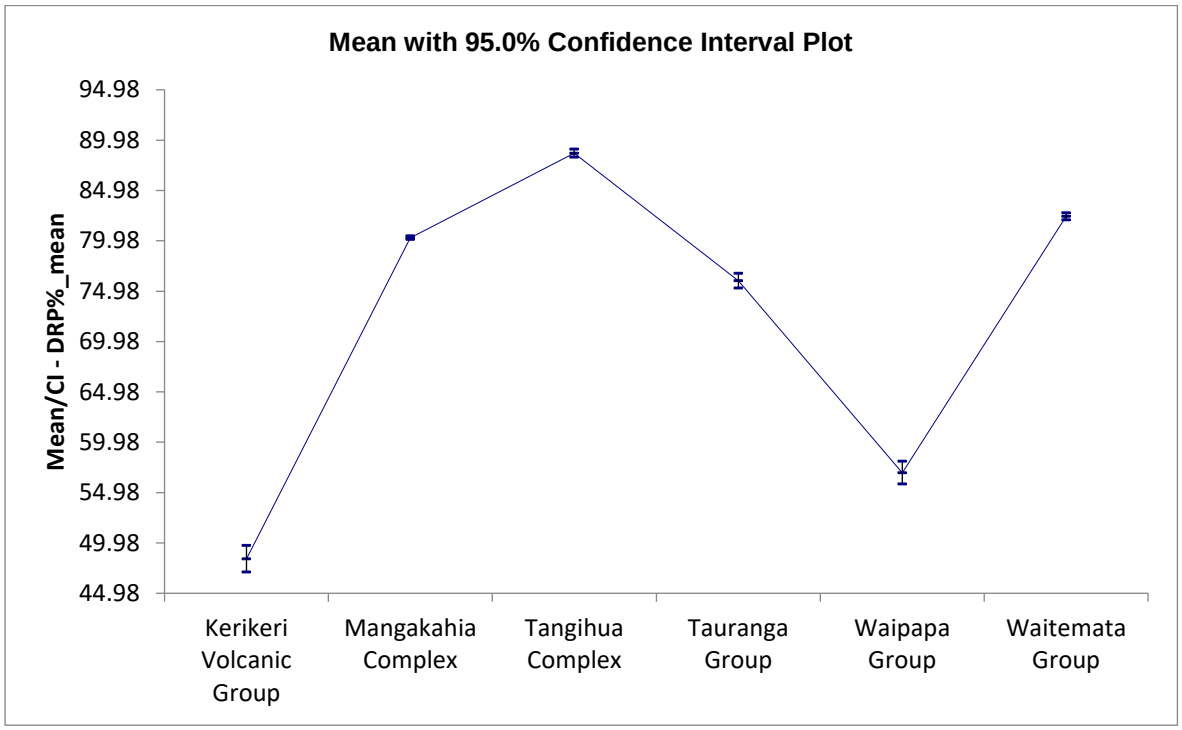

Games-Howell Probabilities (α = 0.05, 0.15)	Kerikeri Volcanic Group	Mangakahia Complex	Tangihua Complex	Tauranga Group	Waipapa Group	Waitemata Group
Kerikeri Volcanic Group		0.0000	0.0000	0.0000	0.0000	0.0000
Mangakahia Complex			0.0000	0.0000	0.0000	0.0000
Tangihua Complex				0.0000	0.0000	0.0000
Tauranga Group					0.0000	0.0000
Waipapa Group						0.0000
Waitemata Group						

Figure E.25. Susceptibility to dissolved reactive phosphorus loss by main geological unit, Tangihua area. Susceptibility to dissolved reactive phosphorus loss is lowest for the low relief and well drained soils (high P-retention) of the Kerikeri Volcanic Group and highest for the high-relief and P-rich rocks of the Tangihua Complex.

The Waipapa Group greywackes have the second lowest susceptibility to dissolved reactive phosphorus loss. These ancient basement rocks are deeply weathered and have a low abundance of inorganic phosphorus. A study of the Waipapa Group greywackes identified a deeply weathered regolith with negligible inorganic phosphorus within the upper few meters and lower overall P concentrations when contrast with the basalt rocks of the Tangihua Complex and Kerikeri Volcanic Complex (Seyers and Walker, 1968; Briggs and Searle, 1975; Heming, 1980; Nicholson et al., 2000).

Mudstones, silt, and sandstones with an appreciable mud content i.e., the Mangakahia Group mudstones and Waitemata Group sandstones, tend to be associated with naturally elevated phosphorus concentrations (Porder et al, 2013). This reflects the association between organic (e.g., inositol hexaphosphate) and inorganic phosphorus and clay ('mud'), including the clay sized oxides and oxyhydroxides of iron and aluminium.

Mudstone rich lithologies also generate clay-rich soils that are often imperfectly to poorly drained (Figure E.26). Soils with poor internal drainage are more susceptible to dissolved reactive phosphorus loss, due to the development of reducing conditions within the soil zone, which also limits P retention (the ability for these soils to 'hold on' to P). For these reasons, the soils of the Mangakahia Complex, Waipapa Group, and Waitemata Group have an elevated susceptibility to dissolved reactive phosphorus loss.

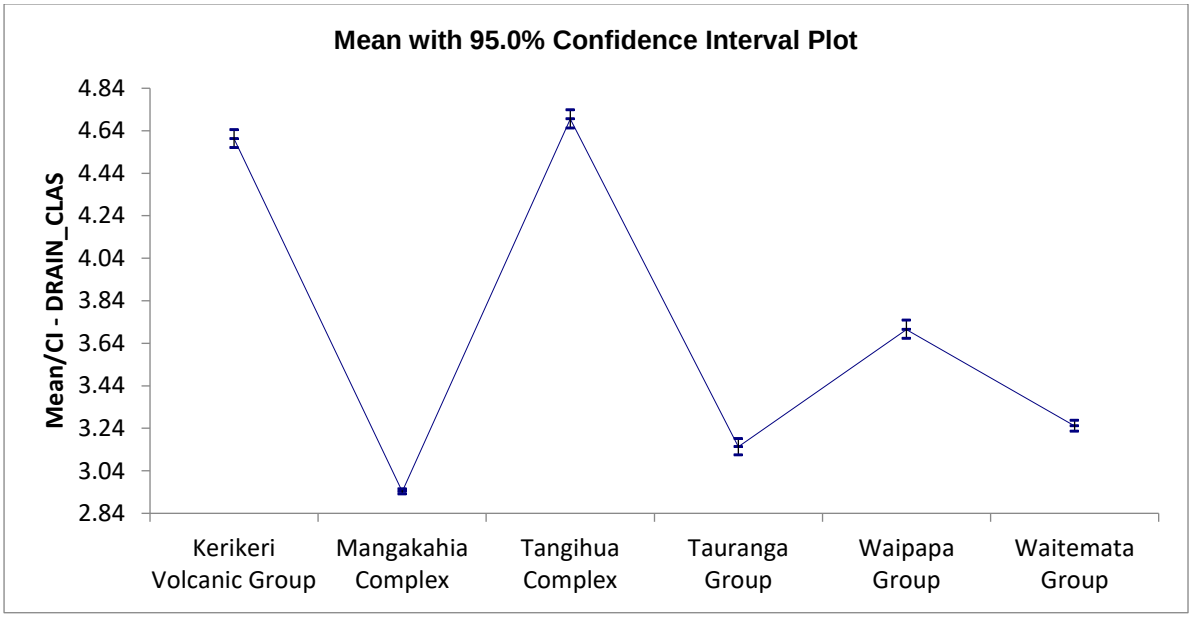

Games-Howell Probabilities (α = 0.05, 0.15)	Kerikeri Volcanic Group	Mangakahia Complex	Tangihua Complex	Tauranga Group	Waipapa Group	Waitemata Group
Kerikeri Volcanic Group		0.0000	0.0288	0.0000	0.0000	0.0000
Mangakahia Complex			0.0000	0.0000	0.0000	0.0000
Tangihua Complex				0.0000	0.0000	0.0000
Tauranga Group					0.0000	0.0005
Waipapa Group						0.0000
Waitemata Group						

Figure E.26. Soil drainage class (FSL, 1:50,000) vs. main geological unit within the Tangihua area. Welch's ANOVA was significant at α = 0.05. Games-Howell post hoc displays a predictable pattern of dissolved reactive phosphorus susceptibility between the main geological units. Soils with imperfect to poor drainage are more susceptible to dissolved reactive phosphorus loss.

The Tauranga Group sediments are associated with a shallow water and imperfectly to poorly drained soils that favour low P retention (Figure E.27). Tauranga Group sediments also host reducing groundwaters (Rissmann et al., 2018b). The Geological Reduction Potential (GRP) layer from the Physiographics of New Zealand dataset demonstrates the variation in the likelihood that groundwater in contact with a geological material will be reduced. Application of Welch's ANOVA and Games-Howell post hoc test to the GRP layer by geological unit displays a high GRP for the Tauranga Group sediments (Figure E.28) and high susceptibility (Figure E.29). Groundwater systems

associated with an elevated GRP tend to have elevated dissolved reactive phosphorus concentrations and generate dissolved phosphorus forms that can be highly mobile (Gschwend and Reynolds, 1987; Rissmann and Lovett, 2016).

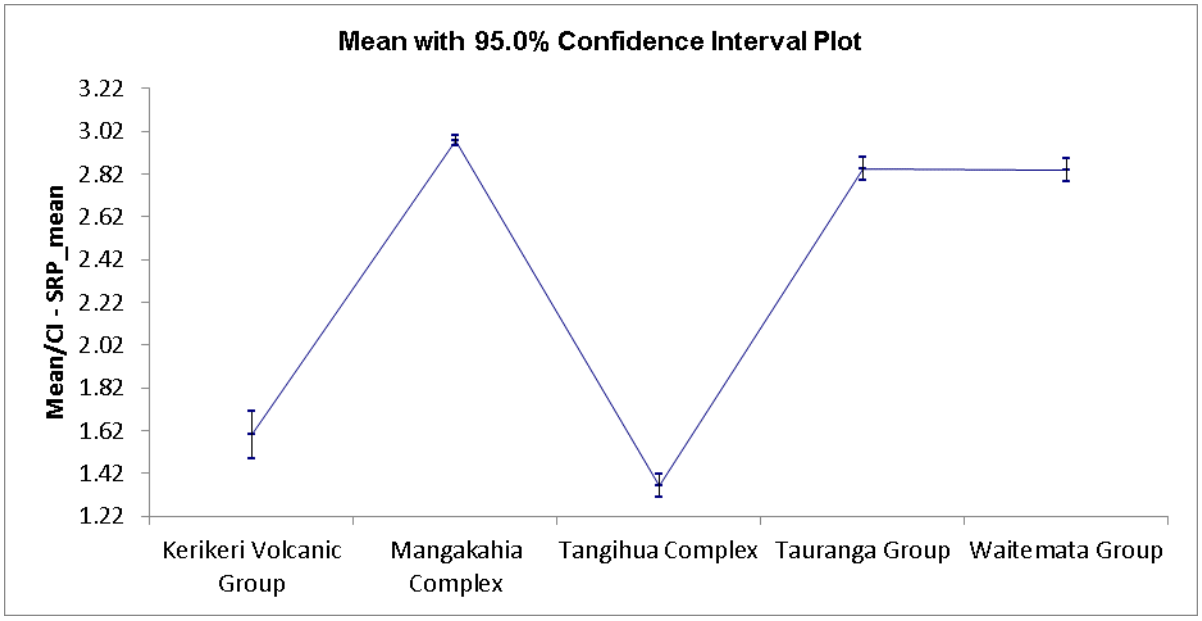

Games-Howell Probabilities (α = 0.05, 0.15)	Kerikeri Volcanic Group	Mangakahia Complex	Tangihua Complex	Tauranga Group	Waitemata Group
Kerikeri Volcanic Group		0.0000	0.0017	0.0000	0.0000
Mangakahia Complex			0.0000	0.0001	0.0001
Tangihua Complex				0.0000	0.0000
Tauranga Group					0.9998
Waitemata Group					

Figure E.27. Soil Reduction Potential (SRP) (PENZ, 1:50,000) vs. main geological unit (Q-Map, 1:250,000) within the Tangihua area. Welch's ANOVA was significant at $\alpha = 0.05$. Games-Howell post hoc displays a predictable pattern of SRP between the main geological units. The Waitemata Group is not significantly different from the Tauranga Group.

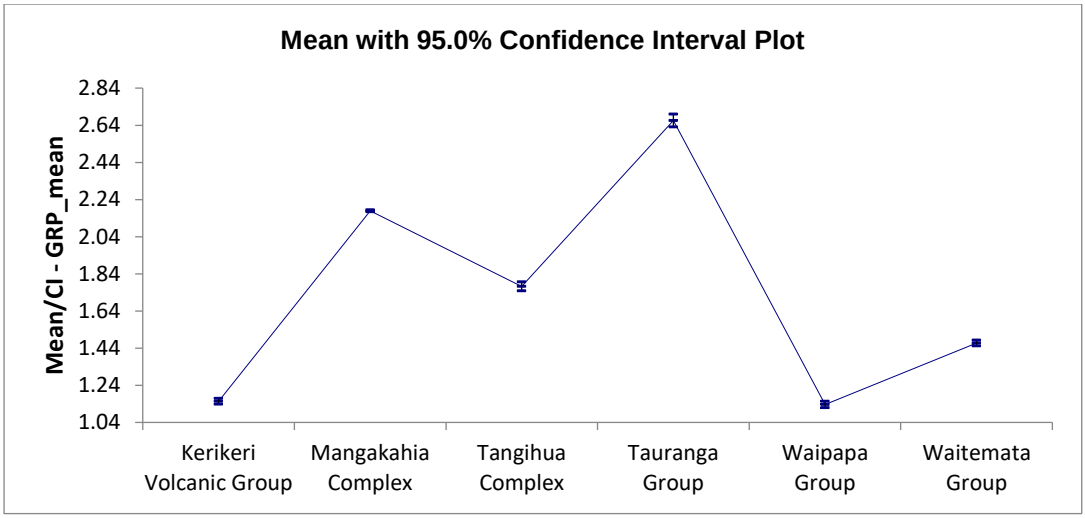

Games-Howell Probabilities (α = 0.05, 0.15)	Kerikeri Volcanic Group	Mangakahia Complex	Tangihua Complex	Tauranga Group	Waipapa Group	Waitemata Group
Kerikeri Volcanic Group		0.0000	0.0000	0.0000	0.7348	0.0000
Mangakahia Complex			0.0000	0.0000	0.0000	0.0000
Tangihua Complex				0.0000	0.0000	0.0000
Tauranga Group					0.0000	0.0000
Waipapa Group						0.0000
Waitemata Group						

Figure E.28. Geological Reduction Potential (GRP) (PENZ, 1:250,000) vs. main geological unit within the Tangihua area. Welch's ANOVA was significant at $\alpha = 0.05$. Games-Howell post hoc displays a predictable pattern of GRP between the main geological units. The Holocene River deposits of the Tauranga Group have the highest GRP and the Kerikeri Volcanic Complex and Waipapa Group the lowest. The Waipapa Group is not significantly different from the Kerikeri Volcanic Group.

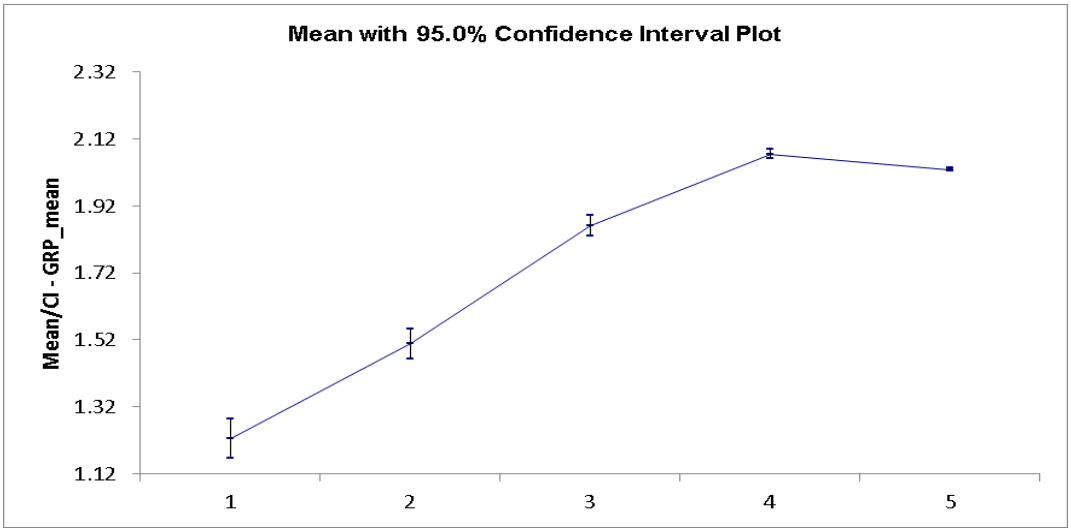

Games-Howell Probabilities (α = 0.05, 0.15)	1	2	3	4	5
1		0.0000	0.0000	0.0000	0.0000
2			0.0000	0.0000	0.0000
3				0.0000	0.0000
4					0.0000
5					

Figure E.29. Geological Reduction Potential (PENZ, 1:250,000) vs. main geological unit (Q-MAP, 1:250,000). Susceptibility to dissolved reactive phosphorus loss increases as GRP increases. This is consistent with redox controls over dissolved reactive phosphorus abundance and mobility (Gschwend and Reynolds, 1987).

The pattern of susceptibility displayed here is consistent with:

i. Contemporary understanding of landscape controls over the abundance and mobility of phosphorus in the environment (Gschwend and Reynolds, 1987; Tiessen, 2008; Gburek et al., 2005; Porder et al., 2013);
ii. The controlling landscape factor and hydrobiogeochemical classification that informs the Physiographic Environments of New Zealand Classification (Rissmann et a., 2019; Pearson and Rissmann, 2021), and;
iii. The spatial pattern of landscape susceptibility and surface and ground water quality provided by earlier pieces of work for the Northland Regional Council (Rissmann et al., 2018a,b; Rissmann & Pearson, 2020; Pearson & Rissmann, 2020).

The significance testing of dissolved reactive phosphorus susceptibility that is presented in Figure E.25 by main geological unit provides context to the natural abundance of P in geological materials including soils, the role of regolith weathering over P depletion, the role of soil drainage, and aquifer reduction potential. All these landscape factors need to be considered to explain the inherent susceptibility of the landscape to dissolved reactive phosphorus loss. A simple map of land use intensity plus soil P-retention is inadequate when seeking to explain the susceptibility of the landscape to dissolved reactive phosphorus loss.

In summary, the association between dissolved reactive phosphorus susceptibility and controlling landscape factors represented by historic soil and geological survey are consistent with established controlling landscape factor theory for areas of heterogenous geology and with historic physiographic classifications of the Northland region (Rissmann et al., 2018b, Rissmann & Pearson, 2020; Pearson & Rissmann, 2020). Notably, *weathering*, *petrochemistry and electron donor abundance are the dominant landscape factors controlling the susceptibility of the landscape to dissolved reactive phosphorus loss* across the Whakapara area.

Whakapara, Wairoa Catchment, Northland

The Whakapara area is dominated by the ancient greywacke basement rocks of the Waipapa Group (41% by area), followed by the unconsolidated alluvium and lacustrine deposits of the Holocene aged Tauranga Group sediments (37%) (Figure E.30). The Kerikeri Volcanic Group (7%) and the Mangakahia Complex (11%) make up a smaller albeit significant area. The Tangihua Complex is negligible (<2% by area). Tauranga group sediments are described as “Unconsolidated to poorly consolidated mud, sand, gravel and peat deposits of alluvial, colluvial and lacustrine origins.”

The Waipapa Group greywackes constitute the steepest geological unit within the Whakapara area, followed by the Kerikeri Volcanic Group. The weak sedimentary rocks of the Mangakahia Complex constitute the lowest relief bedrock unit. The unconsolidated Holocene River deposits of the Tauranga Group occupy the lowest elevation parts of the Whakapara area and are also characterised by the lowest relief.

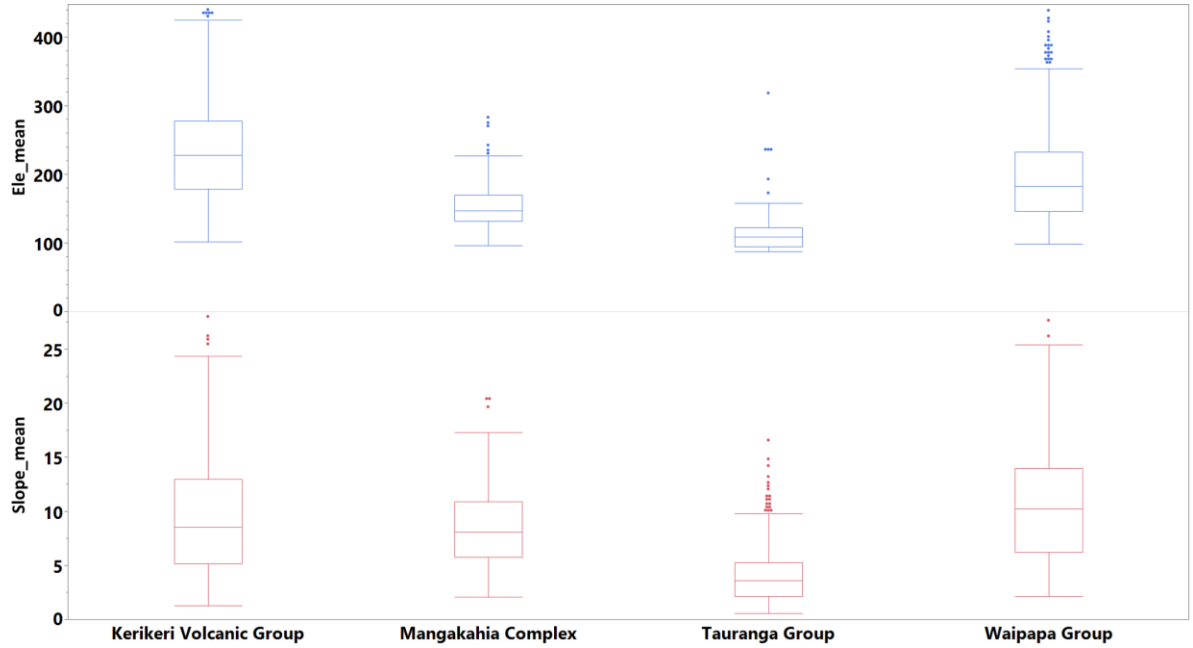

Geological Unit	Elevation (m RSL)	Slope (°)	Min. Elevation	Min. Slope	Max. Elevation	Max. Slope
Kerikeri Volcanic Group	228.0	8.5	101.2	1.3	437.7	28.0
Mangakahia Complex	147.2	8.1	96.2	2.1	283.1	20.4
Tauranga Group	109.1	3.6	87.4	0.6	318.4	16.6
Waipapa Group	182.7	10.2	98.6	2.1	439.0	27.7

Figure E.30. Box and Whisker plots of elevation in metres relative to sea level (m RSL) and slope (°) vs. main geological unit (Q-Map, 1:250,000) across the Whakapara area. Tabulated median, minimum, and maximum values.

According to soil survey (FSL, 1:50,000), clay-rich soils formed in the weak sedimentary sand and mudstones of the Mangakahia Complex are characterised by the lowest permeabilities followed by the soils formed in the Tauranga Group sediments (Figure E.31). Soil P retention is lowest for the Mangakahia Complex and Tauranga Group sediments and highest for the well-drained soils of the Kerikeri Volcanic Complex, with soils formed within the deeply weathered Waipapa Group greywackes having intermediate P-retention values.

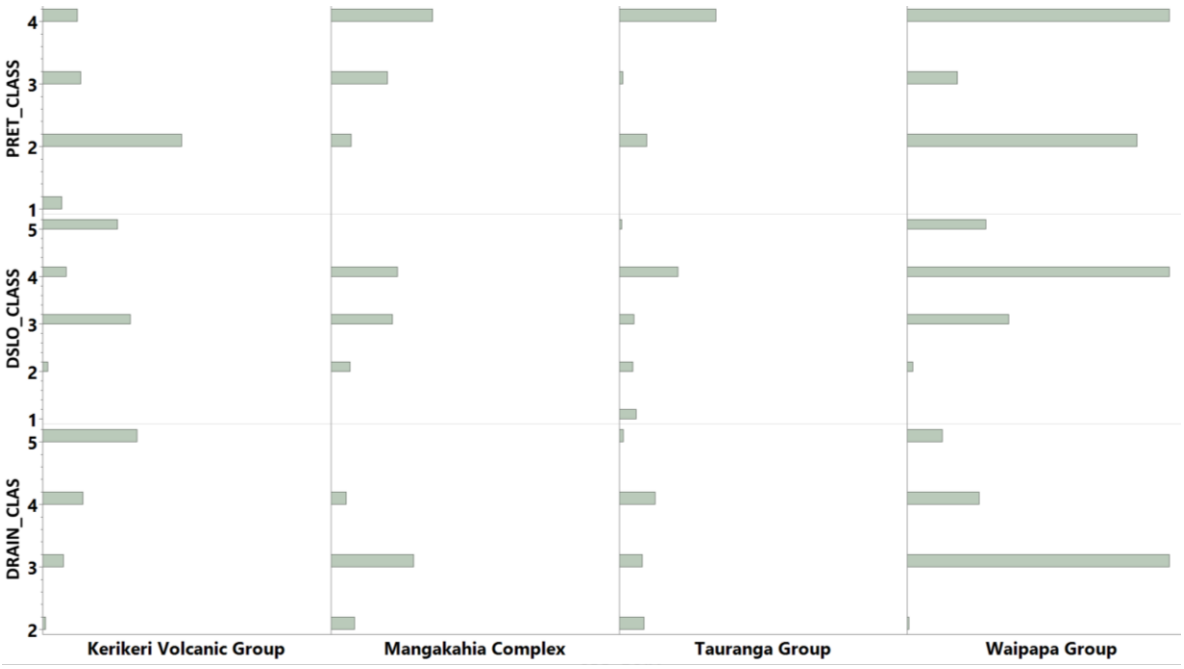

Geological Unit	DSLO	DRAINAGE	PRET	Min. DSLO	Min. DRAINAGE	Min. P-RETENTION	Max. DSLO	Max. DRAINAGE	Min. P-RETENTION
Kerikeri Volcanic Group	4.0	5.0	2	2.0	2.0	1	5.0	5	4
Mangakahia Complex	3.0	3.0	4	2.0	2.0	2	4.0	4	4
Tauranga Group	4.0	3.0	4	1.0	2.0	2	5.0	5	4
Waipapa Group	4.0	3.0	3	2.0	2.0	2	5.0	5	4

Figure E.31. Box and whisker plot of soil P-retention, depth to slowly permeable layer (DSLO), and soil drainage class from the FSL (1:50,000) by main geological unit (Q-Map, 1:250,000) for the Whakapara area. Tabulated median, minimum, and maximum values.

With regards to the Tauranga Group Holocene River deposits there are two distinct subclasses, low elevation and low-relief, and high elevation and high-relief (Figure E.32). The low relief subclass makes up 65% by area (11,380 ha) whereas the high relief subclass makes up 35% by area (6,198 ha). The low-relief subclass has a median water table depth of 1.6 m below ground level (m bgl), whereas the high-relief subclass has a median depth of 12.4 m bgl. Soil survey does not identify any significant variation in soil properties between these two different subclasses despite the low-relief subclass containing a much larger area of poorly drained hydric soils than the high-relief subclass 2 (Rissmann et al., 2020a).

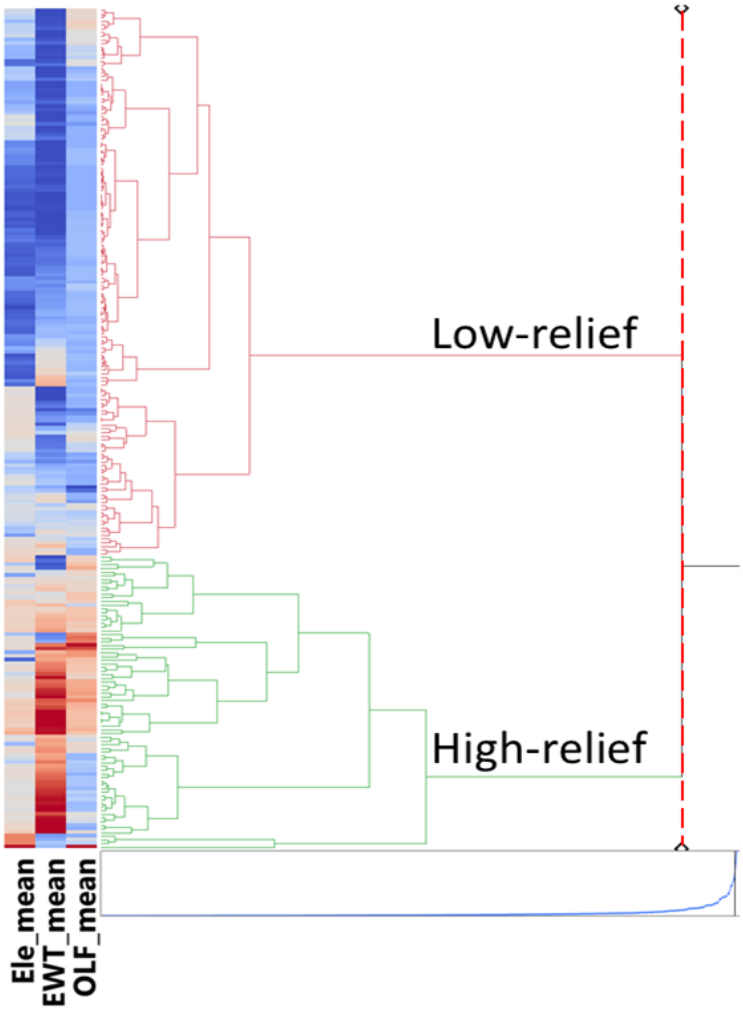

Figure E.32. Hierarchal clustering of the Tauranga Group (Q-MAP, 1:250,000) Holocene River sediments by elevation, slope, and per cent overland flow (OLF) of effective precipitation.

Sediment susceptibility

Application of Welch's ANOVA and the Games-Howell post hoc test to the main geological units of the Whakapara area identify the large area of Tauranga Group Holocene River Deposits as having the highest susceptibility to sediment loss, followed by the deeply weathered Waipapa Group greywackes, and then the Mangakahia Complex (Figure E.33). The low relief Kerikeri Volcanic Group has the lowest susceptibility to sediment loss.

Application of the same test to the two subclasses of the Tauranga Group Holocene River deposits identifies a significant difference in susceptibility to sediment loss, with the highest susceptibility associated with the larger low-relief subclass (Figure E.34).

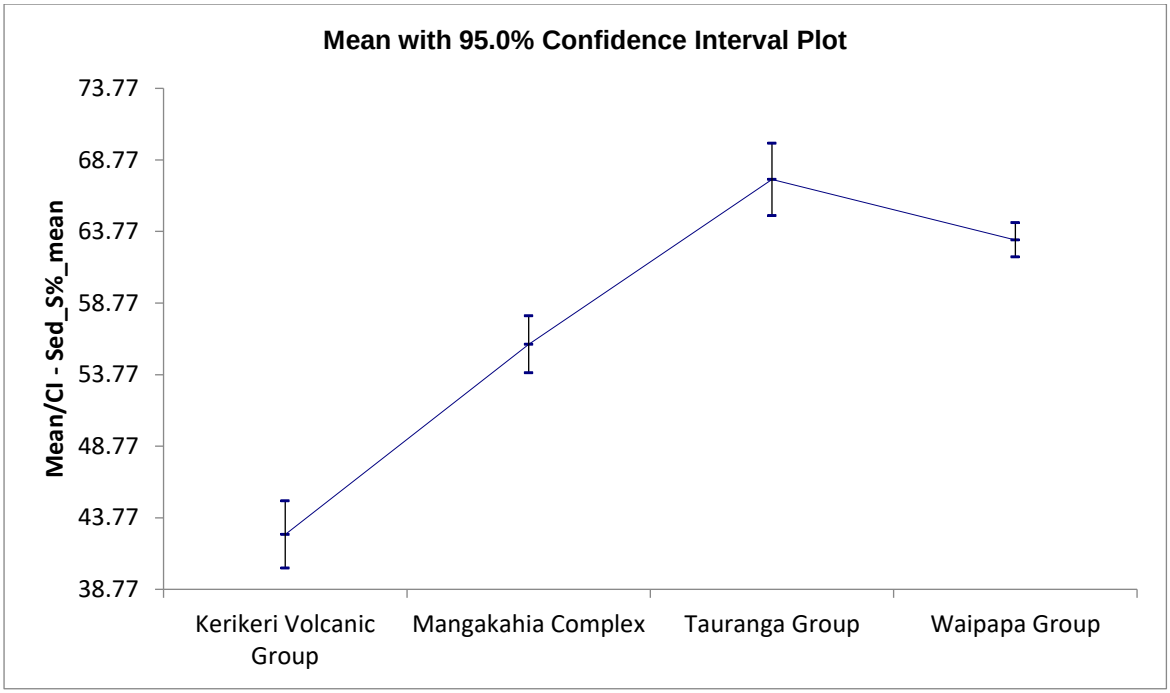

Games-Howell Probabilities (α = 0.05, 0.15)	Kerikeri Volcanic Group	Mangakahia Complex	Tauranga Group	Waipapa Group
Kerikeri Volcanic Group		0.0000	0.0000	0.0000
Mangakahia Complex			0.0000	0.0000
Tauranga Group				0.0159
Waipapa Group				

Figure E.33. Games-Howell post hoc test of the dominant lithologies (Q-Map, 1:250,000) vs. sediment susceptibility for the Whakapara area. Welch's ANOVA was statistically significant at α= 0.05.

The elevated sediment loss susceptibility for the Tauranga Group sediments, is likely a factor of the shallow water table, a dominance of clay soils and reducing conditions within the soils and shallow groundwater system. Runoff is elevated where water tables are shallow and soils imperfectly to poorly drained. High reduction potential in soil and groundwater favours dispersion of unconsolidated clays due to the reductive dissolution of the oxides and oxyhydroxides of iron. Stream bank erosion is another important driver, with subclass 2 of the Tauranga Group occurring in closest proximity to active river channels and their floodplains.

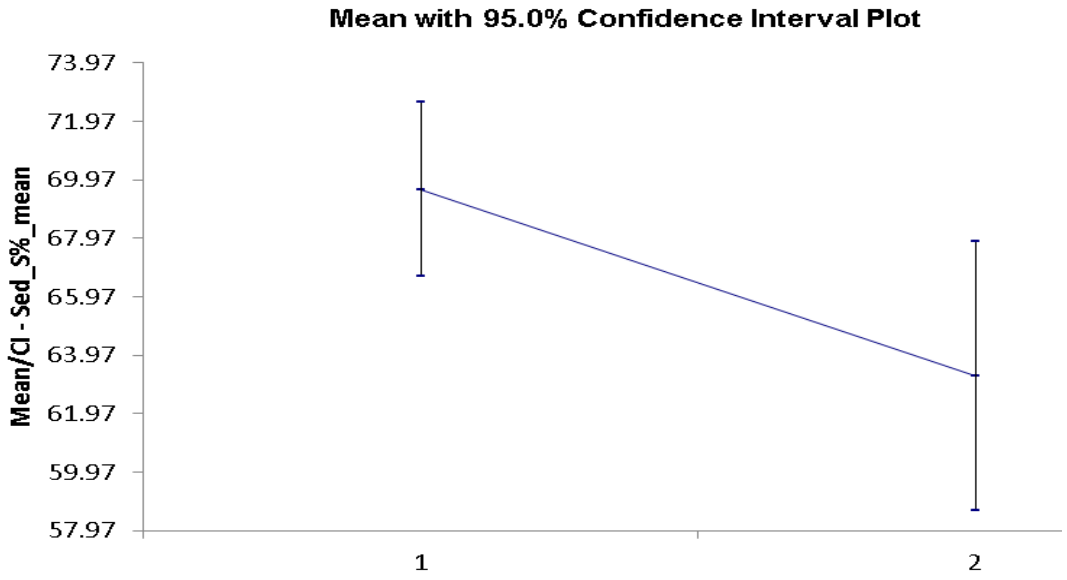

Games-Howell Probabilities (α = 0.05, 0.15)	1	2
Low relief		0.0207
High relief		

Figure E.34. Games-Howell post hoc test of the dominant lithologies (Q-Map, 1:250,000) vs. sediment susceptibility for the two subclasses of the Tauranga Group sediments. Welch's ANOVA was statistically significant at α= 0.05.

Of the bedrock geological units, geostructural setting, weathering, and rock strength once again explain the pattern of sediment susceptibility (Figure E.30). Specifically, the deeply weathered Waipapa Group greywackes have the highest susceptibility to sediment loss followed by the weak sedimentary rocks of the Mangakahia Complex. The strong lava flows of the Kerikeri Volcanic Group have the lowest susceptibility to sediment loss of the bedrock geological units.

In summary, the association between sediment susceptibility and controlling landscape factors represented by historic soil and geological survey are consistent with established controlling landscape factor theory for areas of heterogenous geology and with historic physiographic classifications of the Northland region (Rissmann et al., 2018, Rissmann and Pearson, 2020; McDonald et al., 2020; Pearson and Rissmann, 2020). In summary, *geology, not slope is the first order control over the susceptibility of the landscape to sediment loss across the Whakapara area, an observation that is well supported by sediment generation research* (Morel et al., 2003; Mueller and Pitlick, 2013; Fratkin et al., 2020) and the sediment susceptibility map generated for this study.

Dissolved reactive phosphorus susceptibility

Application of Welch's ANOVA and the Games-Howell post hoc test to the main geological units of the Whakapara area reveal a strong and statistically significant pattern of dissolved reactive phosphorus susceptibility that is explained by the combination of physical and chemical weathering and microbially mediated redox processes (Figure E.35)[45]. Specifically, the deeply weathered greywackes of the Waipapa Group have the lowest susceptibility to dissolved reactive phosphorus loss. A study of the Waipapa Group greywackes identified the deeply weathered regolith with negligible inorganic phosphorus within the upper few meters and lower overall P concentrations when contrast with the basalts of the Kerikeri Volcanic Complex and the weak mud and sandstones

[45] The susceptibility of the Whakapara area to dissolved reactive phosphorus loss is lower than that of the Tangihua area.

of the Mangakahia Complex (Hodgson, 1968; Seyers and Walker, 1968; Briggs and Searle, 1975; Heming, 1980; Nicholson et al., 2000).

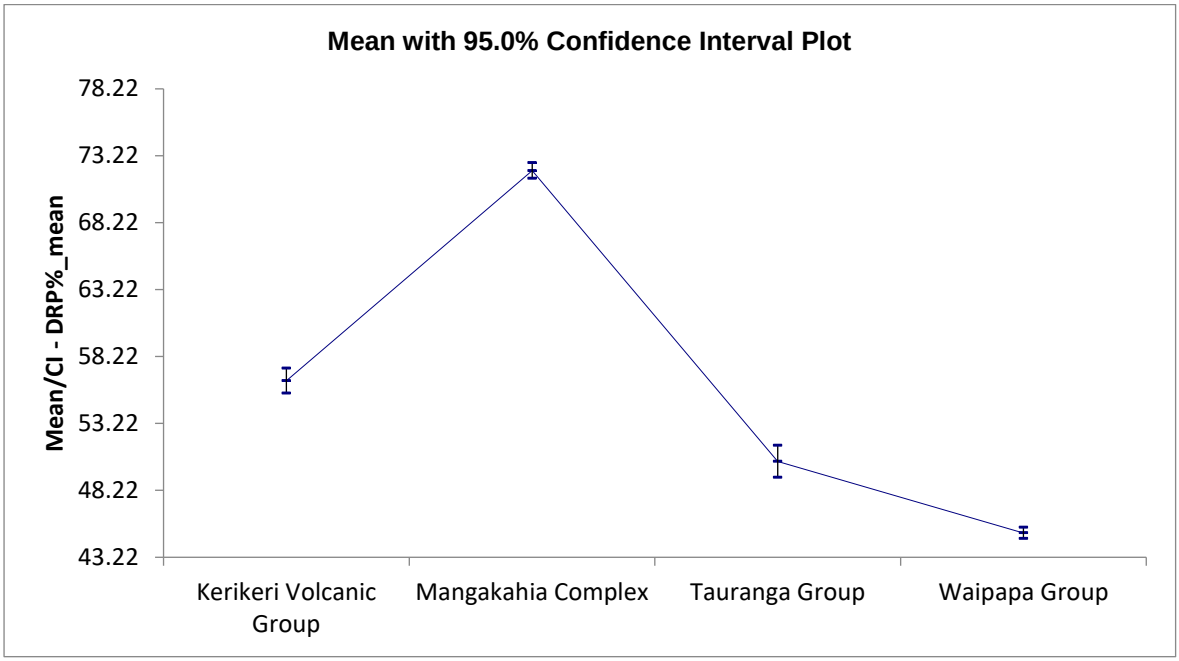

Games-Howell Probabilities (α = 0.05, 0.15)	Kerikeri Volcanic Group	Mangakahia Complex	Tauranga Group	Waipapa Group
Kerikeri Volcanic Group		0.0000	0.0000	0.0000
Mangakahia Complex			0.0000	0.0000
Tauranga Group				0.0000
Waipapa Group				

Figure E.35. Susceptibility to dissolved reactive phosphorus loss by main geological unit, Whakapara area. Welch's ANOVA was significant at $\alpha = 0.05$.

Mudstones, silt, and sandstones with an appreciable mud content i.e., the Mangakahia Group mudstones and Waitemata Group sandstones, are often associated with naturally elevated phosphorus concentrations (Porder et al, 2013). This reflects the association between organic (e.g., inositol hexaphosphate) and inorganic phosphorus and clay ('mud'), including the clay sized oxides and oxyhydroxides of iron and aluminium. Mudstone rich lithologies also generate clay-rich soils that are often imperfectly to poorly drained. Soils with poor internal drainage are more susceptible to dissolved reactive phosphorus loss, due to the development of reducing conditions within the soil zone, which also limits P retention (the ability for these soils to 'hold on' to P). For these reasons, the soils of the Mangakahia Complex have an elevated susceptibility to dissolved reactive phosphorus loss.

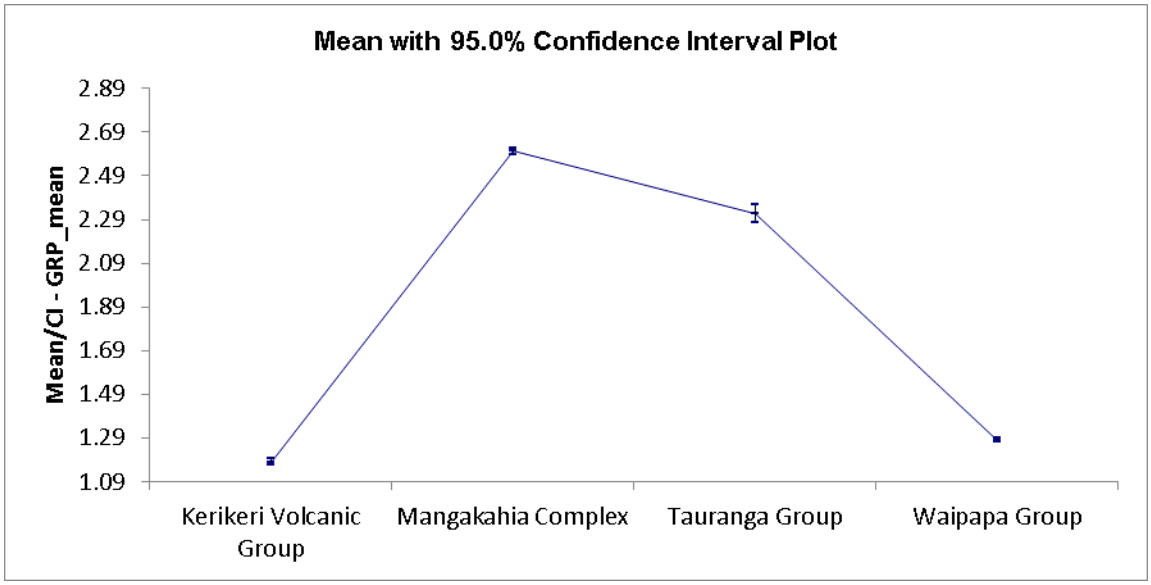

Games-Howell Probabilities (α = 0.05, 0.15)	Kerikeri Volcanic Group	Mangakahia Complex	Tauranga Group	Waipapa Group
Kerikeri Volcanic Group		0.0000	0.0000	0.0000
Mangakahia Complex			0.0000	0.0000
Tauranga Group				0.0000
Waipapa Group				

Figure E.36. Geological Reduction Potential (GRP) (PENZ, 1:250,000) vs. main geological unit within the Whakapara area. Welch's ANOVA was significant at $\alpha = 0.05$.

Although the Kerikeri Volcanic Group is associated with the second highest dissolved reactive phosphorus susceptibility across the Whakapara area, overall susceptibility is low relative to the Mangakahia Complex and the Tangihua area. The Kerikeri Volcanic Complex has elevated dissolved reactive phosphorus susceptibility where steep and the regolith is thin. Where the regolith is deep, soils are well drained with very high P-retention. Soils across the Kerikeri Volcanic Complex are renowned for their ability to sequester super phosphate.

The Tauranga Group sediments have a low susceptibility to dissolved reactive phosphorus loss which is at odds with the abundance of reducing soils and reducing groundwater systems (Figure E.36 and E.37). However, as most Tauranga Group sediments are derived from the mass wasting and erosion of the Waipapa Group greywackes, the concentration of P within the Tauranga Group sediments is likely low, although there is a lack of data to support this assertion.

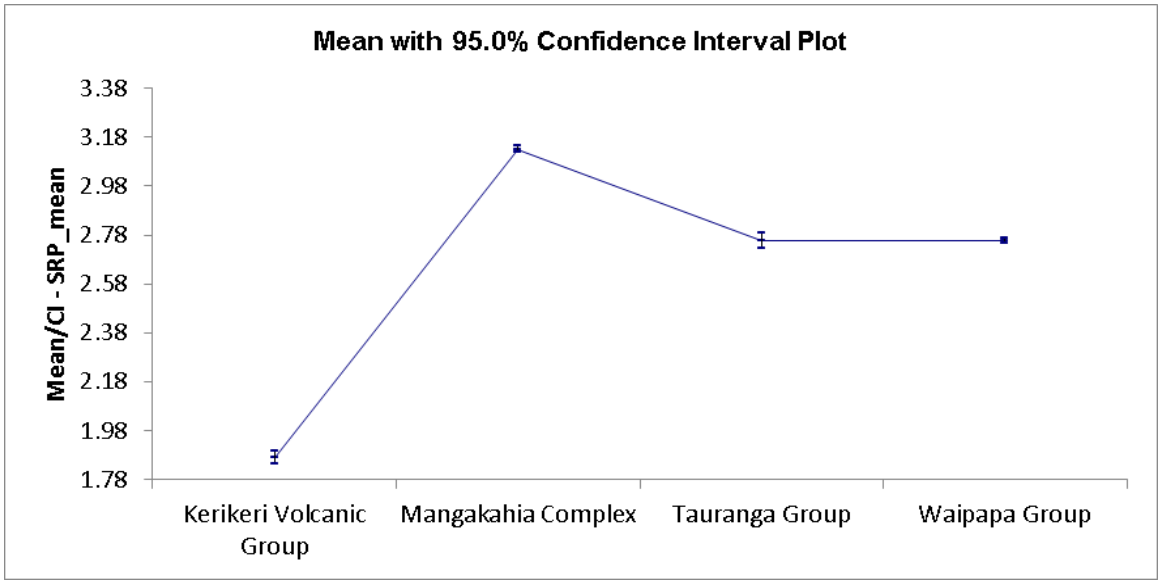

Games-Howell Probabilities (α = 0.05, 0.15)	Kerikeri Volcanic Group	Mangakahia Complex	Tauranga Group	Waipapa Group
Kerikeri Volcanic Group		0.0000	0.0000	0.0000
Mangakahia Complex			0.0000	0.0000
Tauranga Group				1.0000
Waipapa Group				

Figure E.37. Soil Reduction Potential (SRP) (PENZ, 1:50,000) vs. main geological unit (Q-Map, 1:250,000) within the Whakapara area. Welch's ANOVA was significant at α = 0.05. Games-Howell post hoc displays a predictable pattern of SRP between the main geological units. The Waipapa Group is not significantly different from the Tauranga Group.

The significance testing of dissolved reactive phosphorus susceptibility that is presented in Figure E.35 above by main geological unit provides context to the natural abundance of P in geological materials including soils, the role of regolith weathering over P depletion, the role of soil drainage, and aquifer reduction potential. All these landscape factors need to be considered to explain the inherent susceptibility of the landscape to dissolved reactive phosphorus loss. A simple map of land use intensity plus soil P-retention is inadequate when seeking to explain the susceptibility of the landscape to dissolved reactive phosphorus loss.

The pattern of susceptibility displayed here is consistent with:

i. Contemporary understanding of landscape controls over the abundance and mobility of phosphorus in the environment (Gschwend and Reynolds, 1987; Tiessen, 2008; Gburek et al., 2005; Porder et al., 2013);

ii. The controlling landscape factor and hydrobiogeochemical classification that informs the Physiographic Environments of New Zealand Classification (Rissmann et a., 2019; Pearson and Rissmann, 2021), and;

iii. The spatial pattern of landscape susceptibility and surface and ground water quality provided by earlier pieces of work for the Northland Regional Council (Rissmann et al., 2018, Rissmann and Pearson, 2020; McDonald et al., 2020; Pearson and Rissmann, 2020).

In summary, the association between dissolved reactive phosphorus susceptibility and controlling landscape factors represented by historic soil and geological survey are consistent with established controlling landscape factor theory for areas of heterogenous geology and with historic physiographic classifications of the Northland region (Rissmann et al., 2018b, Rissmann and Pearson, 2020; Pearson and Rissmann, 2020). Notably, *weathering*, *petrochemistry and electron donor abundance are the dominant landscape factors controlling the susceptibility of the landscape to dissolved reactive phosphorus loss* across the Whakapara area.

Summary of association testing

Association testing results support established knowledge that multiple different controlling factors interact to determine the susceptibility of the landscape to contaminant loss. Notably, geology is the 1st order control over nitrate-nitrite-nitrogen, particulate phosphorus, sediment, and dissolved reactive phosphorus susceptibility. Geology determines the geostructural setting and associations across a region, including topography, the abundance or otherwise of P, the susceptibility of the regolith to mass wasting, soil type and structure, and the location of microbially mediated redox processes. A failure to recognise the variability in landscape susceptibility as a factor of geological controls will limit the relevance of mitigation or other efforts to reduce losses from the landscape.

For the majority of pollutants evaluated, the pattern of susceptibility is consistent with established controlling factor theory, including the hydrobiogeochemical framework employed by the physiographic approach. For both the Mataura and Wairoa catchments, the data-driven susceptibility layers revealed a similar set of controlling landscape factors to those identified by earlier physiographic classifications and numerical physiographic water quality models (Rissmann et al., 2016, 2018a,b,2019, 2020a,b,c; Rissmann and Pearson, 2020; Pearson and Rissmann, 2020)

A critical observation of this exploratory study and earlier physiographic modelling is that the sensitivity of controlling landscape factors varies with the geological and climatic history of a region. Thus, areas with different geological and climatic histories may exhibit different sensitivities to controlling factors for one or more contaminant. For example, geothermal activity the most sensitive predictor of organic-N, ammoniacal-N, and dissolved reactive phosphorus across the Taupo Volcanic Zone. A failure to consider geothermal activity across this area would result in erroneous interpretations of water quality data (Rissmann et al., 2018b) and soil GHG generation (Rissmann et al., 2011, 2012). Accordingly, it is important to carefully consider not just the soil environment or land use but the geological setting within which a water quality or soil GHG issue manifests. Failure to consider the geological and climatic history of a region can lead to a very poor alignment of mitigations with the factors that control the release of contaminants. This can be especially problematic when small scale plot studies associated with a single soil type (e.g., well drained alluvial gravels), geological, topographic, or climatic setting, are extrapolated to areas with different assemblages of controlling landscape factors.

Radiometric survey provides a measure of the gamma-ray spectra of soil and rock. It registers catchment or regional scale differences in soil and geology that are not represented in historic soil survey. Airborne radiometric and high-resolution topographic survey can therefore discriminate at fine scales the variation in controlling landscape factors that are unique to a catchment or region. In combination with what is an established geophysical theory, radiometric survey provides a means to provide catchment and regionally specific measures of the landscape factors controlling susceptibility to contaminant loss.

However, as this is a new and experimental approach, additional work is required to validate further and understand the outputs, especially when the results suggest new (different) landscape controls. For example, the Tangihua Complex (basaltic rock) across Northland appear to have high dissolved reactive phosphorus susceptibility, whereas the ancient greywacke basement does not. Although

this observation is consistent with petrochemical datasets that identify the Tangihua Complex as containing naturally elevated inorganic phosphorus concentrations (up to 6,000 ppm as P_2O_5) and deeply weathered Waipapa Group greywacke as containing low inorganic phosphorus concentrations, further evaluation is recommended (Syers et al, 1986; Briggs & Searle, 1975; Nicholson et al., 2000; Porder & Ramachandran, 2013). The Northland Regional Council has invested in additional surface monitoring sites and specific hydrochemical and water quality measures to improve their understanding of the spatial and temporal drivers of water quality.

When radiometric survey suggests significantly different soil properties to those that have been mapped at 1:50,000 scale, ground truthing is required. The susceptibility maps generated for the Mataura Catchment are being ground-truthed at sub-catchment and property scales in partnership with farmer-led catchment groups. Ground truthing includes assessing the spatial accuracy of susceptibility maps and radiometrically derived soil and erosion maps at property and paddock scales. Ground truthing includes partnering with land users' local knowledge and the use of soil profile description via hand auger, soil test pits, and soil water (artificial drainage), surface water, and groundwater quality and hydrochemical testing at sub-catchment and property scales. More information on the ground-truthing work is available through Thriving Southland (https://www.thrivingsouthland.co.nz), a rural community initiative to improve water quality and reduce greenhouse gas losses from land-use across the Southland Region.

Finally, Welch's ANOVA and Games-Howell post hoc tests indicate that some susceptibility classes may not be significant different from each other i.e., classes 1 and 2 or 4 and 5 may not be significantly different at α = 0.05 or 0.15. For this reason, we advise against the use of classes for land use modelling. Rather, we recommend the use of the unclassed susceptibility rasters.

References

Berhe, A. A., Barnes, R. T., Six, J., & Marin-Spiotta, E. (2018). Role of soil erosion in biogeochemical cycling of essential elements: carbon, nitrogen, and phosphorus. Annu. Rev. Earth Planet. Sci, 46(1), 521-548.

Boynton, W. R., Garber, J. H., Summers, R., & Kemp, W. M. (1995). Inputs, transformations, and transport of nitrogen and phosphorus in Chesapeake Bay and selected tributaries. Estuaries, 18(1), 285-314.

Ekholm, P., & Lehtoranta, J. (2012). Does control of soil erosion inhibit aquatic eutrophication?. Journal of environmental management, 93(1), 140-146.

Fratkin, M. M., Segura, C., & Bywater-Reyes, S. (2020). The influence of lithology on channel geometry and bed sediment organization in mountainous hillslope-coupled streams. Earth Surface Processes and Landforms, 45(10), 2365-2379.

Gburek, W. J., Barberis, E., Haygarth, P. M., Kronvang, B., & Stamm, C. (2005). Phosphorus mobility in the landscape. Phosphorus: agriculture and the environment, 46, 941-979.

Gschwend, P. M., & Reynolds, M. D. (1987). Monodisperse ferrous phosphate colloids in an anoxic groundwater plume. Journal of Contaminant Hydrology, 1(3), 309-327.

Heming, R. F. (1980). Petrology and geochemistry of Quaternary basalts from Northland, New Zealand. Journal of volcanology and geothermal research, 8(1), 23-44.

Hodgson, W. A. (1968). The diagenesis of spherulitic carbonate concretions and other rocks from Mangakahia Group sediments, Kaipara Harbour, New Zealand. Journal of Sedimentary Research, 38(4), 1254-1263.

Joshi, S. R., Kukkadapu, R. K., Burdige, D. J., Bowden, M. E., Sparks, D. L., & Jaisi, D. P. (2015). Organic matter remineralization predominates phosphorus cycling in the mid-bay sediments in the Chesapeake Bay. Environmental science & technology, 49(10), 5887-5896.

Kleinman, P. J., Fanelli, R. M., Hirsch, R. M., Buda, A. R., Easton, Z. M., Wainger, L. A., ... & Shenk, G. W. (2019). Phosphorus and the Chesapeake Bay: Lingering issues and emerging concerns for agriculture. Journal of Environmental Quality, 48(5), 1191-1203.

Kronvang, B. (1992). The export of particulate matter, particulate phosphorus and dissolved phosphorus from two agricultural river basins: implications on estimating the non-point phosphorus load. Water Research, 26(10), 1347-1358.

McDonald, L., Pearson, L. and Rissmann, C. (2020). Validation of the Northland Sediment Process-Attribute Layer: Erosion Susceptibility Classification. Land and Water Science Report 2020/02. p26.

Moncelon, R., Gouazé, M., Pineau, P., Beneteau, E., Bréret, M., Philippine, O., ... & Metzger, É. (2021). Coupling between sediment biogeochemistry and phytoplankton development in a temperate freshwater marsh (Charente-Maritime, France): Evidence of temporal pattern. Water Research, 189, 116567.

Morel, P., Von Blanckenburg, F., Schaller, M., Kubik, P. W., & Hinderer, M. (2003). Lithology, landscape dissection and glaciation controls on catchment erosion as determined by cosmogenic nuclides in river sediment (the Wutach Gorge, Black Forest). Terra Nova, 15(6), 398-404.

Mortimer, N., & Roser, B. P. (1992). Geochemical evidence for the position of the Caples–Torlesse boundary in the Otago Schist, New Zealand. Journal of the Geological Society, 149(6), 967-977.

Mueller, E. R., & Pitlick, J. (2013). Sediment supply and channel morphology in mountain river systems: 1. Relative importance of lithology, topography, and climate. Journal of Geophysical Research: Earth Surface, 118(4), 2325-2342.

Pearson, L., & Rissmann, C. (2020). Application of Physiographic-based modelling to estimate contaminant load to the Hokianga Harbour.

Pearson, L. and Rissmann, C. (2021). Physiographic Environments of New Zealand: Inherent susceptibility of the landscape for contaminant loss. Land and Water Science Report 2021/25. p60.

Porder, S., & Ramachandran, S. (2013). The phosphorus concentration of common rocks—a potential driver of ecosystem P status. Plant and soil, 367(1), 41-55.

Pound, K. S., Norris, R. J., & Landis, C. A. (2014). Eyre Creek mélange: An accretionary prism shear-zone mélange in Caples terrane rocks, Eyre Creek, northern Southland, New Zealand. New Zealand Journal of Geology and Geophysics, 57(1), 1-20.

Rissmann, Clinton, Andrew Nicol, Jim Cole, Ben Kennedy, Jerry Fairley, Bruce Christenson, Matthew Leybourne, Sarah Milicich, Uwe Ring, and Darren Gravley. "Fluid flow associated with silicic lava domes and faults, Ohaaki hydrothermal field, New Zealand." Journal of Volcanology and Geothermal Research 204, no. 1-4 (2011): 12-26.

Rissmann, C., Christenson, B., Werner, C., Leybourne, M., Cole, J., & Gravley, D. (2012). Surface heat flow and CO2 emissions within the Ohaaki hydrothermal field, Taupo Volcanic Zone, New Zealand. Applied geochemistry, 27(1), 223-239.

Rissmann, C., and Lovett, A. (2016). Hydrochemical analysis for the Otane, Wastewater Treatment Plant. GNS Science Consultancy Report 2016/83.

Rissmann, C., and Pearson, L. (2020). Physiographic Controls over Water Quality State for the Northland Region. Land and Water Science Report 2020/05. p120.

Rissmann, C., Pearson, L., Lindsay, J., and Couldrey, M. (2018a). Sediment Process-Attribute Layer for Northland. Land and Water Science Report 2018/35. p71

Rissmann, C., Pearson, L., and Robson, B. (2020b). Intensive Winter Grazing and Water Quality: Assessing the Importance of Landscape Attributes. Land and Water Science Report 2020/09. p99.

Rissmann, C., Rodway, E., Beyer, M., Hodgetts, J., Pearson, L., Killick, M., Marapara, T.R., Akbaripasand, A., Hodson, R., Dare, J., Millar, R., Ellis, T., Lawton, M., Ward, N., Hughes, B., Wilson, K., McMecking, J., Horton, T., May, D., and Kees, L. (2016). Physiographics of Southland Part 1: Delineation of key drivers of regional hydrochemistry and water quality. Technical Report No. 2016/3. Invercargill, New Zealand: Environment Southland.

Rissmann, C., Pearson, L., Lindsay, J., Couldrey, M., and Lovett, A. (2018b). Application of Physiographic Science to the Northland Region: Preliminary Hydrological and Redox Process-Attribute Layers. Land and Water Science Report 2018/11. p88.

Rissmann, C.W.F., Pearson, L.K., Beyer, M., Couldrey, M.A., Lindsay, J.L., Martin, A.P., Baisden, W.T., Clough, T.J., Horton, T.W. & Webster-Brown, J.G. (2019). A hydrochemically guided landscape classification system for modelling spatial variation in multiple water quality indices: Process-attribute mapping. Science of the Total Environment, 672, pp.815-833.

Rissmann, C., Pearson, L., Joy, K., and Dean, R. (2020a). Mapping Wetness Gradients utilising Radiometric and Satellite Imagery. Land and Water Science Report 2020/10. p58.

Rissmann, C., Pearson, L., Joy, K., and Dean, R. (2020). Mapping Wetness Gradients utilising Radiometric and Satellite Imagery. Land and Water Science Report 2020/10. p58.

Rissmann, C., Pearson, L., Shi, Y., and Lawrence, C. (2020). Radiometric and Terrain Derived Erosion Susceptibility Classification for the Southland Region. Land and Water Science Report 2020/28. p82.

Syers, J. K., Williams, J. D. H., & Walker, T. W. (1968). The determination of total phosphorus in soils and parent materials. New Zealand Journal of Agricultural Research, 11(4), 757-762.

Tiessen, H. (2008). Phosphorus in the global environment. In The ecophysiology of plant-phosphorus interactions (pp. 1-7). Springer, Dordrecht.

Ward, J. C., O'Connor, K. F., & Wei-Bin, G. (1990). Phosphorus losses through transfer, runoff and soil erosion. Phosphorus requirements for sustainable agriculture in Asia and Oceania. Int Rice Res Inst, Manila, Philippines, 167-183.